SYNTHESIS, CHARACTERIZATION AND MOLECULAR MODELING OF DIPHENYL GLYCOLIC ACID-AMINO ACID METAL COMPLEXES

Thesis submitted to the
University of Calicutin partial fulfillment of the
requirements for the award of the degree of

DOCTOR OF PHILOSOPHY IN CHEMISTRY
Under the Faculty of Science

PRANAMYA.N.P

Under the Guidance of

Dr.G.Indira Devi
Associate Professor (Retd.)
&
Dr.Susannah Seth
Associate Professor (Retd.)
&
Dr.Leon Prasanth K.
Assistant Professor

DEPARTMENT OF CHEMISTRY
THE ZAMORIN'S GURUVAYURAPPAN COLLEGE
KOZHIKODE-673 014, KERALA

JANUARY 2024

Dr.G.Indira Devi
Associate Professor (Retd.)
Department of Chemistry
Zamorin's Guruvayurappan College, Calicut
Kerala-673014

CERTIFICATE

This is to certify that the thesis entitled, **"Synthesis, Characterization and molecular modeling of Diphenyl glycolic acid- amino acid metal complexes"** is an authentic record of the research work carried out by Ms. Pranamya.N.P under my supervision in fulfilment of the requirements for the degree of Doctor of Philosophy in Chemistry of the Zamorin's Guruvayurappan College, Calicut and further that no part thereof has been presented before for any other degree.

ZGC, Calicut

Dr.G.Indira Devi
(Supervising Teacher)

Dr.Susannah Seth
Associate Professor (Retd.)
Department of Chemistry
Malabar Christian College, Calicut
Kerala-673014

CERTIFICATE

This is to certify that the thesis entitled, **"Synthesis, Characterization and molecular modeling of Diphenyl glycolic acid- amino acid metal complexes"** is an authentic record of the research work carried out by Ms. Pranamya.N.P under my supervision in fulfilment of the requirements for the degree of Doctor of Philosophy in Chemistry of the Zamorin's Guruvayurappan College, Calicut and further that no part thereof has been presented before for any other degree.

MCC, Calicut
(Co-Guide)

Dr. Susannah Seth

Dr.Leon Prasanth K
Assistant Professor
Z.G.College P.O
Department of Chemistry
Zamorin's Guruvayurappan College, Calicut
Kerala-673014

CERTIFICATE

This is to certify that the thesis entitled, **"Synthesis, Characterization and molecular modeling of Diphenyl glycolic acid- amino acid metal complexes"** is an authentic record of the research work carried out by Ms. Pranamya.N.P under my supervision in fulfilment of the requirements for the degree of Doctor of Philosophy in Chemistry of the Zamorin's Guruvayurappan College, Calicut and further that no part thereof has been presented before for any other degree.

ZGC, Calicut

Dr.Leon Prasanth.K
(Co-Guide)

DECLARATION

I hereby declare that this thesis entitled, **"Synthesis, Characterization and molecular modeling of Diphenyl glycolic acid- amino acid metal complexes"** submitted to the Zamorin's Guruvayurappan College, Calicut in fulfilment of the requirements for the degree of Doctor of Philosophy in Chemistry is a bonafide research work done by me under the supervision and guidance of Dr.G.Indira Devi, Associate Professor (Retd.), Department of Chemistry, Zamorin's Guruvayurappan College, Calicut. Dr. Susannah Seth, Associate Professor (Retd.), Department of Chemistry, Malabar Christian College, Calicut, Dr. Leon Prasanth K. Assistant Professor Department of Chemistry, Zamorin's Guruvayurappan College, Calicut. I further declare that this thesis has not previously formed the basis of any degree, diploma or other or other similar title.

ZGC, Calicut **Pranamya.N.P**

Dedicated to
To My parents who strengthen me with their love and affection
To My husband who shares my happiness and worries
To My little angel who inspired me with her cute smile

ACKNOWLEDGEMENT

First and foremost to Almighty God for giving endless blessing during this work as a part of his generous help throughout my life.

I wish to express my deep sense of gratitude and respect to Dr.G.Indira Devi, Associate Professor (Retd), Department of Chemistry, Zamorin's Guruvayurappan College, Calicut for her unfailing encouragement, outstanding guidance, valuable suggestions and support throughout this work. I am indebted to her giving me considerable freedom of thought and expression which I enjoyed during my research period.I thank her with all my heart. I also thank Dr. Sabu.P.G. for the support and care extended for me. I wish to acknowledge my heartfelt thanks to Dr.Susannah Seth, Associate Professor (Retd), Department of Chemistry, Malabar Christian College, Calicut (Co-Guide) for her meticulous supervision,constant encouragement, and support throughout this work. I take this opportunity to thank Dr.Leon Prasanth.K, Assistant Professor, Department of Chemistry, Zamorin's Guruvayurappan College, Calicut (Co-Guide) for his support throughout this work.

I sincerely express my gratitude towards Dr. Rugmini Ammal, Head of the Department of Chemistry, Zamorin's Guruvayurappan College, Calicut and former heads Dr.D.K.Babu and Dr.Malini.P.T. for providing me the necessary facilities. I would

like to express my gratitude to other teachers and non-teaching staff of this department for their valuable help and support. I would like to express my gratitude to Dr. Rajan.P. P and Dr. Arun Kumar, Dr. Anoop and their research scholars of Department of Botany, ZGC Calicut for assisting me to conduct antifungal activity studies. I take this opportunity to thank Dr.Rajani, Principal Zamorin's Guruvayurappan College, Calicut and former Principal Dr. Ramachandran for their co-operation and support which helped me to complete my research work.

I am thankful to CSIF-Calicut University, Department of Chemistry-Calicut University, Department of Physics-St.Thomas College, Thrissur and NIT Calicut for carrying out spectral and physico-chemical analysis necessary for my research work. I am also thankful to Dr.K.Muraleedharan and Neenu Krishna.P.U for conducting the molecular modeling studies.

My heartfelt thanks to all research scholars of the Department of Chemistry, ZGC, Calicut, especially to Ali Hassan. M, Pravisha. K and Nasheetha Rahman. T. T for their help, co-operation and support.

Most importantly, I would like to thank my father, Preman, mother, Nisha, My sister Prabhisha. K and my brother, Sreegokul for their love, support and encouragement in every hard situations. I am deeply indebted to my husband Sreejesh.K, without him I couldn't have completed this research. His constant support and

encouragement helps me throughout the research period. I am also grateful to my daughter Dhruvika.K for giving me humble time. I sincerely remember and acknowledge the moral support and help extended by my family members and in-laws.

Pranamya.N.P

ABSTRACT

Coordination chemistry is a branch of inorganic chemistry which deals with metals, ligands and complexes. Due to the wide range of applications of coordination compounds they are gaining momentum in the area of research for the last few decades. A coordination compound may be defined as an innermost metal atom/ion bounded by a sheath of ions/ molecules called ligands by the coordinate bonds. The splendid beauty of nature around us is the foremost contribution of coordination chemistry. We may wonder how, but it is playing a vital role in our life. The chlorophyll which contributes greenery to our eyes, the blood flows through our body, everything and anything around us is a contribution to coordination chemistry.The applications of coordination complexess encompass various fields such as metallurgical processes, electroplating, water softening, dyes, color photography, nuclear fuels, toxicology, medicine, catalysis, material science etc.

Out of many flexible multifunctional ligands, amino acids and Diphenyl glycolic acid are effective due to their wide range of applications in analytical, catalytic, corrosion and biological fields.So we have chosen these compounds (diphenyl glycolic acid and various amino acids such as tyrosine,glycine,histidine,valine and leucine) as the initial materials for the formation of ligands. Diphenyl Glycolic acid-amino acids are condensed together and are

coordinated to the various metal ions. The formation of the ligands and metal complexes was studied using various analytical techniques as IR, UV, Thermogravimetric analysis (TG, DTA), X-ray diffraction. Various applications such as antifungal activity,corrosion inhibition efficiency and catalytic activity of the compounds have been studied. Also the molecular modeling studies of the compounds have been studied.

Keyword: Diphenyl glycolic acid, Aminoacid, Corrosion inhibition studies, Catalytic Studies, Antifungalstudy

സംഗ്രഹം

ഘടനാപരമായ ക്രമീകരണങ്ങളിലെ വ്യതിരിക്തതയും വിവിധ മേഖലയിലെ പ്രയോഗസാധ്യതയും മൂലം രസതന്ത്രത്തിൽ പ്രത്യേക സ്ഥാനമുള്ളവയാണ് ഏകോപന അഥവ സമന്വയ സംയുക്തങ്ങൾ. വൈവിധ്യമാർന്ന മേഖലകളിൽ ഉപയോഗിക്കപ്പെടുന്നു എന്നതിനാൽ തന്നെ ധാരാളമായി പഠനവിധേയമാകുന്ന ഒരു ശാഖകൂടിയാണിത്. ഒരു കേന്ദ്ര ആറ്റമോ അയോണോ അലോഹ ആറ്റങ്ങളാലോ അല്ലെങ്കിൽ ലിഗാർഡുകൾ എന്ന് വിളിക്കപ്പെടുന്ന ആറ്റങ്ങളുടെ ഗ്രൂപ്പുകളാലോ ചുറ്റപ്പെട്ടിരിക്കുന്ന ഒരു രാസസംയുക്തമാണ് ഏകോപന സംയുക്തങ്ങൾ. ഉചിതമായ ലിഗാന്റ്ഡുകൾ തിരഞ്ഞെടുത്ത് ആസൂത്രണം ചെയ്ത ഗുണങ്ങളുള്ള വിവിധതരം ഏകോപന സംയുക്തങ്ങൾ നിർമ്മിക്കുകയും അവയുടെ രാസഗുണങ്ങൾ , സ്വഭാവങ്ങൾ എന്നിവ മനസ്സിലാക്കുകയും ചെയ്യുന്നു.

ജീവശാസ്ത്രപരമായ വ്യവസ്ഥിയിൽ പ്രത്യേകിച്ച് മനുഷ്യരിലും സസ്യജാലങ്ങളിലും അവ സുപ്രധാന പങ്ക് വഹിക്കുന്നു. രക്തത്തിലെ ഹീമോഗ്ലോബിൻ മനുഷ്യ ശരീരത്തിലെ അത്യന്താപേക്ഷിതമായ ഇരുമ്പിന്റെ ഏകോപന സംയുക്തമാണ്. കൂടാതെ സസ്യജാലങ്ങളുടെ ജീവന്റെ തുടർച്ചക്കാവശ്യമായ ക്ലോറോഫിൻ, മഗനീഷ്യത്തിന്റെ ഒരു ഏകോപന സംയുക്തമാണ്. വിറ്റാമിൻ ബി 12, ഡൈകൾ, പിഗ്മെന്റുകൾ എന്നിവ സമന്വയ സംയുക്തങ്ങൾക്ക് ഉദാഹരണങ്ങളാണ്.

ഈ ശാസ്ത്രപ്രബന്ധത്തിൽ വിവിധ അമിനോ ആസിഡുകളും ബെൻസിലിക് ആസിഡും ചേർന്ന് നിർമ്മിച്ച വ്യത്യസ്ത ലിഗാന്റ്ഡുകളെയും അവിടെ വിവിധതരം ഏകോപന സംയുക്തങ്ങളെയും കുറിച്ച് പ്രതിപാദിച്ചിരിക്കുന്നു. ഐ.ആർ,യു.വി, തെർമോഅനലിറ്റിക്കൽ ടെക്നിക്കുകൾ (ടി.ജി, ഡി.ടി.എ, ഡി.ടി.ജി) എക്സ്-റേ ഡൈഫ്രേയ്ഷൻ ടെക്നിക്കുകൾ എന്നിവ ഉപയോഗിച്ച് പുതുതായി നിർമ്മിച്ച ലിഗാന്റ്ഡുകളെയും അവയുടെ വ്യത്യസ്ത സംയുക്തങ്ങളെയും പറ്റി പഠിച്ചിരിക്കുന്നു. അവയുടെ ബന്ധനം ആകൃതി എന്നിവയെ കുറിച്ച് മനസ്സിലാക്കുകയും ചെയ്തിരിക്കുന്നു. അതിനോടൊപ്പം അവയുടെ വ്യത്യസ്ത ഗുണങ്ങളും അപഗ്രഥിക്കുന്നു. ലോഹനാശനം തടയാനുള്ള കഴിവ്, ഉൽപ്രേരകശേഷി , ആന്റിഫംഗൽ പ്രവർത്തനം എന്നീ ഗുണങ്ങൾ വിശദപഠനം നടത്തുകയും പുതുതായി നിർമ്മിച്ച ലിഗാന്റ്ഡുകളുടെ കമ്പ്യൂട്ടേഷണൽ രീതികൾ പഠനവിധേയമാക്കുകയും ചെയ്തിരിക്കുന്നു.

സൂചകപദങ്ങൾ: ഡൈഫീനൈൽ ഗ്ലൈക്കോളിക് ആസിഡ്(ബെൻസീലിക് ആസിഡ്), അമിനോ ആസിഡ്, ലോഹനാശനശേഷി, ഉൽപ്രേരകശേഷി, ആന്റിഫംഗൽ പ്രവർത്തനം

PREFACE

Coordination chemistry is a wide area of research from nineteenth century due to their diverse applications in the different fields of science. Transition metal complexes having electronegative atoms like sulphur, nitrogen and oxygen play a vital role in coordination chemistry. Transition metal complexes with amino acids as ligands have been the widely studied topic nowadays. Out of many flexible multifunctional ligands, amino acids and Diphenyl glycolic acid are effective due to their wide range of applications in analytical, catalytic, corrosion and biological fields.

The metal complexes of amino acids and Diphenyl glycolic acid have been a source of attraction to the research world due to their antifungal, antibacterial, catalytic and corrosion inhibition activities. Recent studies on the synthesis, characterization and wide range of applications in the various fields are promising and favourable for further research. Hence the synthesis of various Diphenyl glycolic acid-amino acid condensed ligands and their transition metal complexes are considered to be interesting.

The present investigation mainly focused on the synthesis, characterization and application study of the Diphenyl glycolic acid-amino acid ligands and their transition metal complexes. Five new ligands Diphenyl glycolic acid-tyrosine, Diphenyl glycolic acid glycine, Diphenyl glycolic acid-histidine, Diphenyl glycolic acid-valine,

Diphenyl glycolic acid-leucine and their transition metal complexes have been synthesized and studied extensively with the aid of physicochemical studies. The results are summarized in part I.

The thermal studies of the selected complexes were carried out using T.G. All the TG curves were subjected to kinetic analysis and kinetic parameters namely order of reaction, activation energy, entropy of activation, enthalpy of activation and free energy of activation are evaluated using the mechanistic and non-mechanistic equations. The results of the studies have been reported in part II.

Based on the X-ray powder diffraction pattern the crystal lattice and cell dimensions of selected complexes HBT, HBG and HBH have been reported in part III. The orthorhombic crystal structure was suggested for the complexes.

Part IV briefly explains the details of the corrosion inhibition efficiency of the newly synthesized Diphenyl glycolic acid-amino acid ligands in 0.5M HCl acid media.

The investigation of the antifungal activity of the ligands and their selected metal complexes against various fungal strains carried out and are described in the Part V.

Another potential application of the selected complexes as an efficient catalyst for the dye degradation is investigated and summarized in Part VI.

The molecular modeling studies of the newly synthesized ligands were conducted and the geometrical optimization, NBO analysis and MEP data of the ligands are summarized in part VII.

A detailed list of references arranged in serial order is given at the end of each part and the thesis concludes with a brief summary.

The research work presented in this thesis has partly been published/under publication as indicated.

CONTENTS

ABBREVIATIONS

HBT	-	Diphenyl glycolic acid-Tyrosine
HBG	-	Diphenyl glycolic acid-Glycine
HBH	-	Diphenyl glycolic acid-Histidine
HBV	-	Diphenyl glycolic acid-Valine
HBL	-	Diphenyl glycolic acid- Leucine
M	-	Central metal ion in the complex
L	-	Ligand moiety in a complex
B.M	-	Bohr Magneton
DMSO	-	Dimethyl sulphoxide
DMF	-	Dimethyl formamide
MS	-	Mild Steel

PART 1

SYNTHESIS AND CHARACTERIZATION

CHAPTER 1

A BRIEF OUTLINE OF DIPHENYL GLYCOLIC ACID AND AMINO ACID COMPLEXES

1.1 Introduction

The race of inorganic chemistry instigates its expedition from minerals and ores, as its name suggests, the non-living chemistry which eventually steps forward to miscellaneous wings of chemistry, for instance coordination chemistry, organometallic chemistry, bioinorganic chemistry etc. The most relevant developments happened in the field of coordination chemistry only about five decades ago. The world of coordination chemistry transpires from the efforts of two prominent scientists, Werner and Jorgenson. Here begins the era of coordination chemistry and progress is going on till the twenty-first century. Explanations of the stability of the complexes, nature of the chemical bonds, structure and reactivity were predicted by various theories, namely the electronic theory of Sidgwick, crystal field theory, Ligand field theory and molecular orbital theory. Coordination chemistry remains a versatile field in the domain of chemistry due to its important role in the progress of chemistry. The theories related to the structure and chemical bonding were analyzed by taking coordination complexes as the investigating ground. The application of quantum mechanical chemistry to the chemical bonding in coordination compounds has resulted in the formation of modern coordination theories such as molecular orbital and ligand field theories. Recently, a major breakthrough happened in the field of coordination chemistry through the upcoming of molecular modeling studies of coordination complexes.

The splendid beauty of nature around us is the foremost contribution of coordination chemistry. We may wonder how, but it is playing a vital role in our life. The chlorophyll which contributes greenery to our eyes, the blood flows through our body, everything and anything around us is a contribution to coordination chemistry. Simply, we can outline coordination chemistry as a branch of inorganic chemistry which deals with metals, ligands and complexes. A coordination compound may be defined as a innermost metal atom or ion bounded by a sheath of ions or molecules by the dative bonds, which are also known as coordinate bonds. The process of coordination is an acid-base reaction. The groups of molecules bonded directly to the metal atom are called ligands. The stability of the complex is enhanced by an increase in the basicity of the ligand or increase in acidity of metal. Coordination complexes are compounds that have a metal center that is bound to ligands (atoms, ions, or molecules that contribute electrons to the metal). These complexes can be neutral or charged. When the complex is charged, it is stabilized by neighbouring counter-ions.

The applications of coordination complexess encompass various fields such as metallurgical processes, electroplating, water softening, dyes, color photography, nuclear fuels, toxicology, medicine, catalysis, material science etc. The coordination compounds are used in the extraction of cobalt and nickel by hydro-metallurgical processes which require a lot of complex ions.

The use of EDTA catalysts is becoming increasingly popular in the polymer industry. The use of coordination complexes such as Phthalocyanine as dyes for fabrics is common in the pigment industry. Some of the cyanide complexes are used as a protective layer on surfaces for electroplating finds applications in photography. Hydrometallurgy involves the extraction of metals from ores using aqueous solutions by precipitating a metal of interest over the other metals in the solution present in the sample.

Transition metal complexes are a widely interesting topic in coordination chemistry as a result of their remarkable magnetic properties; abnormal arrangement features and significance in biological systems [1-4].The cations of the transition metal ions have a tendency to form complexes by accepting electrons from the ligands which possess the lone pair of electrons. The small size and greater positive charge density makes the transition metal cations receive the lone pairs of electrons from the ligand. Transition metal complexes act a vital role in agriculture, pharmaceutical and industrial chemistry. One of the most important ligands used in transition metal complex formation is the Schiff base, which is formed by the condensation reaction of primary amines and aldehydes or ketones[5]. Copper is a moderately active metal with electronic configuration $3d^{10}4s^{1}$ which dissolves in most acids and alkalis. It appear in nature as a metal, as sulphide, as arsenide, as carbonate, as acetate and as sulphate etc.

A numerous copper compounds are used as pesticides, chemicals and fungicides. Copper complexes exhibit excellent activities, such as anticancer[6], antitumor[7], antibacterial[8], antifilarial[9] and antiviral[10] drugs. The rate of hydrolysis of copper complexes is 10-50 times greater than a normal Cu (II) ion. Enhancement in the antiulcer activity of Cu (II) complexes is observed in comparison with its parent ligand, Salicylidine anthranilic acid[11]. The Schiff base obtained from salicylaldehyde, 2, 4-dihydroxy-benzaldehyde, glycine and L-alanine and their Cu, Ni, Zn and Co metal complexes possess antitumor activity[12]. Cobalt is another transition metal having a wide range of applications in the manufacture of ceramics and enamels, coloring materials, fire retardants, pigments in paints, metal preservatives and water purification etc. It has an electronic configuration of $3d^7 4s^2$. Sahare[13] et al synthesized the transition metal complexes of 2-hydroxy-5-methylbenzophenone with 2-phenylethylamine and they are characterized by micro analytical analysis, FT-IR, ^{1}HNMR, magnetic measurements, electronic spectra and thermal analysis methods and the complexes found to have various geometries such as octahedral, tetrahedral and square planar.

Amery[14] et al synthesized and characterized a bidentate Schiff base derived from benzaldehyde with 1,2-diphenyl-3-methyl-4-amino-5-oxo-pyrazole and their complexes of Mn (II), Co (II), Ni (II), Cu (II), Zn (II) and Cd (II) with the aid of metal and elemental analysis, FTIR, electronic spectra, molar conductivity, magnetic

susceptibility and mole ratio and they are octahedral in geometry. From the FTIR, UV-Visible, proton and ^{13}C NMR, magnetic moment and conductivity measurements, the tetrahedral geometry of Ni(II)), Zn(II), Cd(II) and Sn(II) metal with 4-amino-5-(pyridyl)-4H-1,2,4-triazole-3-thiol and square structure of the Cu(II) complexes were confirmed[15]. New tridentate schiff base, quinoxaline-2-carboxalidine-2-amino-5-methylphenol and their five metal complexes have been synthesized and their square planar, tetrahedral and octahedral structure have been predicted by various spectroscopic techniques[16].

Diphenyl Glycolic acid is a white crystalline molecule with the formula $C_{14}H_{12}O_3$ or $(C_6H_5)_2$(HO)-C-(COOH) prepared by the heating of benzil, ethanol and potassium hydroxide mixture or by the rearrangement of benzyl by the dimerisation of the benzaldehyde. Rosa Carballo[17] et al synthesized two new novel complexes of Zinc(II) with 1, 10-phenanthroline and one of three different α-hydroxycarboxylates (HL′) derived from the α-hydroxycarboxylic acids (H_2L') (2-methyllactic, H_2mL; mandelic, H_2M or benzilic, H_2B). They also studied the effect of the classical and non-classical hydrogen bonding and of the π-π and C-H…π interactions in the 3D supramolecular arrangement of these molecular complexes. Some higher carboxylic acids and hydroxycarboxylic acids undergo reaction with anhydrous Cu (II) acetate in toluene under reflux conditions. Baranwal[18] and his co-workers suggest antiferromagnetic coupling between two copper

atoms using the magnetic moment measurement and electron spin resonance spectral data. The molecular weight determination confirms the dinuclear nature of the complexes. There are a few metal complexes derived from Diphenyl Glycolic acid and the reviews about the complexes are given here.

The different substituents in the Diphenyl Glycolic acid and its derivatives were synthesized and their antimicrobial studies were done by R. Sudha[19] et al.Yongcai[20] et al have prepared and characterized the Cu(II) and Cd (II) complexes of Diphenyl Glycolic acidand [(1,10)-phen]. Rosa Carballo[21] et al has prepared a nickel (II) mixed-ligand complex with benzilate and the N, N-chelating aromatic amine 1, 10-phenanthroline.Magnetic and electronic studies proposed an octahedral geometry for the complex. G.Indiradevi[22] synthesized the thermally stable fungicides from Benzilic acid-amino acid complexes of transition metals like Ni, Cu, Mn and Co and their structure was determined by various methods such as molar conductance, elemental analysis, and spectral measurements and by using magnetic and conductance data. Electronic spectra assigned an octahedral structure for the Co (II) complex. G.Indiradevi[23] et al also synthesized a series of complexes on condensation of Diphenyl Glycolic acid with alanine. An octahedral geometry was assigned to the Cu, Ni, Mn and Co complexes.

Issa[24] et al synthesized Mn (II), Co (II), Ni (II), Cu (II) and Cd (II) complexes of benzilic and mandelic esters and the spectral studies shows that the Ni complexes are octahedral, whereas the Co and Cu analogous are distorted octahedral.Complexes of acetates of U (IV), Th (IV) and La (III) with the ligands p-amino benzoic acid, m-amino benzoic acid, Diphenyl Glycolic acidand phthalic acid have been prepared by Singh[25] et al. They characterized the complexes on the basis of IR and reflectance spectra and magnetic susceptibility data. Maumoud[26] et al synthesized 1,3,4-thiadiazole by reaction of potassium xanthate with con.H_2SO_4 (0-3°C) and characterized by TLC,MP,FT-IR and ^{1}H-NMR spectral data. The potassium xanthate has been prepared by reaction of Diphenyl Glycolic acidhydrazide with carbon disulphide in potassium hydroxide. The non-linear optical properties of the Diphenyl Glycolic acidcrystals were studied by Felicita[27] and co-workers. The crystals were synthesized by a slow evaporation method and the unit cell parameters were evaluated by single crystal and powder x-ray diffraction techniques. Also, the SHG efficiency of the crystals is also measured.

Salim[28] et al obtained benzil hydrazones by the reaction of acetophenone or its derivatives and benzophenone or its derivatives with Diphenyl Glycolic acidhydrazide. The characterization of the compounds was done by IR, ^{1}H-NMR, ^{13}C NMR and UV spectroscopy. Synthesis and study of the Cobalt-Diphenyl Glycolic acid complexes having the general formula [ML_4Cl_2] and

$[ML_4](ClO_4)_2$ have been carried out by Jerome and Merina[29]. The IR spectra indicate that the carbonyl group is coordinated with metal and the compound acts as a monodentate ligand, and also the UV data suggest an octahedral geometry for the complexes, which is supported by the magnetic moment measurements. Jerome[30] et al prepared and characterized the Mn (II) Diphenyl Glycolic acidcomplexes with the general formula $[ML_4Cl_2]$ and $[ML_6](ClO_4)_2$. The conductance measurement suggests that chloride and perchlorate complexes behave as a 1:2 electrolyte and the electronic spectra suggest octahedral geometry of the complexes. Also, the IR data shows Diphenyl Glycolic acidacting as a monodentate ligand in which the carbonyl group is coordinated with the metal ion.

Smith[31] et al evaluated the physiological properties of the newly synthesized amino esters of Benzilic acids. These compounds exhibit an enhanced anticholinergic activity than atropine and one among the compounds exhibits antihistamine activity. The equilibria and the kinetics of the Fe(III) complexes with different α-Hydroxycarboxylic acids(glycolic, DL-lactic, DL-malic, and benzilic acids) were studied using the stopped-flow method by Mentasti[32,33].The spectral and thermal study of the nano-sized, oxo-centered, trinulcear carboxylate-bridged chromium(III) complexes of hydroxycarboxylic acids were conducted by Baranwal[34] and his co-workers. The structural study of the condensed products of acephenone or its derivatives and benzophenone and its derivatives

with Diphenyl Glycolic acidhydrazide carried out by Salim[35]et al. The characterisation of 5-(mercapto-1,3,4-thiadiazole-2yl)α,α-(diphenyl)methanol, which have been synthesized by the ring closure of potassium xanthate, which is the condensed product of Diphenyl Glycolic acidwith carbon disulphide in potassium hydroxide[36].

Amino acids are compounds having a carboxylic acid chain attached to the carbon containing an amino acid group. The essential elements of an amino acid are carbon (C), hydrogen (H), oxygen (O) and nitrogen (N), although other elements are present in the side chains of certain amino acids. Amino acids are water soluble, amphoteric compounds which act as a buffer over a wide range of pH due to their capability to form both acidic as well as basic salts due to the presence of amino and carboxyl groups. The presence of active groups helps them to be involved in various reactions to form products such as esters, amides, amines, polymers, polypeptides, hydroxy acids, ketoacids, short and long chain acids. The presence of two effective donor atoms, NH_2 and COO^- groups, in the skeletal structure makes the amino acid a potential coordinating ligand. Amino acids are the basic constituents of proteins and also they play a vital role in processes such as neurotransmitter transport and biosynthesis. The history of the amino acid began in the early nineteenth century when the compound asparagines was isolated from the asparagus by the

French chemists Louis-Nicolas Vauquelin and Pierre Jean Robiquet[37].

Amino acid complexes play an important role in the history of medicine. They have a high potential to act as antimicrobial agents. In complexation with the metal atom, they seem to raise the ability to act against microbes such as bacteria and fungus. Novel complexes have been prepared by the reaction of salicylaldehyde and o-pheneylenediamine with Cr (VI), Cr (III), Pb (II) and TiO (IV) ions. The ligand doesn't show any activity against the bacteria, but on complexion with Pb (II) ion it shows an amazing effect against both gram positive and gram negative bacteria in this study concluded by Ajaily[38]*et al.* The antifungal and antibacterial activities of Co(II), Cu(II), Ni(II), and Zn(II) metal complexes derived by condensation of *β*-diketones with glycine, phenylalanine, valine, and histidine,which act as bidentate towards metal ions (cobalt, copper, nickel, and zinc) have studied using agar method. The high potential to act as cytotoxic agents was also determined by Zahid[39] and his coworkers.

A new ligand 2N-salicylidene-5-(p-nitrophenyl)-1,3,4-thiadiazole, HL and a total of five new metal complex derivatives with the metal ions Vo(II), Co(II), Rh (III), Pd(II) and Au(III) have been successfully prepared in alcoholic medium by Emad Yousif[40] et al. The complexes obtained are characterized quantitatively and qualitatively by using micro elemental analysis, FTIR, UV–Vis, mass, ^{1}H &^{13}C NMR, magnetic susceptibility and conductivity

measurements. The preliminary in vitro antibacterial screening activity revealed that complexes 1–5 showed moderate activity against tested bacterial strains *Staphylococcus aureus, Salmonella typhi and Escherichia coli* and slightly higher compared to the ligand. Amino acid complexes with trivalent metal ions Al (III) and Fe (III) derived from the condensation of ortho-tyrosine and trans-4-hydroxyproline were investigated by ^{1}H and ^{13}C highresolution NMR, Laser Desorption Mass Spectrometry (LD-MS), and MS/MS experiments. The binding sites are COOH and NH_2 functional groups of ligands, while their phenolic and alcoholic groups, which did not participate in the metal coordination[41].

Inhibition efficiency of various metal complexes Cu (II), Co (II), Ni (II) and Mn (II) with, schiff bases synthesized from o-phthalaldehyde and amino acids, viz., glycine L-alanine, L-phenylalanine, then screened against three fungi. Neelakantan[42] et al suggested that Cu (II) and Ni (II) complexes exhibit inhibition of all the studied microorganisms. However, Co (II) and Mn (II) complexes exhibit less activity and VO (II) complexes exhibit no inhibition efficiency towards the microorganisms. Cu (II), Ni (II) and Co (II) metal complexes of 3-(2-hydroxy-3-ethoxybenzylideneamino)-5-methyl isoxazole and 3-(2-hydroxy-5-nitroben-zylidene amino)-5-methyl isoxazole were screened for the antifungal activity against Aspergillus niger and Rhizoctonia solani. According to chelation theory, the metal complexes show better efficiency than that of ligands as explainedby the study[43, 44].

The increased lipophilicity that leads to the breakdown of the permeability barrier of the cell was explained by Gupta[45] and Cukurova Liet al[46]. The Cu(II) complexes exhibit more activity than other metal complexes, which may be due to the higher stability constant of the Cu(II) complexes.

A Schiff base ligand derived from acetoacetanilide and 1,3-diaminopropane were tested for their antimicrobial activities to assess their inhibiting potential. The antifungal activity of the ligands and their metal complexes were evaluated by agar diffusion method against the fungi Candida albicans and Fusarium oxysporum [47]. The Cr(III), Mn(III), and Fe(III) complexes of Schiff base ligand derived from 1,4-dicarbonyl-phenyldihydrazide and chromene-2,3-dione exhibits greater antifungal activity against Aspergillus sp but show lesser activity towards Rhizoctonia sp. The Cr (III) and Fe (III) complexes are more effective against Penicillium sp[48]. Panchal[49] et al synthesized some mixed ligand complexes of transition metal ions Mn(II), Co(II), Ni(II), Cu(II), Zn(II) and Cd(II) by condensing the salicylidene-glycine and 2,2'-bipyridylamine or di(benzylidene)-1,8-diaminonaphthalene. Using the disc-diffusion method the compounds were tested against the pathogenic bacteria S. typhi, E. coli, and Serratia marcescens. The antibacterial study of a series of new Iron (II) schiff base amino acid complexes prepared by condensing amino acid and sodium 2-hydroxybenzaldehyde-5-sulfonate has been conducted and also the effect of HCl on the complexes studied spectrometrically. The

results showed good antibacterial activity against the *Bacillus cereus, Pseudomonas aeruginosa and Micrococcus bacteria* [50].

The biological study of the tridentate Schiff base formed by condensing 2-aminobenzimidazole with salicyladehyde and its Zn complex has been studied [51].Metal complexes of novel Schiff base derived from condensation of leucine and salicyldehyde were screened against bacterial(B. sabtilus, S. aureus and E.coli) and fungal(A. flavus, A. alternateand A. niger.) species. The newly prepared compounds and their metal complexes showed a higher effect on all bacterial and fungal stains but maximum activity was shown by Cobalt complex against B. sabtilus and A. flavus[52]. Yiheyis Bogale Zemede[53] et al synthesized and characterized Four Schiff bases,namely4-((thiophene-2-yl)methyleneamino) phenylsulphonamide(1),(2E)-2-((5-((E)-(2-hydroxyphenylimino) methyl) thiophene-2-yl)methyleneamino)phenol(2),2-(5-methoxy-2-hydroxybenzylideneamino)phenol(3) and N,N'-bis((thiophene-2yl)methylene)benzene-1,2-diamine (4) by IR, 1H NMR, Uv-Vis, mass spectral and elemental analyses techniques. Corrosion inhibition efficiency of these Schiff bases were evaluated using weight loss method in a 0.1MHCl solution for mild steel and they investigated a good inhibitory action against corrosion of mild steel in the medium. The Schiff bases were also screened for their in vitro antimicrobial activities against S. aureus, K.pneumoniae, C. albicans and C. krusei hence the result revealed that, except 4 all

the synthesized Schiff bases showed significant antimicrobial activity against all microbes under the study.

Jayeeta[54] synthesized the peroxovanadium complexes of phenylalanine and aspartic acid and studied the biological relevance of the complexes, which included the discovery of the natural product amvadin in mushrooms. Milan[55] et al synthesized and characterized Cobalt complexes of type $[CoLX]^{*}$ and [CoLXY] and their three isomers, cis-α, cis-β and trans forms, where L is the quadridentate ligand ethylenediamine-N,N'-di-(S)-α-isovalerate. Gallic acid-amino acid (alanine, leucine, isoleucine, and tryptophan) complexes of Europium were synthesized and studied using potentiometric studies and molecular modeling studies using the DFT method by Mohamed Taha[56] et al. Soliman[57] et al studied the ternary copper (II) complexes of the salicylidene-2-aminothiophenol (L) and glycine, alanine, valine and histidine amino acids. They were found to have five coordinated square bipyramidal distorted trigonal bipyramidal (SBPTBP) geometry and their thermodynamic parameters were reported. New Fe(II) Schiff base compounds derived from the condensation of o-hydroxynaphthaldehyde with L-alanine, L-phenylalanine, L-aspartic acid, L-histidine and L-arginine have undergone antibacterial studies and the results show that the metal complexes are potential compared to that of Schiff base-amino acid ligands[58]. Adam[59] et al studied the catalytic efficiency of the mono-oxovanadium (IV) complexes of acetylacetonate, curcumin

and N,N′-bis(2-pyridyl)thiourea for the oxidation of 1-octene by aqueous H_2O_2 in acetonitrile and they exhibits high activity to the production of epoxy product with low chemoselectivity. Catalytic applications of the copper complexes of N_6O_4 macrocyclic ligands have been studied by Zhen[60] et al for alcohol oxidation. The catalytic oxidation of styrene using O_2 as the oxidant has been carried out by Hongxin[61] et al and the catalysts are active at room temperature and the importance of solvent has been investigated. Rahmani[62] et al studied the catalytic reduction of dyes using the $NaBH_4$ as the reducing agent which was monitored by UV-vis spectroscopy and the studies revealed that the catalyst showed conversion ability up to 97% and its activity retained after 5 consecutive reactions. The catalytic study of the amino acid L-valine Cu (II) complex on cross-linked styrene-divinylbenzene carried out by Valodkar[63] et al and prove to act as versatile catalysts in the oxidation of various substrates such as benzyl alcohol, cyclohexanol and styrene in presence of *t*-butyl hydroperoxide as oxidant.

The Co(II), Ni(II) and Cu(II) chloro complexes of Benzilic hydrazide (BH) have undergone the catalytic degradation of AB25, IC and AB92 dyes using H_2O_2 and studies reveal that activity is dependent on metal ion and the activity decreases in the following order Cu(II)[Ni(II)[Co(II) for the three target dyes[64]. Homogeneous oxidation of 1,2-cyclohexene using Ni(II)-, Cu(II)- and Zn(II)-complexes (M-SSA) of salicylidene anthranilate sodium salt ligand

as catalyst was investigated by Hany[65] et al and among the complexes Cu-SSA shows the highest catalytic potential followed by Ni-SSA and Zn-SSA complexes. The reduction of p-nitrophenol to p-aminophenol catalyzed by the nickel(II) adamantane complexes has been investigated by UV–visible spectrophotometry by Zhou[66] and co-workers. Adam[67] et al studied the Catalytic efficiency of VO-complexes is measured in the symmetric and asymmetric oxidation of sulfides by using an aqueousH_2O_2 and the temperature study also have been carried out. The catalytic potential of Cu (II) and Co (II) pyridinylimino phenolate complexes for the (ep)oxidation of 1,2-cyclooctene by an aqueous H_2O_2 under alternative conditions has also been investigated[68].

B. El Ibrahimi[69] et al reviewed the application of amino acids and their derivatives as corrosion inhibitors for metallic alloy materials. Amino acids are one of the encouraging compounds which can be used as safe corrosion inhibitors and they are environmentally friendly, nontoxic, biodegradable and relatively cheap. Also, the development of computational modeling helps to understand the inhibition mechanism of those compounds and to develop the recently plannned inhibitors. Through the review, the ability of some amino acids to protect metal against corrosion through new systems like self-assembly monolayer (SAM) and smart coating systems has been studied. Kabanda[70] et al performed the quantum mechanical calculations and molecular dynamics studies of five amino acid derivatives which predict that amino acid derivatives

have a high tendency to interact with the metal surface by donating electrons through their amino groups and accepting electrons through their carboxylic group. Corrosion inhibition study of alkylamides derived from α-amino acids was investigated and the inhibitor efficiency displayed a relationship with an alkyl chain that increased in four carbon lengths, and observed an increase of 20% of inhibitor efficiency and also increase in toxicity[71].

Statistical modeling of the corrosion inhibition process by twenty-one pyridazine derivatives for mild steel in acidic medium was investigated by the QSR approach by Assiri[72] et al. The study reveals that PCR and ANN methods are relevant in comparison with the PLS model. Revathi[73] and Abraham studied the inhibition efficiency of propyl benzimidazole at different concentrations at various temperatures using PDP, EIS, adsorption and surface studies and basic computational calculations. Efficiency increases with concentration and shows an inverse relationship with protection efficiency and the adsorption studies obey the Langmuir adsorption isotherm except for all cases except for that in 1.5 HCl at 313K Temkin adsorption isotherm. The corrosion inhibition efficiency of mild steel in 0.25M HNO_3 by the benzimidazole bearing 1,3,4-oxadiazole derivative, 5-((2-propyl-1H-benzo[d]imidazol-1-yl)methyl)-1,3,4-oxadiazole-2-thiol (PBIMOT) have been studied by Rugmini[74] et al. Surface studies and quantum mechanical studies are also conducted.

Three 1,3,4-oxadiazole derivatives viz 5-((2-methl-1H-benzo[d]imidazol-1-yl) methyl)-1, 3, 4-oxadiazole-2-thiol (MBIMOT), 5-((2-ethyl-1H-benzo[d]imidazol-1-yl) methyl)-1, 3, 4-oxadiazole-2-thiol (EBIMOT) and 5-((2-propyl-1H-benzo[d]imidazol-1-yl) methyl)-1, 3, 4-oxadiazole-2-thiol (PBIMOT) have undergone corrosion study in sulphuric acid towards the mild steel[75]. Also, the inhibitive properties of the 4-(4-hydroxy-3-methoxybenzylidene amino)-4-H-1,2,4-triazole-3, 5-dimethanol, HMATD against mild steel in 0.5M HCl have been determined by weight loss measurements and electro analytical methods. Polarization studies suggest it to be a mixed type inhibitor by inhibiting both cathodic and anodic reactions. The metal surface obeys Langmuir adsorption isotherm was predicted by adsorption studies and various kinetic and thermodynamic parameters have been calculated from the adsorption studies[76].Anna[77] et al synthesized and studied the diffraction patterns, spectroscopic, electrochemical and antiproliferative activity of Ruthenium-Nitrosyl complexes with Glycine, L-Alanine, L-Valine,L- Proline, D-Proline, L-Serine,L-Threonine and L-Tyrosine.

Shainy[78] et al studied the interaction of inhibitor on the mild steel surface and corrosion inhibition efficiency of mild steel in HCl using a biomolecule, Pyoverdine, with the help of various methods, i.e.gravimetric, electrochemical impedance spectroscopy and polarization techniques at various temperatures. Surface morphology of the mild steel was done using SEM and AFM.

Murlidharan et al studied 3-methyl-2,6-diphenyl piperidin-4-one and 2- phenyl decahydro-quinoline-4-one as corrosion inhibitor for mild steel in acidic solutions and effect on hydrogen permeation by weight loss and various electrochemical methods and studies concluded that inhibitors act as cathodic inhibitor[79] . 1-aryl-2,5-Dithio-hydrazodicarbonamides and their triphenyltin and dibutyltin complexes were analyzed for corrosion inhibition in hydrochloric acid at 25°C by electrochemical polarization technique by Rastogi[80] et al. Nabel A. Negm[81] and co-workers synthesized some new hydrazine surfactants for inhibition of carbon steel alloys in acidic media .

The monoclinic crystal structure of the Co (II), Mn (II) and Fe (III) complexes with an asymmetric tetradentate Schiff base ligand derived from dehydroacetic acid, 4-methyl-*O-phenylenediamine* and salicylic aldehyde was predicted using the powder X-ray diffraction data[82].The crystallinity of the three novel quadridentate Schiff base complexes, [Cu(OIAC)Cl2], [Co(OIAC)Cl2] and [Ni(OIAC)Cl2] [OIAC, a Schiff base ligand: (([2-oxo-1H-indol-3-ylidene]amino)chitosan)] were analysed by X-ray diffraction technique and the studies reveals that the Schiff base (OIAC) has less crystallinity when compared to the complexes of chitosan[83]. Hishashi and Akito[84] determined the structural changes of chloride and bromide complexes, $[Ni(Et_2en)_2(H_2O)_2]Cl_2$ and $[Ni(Et_2en)_2]Br_2$ by X-ray and DSC studies. The transformation of the compounds

from an anhydrate state to a hydrous state and vice versa was studied and their structure confirmed by the powder XRD data.

Selwis[85] et al synthesized crystalline Co (II), Ni (II), Cu (II) and Zn (II) complexes and the patterns predict that Co(II) and Zn (II) complexes show isostructural crystallinity which is greater than that of Ni (II) and Cu (II) complexes. Padma Priya[86] et al proposed an octahedral geometry for the Ru(III) complexes on the basis of the X-ray study which also predicts that the complex crystallizes in an orthorhombic type of lattice with dimensions like a-1.104, b-1.245 and c-1.201 Å. The monoclinic crystal structure for the Cr (III) complexes with lattice parameters a = 4.6549, b = 8.2856, c = 5.0549, b = 90.626, a = g = 90 and volume = 194.95 have been calculated by using computer programme FullProf suite by Parveen Rathi[87] et al. The crystalline size of 29 nm suggesting the nanocrystalline nature of Pt (II) complexes of Schiff base ligands derived from 4-aminoantipyrine and a few substituted aldehydes was calculated using Scherrer's formula by Shiju[88] et al.

The crystalline nature of the Schiff bases derived from 2-nitrobenzaldehyde with amino acids (glycine, methionine) and their Co(II), Ni(II) and Cu(II) complexes were studied by Bibhesh[89] et al and the density and particle size of the metal complexes have been also estimated. The cubic symmetry for the Co(II) and Ni(II) complexes and hexagonal or tetragonal systems for Zn(II) complexes of the novel Schiff base ligand 2-((2-hydroxynaphthalen-1-yl)methylene)-N-(4-phenylthiazol-2-

yl)hydrazinecarboxamide was studied by Nagesh and Mruthyunjayaswamy[90].The powder XRD pattern of the Cu(II), Co(II), Ni(II) and Zn(II) complexes of the Schiff base ligand 2-(4-(dimethylamino)benzylidene)-N-(4-phenylthiazol-2-yl)hydrazinecarboxamide have been studied by Nagesh[91] et al. The Cu(II) and Co(II) belong to the hexagonal or tetragonal system, whereas the Zn(II) complex possesses cubic symmetry.

Ali[92] et al carried out the spectra thermal characterization of pyrazinamide metal complexes and their octahedral geometry is converted to tetrahedral during their thermal decomposition. The decomposition mechanism and the thermodynamic parameters of the decomposition steps are determined. Alothman[93] studied the different decomposition stages of the complexes and also the decomposition kinetics of these complexes using Coats-Redfern and Horowitz-Metzger methods. The high energy values obtained indicate the thermal rigidity of them. The thermal study of the [Cu (tmeda)(cinnamate)$_2$].7H_2O complex has been evaluated by Batool[94] with the help of thermogravimetric analysis and they also carried out their antimicrobial study. Thermal study of the Zn (II), Cd (II) and Hg (II) Complexes of Some *N*-Alkyl-*N*-Phenyl-Dithiocarbamates conducted using thermogravimetric analysis (TGA) and differential scanning calorimetry (DSC) by Damian[95] and co-workers.

The thermal studies of Co (II), Ni (II), Cu (II), Zn (II) and Pd (II) complexes of N^4-morpholinyl isatin-3-thiosemicarbazone have

been carried out by Sawaf [96] et al. These studies explained that the thermal stability of the investigated complexes is higher than their parent ligand. Sonabati[97] et al studied kinetic data of copper (II) with azo compounds of 5-amino-2-(aryldiazenyl) phenol using TG analysis. The calculated values of Ea, A, S*, H* and G* for the decomposition steps for ligands and their metal complexes are studied. The thermogravimetric method along with the Freeman-Carroll method was used for analyzing the thermal stability of the terpolymer ligand metal complexes and for the calculation of activation energy[98]. The thermal study of the mixed ligand derived from the condensation of Glutamic acid with the nitriloacetic acid and its Cu (II), Ni (II), Co (II) and Zn (II) complexes were conducted using TG-DTG calculations by Isamil[99] et al.

Different thermal methods have been employed to study the structural details of the organotin(IV) complexes of S –benzyl –β– N –(2-hydroxyphenyl) –methylen- dithiocarbazate (L 1), S – benzyl –β–N –(benzoylphenyl) –methylendithiocarbazate (L 2), N –methyl - S –benzyl –β–N –(2-hydroxylphenylethylidene) – dithiocarbazate (L 3) ligands in the nitrogen atmosphere by Deo[100].Mandour[101] et al analysed the chemical structures of the copper complex of the novel azo ligand (L) Bis-(1,5- dimethyl-4-[(E)-(3- Methyl phenyl)diazenyl]-2- phenyl-1,2-dihydro-3H-pyrazol-3-one) using TG-DTG curves. The complex started to decompose from the 222-324°C range and the decomposition ended in the 683-820°C range. The various steps involved and the decomposed

products were explained using the TG-DTG curve. The mechanism for the thermal decomposition has also been represented in the study.The structural characterization of diorganotin complexes of Schiff base derived from 4-(diethylamino) salicylaldehyde and L-tyrosine was carried out by Lexing[102] et al.

A series of publications reports on the catalytic activity of transition metal complexes on dye degradation have been reported. Oxidative and hydrolytic DNA cleavage by Cu(II) complexes of salicylidene tyrosine and 1,10 phenanthroline(1) or 2,2'bipyridine (2) was studied by Reddy[103] et al and the catalytic ability follows the order: 1>2. The theoretical models of the electronic and molecular structures of asparagine, aspartic acid, glutamine and glutamic acid were established and the results can be used to predict the direction of the inhibition reactions and the sites for nucleophilic/electrophilic attacks. From the results Eddy[104] reveals that the sites for nucleophilic attacks in aspartic acid glutamine are at the nitrogen atom but at the carbon atom for asparagine and glutamic acid. The sites for electrophilic attacks are at the oxygen atom, carbon atom, oxygen atom and nitrogen atom. Laila[105] et al synthesized azomethine amino ligands derived from condensation of 3-methoxysalicylaldehyde (MS) or 4-diethylamino salicylaldehyde (DS) with α-amino acids (L-phenylalanine (P) and DL-tryptophan (T)) and characterized using the elemental analysis, infrared spectra, ultraviolet-visible and thermal analysis (TGA) in dynamic air atmosphere. Biological analysis of the compounds and

interaction of the complexes with CT-DNA was monitored using spectral studies.

The experimental charge densities for $(C_5H_5)Mn(CO)_3$, $(\eta^6\text{-}C_6H_6)Cr(CO)_3$, and $(E)\text{-}\{(\eta^5\text{-}C_5H_4)\text{-}CF{=}CF(\eta^5\text{-}C_5H_4)\}(\eta^5\text{-}C_5H_5)_2Fe_2$ were studied with the help of the quantum theory of atoms in molecules (QTAIM) by Farugia[107] et al. DFT studies of Fe, Co, Ni, or Zn metal complexes of tetradendate ligand 1,5-bis(2-pyridylmethyl)-1,5-diazacyclooctane (L^8py_2) conducted by Fox[108] et al reveal that the Co(II) and Zn(II) thioethers exhibit weaker M-S bonding than Ni(II). TDDFT studies of the unsymmetrical tetradentate Schiff base complexes have been analysed by Julieta[109] and Co-workers. Masahiro[110] et al conducted the theoretical analysis of the L-alanine and L-homocysteine- Cu(II) complexes at different pHs depending on the formation mechanism.

DFT calculations of the two dinuclear Ni (II) complexes of (2-[1-(3-methylamino-propylimino)-ethyl]-phenol) have been studied[111]. A combined experimental and theoretical study of the chiral Schiff base copper catalyst has been conducted by Bania[112] et al. Rosa[113] et al carried out the theoretical study of the coelenteramide-containing fluorescent proteins. Yuan[114] et al conducted the DFT studies to study the selectivity and sensitivity of a triazole-Schiff base, 4-(5-Chloro-2-hydroxybenzylidene amino)-1H-1, 2, 4-triazole-5(4H)-thione towards Zn^{2+} over Cd^{2+} using the fluorescence spectrometry. Theoretical study of electrophilic versus nucleophilic character of transition metal complexes of

phosphinidene has been carried out by Frison[115] et al at the DFT levels. The metal complexes of glipizide were synthesized; characterization and metal percent was determined with AAS[116] .The study of unusual behaviour of the actinide elements which are short-lived and scarce is highlighted by Korey and Co-workers[117].

The photocatalytic degradation of methylene blue by cobalt–beta hydroxyl benzoate complexes was studied by sangeetha[118] et al and the results show that Co-bhb act as an excellent catalyst.The application of cobalt bicarbonate complexes in elimination of organic pollutants was studied by Aihua[119] and co-workers. Thermal and kinetic studies of the transition metal complexes of some thiosemicarbazones have been reported[120]. West and his co-workers also reported a number of transition metal complexes of thiosemicarbazones[121-127]. R.Reddy[128] et al investigated the mixed ligand complexes of Ni(II) with uridine and amino acids ,L-alanine,L-phenylalanine and L-tryptophan. Jamuna[129] et al studied the antibacterial activity of the transition metal complexes of Schiff base derived from 5-methyl-2- thiophene carboxaldehyde and 4-amino-3-hydroxy benzoic acid. The study reveals that these metal complexes are effective against E. faicalis and S. aureus. The antibacterial activity of Schiff bases derived from 4-(diethylamino)-2-hydroxybenzaldehyde and 4-nitrobenzohydrazide and their transition metal complexes were studied by Charity[130] and co-workers. The results shows that the compounds except Mn(acac) complex are inefficient against the gram +ve bacteria.

The thermal behaviour and kinetics of dihydrobis(2-mercaptobenzothiazolyl)borate and their various transition metal complexes(Co(II), Ni(II) and Cu(II)) were studied by ahmad[131] et al. The corrosion inhibition efficiency of N-cetyl-3-(2-methoxycarbonylvinyl)pyridinium bromide for X70 steel in 5M HCl is investigated by gravimetric and electrochemical methods. The inhibitive action of compounds was confirmed by the theoretical calculations done by quantum chemical and molecular dynamics simulation methods[132].

Francis K. Ngounoue[133] et al prepared a series of Schiff base transition metal complexes by using, 4-hydroxypent-3-en-2-ylideneaminophenol as ligand. The spectroscopic studies using IR, UV, elemental analysis and conductivity proves that the obtained Schiff base ligand acts as a tridentate ligand and the metal complexes of Fe(III), Mn(II) and Co(II) showed the tetrahedral geometry. Antibacterial studies of the prepared metal complexes have shown more potency against four strains of bacteria and four strains of fungus as compare to Schiff ligands. The Schiff base ligand and its transition metal complex have also showed fantastic free scavenging property on comparison with garlic acid. Gajendra Kumar[134] et al reported the synthesis and characterization and antimicrobial activity of noval Schiff base and its transition metal complexes (Cu, Ni and Co) from 2-amino-4-ethyl-5-hydroxybenzaldehyde and thiocarbohydrazide.

Vatsala Pawar[135] et al synthesized a oxovanadium complex of Schiff base formed by condensation of acetyl acetone with semicarbazide hydrochloride and thiosemicarbazide in methanol. The prepared Schiff base and its metal complex was screened for the inhibiting activities against various strains of bacteria like Bacillus licheniformis, Eschericha coli and Micrococcus luteus and were compared with standard antibiotics. The results show that all compounds exhibit strong to moderate activity. Cobalt complex of Schiff base derived from acetyl acetone and leucine undergone antifungal studies by Mohammed[136] and his co-workers. The cobalt complex shows better efficiency compared to its parent ligand. Sharda D Dakore[137] et al obtained a new Schiff base on condensation of 4-aminoantipyrine, 2-furan carboxaldehyde and acetylacetone. After that noval Schiff base complexes of N2O2 type have been synthesized by using chlorides of transition metals like Co(II), Ni(II), Cu(II), Zn(II). The metal complexes were prepared by non template methods by using triethylamine as a catalyst. The complexes were characterized by IR, NMR, EPR spectroscopy, magnetic moment, conductance, thermal analysis (TGA and DTA) and powered X-Ray (XRD) analysis. Square planar structure was confirmed from the magnetic moment values. Moderate activity was observed for Schiff base metal complexes against various strains of microbes like Staphylococcus typhus, Staphylococcus aureus, Escherichia coli, Bacillus subtilis.

Mojtaba[138] et al carried out the catalytic study of the oxo-diperoxo tungsten(VI) complex, and they found to be an excellent catalyst for the selective oxidation of sulfide to sulfoxide. R.A.Ahmadi and S.Amani[139] prepared azo group containing Schiff base ligand such as 1-{3-[(3-hydroxypropylimino)methyl]-4-hydroxyphenylazo}-4-nitrobenzene (2a), 1-{3-[(3-hydroxypropylimino)methyl]-4-hydroxyphenylazo}-2-chloro-4-nitrobenzene (2b) and 1-{3-[(3-hydroxypropylimino)methyl]-4-hydroxyphenylazo}-4-chloro-3-nitrobenzene (2c) and their Cu(II) and Co(II) complexes. They have been characterised using FTIR UV, ^{13}C- and ^{1}H-NMR spectroscopic techniques and TG analysis. Banzod[140] derived a novel Schiff base ligand from terephthaladehyde and isoniazid and their metal complexes. The prepared compounds were analyzed by using elemental analyses, IR and electronic spectra, magnetic moment measurements and thermogravimetric analysis. The kinetic parameters calculated from the thermal data by both Coats-Redfern and Broido equations. Y.Boughoues[141] et al synthesized new amine derivatives namely 2-[(phenylamino)methyl]phenol, 2-{[(4-hydroxyphenyl)amino]methyl}phenol, 2-[(2-hydroxybenzyl) amino]benzonitrile and 2-{[(3-chlorophenyl) amino]methyl}phenol and their corrosion inhibition efficiency was studied by means of electrochemical measurements and morphological studies. The theoretical confirmation of the outcome is done with the assistance of techniques such as Density functional theory and molecular dynamics simulation.

S D Dakore[142] et al prepared a new Schiff base from 4-amino antipyrine, 2-thiophene carboxaldehyde and acetyl acetone. After that Schiff bases complexes of N_2O_2 type have been prepared by using various transition metals like Co(II), Cu(II), Ni(II) and Zn(II). The metal complexes were characterized by various methods like IR, NMR, EPR spectroscopy, magnetic moment, conductance, thermal analysis (TGA and DTA) and powered X-ray (XRD) analysis. The compounds undergone antimicrobial studies against various strains of microbes like Staphylococcus typhi, Staphylococcus aureus, Escherichia coli and Bacillus subtilis. The results shows that Cu(II) and Zn(II) complexes were found to be moderately active against Cu(II) and Zn(II) complexes were moderately active against all strains of bacteria.M.B.Fugu[143] et al reacted alcoholic solution of vanillin with 2-aminophenol to synthesize a new Schiff base. Using different salts of transition metals different transition metal complexes of the prepared Schiff base have been synthesized and charcterised by various methods like microanalysis, conductivity, solubility and spectral studies. The antimicrobial screening of metal complexes against various strains of bacteria like E. coli, S. typhi, Klebsiella pneummiae were conducted. The results have concluded that some of the complexes were active against the microoraganisms.

K.R.Patel[144] et al studied the thermal stability of the metal complexes of the Schiff base derived from heterocyclic compound and its kinetic parameters such as energy of activation (Ea), enthalpy (ΔH#), entropy (ΔS#) and Gibbs energy (ΔG#), were calculated from the TGA data. The catalytic degradation study of

Silver and Magnetite Nanoparticles Functionalized with a Poly(ionic liquid) based on Quaternized Dialkylethanolamine with 2-Acrylamido-2- methylpropane Sulfonate-co-Vinylpyrrolidone was conducted by A.M.Atta[145] et al. Using the kinetic study, various kinetic parameters such as activation energy, enthalpy, and entropy have been calculated. R.Joshy[146] et al synthesized the triorganotin(IV) complexes of Schiff base (E)-4-amino-3-(2-(4-hydroxybenzylidene)hydrazinyl)- 1H-1,2,4-triazole-5(4H)-thione (HL), and the antifungal activity were tested and the results were validated by in silico molecular docking studies.

Hossain Mohammad Zakir[147] et al derived a Schiff base by the condensation of benzoin thiosemicarbazone from benzoin and thiosemicarbazone. Their Co(II) and Ni(II) complexes were synthesized and their characterization was done with the aid of elemental analysis and IR spectra. These complexes have undergone antibacterial study by the disc diffusion technique. The Cobalt complex exhibits higher inhibition efficiency when compared to that of its parent ligand and its nickel complex. Rekha Nalawade[148] et al prepared a thiocarbohydrazide derivative named N'',N''- bis[(E)-4- Fluorophenyl)methylidine]thiocarbonhydrazide by the condensation between thiocarbohydrazide and p- fluoro benzaldehyde in ethanol medium. The complexes were characterized by elemental analysis, UV-Visible, IR and NMR spectroscopic techniques. The antimicrobial screening of the synthesized compounds have been carried out and the study reported that the prepared compound act as an efficient antimicrobial agent.

Few macrocyclic transition metal complexes have been reported by the [2+2] condensation of thiocarbohydrazide and isatin in presence of trivalent transition metal salts by D.P. Singh[149] and his co-workers. A five coordinate square pyramidal geometry was confirmed for the complexes which were confirmed by the assistance of elemental analysis, conductance measurements, magnetic measurements and mass spectral studies. The compounds were undergone antimicrobial studies against various strains of bacteria viz. Staphylococcus aureus, Bacillus subtilis, Escherichia coli, Pseudomonas aeruginosa and selected fungal strains i.e. Aspergillus niger, Aspergillus flavus (molds), Candida albicans, Saccharmyces cerevisiae (yeasts). Dharam Pal Singh[150] et al synthesized a series of new Schiff base metal complexes from a tetradentate macrocyclic ligand. The Schiff base ligand was prepared by reaction between dibenzoyl and dithiocarbohydrazide and also their transition metal complexes were prepared by template synthesis method. The structure of the compounds were determined by many elemental analysis, conductance measurements, molecular weight determinations, magnetic measurements and various spectral method such as electronic, NMR, Infrared and Far infrared spectra. The five coordinated square pyramidal geometry was suggested for all the complexes by the electronic spectra along with magnetic moments.

1.2. Objectives and Scope of the investigation

The motive of the research is the high potential of Diphenyl Glycolic acid and its derivatives in various disciplines, such as pharmacology, corrosion chemistry, NBO study and many other

analytical applications. The extensive literature survey on the amino acid metal complexes revealed that the scope of the amino acid metal complexes with Diphenyl Glycolic acid is yet to be studied. An amino acid metal complex on condensation with Diphenyl Glycolic acid is not so far reported. Evidence shows that such ligands have plenty of opportunities in biological activities viz, antifungal, antibacterial, antiviral and antitumour etc.

The objectives of our study consist of the following lessons:

I. To synthesize and characterize the Dipheny glycolic acid - amino acids (Tyrosine, Glycine, Valine, Leucine and Histidine) ligands and their transition metal complexes. The condensation of the Dipheny glycolic acid -amino acid has been visible by the clear color change of the solution and they crystallized out of the solution.

II. To accomplish the Thermogravimetric analysis of some of the ligands and their complexes

III. To accomplish the powder X-ray diffraction studies of some of the ligands and their complexes.

IV. To carry out the corrosion inhibition study of the prepared ligands.

V. To perform in vitro antifungal screening of the selected ligands and complexes.

VI. To conduct the catalytic study of the selected complexes of ligands.

VII. To carry out DFT studies of all the ligands.

References:

1. Bharti, N., Maurya, M. R., Naqvi, F., & Azam, A. (2000). *Bioorg. Med. Chem. Lett.*, *10*(20), 2243.
2. Johnson, D. K., Murphy, T. B., Rose, N. J., Goodwin, W. H., & Pickart, L. (1982). *Inorg. Chim.Acta*, 67,159.
3. El-Shahawi, M.S. (1991). *Anal. Sci*., 7, 443.
4. Mishra, A. P., Srivastava, S. K., & Srivastava, V. (1996). *J. Indian Chem. Soc*., 73, 261.
5. Dhar, D. N., & Taploo, C. L. (1982). *J.Sci. Ind.Res*. 41, 501.
6. Quiroga, A. G., Perez, J. M., Montero, E. I., West, D. X., AIonso, C. & Ranninger, C. N. (1999). *J.lnorg. Biochem*., 75, 293.
7. French, F. A., & BIanz Jr, E. J. (1966). *J.Med.Chem*., 9, 585.
8. Dobek, A. S., Klayman, D. L., Dickson Jr, E. T., Scovill, J. P., & Tramont, E. C. (1980). *Antimicrob. Agents Chemother.*,18, 27.
9. Klayman, D. L., Lin, A. J., McCall, J. W., Wang, S. Y., Townson, S., Grogl, M., & Kinnamon, K. E. (1991). *J.Med Chem*., 34, 1422.
10. Shipman Jr, C. , Smith, S. H., Drach, J.C.& Klayman, D.L. (1986). *Antiviral Res*., 6, 197.
11. Parashar, R. K., Sharma, R. C. & Mohan, G., (1989). *Biol. Trace Elem. Res*., 23, 145.
12. Gaowen, Y., Xiaping, X., Huan, T. & Chenxue, Z. (1995). *Chem. Abstr.*, 123, 101089.
13. Sahare, A.B. & Mohod, R.B. (2020). *Rasayan J. Chem.*, 13,647.
14. Al-Amery, M. H., (2012). *Iraqi J. Sci*., 53, 704.
15. Haddad, R., Yousif, E. & Ahmed, A., (2013). *SpringerPlus*, 2, 1.
16. Sebastian, M., Arun, V., Robinson, P. P., Varghese, A. A., Abraham, R., Suresh, E. & Yusuff, K. M. (2010). *Polyhedron*,29, 3014.
17. Carballo, R., Covelo, B., Fernández-Hermida, N., Lago, A. B., & Vázquez-López, E. M. (2009). *J. Mol. Struct., 936*, 87.

18. Baranwal, B. P., Das, S. S., & Singh, P. (1998). *Synth. React. Inorg. Met.-Org. Chem.,28*, 1689.

19. Sudha, R., Charles, C. K., & Nithya, G., (2015). *Int. J. ChemTech Res*., 8, 383.

20. Qiu, Y., Wang, K., Liu, Y., Deng, H., Sun, F., & Cai, Y. (2007). *Inorganica Chim. Acta*, *360*, 1819.

21. Carballo, R., Covelo, B., Fernández-Hermida, N., Lago, A. B., & Vázquez López, E. M., (2011). *J. Chem. Crystallogr*., *41*, 1949.

22. Indiradevi, G. (2019). *IJEEFUS*, 1, 71.

23. Indiradevi, G., Pranamya, N. P., & Ali Hassan, M. (2019). *WJPLS*, 5, 71.

24. Issa, Y.M. , Waheed, F.,.Hussein, A. A., & Issa, R.M. (1995). *Transit. Met. Chem*., 5, 423.

25. Singh, M., & Singh, A. (1979). *J. Indian Chem. Soc*., 56, 1249.

26. Mahmaud, M.J., Redha, I.B.., Shaimaa, A.S. & Ismael, Y.M. (2013). *IHJPAS*, 26.

27. Vimala, J.F., Lawrance, M. & Prakash, J.T.J. (2011). *Elixir Crystal Growth*, 41, 5664.

28. Mohammed, S.J., & Zubair, F.G. (2017). *Open Access Journal of Chemistry*, 1, 1.

29. Rozario, M.J. & Merina, J. (2016). *IJSR*, 5(8), 164.

30. Rozario, M. J. & Merina, J. (2016). *IJSR*, 5(7),164.

31. Buehler, C. A., Smith, H. D., Glenn, D. M., & Tal ah K V. (1958). *I. Ory Chem.,* 23, 1432.

32. Mentasti, E. (1979). *Inorg. Chem.*, 18, 6.

33. Cicek, V., Ozdemir M. & Apblett, A.W., (2013). *Int. J. Chem.*, 5, 1916.

34. Baranwal, B. P., Fatma, T. & Varma, A. (2009). *J. Mol. Struct*., 920, 472.

35. Mohammed,S. J. & Zuhair, F. G. (2017*). IJRRR*, 10, 19.

36. Mahmoud, M. J., Redha, I. B., Shaimaa, A. S. & Ismaeel, Y. M. (2013). *Ibn Al-Haitham Jour. for Pure & Appl. Sci.,* 26, 1.

37. Pines, M. (1991). The Structures of Life: Discovering the Molecular Shapes that determine Health or Disease, National Institute of General Medical Sciences.

38. El- Ajaily, M. M., Abdlseed, F. A. & Ben-Gweirif, S., (2007). *E-Journal of Chemistry*, 4, 461.

39. Chohan, Z. H., Arif, M., Akhtar, M. A. & Supuran, C. T., (2006). *Bioinorg. Chem. Appl*, 2006.

40. Yousif, E., Majeed, A., Khulood, Al-Sammarrae, K., Salih, N., Salimon, J., & Abdullah, B. (2017). *Arab.J.Chem.*, 10, 1639.

41. Aiello, D., Furia, E., Siciliano, C., Bongiorno, D & Napoli, A., (2018). *J. Mol. Liq. ,* 269, 387.

42. Neelakantan, M.A., Rusalraj, F., Dharmaraja, J., Johnsonraja, S., Jeyakumar, T. & Pillai, M.S. (2008). *Spectrochim Acta*, 71, 1599.

43. Raman, N., Kulandaisamy, A., Shanmugasundaram, A. &Jeyasubramanian, K. (2001).*Trans Met Chem.*, 26, 131.

44. Prashanthi, Y., Kiranmai, K., Subhashini, NJP. & Shivaraj, S., (2008). *Spectrochim Acta*, 70, 30.

45. Singh, R.V., Swaroop,R. & Gupta, N., (1997). *Main Group Met Chem.*, 20, 387.

46. Cukurovali, A., Yilmaz, I. Ozmen, H. & Ahmedzade, M. (2002). *Trans Met Chem*., 27, 171.

47. Santhi, S. &Radhakrishnan Namboori, C. G., (2013). *Int J ChemTech Res*., 5, 1750.

48. Kumar, G., Devi, S., Johari, R. & Kumar, D., (2012). *Eur J Med Chem.*, 52, 269.

49. Panchal, P. K. & Patel, M. N. (2004). *Synth. React. Inorg. Met. Org. Chem.*, 34, 1277.

50. Shaker, A. M., Nassr, L. A., Adam, M. S. & Mohamed, I. M. (2013). *J Korean Chem Soc.*, 5, 560.

51. Ahmed, N., Riaz, M., Ahmed, A., & Bhagat, M. (2015). *Int. J. Inorg. Chem.*

52. Pervaiz, M., Ahmad, I., Yousaf, M., Kirn, S., Munawar, A., Saeed, Z., Adnan, A., Gulzar, T., Kamal, T., Ahmad, A., &

Rashid, A. (2019). *Spectrochim Acta A: Mol Biomol Spectrosc.*, 206, 642.

53. Zemede, Y. B., & Kumar, A. (2014). *Int. J. ChemTech Res.*, 7, 279.

54. Bhattacharjee, J., (2016), *IRJIMS*, 2, 07.

55. Strasak, M. & Majer, J. (1983). *Inorganica Chim. Acta*, 70, 231.

56. Taha, M., Khan, I. & Coutinho, J. A., (2016). *J. Inorg Biochem.*,157, 25.

57. Soliman, A. A., & Mohamed, G. G. (2004).*Thermochim. Acta*, 421, 153.

58. Abdel-Rahman, L. H., El-Khatib, R. M., Nassr, L. A., Abu-Dief, A. M. and Lashin, F.E.D. (2013). *Spectrochim Acta A: Mol Biomol Spectrosc.*,111, 266.

59. Adam, M. S. S., Youssef, M. M., Aboelghar, M. F., Hafez A. M. & El- Ayaan, U. (2017). *Appl Organomet. Chem.*, 31, 3650.

60. Ma, Z., Wang, Q., CBA Alegria, E., C. Guedes da Silva, M. F., MDRS Martins, L., Telo, J. P. & JL Pombeiro, A. (2019). *Catalysts*, 9, 424.

61. Chai, H., Cao, Q., Dornan, L. M., Hughes, N. L., Brown, C. L., Nockemann, P. & Muldoon, M. (2017). J., *Eur. J. Inorg. Chem.*, 2017, 5604.

62. Rahmani, A., Rahmani, H. & Zonouzi, A., (2020). *Mater. Today Commun.*, 25, 101304.

63. Valodkar, V.B., Tembe, G.L., Ravindranathan, M., Ram R.N., & Rama, H.S. (2004). *J. Mol. Catal. A: Chem*., 208, 21.

64. El-Ghamry, H., El-Sharkawy. R., & Gaber, M. (2014). *J. Iran Chem Soc*., 11,379.

65. El-Lateef, H. M. A., Adam, M. S. S., & Khalaf, M. M. (2018). *J. Taiwan Inst. Chem. Eng.*, 88, 286

66. Zhou, Y. H., Wang, S. Q., Chen, L. Q., Gong, D. Y., Ni, P., & Cheng, Y. (2017). *Transit Met Chem.*, 42, 175.

67. Adam, M. S. S., El-Lateef, H. M. A., & Soliman, K. A. (2018). *J. Mol. Liq.*, 250, 307.

68. Adam, M. S. S., & Mohamad, A. D.M., (2018). *Polyhedron*, 151, 118.

69. El Ibrahimi, B., Jmiai, A., Bazzi. L.& El Issami, S. (2020). *Arab. J. Chem.*, 13, 740.

70. Kabanda, M. M., Obot,I. B., & Ebenso, E. E., (2013). *Int. J. Electrochem. Sci.*, 8, 10839.

71. Olivares-Xometl, O., Likhanova, N.V., Domınguez- Aguilar, M.A., Arce, E., Dorantes, H. & Arellanes-Lozada, P., (2008). *Mater. Chem. Phys.*, 110, 344.

72. Assiri, H., Driouch, M., Lazrak, J., Bensouda, Z., Elhaloui, A., Sfaira, M., Saffaj, T., & Taleb, M. (2020). *Heliyon*, 6.

73. Mohan, R., & Joseph, A. (2018). *Egypt. J. Pet.*, 27, 11.

74. Ammal, P. R., Prajila, M. & Joseph, A., (2017). *J Bio Tribo Corros.*, 3, 47.

75. Ammal, P. R., Prajila, M. & Joseph, A., (2018). *J. Environ. Chem. Eng.*, 6, 1072.

76. Ammal, P. R., Prajila. M., & Joseph, A. (2018). *Egypt. J. Pet.*, 27, 307.

77. Rathgeb. A., Bohm, A., Novak, M. S., Gavriluta, A., Do□mo□to□r, O., Tommasino, J. B., & Arion, V. B. (2014). *Inorg. Chem.*, 53, 2718.

78. Shainy, K. M., Ammal, P. R., Unni, K. N., Benjamin, S., & Joseph,A. (2016). *J Bio Tribo Corros.*, 2, 20.

79. Muralidharan, S., Chandrasekar, R., & Iyer, S. V. K. (2000). *J. Chem. Sci.*, 112, 127.

80. Singh, M. M., Rastogi, R. B., Upadhyay, B. N., & Yadav, M., *Mater. Chem. Phys.*, 80, 283(2003).

81. Negm, N. A., Kandile, N. G., Badr, E. A. & Mohammed, M. A., (2012). *Corros. Sci.*, 65, 94.

82. Munde, A. S., Jagdale, A. N., Jadhav, S. M. & Chondhekar, T. K. (2010). *J. Serb. Chem. Soc., 75*, 349.

83. Antony, R., David, S. T., Saravanan, K. Karuppasamy, K., & Balakumar, S. (2013). *Spectrochim Acta A: Mol Biomol Spectrosc.*,103, 423.

84. Konaka, H., & Sasaki, A. (2020). *Crystals*, 10, 106.

85. Joseyphus, R. S., Dhanaraj, C. J., & Nair, M. S. (2006). *Trans. Met. Chem.*, 31, 699.

86. Priya, N. P., Arunachalam, S., Manimaran, A., Muthupriya, D., & Jayabalakrishnan, C. (2009). *Spectrochim Acta A: Mol Biomol Spectrosc.*, 72, 670.

87. Rathi, P., Singh, D. P. & Surain, P., (2015). *C. R. Chimie*, 18, 430.

88. Shiju, C., Arish, D., Bhuvanesh, N. & Kumaresan, S. (2015). *Spectrochim Acta A: Mol Biomol Spectrosc.*, 145, 213.

89. Singh, B. K., Rajour, H. K., & Prakash, A. (2012). *Spectrochim Acta A: Mol Biomol Spectrosc.*, 94, 143.

90. Nagesh, G.Y., & Mruthyunjayaswamy, B.H.M. (2015). *J. Mol. Struct.*, 1085, 198.

91. Nagesh, G.Y., Raj, K. M., & Mruthyunjayaswamy, B.H.M. (2015). *J. Mol. Struct.*, 1079, 423.

92. Ali, A. E., Elasala, G. S., Mohamed, E. A., Kolkaila, S. A. (2019). *Heliyon*, 5.

93. Alothman, A. A., Albaqami, M. D., & Alshgari, R. A. (2021). *J. Mol. Struct.*, 1223, 128984.

94. Batool, S. S., Gilani, S. R., Zainab, S. S., Tahir, M. N., Harrison, W. T., Haider, M. S., & Shoaib, M., (2020). *Polyhedron*, 178, 114346.

95. Onwudiwe, D. C., & Ajibade, P. A. (2012). *Int. J. Mol. Sci.*, *13*, 9502.

96. El-Sawaf, A. K., El-Essawy, F., Nassar, A. A., & El-Samanody, E. S. A., (2018). *J. Mol. Struct.*,1157, 381.

97. El-Sonbati, A.Z., Diab, M.A., El-Bindary, A.A., Shoair, A.F., Hussein, M.A., & El-Boz, R.A., (2017). *J. Mol. Struct*, 1141, 186.

98. Gurnule, W. B., Rathod, Y. U., Belsare, A. D., & Das, N. C. (2020). *Mater. Today*: Proc., 29, 1044.

99. Isamil, E. H., AlBlewi, F. F., Soliman. N., & Khalil, M. M. H. (2016). *J Therm Anal Calorim*., 125, 289.

100. Kumar, D. N. (2021). *J. Mol. Struct.*, 1227, 129569.

101. Mandour, H. S., Abouel- Enein, S. A., Morsi, R. M. M. & Khorshed, L. A., (2021). *J. Mol. Struct.*,1225, 129159.

102. Chen, L., Wang, L., An, W., Wang, R. & Tian, L. (2020). *Inorg. Nano-Met. Chem.*, 50, 872.

103. Reddy, P. R. & Shilpa, A. (2011). *Polyhedron*, 30, 565.

104. Eddy, N. O. (2010). *Molecular Simulation*, 36, 354.

105. Rahman, L. H. A., Abu-Dief, A. M., Hashem, N. A., & Seleem, A. A. (2015). *Int. J. Nano. Chem.*, 1, 79.

106. Dostani, M., Kianfar, A. H., Mahmood, W. A. K., Dinari, M., Farrokhpour, H., Sabzalian, M. R., & Azarian, M. H. (2017). *Spectrochim Acta A: Mol Biomol Spectrosc.*, 180, 144.

107. Farrugia, L. J., Evans, C., Lentz, D., & Roemer, M. (2009). *J. Am. Chem. Soc*., *131*, 1251.

108. Fox, D. C., Fiedler, A. T., Halfen, H. L., Brunold, T. C., & Halfen, J. A. (2004). *J. Am. Chem. Soc*., 126, 7627.

109. Gradinaru, J., Forni, A., Druta, V., Tessore, F., Zecchin, S., Quici, S., & Garbalau, N., (2007). *Inorg. Chem.*, 46, 884.

110. Kunimoto, M., Sadaoka, Y., Nakanishi, T., Osaka. T., & Homma, T. (2016). *J. Phys. Chem.*, 120, 15722.

111. Naiya, S., Drew, M.G., Estarellas, C., Frontera, A., & Ghosh, A. (2010). *Inorganica Chim. Acta*, 363, 3904.

112. Bania, K. K., Karunakar, G. V., Sarma, B., & Deka, R. C. (2014). *ChemPlusChem*, 79, 427.

113. Alieva, R. R., Tomilin, F. N., Kuzubov, A. A., Ovchinnikov, S.G. & Kudryasheva, N. S. (2016). *J. Photochem. Photobiol B,* 162, 318.

114. Yuan, C., Liu, X., Wu, Y., Lu, L., & Zhu, M. (2016). *Spectrochim Acta A: Mol Biomol Spectrosc.*,154, 215.

115. Frison, G., Mathey, F., & Sevin, A. (1998). *J. Organomet. Chem.*, 570, 225.

116. Ali, H. R., Saleh, G. A., Hussein, S. A., & Hassan, A. I. (2013). *Der Pharma Chem.*, 5, 156.

117. Carter, K. P., Shield, K. M., Smith, K. F., Jones, Z. R., Wacker, J. N., Arnedo-Sanchez, L. & Abergel, R. J. (2021). *Nature*, 590, 85.

118. Sangeetha, S., Krishnamurthy, G. & Raghavan, M. S. (2019). *Mater. Sci. Semicond. Process.*, 101, 164.

119. Xu, A., Li, X., Ye, S., Yin, G., & Zeng, Q. (2011). *Appl.Catal. B: Environ.*,102, 37.

120. Jadhav, V.A., & Vandre, A.G. (1995). *J. Indian Chem. Soc*., 72, 747.

121. El-Saied, F.A., El-Asmy, A.A., Kaminsky, W., & West, D.X. (2003). *Transition Met. Chem*., 28, 954.

122. Swearingen, J.K., Kaminsky, W., & West, D.X. (2002).*Transition Met. Chem.*, 27, 724.

123. Swearingen, J.K., & West, D.X., (2000). *Transition Met. Chem.*, 25, 241.

124. West, D.X., Swearingen, J.K., & El-Sawaf, A.K. (2000). *Transition Met. Chem.*, 25, 80.

125. West, D.X., Beraldo, H., Nassar, A.A., EI-Saied, F.A., & Ayad, M.I. (1999). *Transition Met. Chem*., 24, 421.

126. Ackerman, L.J.,Webb, J.W. & West, D.X. (1999). *Transition Met. Chem*., 24, 558.

127. El-Sawaf, A.K., West, D.X., EI-Saied, F.A., & El-Bahnasawy, R.M. (1998). *Transition Met. Chem*., 23, 649.

128. Reddy, P. R., & Reddy, A. M. (2000). *Chem.Sci.J.*,112, 593.

129. Jamuna, K., Naik, B. R., Sreenu, B., & Seshaiah, K., (2012). *J. Chem. Pharm. Res.*, 4, 4275.

130. Dikio, C. W., Ejidike, I.P., Mtunzi, F. M., Klink, M. J., & Dikio, E. D. (2017). *Int J Pharma Sci.*, 9, 257.

131. Ahmad, N., Alam, M., Kumar, P., Hashmi, A. A., & Wahab, R. (2013). *Asian J. Chem*., 25, 10386.

132. Xia, G., Jiang, X., Zhou, L., Liao, Y., Duan, M., Wang, H., Pu, Q. & Zhou, J. (2015). *Corros. Sci.*, 94, 224.

133. Ngounoue, F. K., Mainsah, E. N., Conde, A. M., Paboudam, A. G., Ntum, S. E., Ndamukong, W.K., Vanessa, C. M., & Ndifon, P. T. (2015). *Der Pharma Chemica*, 7(5), 101.

134. Kumar, G., Kumar, A., Shishodia, N., Garg, Y.P., & Yadav, B.P. (2011). *J. Chem*., 8, 1872.

135. Pawar, V., Joshi, S., & Uma, V. (2011). *Biokemistri*., 23, 21.

136. Mohammed, A. S., Abubakar, F., & Aye, A. E., (2017). *J. Appl. Chem*., 10, 68.

137. Dakore, S. D., Kamble, V., & Bisal, P. (2017). *J. Chem Studies*, 5, 110.

138. Bagherzadeh, M., Esmailpour, P., Abbasi, A., Akbari, A., & Amini, M. (2018). *J. Coord. Chem*, 71, 3405.

139. Ahmadi, R. A., & Amani, S. (2012). *Molecules*,17, 6434.

140. Bansod, A. D. (2021). *International Journal of Scientific Development and Research*,, 6, 226.

141. Boughoues, Y., Benamira, M., Messaadia, L., Bouider, N. & Abdelaziz, S. (2020). *RSC Adv*., 10, 24145.

142. Dakore, S. D., & Kamble. V. T. (2016). *JOCPR*, 8, 211.

143. Fugu, M. B., Ndahi, N. P., Paul, B. B., & Mustapha, A. N. (2013). *J. Chem. Pharm. Re*., 5, 22.

144. Patel, K. R., Patel, D.,& Patel, A. (2013). *Indian J. Appl. Res.*, 3.

145. Atta, A.M., Moustafa, Y. M., Al-Lohedan, H. A., Ezzat, A. O., & Hashem, A. I. (2020). *ACS Omega*, 5, 2829.

146. Joshi, R., Kumari, A., Singh, K., Mishra, H., & Pokhari, S. (2020). *J. Mol. Struct*, 1206, 127639.

147. Hossain, M., Mele, J., & Shaikh, M. M. A. (2016). *Asian J. Med. Pharm. Res.*, 6, 32.

148. Nalawade, R., Nalawade, A., Shejwal, R., & Anuse, M. (2017). *IJESI*, 6, 46.

149. Singh, D., Kumar, K., & Sharma, C. (2010). *European Journal of Medicinal Chemistry*, 45, 1230.

150. Singh, P. D., & Kumar, R. (2007). *J. Serb. Chem. Soc*., 72, 1069.

CHAPTER 2

MATERIALS, METHODS AND INSTRUMENTS

The current section summarizes about the general reagents utilized and gives a brief account about the purification methods employed. It also provides an overview of the theories and methods of various analytical and physical techniques used to characterize ligands and their transition metal complexes. Additionally, the procedures used for corrosion studies, DFT, and molecular modeling studies are briefly described.

2.1 REAGENTS

Analar grade samples of Diphenyl glycolic acid, L-Tyrosine, L-Valine, L-Leucine, L-Glycine, L-Histidine supplied by Merck, Sigma Aldrich were used as received, for the preparation of ligands. The metal salts used for the preparation of complexes were chromium acetate, manganese acetate, ferric chloride, cobalt acetate, nickel acetate, copper acetate, zinc acetate and cadmium acetate. During the preparation of complexes AR grade samples of metal salts were used. Spectroscopic grade samples of the solvents were employed for the spectral measurements. All other commercial reagents and solvents used for the synthesis and characterization of compounds such as NaOH, CH_3COONa, KOH, HCl, methanol, ethanol DMF, DMSO, $CHCl_3$ etc were used as received.

2.2 EXPEIMENTAL TECHNIQUES

A brief account about the methods employed for the characterization of ligands and their metal complexes have been

described below and thesynthetic procedures for the ligand and its transition metal complexes are described in the imminent chapters.Various physicochemical methods and spectral studies employed for elucidating the structure and geometry of the complexes. Physicochemical method involves conductivity measurements and magnetic susceptibility measurements. Spectral studies were the IR and UV-Visible measurements. The X-ray diffraction and thermogravimetric studies were also conducted.

2.2.1 CHN Measurements

Thecarbon,hydrogen and nitrogencontents of the ligands and their metal complexes were determined by analysis on anElementar make Vario EL III model CHNS analyzer. The metal content of the complexes was determined using the specifiedmethods.

2.2.2 Metal percentage analysis

Themetal percentage in the complexes was estimated using standard methods[1]suchas volumetric, gravimetric, andpyrolysismethods. The volumetric estimation of the metal content in the complexes was done by dissolving the complexes in a mixture of nitric, hydrochloric, and perchloric acids. A known amount of complexes(0.2-0.3g) was digested with a concentrated nitric acid-perchloric acid mixture andthenwith concentrated HCl. Repeatthis process two or three times by adding anewamount of hydrochloric acid. The resulting solution was then quantitatively

adjusted to 100 ml. The metal content in the complex is estimated based on the specific volume of this solution.

Copper content was determined by iodometric titration by adding KI and titrating ther eleased iodine with standard sodium thiosulfate. Zinc and Manganese were estimated volumetrically by complexometric titration using standard EDTA with Eriochrome black –T as indicator Nickel was determined as dimethyl glyoxymate byprecipitation using a gravimetric method. Estimation of cobalt and cadmium was performed by complexometric titration using standard EDTA solution and xylenol orange indicator.

The metal content of all complexes was estimated using the pyrolysis method. Approximately 0.2g of the composite was weighed into a quartz crucible and heated vigorously. During intense heating, the organic components of the metal complex are burned and the remaining metal oxides are balanced.Metal content was calculated from the weight loss of metal oxides.

2.2.3 Determinationof Molar Conductivity

The molar conductivity of the complexat a concentration of approximately 10^{-3} M was determined at28±2°C using a Philips conductivity bridge.

2.2.4 Magnetic measurements

Themagnetic properties of the ligand and its complexes were studied using the Gouy balance. The measurements done at room temperature using the $Hg[Co(NCS)_4]$ as calibrant.By considering

the magnetic contribution of various atoms and structural units[2,3] diamagnetic corrections were applied using the Pascal constants. The effective magnetic moment $\mu_{eff}$was calculated from the modifiedformulashownbelow,

$$\mu_{eff} = g\sqrt{\chi_m} .T$$

Where χ_m is the molar susceptibility corrected for diamagnetism and T is the absolute temperature. The theoretical value of magnetic moments calculated using the formula

$$\mu_{eff} = g \sqrt{J (J+1)}$$

2.2.5. Electronic Spectra

The solid state electronic spectra[4] of the ligands and their complexes were recorded using a UV-VISspectrophotometer model JascoV-550. These spectral studies carried out to assist the structural information obtained from magnetic studies.

2.2.6. Infrared Spectra

IR spectroscopy is a powerful tool for the determination of the molecular structure and identification. The characteristic bands of a group appear at a specificfrequency,regardless of the molecule in which the group is present hence it named as the finger print spectroscopic method. IR studies of the presentligand and its metal complexes[5] were recorded using a Jasco-FT-IR-4100 model spectrometer in the range 4000–400cm using the KBrdisc method.

2.2.7. X-ray Diffraction study

The XRD studies of selected ligands and their metal complexes were recorded using anAeris research benchtop X-ray diffractometer in the range10-90 2θ values. X-ray crystallographic studies were carried out for the determination of lattice type and unit cell dimension of complexes. X-ray pattern plots 2θ against intensity of diffraction used for finding interplanar spacing (d).

2.2.8. Thermogravimetry

Thermal analysis of the complexes, TG-DTA and DTG wasperformed on a thermogravimetric analyzer TGA Q50 V20.13 Build 39 model fitted with a thermal analyzer controller in air atmosphere with a heating rate of 10^{o} C/min at NIT, Calicut.

2.2.9. Corrosion Inhibition studies

Corrosion inhibition studies were carried out at the Department of Chemistry, The Zamorin's Guruvayurappan College, Calicut. The inhibition efficiency, corrosion rate and the adsorptions studies from the weight loss method was calculated. The details of the study are discussed in Part IV.

2.2.10. Antifungal studies

Antifungal studies of the ligands and its selected complexes were conducted at the Department of Chemistry, The Zamorin's Guruvayurappan College, Calicut in collaboration with the Department of Botany, The Zamorin's Guruvayurappan College, Calicut. The antifungal studies of the ligand and complexes against

various fungal strains Pencillium sp., Fusarium sp., Pythium sp., Lasiodiplodia theobromae and Aspergillus sp.were studied using potato dextrose agar medium[6]. The details of the studies carried out are explained in Part V.

2.2.11. Catalytic studies

The catalytic degradation study of the hazardous dyes like methylene blue and methyl orange has been carried out at the Department of Chemistry, The Zamorin's Guruvayurappan College, Calicut. The study was monitored using UV spectrophotometer and is explained in Part VI .

2.2.12. Molecular Modeling studies

Molecular Modeling studies of ligands were performed at the Department of Chemistry, University of Calicut. For computational studies, the molecules are optimized by DFT (B3LYP) method with the 6-31+G (d, p) basis sets, using the Gaussian 09program. Details of the DFT studies are discussed in Part VII.

References :

1. Vogel A.I. (1962). "A text book of Quantitative Inorganic Analysis" , ELBS and Longman, London,1048.

2. Figgis B.N., & Lewis, J. (1964). "Progress in Inorganic Chemistry", *Inter Science*, New York, 6.

3. Earnshaw, A., King, E.A., & Larkworthy, L.K. (1968). *J.Chem.Soc*.,Sect.A, 1048

4. Figgis, B.N.and Nyholm, R.S., (1959). *J.Chem.Soc*., 388.

5. Venanzi, L.M., Dyer, G. and Hartel, J.G. (1965). *J.Chem.Soc*.,1293.

6. Singh, H.L. (2007).*Inorg.Chem.Indian J*., 2, 135.

CHARACTERIZATION STUDIES OF THE DIPHENYL GLYCOLIC ACID – AMINO ACID LIGAND AND ITS METAL COMPLEXES

CHAPTER 3

STUDIES ON Cr (III), Mn (II), Fe (III), Co(II),Ni (II), Cu (II), Zn (II), Cd (II) COMPLEXES OF DIPHENYL GLYCOLIC ACID-TYROSINE LIGAND (HBT)

3.1 Introduction

L-Tyrosine or 4-hydroxyphenylalanine is a non-essential amino acid produce from phenylalanine with a polar side group. The word tyrosine originated from the Greek word ‘tyros’ meaning cheese, as it was first isolated from casein from cheese by German Chemist Justus Von Liebig. Tyrosine has a special role in the signal transduction processes and functions as a receiver of phosphate groups that are transferred by the way of protein kinases. In photosynthesis, tyrosine residue acts as an electron donor in the reduction of oxidized chlorophyll. Tyrosine is a precursor to neurotransmitter and also used to improve the mental health performance to reduce the stress hormone levels. Tyrosine helps in the preparation of several important substances including Dopamine, Adrenaline, Noradrenalin, thyroid hormones and Melanin.

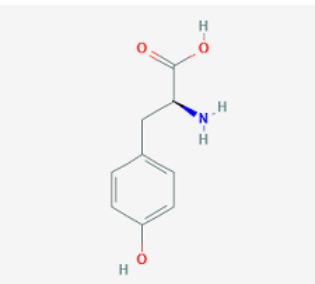

Fig.1. Tyrosine

Theoretical study of complexes of tyrosine with biologically important metal cations in aqueous solutions was reported by Agnieszka[1]. Baul[2] et al synthesized and characterize the crystal structure and supramolecular features of bicycloazastannoxides derived from Schiff bases derived from L-tyrosine. Anna[3] et al synthesized and studied the diffraction patterns, spectroscopic, electrochemical and antiproliferative activity of Ruthenium-Nitrosyl complexes with L-Glycine, L-Alanine, L-Valine,L-Proline, D-Proline, L-Serine,L-Threonine and L-Tyrosine.The square pyramidal ternary Cu(II) complexes [Cu(II)(saltyr)(B)](1,2), saltyr= Salicylidine-tyrosine, B=1,10,phenanthroline(1) or 2,2'-bipyridine(2) were synthesized and DNA binding and cleavage study was determined by Reddy[4] et al. The structural characterization of diorganotin complexes of Schiff base derived from 4-(diethylamino)salicylaldehyde and L-tyrosine were carried out by Lexing[5] et al.

HBT is a potential bidentate ligand which has been prepared and their transition metal complexes have also been synthesized. The elucidation of the structure of the HBT ligand and its complexes predicted using various spectral and physicochemical methods.

3.2 Experimental

3.2.1 Materials and Method

Diphenyl glycolic acid, L-Tyrosine, L-Glycine, L-Histidine, L-Valine, L-Leucine and metal salts were used without purification. The solvents were purified using standard procedure. The melting points of the ligand and the complexes were recorded with the melting point apparatus. The Gouy balance is used to determine the magnetic susceptibility of the complexes. The characterization of the compounds conducted with the aid of elemental analysis, Fourier-transform infrared (FT-IR), electronic, thermal methods and powder XRD studies. This chapter describes the method of characterization of diphenyl glycolic acid-tyrosine ligand and its various transition metal complexes in detail.

3.2.2 Preparation of HBT

0.1 M solution of diphenyl glycolic acid in aqueous ethanol was mixed with 0.1 M ethanolic solution of tyrosine potassium salt and refluxed for 3 hours on water bath[6]. The resulting solution concentrated for few minutes and the ligand crystallizes out and washed with ethanol and dried over anhydrous $CaCl_2$. The melting point was found to be 290^0C.

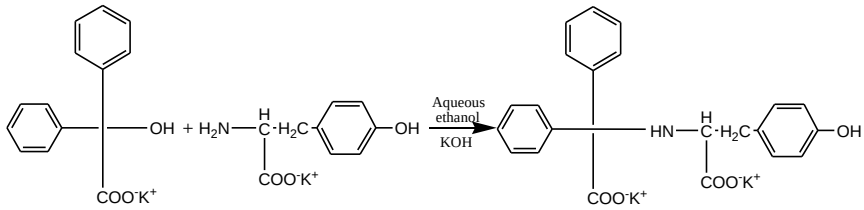

Scheme 1.The reaction pathway of the ligand HBT

3.3 Results and Discussion

3.3.1 Characterization of the ligand

The ligand is characterized by CHN analysis, IR, UV spectral studies. The description of the ligand is discussed in the following sections.

3.3.1.1 Micro analytical data

The newly synthesized ligand having the molecular formula $C_{23}H_{19}NO_5$ is pale yellow in colour. Elemental analysis data is in good agreement with the suggested molecular formula. **(Table.1).**Theligand is soluble in all common solvents such as methanol, ethanol, DMSO, DMF etc.

Table 1. Analytical data of ligand (HBT)

Compound	Molecular Weight	Melting point	Colour	yield	Elemental Analysis Found(Calculated)		
					C	H	N
$C_{23}H_{19}NO_5$	389	290^0C	Pale yellow	80	70.82 (70.95)	4.78 (4.88)	3.56 (3.59)

3.3.1.2 IR spectrum

The FT-IR spectrum of the ligand was recorded in the range 4000-400 cm^{-1} and presented in Fig.2and the IR values are shown in Table.2. The sharp peak at 3207 cm^{-1} may be attributed to O-H stretching vibration. The broad band at 3437 is assigned to the N-H stretching vibration. The bands at 1609 and 1416 cm^{-1} are assigned to υ (COO_{asymm}) and υ (COO_{symm}) respectively. The υ (C=O) band is at 1732 cm^{-1} and the υ (C-O) band is at 1244 cm^{-1}.[6]

Table 2.IR spectral data

No.	**Compound**	**υ(N-H)**	**υ (O-H)**	**υ(COO_{asymm})**	**υ(COO_{symm})**	**υ(C=O)**	**υ (C-O)**
1.	$C_{23}H_{19}NO_5$	3437	3207	1609	1416	1732	1244

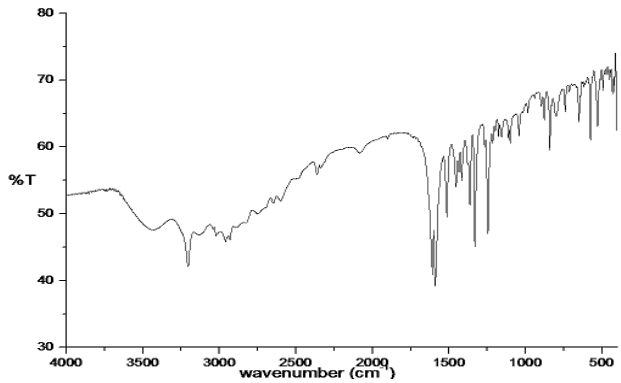

Fig.2. IR spectrum of the ligand

3.3.1.3. Electronic spectrum

The solid state uv-visible[7] spectrum of the ligand was recorded in the region 200-900 nm (fig.3) and the electronic spectral data is given in Table 3.The compound gives peaks at 279,342 and 367 nm in which former peak indicates the n→π* transition and the latter may be due toπ→π* transition.

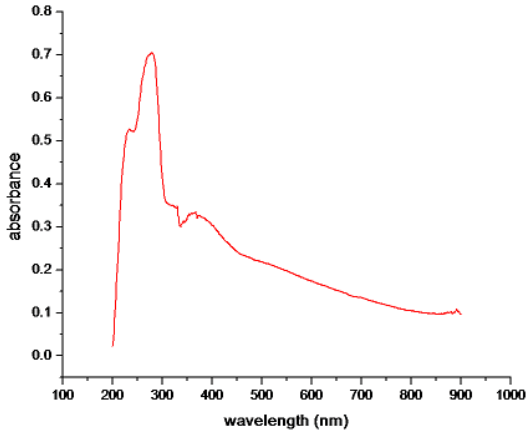

Fig.3. Electronic spectra of ligand

Table 3. Electronic spectral data

No.	Compound	Band nm	cm^{-1}	Assignments
1.	$C_{23}H_{19}NO_5$	279	35842	n→π*
		342	29239	π→π*
		367	27247	π→π*

3.2.3 Preparation of the transition metal complexes

The metal complexes were prepared by adding the metal acetate/chloride solution dropwise to the hot ethanolic solution of HBT solution. A pinch of sodium acetate trihydrate was added and was refluxed for 1 hour, and cooled to room temperature. The crystalline precipitate was collected and washed several times with water and dried in dessicator.

3.3.2Characterization of the transition metal complexes

The metal complexes were found to be insoluble in water and soluble in dilute hydrochloric acid and partially soluble in organic solvents like alcohol, DMF, DMSO, etc. The complexes have undergone elemental analysis, magnetic measurements, electronic and infrared spectral studies, molar conductance measurements and thermal analysis. The data obtained helped to predict the properties, structure and geometries of the complexes.

3.3.2.1 Elemental Analysis

The elemental analysis of the metal complexes was conducted by the standard methods[8]. CHN analysis carried out to found the percentage of carbon, hydrogen and nitrogen. Ligand act as both bidentate and tridentate in some metal complexes. The metal complexes are formed in both 1:1 and 1:2 ratios. The details of the metal complexes are described in the following sections. The Analytical data is depicted in table 4.

Table.4. Molecular formulae, colours, elemental analysis data, conductivity and magnetic moments of the complexes

Compound	**Molecular Weight**	**Melting point**	**Colour**	**yield**	**Ω^{-1}**	**μ_{eff}**	**M%**
$C_{23}H_{19}NO_5$(HBT)	391.43	290^0	Pale yellow	80		-	-
$Cr(BT)(H_2O)_4$	515.43	$>300^0$	Dark green	70	8.55	1.52	10.08 (10.27)
$Mn(BT)_2(H_2O)_2$	873.79	$>300^0$	Light brown	70	20.55	5.68	6.28 (6.36)
$Fe(BT)(H_2O)_2Cl_2$	554.27	$>300^0$	Light brown	70	9.73	3.18	10.07 (10.12)
$Co(BT)(H_2O)_4$	522.36	$>300^0$	Pink	60	4.56	4.32	11.28 (11.90)
$Ni(BT)_2(H_2O)_2$	877.69	$>300^0$	Bluish green	60	4.79	3.38	6.68 (6.40)
$Cu(BT)(CH_3COO)_4$	690.98	$>300^0$	Brown	80	17.36	2.18	9.19 (9.28)
$Zn(BT)(CH_3COO)_4$	692.81	$>300^0$	White	70	19.35	DIA	9.17 (8.94)
$Cd(BT)(H_2O)_2$	539.841	$>300^0$	White	60	20.32	DIA	20.82 (20.14)

3.3.2.2 Infrared studies

The characteristic IR spectra of the metal complexes of the spectra are given in Table.5. The IR band in the region 3500-3100 cm^{-1} due to υ (OH) stretching vibrations in the metal complexes indicating that the presence of water coordinated to the metal which is further supported by the new peaks in the regions of 750-850 cm^{-1} [9,10]. The C-O stretch at 1244 cm^{-1} is red shifted to 1170-1200 cm^{-1} suggests the participation of carboxylate in the complexation. The bands at 1590 cm^{-1} and 1344 cm^{-1} assigned to

the υ (COO_{asymm}) and υ (COO_{symm}) respectively, a shift to lower frequencies indicating the reduction of electron density in the oxygen in carboxylate group when coordinate to the metal ion. The difference between υ (COO_{asymm}) and υ (COO_{symm}) is greater than 140 cm^{-1} suggesting unidentate nature of acetate group. New absorption bands in the region 500-700 cm^{-1} assigned to υ (M-O) stretching vibrations[11-13](Fig.4-8).

Table.5. IR spectral assignments of the metal complexes

Sl.No	Compound	υ(O-H)	υ(N-H)	υ (COO_{asymm})	υ (COO_{symm})	υ(H_2O)	υ (M-O)
1	$C_{23}H_{19}NO_5$(HBT)	-	3207	1609	1416	-	-
2	$Cr(BT)(H_2O)_4$	3834	3286	1591	1344	858	698
3	$Mn(BT)_2(H_2O)_2$	3891	3053	1575	1336	845	675
4	$Fe(BT)(H_2O)_2Cl_2$	3521	3205	1512	1380	853	649
5	$Co(BT)(H_2O)_4$	3621	3212	1507	1384	821	695
6	$Ni(BT)_2(H_2O)_2$	3640	-	1566	1382	754	615
7	$Cu(BT)(CH_3COO)_4$	-	3208	1588	1406	-	655
8	$Zn(BT)(CH_3COO)_4$	-	3209	1562	1395	-	687
9	$Cd(BT)(H_2O)_2$	3606	3193	1532	1402	858	689

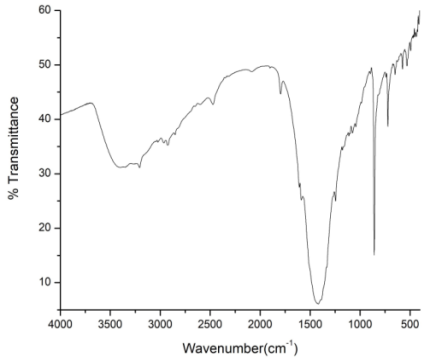

Fig.4. IR spectrum of the CdBT complex

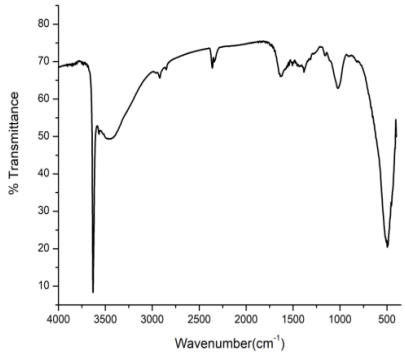

Fig.5. IR spectrum of the CoBT complex

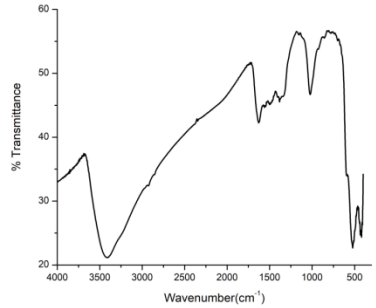

Fig.6. IR spectrum of the CuBT complex

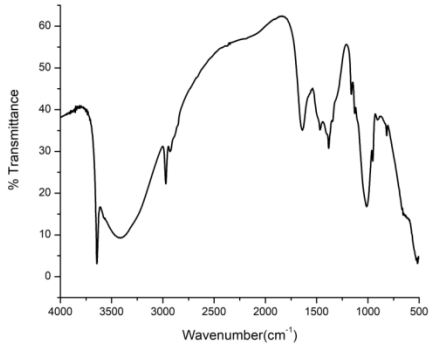

Fig.7. IR spectrum of the NiBT complex

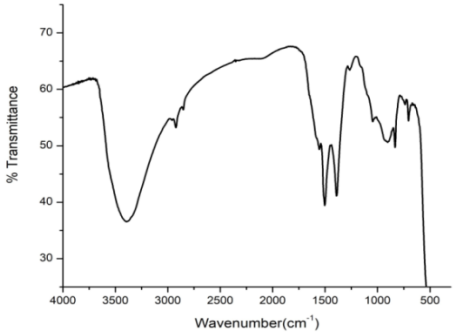

Fig.8. IR spectrum of the ZnBT complex

3.3.2.3Electronic spectra

The solid state electronic spectrum of the ligand was recorded in the range 200-900 nm and it exhibits bands at 279,342 and 367 nm. The bands attributed to the n→π*and π→π* transitions respectively. The shift in the value of the bands from the ligand to the complexes explains the coordination occur between the metal ion and the ligand.

Chromium (III) ion is having d^3 configuration. They exhibits three spin-allowed transitions i.e. ^4A_2g (F) → ^4T_2g (F) (v_1), ^4A_2g (F) → ^4T_1g (F) (v_2), ^4A_2g (F) → ^4T_1g (P) (v_3). In the current work bands at 330, 354 and 594nm respectively for π→π*, n→π* and ^4A_2g (F) → ^4T_1g (F) transitions suggests their octahedral stereochemistry. Manganese (II) ion with d^5 configuration is capable of forming spin-free as well as spin-paired complexes but due to their additional stability of the half-filled d-shell they preferably form spin-free complexes. According to Tanabe-Sugano diagram the three lowest energy states in order to increasing energy are $^4T_1$ (G), $^4T_2$ (G) and $^4A_1$, ^4E (G). Here Mn (II) complexes show low intensity weak bands at 330 nm due to n→π* and 419 nm ^6A_1g→^4T_1g (G) which have been assigned to transitions, and respectively, in an octahedral field of Mn (II) ion.

The iron(II) ion having [Ar] $3d^6$ electronic configuration and ground state of high spin system ^5D splits into the ground state is ^5T_2g and the only excited state of the same spin multiplicity is the

^5E_g state in weak octahedral fields. The spectra consists of three bands 1080.03 nm, 625 nm and 470 nm in which the high energy bands may be charge transfer in nature. The remaining two low energy bands may be assigned to $^5T_2g \rightarrow {}^5Eg$ transition, which corresponds to 10Dq.In the current work absorption band of Fe (III) complex are in the range 282 and 330 nm assigned to $\pi \rightarrow \pi^*$, $n \rightarrow \pi^*$ transition. A strong charge transfer band is observed at 389 nm due to CT transition. From spectral data, an octahedral geometry is proposed for the Fe (III) chelate.

The electronic configuration of Co(II) ion is d^7 and in the octahedral ligand field its ground state may be either t_2g^5, eg^2 in weak-field or t_2g^6, eg^1 in strong-field[14,15]. Normally cobalt complexes are in tetrahedral and octahedral environment but rarely in planer environment. The octahedral Cobalt(II) complexes are pink or reddish brown in color. The ground state of Cobalt(II) in octahedral environment is ^4T_1g or ^2Eg. A band near 908-704 nm can be assigned to transition $^4T_1g \rightarrow {}^4T2g$ (υ_1). In addition to this band, a multiple band is observed in the visible region near 426-412 nm can be assigned to ^4T_1g (F) $\rightarrow {}^4T_1$ (P) (υ_3) transition. The transition ^4T_1g (F) $\rightarrow {}^4A_2g$ (υ_2) is two electron transition and observed at 686-534 nm. In the present work Cobalt(II) metal complexes two bands present in electronic spectra of Co(II) at 255,355 and 345 nm. It is assignable to octahedral geometry.

The Nickel(II) complexes having the atomic ground state ^3F with the ground state term in an octahedral field is ^3A_2g, in tetrahedral field is ^3T, where as in square planar complexes is ^1A_1g.The electronic spectrum in octahedral co-ordination shows three main bands in the regions 1,000-790 nm (υ_1), 612-519 nm (υ_2), 378-353 nm (υ_3). The bands υ_1, υ_2 and $\upsilon 3$ may be assigned as ^3A_2g (F) → ^3T_2g (F) (υ_1), ^3A_2g (F) → ^3T_1g (F) (υ_2) and ^3A_2g (F) → ^3T_1g (P) (υ_3) transitions respectively. In the current work nickel chelate exhibits three bands in the region 254,330 and 664 nm. Using energy level diagram these band are assigned to the transition ^3A_2g (F) → ^3T_2g (F) (υ_1), ^3A_2g (F) → ^3T_1g (F) (υ_2) and ^3A_2g (F) → ^3T_1g (P) (υ_3) respectively, for an octahedral stereochemistry[16].

The electronic configuration of copper(II) is d^9 and the ground state being ^2D.The ground state of the octahedrally coordinated copper(II) ion is ^2E_g, in tetrahedral field is ^2T_2g, where as for the square planer complexes is ^2B1g. The d^9 configuration undergoes tetragonal distortion because of Jahn-Teller distortion and leads to splitting of the ^2Eg and ^2T_2g levels in to ^2B_1g, ^2A_1g and ^2B_2g, ^2Eg levels, respectively[17]. The Cu(II) complex electronic spectrum shows a broad band in the region 478-700 nm and is assignable to C-T transition. The electronic spectra of Zn(II) and Cd(II) complexes is not possible since there is no unpaired electrons and the‘d’ sub shell is completely filled. They show charge transfer transitions in the range of 280-350 nm and they are diamagnetic in

nature. Most of the complexes are tetrahedral even though some octahedral complexes have also been reported.

Table6. Electronic spectral bands and their assignments of the metal complexes

Sl. No	Compound	Wave number(nm)	Wavelength (cm^{-1})	Transition
1	Ligand(HBT)	279 342 367	30303 28248 16835	$\pi\rightarrow\pi^*$ $n\rightarrow\pi^*$ $n\rightarrow\pi^*$
2	$Cr(BT)(H_2O)_4$	330 354 594	30303 23866 16835	$n\rightarrow\pi^*$ $n\rightarrow\pi^*$ $^3A_2g(F)\rightarrow{}^3T_1g(F)$
3	$Mn(BT)_2(H_2O)_2$	330 419	35460 30303	$n\rightarrow\pi^*$ C-T
4	$Fe(BT)(H_2O)_2Cl_2$	282 330 389	35460 30303 25706	$\pi\rightarrow\pi^*$ $n\rightarrow\pi^*$ $n\rightarrow\pi^*$
5	$Co(BT)(H_2O)_4$	255 330 645	39215 30303 28985	$\pi\rightarrow\pi^*$ $n\rightarrow\pi^*$ $^4T_1g(F)\rightarrow{}^4A_2g$
6	$Ni(BT)_2(H_2O)_2$	254 330 664	39370 30303 15060	$\pi\rightarrow\pi^*$ $n\rightarrow\pi^*$ $^3A_2g(F)\rightarrow{}^3T_1g$
7	$Cu(BT)(CH_3COO)_4$	449	20040	C-T
8	$Zn(BT)(CH_3COO)_4$	330 342	30303 29239	$n\rightarrow\pi^*$ $n\rightarrow\pi^*$
9	$Cd(BT)(H_2O)_2$	288 330	34722 30303	$\pi\rightarrow\pi^*$ $n\rightarrow\pi^*$

3.3.2.4Molar conductance

The molar conductance values of the 10^{-3} solution of the HBT ligand and its metal complexes in DMSO were observed to be in the range of 4-20$ohm^{-1}cm^2mol^{-1}$. The low values of

conductance[18]suggest that the complexes behave as non-electrolytes and are neutral in nature.

3.3.2.5Magnetic measurements

The magnetic moment values of the complexes helps in the prediction of their structure along with their electronic spectra. The Cr (III) complex possesses magnetic moment of 1.52 BM. It is suggested that if the measured value of the metal complex is in the range of 1.2- 2.5 BM, they possess to have an octahedral geometry. Magnetic moment values of a low spin Mn (II) complex having octahedral geometry are nearly 2.5 BM and that of high spin octahedral Mn (II) complex is between 5.64 and 6.15 BM. In the current case the complex possess a value of 5.68 BM which suggests the octahedral nature of the complex. Fe (III) complex have a magnetic moment value of 3.18 BM which corresponds to three unpaired electrons and they possess to have an octahedral geometry. Co(II) complexes with one unpaired electron can either form octahedral as well as square planar complexes but complexes with three unpaired electrons may form either tetrahedral or octahedral complexes. In the present case Co (II) complex have a magnetic moment value of 4.32 BM suggesting their octahedral geometry[19]. Octahedral Ni (II) complexes have a magnetic moment values in the range of 2.60-3.30BM, due to spin-orbit coupling or higher state mixing with ground state. The Ni (II) complex with a magnetic moment value of 3.38 BM indicates its octahedral

geometry. The magnetic moment value of copper complex is 2.18 BM corresponding to their one unpaired electron suggesting their octahedral geometry[20,21]. Zn (II) complex and Cd (II) complexes are diamagnetic in nature.

3.3.2.6 X-ray diffraction

The XRD pattern of the ligand and metal complexes gives a brief account of crystal lattice structure, interplanar distance, crystalline size etc. PXRD studies were discussed in Part III.

The proposed structures of the complexes arethe follows:

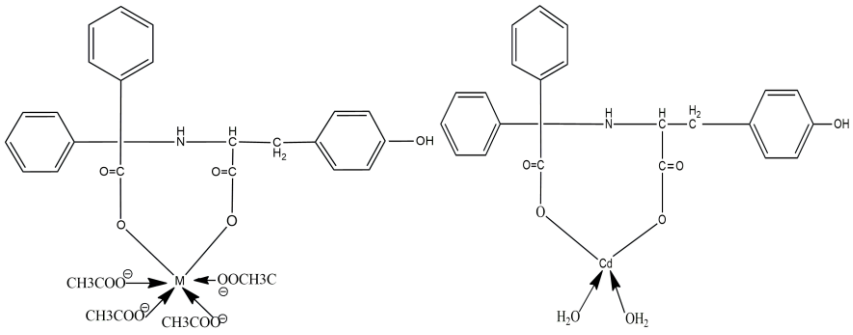

[M=Cu, Zn]

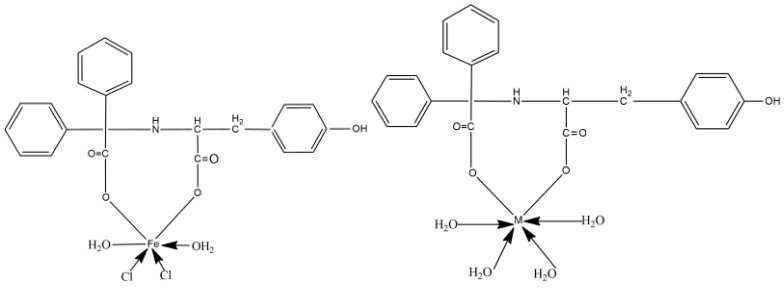

[M= Co]

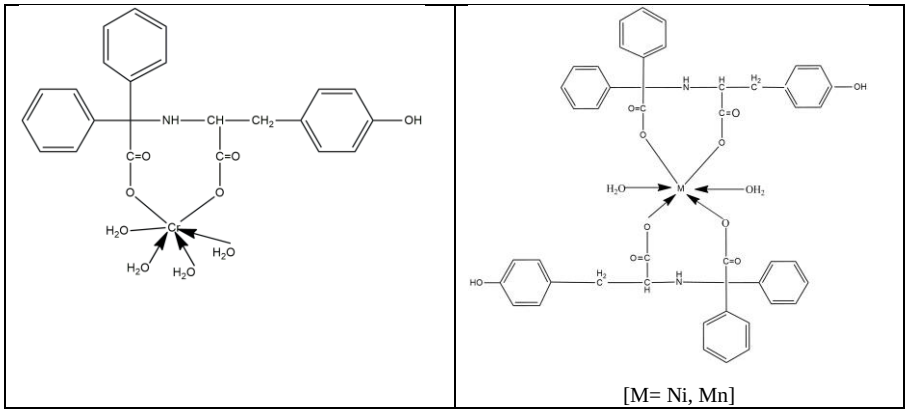

Fig.9. Structure of metal complexes of the ligand HBT

CHAPTER 4

STUDIES ON Cr (III), Mn (II), Fe (III), Co (II), Ni (II), Cu (II), Zn (II), Cd (II) COMPLEXES OF HBG

4.1 Introduction

Glycine or 2-Aminoethanoic acid is the simple, non-essential and the only proteinogenic amino acid with achiral carbon centre. Glycine is a colorless, sweet tasting crystalline compound soluble in pyridine and partially soluble in ethanol. The name glycine comes from the Greek word means “sweet tasting”. It was first discovered by French chemist Henri Braconnot when he hydrolyzed gelatin by boiling it with sulfuric acid. Glycine is a precursor to proteins and is an inhibitory neurotransmitter in the central nervous system. Glycine provides improved bone health and brain function. Glycine can promote the quality of our sleep and have the ability to lower core boy temperature.

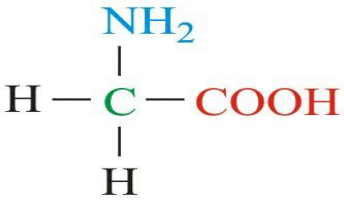

Fig.10. Glycine

Synthesis and characterization of the Schiff base derived from salicyaldehyde and glycine and their complexes with Lanthanide elements were reported by Zhang et al[22]. A series of organotin(IV) complexes were derived by the condensation of 1H-indole-2,3-dione,5-chloro-1-H-indole-2,3-dione and α-amino acids(phenyl alanine, isoleucine and glycine) and characterized by Har Lal and Jangbhadur[23].Hamza[24] et al conducted the theoretical study of reaction mechanism of formaldehyde and glycine Schiff base using Spactum '08 software semi-empirical/parametric model (PM3) and Density Functional Theory [RB3LYP/6-31G (d)] calculations. The synthesis and characterization of the Schiff bases derived from vanillin and amino acids (glycine, L-serine, L-tyrosine and L-phenylalanine and their Fe(III) complexes have been prepared by Shaheen[25] et al and their characterization carried out by various physicochemical and spectral methods. ((E)-2-((2-hydroxy-1,2-diphenylethylidene) amino) propanoic acid).and their Cu(II), Ni(II), Co(II), Zn(II) and Fe(II) complexes were synthesized and characterized by Nuha et al[26].

HBG is a potential bidentate ligand which has been prepared and eight transition metal complexes have also been synthesized. The elucidation of the structure of the HBG ligand and its complexes studied using various spectral and physicochemical methods.

4.2 Experimental

4.2.1 Preparation of HBG

0.1 M solution of diphenyl glycolic acid in aqueous ethanol was mixed with 0.1 M ethanolic solution of Glycine potassium salt and refluxed for 3 hours on water bath. The resulting solution concentrated for few minutes and the ligand crystallizes out and washed with ethanol and dried over anhydrous $CaCl_2$. The melting point was found to be 242^0 C.

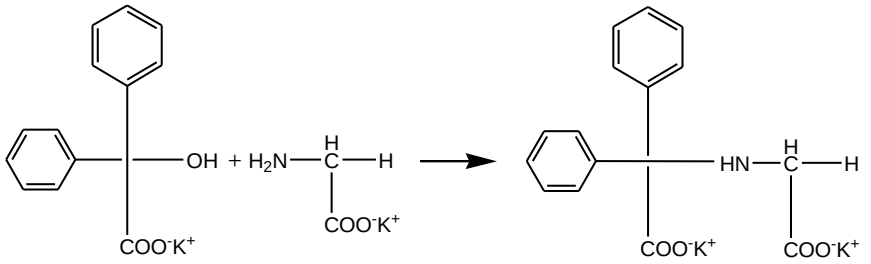

Scheme.2.The reaction pathway of the ligand HBG

4.3 Results and Discussion

4.3.1. Characterization of the ligand

The ligand is characterized by CHN analysis, IR, UVstudies. The description of the ligand is discussed in the following sections.

4.3.1.1 Micro analytical data

The newly synthesized ligand having the molecular formula $C_{16}H_{13}NO_4$is white crystalline powder. Elemental analysis data is in good agreement with the suggested molecular formula. (Table.7).The ligand is soluble in all common solvents such as methanol, ethanol, DMSO, DMF etc.

Table.7. Analytical data of ligand (HBG)

Compound	Molecular Weight	Melting point	Colour	yield	Elemental Analysis Found(Calculated)		
					C	H	N
$C_{16}H_{13}NO_4$	283	242^0 C	Pale yellow	80	71.02 (70.95)	4.64 (4.88)	3.54 (3.59)

4.3.1.2. IR spectrum

Table 8.IR spectral data

No.	Compound	υ(N-H)	υ (O-H)	$\upsilon(COO_{asymm})$	$\upsilon(COO_{symm})$	υ(C=O)	υ (C-O)
1.	$C_{16}H_{13}NO_4$	3453	-	1593	1491	1726	1254

The FT-IR spectrum of the ligand was recorded in the range 4000-400 cm^{-1} and presented in fig.11. The band at 3437 cm^{-1} is assigned to the N-H stretching vibration. The bands at 1593 and 1491 cm^{-}

[1]are assigned to υ (COO_{asymm}) and υ (COO_{symm}) respectively. The υ (C=O) band is at 1726 cm^{-1} and the υ (C-O) band is at 1254 cm^{-1} and the IR values are shown in table 8.[6]

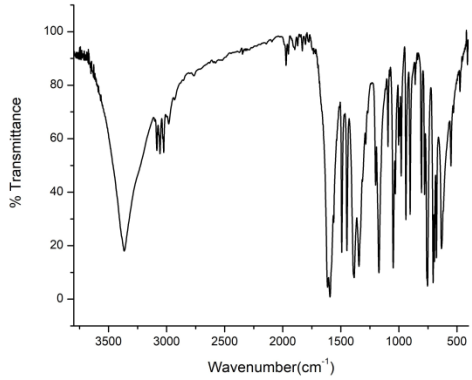

Fig.11. IR spectrum of the ligand

4.3.1.3. Electronic spectrum

The solid state uv-visible spectrum of the ligand was recorded in the region 200-900 nm (fig.12) and the spectral data is given in table 9.The compound gives peaks at 260 nm indicates the π→π* transition.[7]

Table 9. Electronic spectral data

No.	Compound	Band nm	cm^{-1}	Assignments
1.	$C_{16}H_{13}NO_4$	260	38461	π→π*

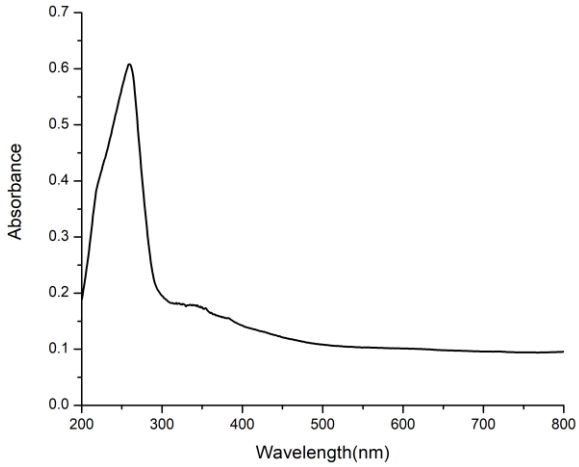

Fig.12. Electronic spectra of ligand

4.3.2. Preparation of the transition metal complexes

The metal complexes were prepared by adding the metal acetate/chloride solution drop wise to the hot ethanolic solution of HBG solution. A pinch of sodium acetate trihydrate was added and was refluxed for 1 hour, and cooled to room temperature. The crystalline precipitate was collected and washed several times with water and dried in dessicator.

4.3.3. Characterization of the transition metal complexes

The metal complexes were found to be insoluble in water and soluble in dilute hydrochloric acid and partially soluble in organic solvents like alcohol, DMF, DMSO, etc. The complexes have undergone elemental analysis, magnetic measurements, electronic and infrared spectral studies, molar conductance measurements and

thermal analysis. The data obtained helped to predict the properties, structure and geometries of the complexes.

4.3.3.1 Elemental Analysis

The elemental analysis of the metal complexes was conducted by the standard methods.[8] CHN analysis carried out to found the percentage of carbon, hydrogen and nitrogen. Ligand act as both bidentate and tridentate in some metal complexes. The metal complexes are formed in both 1:1 and 1:2 ratios. The details of the metal complexes are described in the following sections. The analytical data of the HBG and its metal complexes are tabulted in table 10.

Table.10. Molecular formulae, colours, elemental analysis data, conductivity and magnetic moments of the complexes

Compound	**Molecular Weight**	**Melting Point (^{0} C)**	**Colour**	**yield**	**Ω^{-1}**	**μ_{eff}**	**M%**
$C_{16}H_{13}NO_4$(HBG)	283	242	Pale yellow	80	2.56	-	-
$Cr(BG)_2(CH_3COO)_2$	740	>300	Dark green	60	3.72	4.46	7.02 (6.92)
$Mn(BG)_2(H_2O)_2$	656.94	>300	Dark Brown	70	9.8	1.82	8.36 (8.28)
$Fe(BG)(H_2O)_2Cl_2$	554.27	>300	Light Brown	70	10.12	3.26	10.07 (10.12)
$Co(BG)_2(H_2O)(CH_3COO)$	522.36	>300	Pink	60	5.4	3.98	11.28 (11.90)
$Ni(BG)(H_2O)_4$	415.69	>300	Bluish Green	60	7.3	3.16	14.11 (14.06)
$Cu(BG)(CH_3COO)_4$	582.55	>300	Coffee Brown	60	4.5	1.32	10.90 (10.86)
$Zn(BG)(H_2O)_4$	422.37	>300	White	70	6.8	DIA	15.47 (15.36)
$Cd(BG)(H_2O)_2$	431.41	>300	White	60	7.2	DIA	26.05 (25.54)

4.3.3.2 Infrared studies

The characteristic IR spectrums of the metal complexes of the spectra are given in Table.11 and are represented in fig 13-18. The IR band in the region 3400-3600 cm^{-1} due to υ (OH) remains in the metal complexes indicating that the hydrogen atom of the OH group of the water molecules which is further supported by the peaks at 800 cm^{-1} region.[9, 10] The N-H stretching peak observed at 3437 cm^{-1} is shift from its position may be due to the presence of new O-H stretching bands in that particular region. The C-O stretch at 1244 cm^{-1} is red shifted to 1170-1200 cm^{-1} suggests the participation of enolic –OH in the complexation. The bands at 1590 cm^{-1} and 1344 cm^{-1} assigned to the υ (COO_{asymm}) and υ (COO_{symm}) respectively, a shift to lower frequencies indicating the reduction of electron density in the oxygen in carboxylate group when coordinate to the metal ion. The difference between υ (COO_{asymm}) and υ (COO_{symm}) is greater than 140 cm^{-1} suggesting unidentate nature of acetate group. New absorption bands in the region 460-560 cm^{-1} assigned to υ (M-O) stretching vibrations.[11-13]

Table 11. IR spectral assignments of the metal complexes

No	Compound	υ(O-H)	υ(N-H)	υ (COO_{asymm})	υ (COO_{symm})	υ(H_2O)	υ (M-O)
1	$C_{16}H_{13}NO_4$(HBG)		3453	1593	1491		-
2	$Cr(BG)_2(CH_3COO)_2$	3448	-	1622	1444	829	637
3	$Mn(BG)_2(H_2O)_2$	3389	-	1599	1446	814	638
4	$Fe(BG)(H_2O)_2Cl_2$	3456	-	1613	1447	832	673
5	$Co(BG)_2(H_2O)(CH_3COO)$	3492	3687	1598	1448	856	674
6	$Ni(BG)(H_2O)_4$	3358	3612	1565	1409	848	525
7	$Cu(BG)(CH_3COO)_4$	-	-	1647	1446	-	695
8	$Zn(BG)(H_2O)_4$	3358	3596	1654	1492	836	622
9	$Cd(BG)(H_2O)_2$	-	3480	1639	1446	842	696

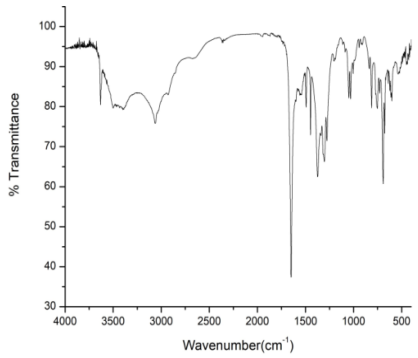

Fig.13. IR spectrum of the CoBG complex

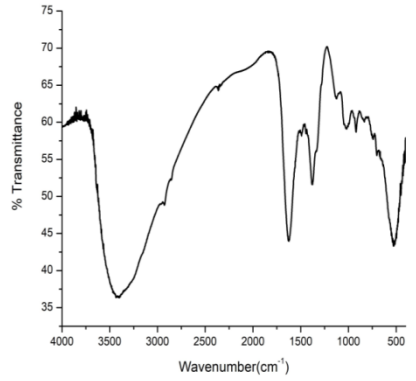

Fig.14. IR spectrum of the CrBG complex

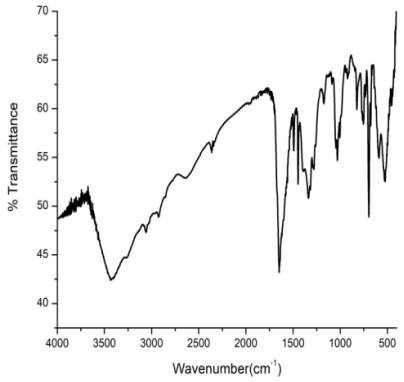

Fig.15. IR spectrum of the CuBG complex

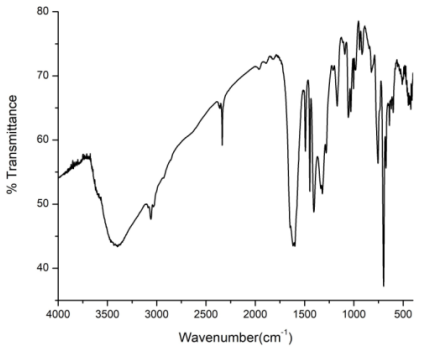

Fig.16. IR spectrum of the FeBG complex

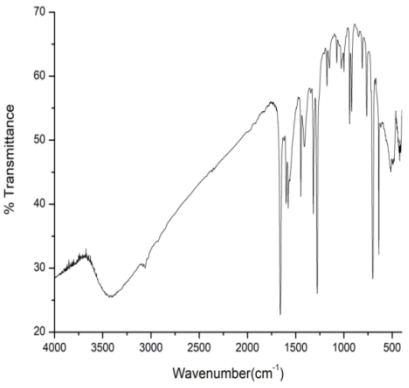

Fig.17. IR spectrum of the MnBG complex

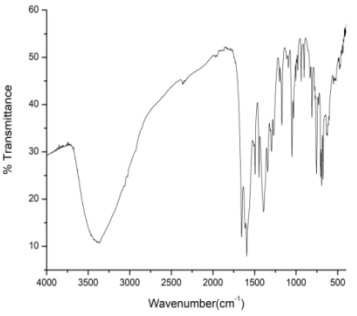

Fig.18. IR spectrum of the ZnBG complex

4.3.3.4 Electronic spectra

The ligand UV spectrum exhibits band at 260 nm attributed to the $\pi \rightarrow \pi^*$ and $n \rightarrow \pi^*$ transitions respectively. The shift in the value of the bands from the ligand to the complexes explains the

coordination occur between the metal ion and the ligand. Chromium (III) ion with d^3 configuration shows three spin-allowed transitions i.e. ^4A_2g (F) → ^4T_2g (F) (v_1), ^4A_2g (F) → ^4T_1g (F) (v_2), ^4A_2g (F) → ^4T_1g (P) (v_3) at 264 nm, 423 nm and 584 nm respectively suggesting the octahedral stereochemistry of the chromium complexes. The octahedral geometry of Mn (II) ion is confirmed by the appearance of bands at 248 and 342 nm. According to Tanabe-Sugano diagram the three lowest energy states in order to increasing energy are $^4T_1$ (G), $^4T_2$ (G) and $^4A_1$, ^4E (G). Manganese (II) ion belongs to d^5 system may form either high-spin or low-spin complexes. They show two low intense band at 406nm due to ^6A_1g→^4A_1g (G) transition and another at 687nm ^6A_1g →^4T_1g (G) transition which is in accordance with an octahedral geometry. Here Mn (II) complexes show intense bands at 342 nm due to ^6A_1g→^4A_1g (G) which has been assigned to transitions in an octahedral field of Mn (II) ion. The iron (III) ion having absorption band in the range 336nm assigned to^5T_2g→^5Eg transition. A strong charge transfer band is observed at 388 nm. From spectral data, an octahedral geometry is proposed for the Fe (III) chelate.

The transition ^4T_1g (F) →^4T_2g(P) (υ_1), ^4T_1g (F) → ^4A_2g (υ_2) and ^4T_1g (F) → $^4T_1$ (P) (υ_3) is two electron transition and observed at 686-534 nm for Co(II) complexes. In the present work cobalt (II) metal complexes two bands present in electronic spectra of Co (II) at 525 and 660 nm. It is assignable to octahedral geometry.[14,15] The absorption band at 237,386 and 667 nm are due to the transition$n\rightarrow\pi^*$,^3A_2g (F) → ^3T_1g (F) (υ_2) and ^3A_2g (F) → ^3T_1g (P)

(υ_3) respectively, for an octahedral stereochemistry of Ni(II) chelate.[16] The Cu(II) complex electronic spectrum shows a broad band in the region 478-700 nm and is assignable to d-d transition. The band at 634 nm suggests their octahedral geometry.[17,18]

The electronic spectra of Zn (II) and Cd (II) complexes is not possible since there is no unpaired electrons and the'd' sub shell is completely filled. They show charge transfer transitions in the range of 399-420 nm and they are diamagnetic in nature. Most of the complexes are tetrahedral even though some octahedral complexes have also been reported. The spectral values are shown in table 12.

Table.12. Electronic spectral bands and their assignments of the metal complexes

Sl.No	Compound	Wave number(nm)	Wavelength (cm^{-1})	Transitions
1	$Cr(BG)_2(CH_3COO)_2$	264 423 584	37879 23640 17123	$^4A_2g(F)\rightarrow\ ^4T_2g$ (F) $^4A_2g(F)\rightarrow\ ^4T_1g$ (F) $^4A_2g(F)\rightarrow\ ^4T_1g$ (P)
2	$Mn(BG)_2(H_2O)_2$	248 342	40322 29240	$n\rightarrow\pi^*$ $^6A_1g\rightarrow\ ^4A_1g$ (G)
3	$Fe(BG)(H_2O)_2Cl_2$	336 388	29761 25773	$^6A_1g\rightarrow\ ^4Eg$ $^6A_1g\rightarrow\ ^4A_1g$ (G)
4	$Co(BG)_2(H_2O)(CH_3COO)$	525 660	19047 15151	$^4T_1g\rightarrow\ ^4T_2g$ $^4T_1g\rightarrow\ ^4A_2g$
5	$Ni(BG)(H_2O)_4$	237 386 667	42194 25906 14992	$n\rightarrow\pi^*$ $^3A_2g\rightarrow\ ^3T_1g(F)$ $^3A_2g\rightarrow\ ^3T_1g(P)$
6	$Cu(BG)(CH_3COO)_4$	634	15772	$^2B_1g\rightarrow\ ^2A_2g$
7	$Zn(BG)(H_2O)_4$	229 262 344	43668 38167 29069	$n\rightarrow\pi^*$ $\pi\rightarrow\pi^*$ $\pi\rightarrow\pi^*$
8	$Cd(BG)(H_2O)_2$	235 266	42553 37594	$n\rightarrow\pi^*$ $\pi\rightarrow\pi^*$

4.3.3.5 Molar conductance

The molar conductance values of the 10^{-3} solution of the HBG ligand and its metal complexes in DMSO were observed at room temperature and all the chelates exhibits low values of conductance in the range of 4-20ohm^{-1}cm^{2}mol^{-1} suggesting the non-electrolytic nature.[19]

4.3.3.6 Magnetic measurements

The magnetic moment values of the complexes helps in the prediction of their structure along with their electronic spectra. The Cr (III) complex possesses magnetic moment of 1.82 BM. It is suggested that if the measured value of the metal complex is in the range of 1.2- 2.5 BM, they possess to have an octahedral geometry. Magnetic moment values of a low spin Mn (II) complex having octahedral geometry are nearly 2.5 BM and that of a high spin Octahedral Mn (II) complex is between 5.64 and 6.15 BM. In the current case the complex possess a value of 4.46 BM which suggests the octahedral nature of the complex. Fe (III) complex have a magnetic moment value of 3.26 BM which corresponds to three unpaired electrons and they possess to have an octahedral geometry. Co(II) complexes with one unpaired electron can either form octahedral as well as square planar complexes but complexes with three unpaired electrons may form either tetrahedral or octahedral complexes.[20] In the present case Co(II) complex have a magnetic moment value of 3.98 BM suggesting their octahedral

geometry. Octahedral Ni(II) complexes have a magnetic moment values in the range of 2.60-3.30BM, due to spin-orbit coupling or higher state mixing with ground state.[21,22] The Ni(II) complex with a magnetic moment value of 3.26 BM indicates its octahedral geometry. The magnetic moment value of copper complex is 1.32 BM corresponding to their one unpaired electron suggesting their octahedral geometry. Zn(II) complex and Cd(II) complexes are diamagnetic in nature.

4.3.3.7 Thermal analysis

The metal complexes were subjected to thermal studies with the aid of TG-DTA, DTG data and is discussed in Part II. The data provides information about the kinetic parameters, mechanism of decomposition and probable assignments in the decomposition curve. The kinetic parameters studied by non isothermal method.

4.3.3.8 X-ray diffraction

The XRD pattern of the ligand and metal complexes gives a brief account of crystal lattice structure, interplanar distance, crystalline size etc. PXRD studies were discussed in Part III.

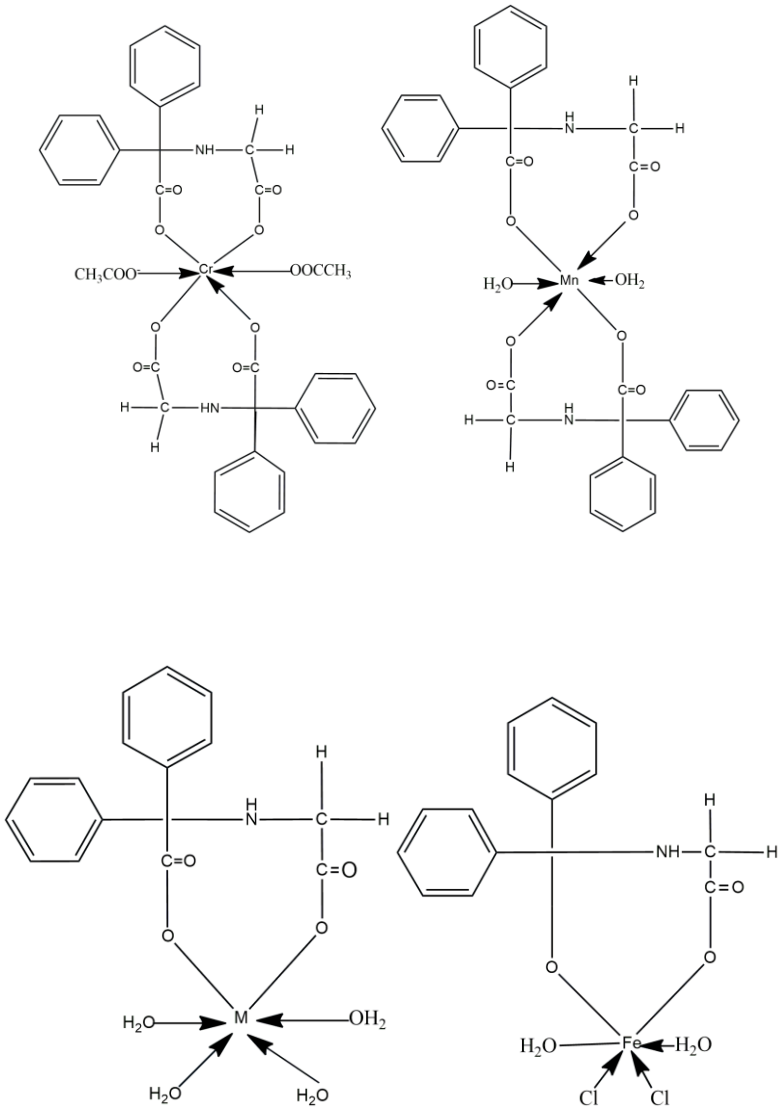

(M = Ni, Zn)

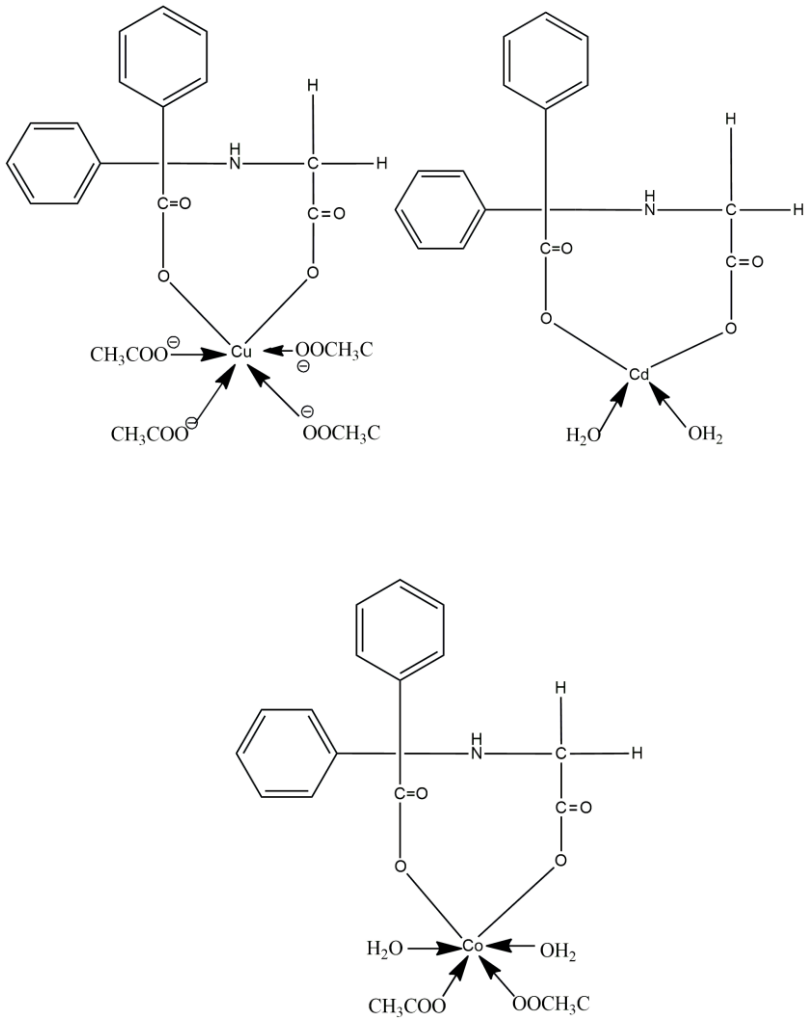

Fig.19. Structure of metal complexes of the ligand HBG

CHAPTER 5

STUDIES ON Cr (III), Mn (II), Fe (III), Co (II), Ni (II), Cu (II), Zn (II), Cd (II) COMPLEXES OF HBH

5.1 Introduction

Histidine or 2-Amino-3-(1H-imidazol-4-yl)propanoic acid is a semi-essential amino acid which plays an role in immunity, gastric secretion, protein biosynthesis and sexual functions. Histidine was first isolated by German physician Albrecht Kossel and Sven Gustaf Hedin. It is the precursor of histamine, carnosine biosynthesis and also serves as biomarker for skeletal muscle damage. Histidine is used for rheumatoid arthritis, allergic diseases, ulcers and anemia caused by kidney failure or kidney dialysis. Histidine is an odorless, white crystalline powder soluble in water.

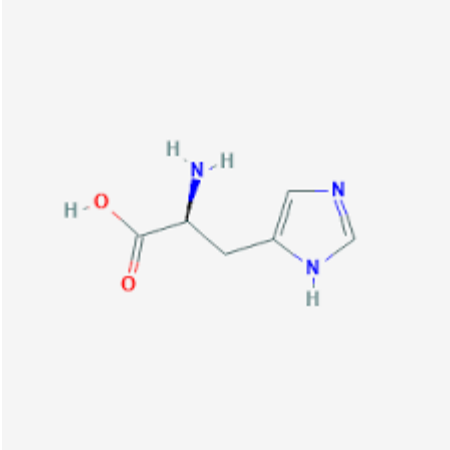

Fig.20. Histidine

Histidine analogues obtained by the reaction between L-Histidine and 3,5-di-*tert*-butyl-2-hydroxybenzaldehyde and their five novel tin complexes have been prepared by Ariadna[28] et al. The corrosion inhibition efficiency of the complexes of L-Histidine Schiff base derived from 2, 4-dihydroxybenzaldehyde and 2-hydroxy-1-naphthaldehyde have been synthesized by Baradie[29] et al. Template synthesis of Schiff base derived from quinoxaline-2-carboxaldehyde and L-histidine and their metal complexes were synthesized by Manju[30] et al. The antimicrobial activities of manganese (III) complexes of (2-hydroxy-1-naphthalidene)-histidine was evaluated by Sakiyan[31] and coworkers. Neelofar[32] reveals the excellent antioxidant and antimicrobial activities of tin (II) complexes of various Schiff base derivatives of 2-hydroxy-1-naphthaldehyde (HN) with L-histidine.

HBH is a potential bidentate ligand which has been prepared and eight transition metal complexes have also been synthesized. The elucidation of the structure of the HBH ligand and its complexes studied using various spectral and physicochemical methods.

5.2 Experimental

5.2.1 Preparation of HBH

0.1 M solution of diphenyl glycolic acid in aqueous ethanol was mixed with 0.1 M ethanolic solution of histidine potassium salt and refluxed for 3 hours on water bath. The resulting solution

concentrated for few minutes and the ligand crystallizes out and washed with ethanol and dried over anhydrous $CaCl_2$. The melting point was found to be 292˚C. The analytical data of the HBH ligand and its metal complexes is discussed in table.13.

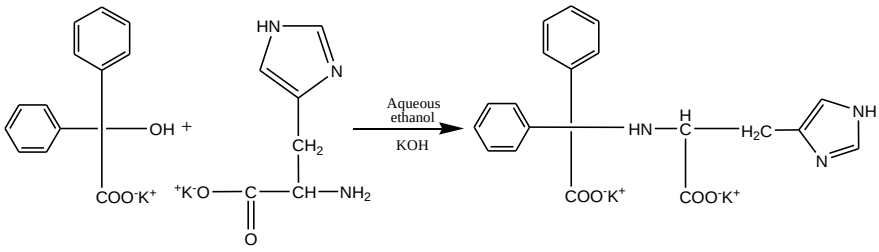

Scheme.3. Scheme of preparation of HBH ligand

5.3 Results and Discussion

5.3.1 Characterization of the ligand

5.3.1.1 Micro analytical data

The newly synthesized ligand having the molecular formula $C_{20}H_{13}N_3O_4$is white crystalline powder. Elemental analysis data is in good agreement with the suggested molecular formula. (Table 13).The ligand is soluble in all common solvents such as methanol, ethanol, DMSO, DMF etc.

Table.13. Analytical data of ligand (HBH)

Compound	Molecular Weight	Melting point	Colour	yield	Elemental Analysis Found(Calculated)		
					C	H	N
$C_{20}H_{19}N_3O_4$	365	292^0	Pale yellow	80	65.24 (65.68)	4.82 (5.19)	10.98 (11.49)

5.3.1.2 IR spectrum

The FT-IR spectrum of the ligand was recorded in the range 4000-400 cm^{-1} and presented in fig.21 and the values are given in table.14The sharp peak at 3367cm^{-1} may be attributed to N-H stretching vibration. The bands at 1652 and 1492 cm^{-1} are assigned to υ (COO_{asymm}) and υ (COO_{symm}) respectively. The υ (C=O) band is at 1861 cm^{-1} and the υ (C-O) band is at 1172 cm^{-1}.[6]

Table.14 IR spectral data

No.	Compound	υ(O-H)	υ (N-H)	υ(COO_{asymm})	υ(COO_{symm})	υ(C=O)	υ (C-O)
1.	$C_{20}H_{17}N_3O_4$	3367	2954	1652	1492	1861	1172

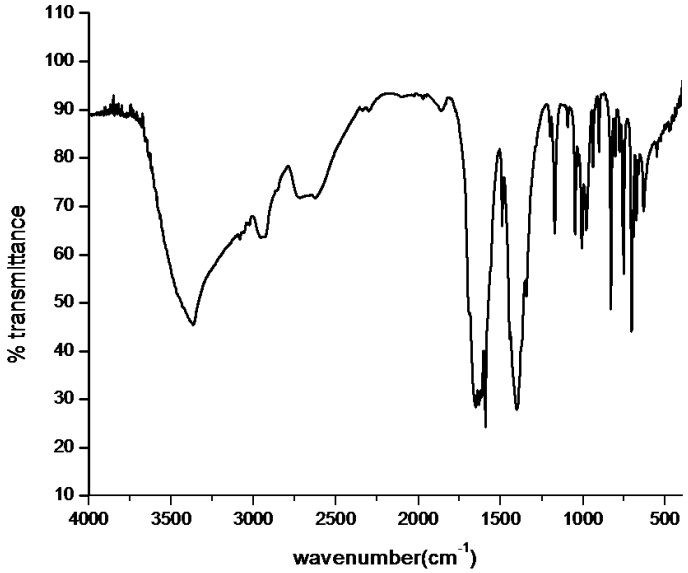

Fig.21. IR spectrum of HBH ligand

5.3.1.3 Electronic spectrum

The solid state uv-visible spectrum of the ligand was recorded in the region 200-900 nm **(**fig.22**)** and the values are given in table.15**.**The compound gives peaks at 254 nm in which former peak indicates the $\pi \rightarrow \pi^*$ transition.[7]

Table.15. Electronic spectral data

No.	Compound	Band nm	cm^{-1}	Assignments
1.	$C_{20}H_{17}N_3O_4$	254	38461	$\pi \rightarrow \pi^*$

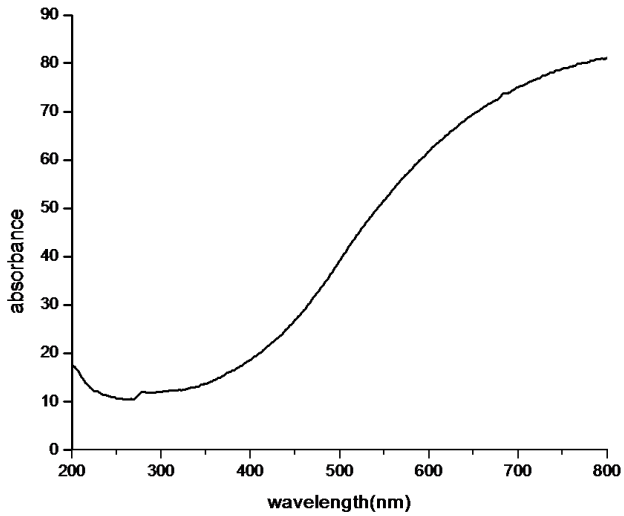

Fig.22. Electronic spectrum of HBH ligand

5.4.1Preparation of the transition metal complexes

The metal complexes were prepared by adding the metal acetate/chloride solution drop wise to the hot ethanolic solution of HBH solution. A pinch of sodium acetate trihydrate was added and was refluxed for 1 hour, and cooled to room temperature. The crystalline precipitate was collected and washed several times with water and dried in dessicator.

5.5.1 Characterization of the transition metal complexes

The metal complexes were found to be insoluble in water and soluble in dilute hydrochloric acid and partially soluble in organic solvents like alcohol, DMF, DMSO, etc. The complexes undergo elemental analysis, magnetic measurements, electronic and infrared spectral studies, molar conductance measurements and thermal analysis. The data obtained helped to predict the properties, structure and geometries of the complexes.

5.5.1.1 Elemental Analysis

The elemental analysis of the metal complexes was conducted by the standard methods.[8] CHN analysis carried out to found the percentage of carbon, hydrogen and nitrogen. Ligand act as both bidentate and tridentate in some metal complexes. The metal complexes are formed in both 1:1 and 1:2 ratios. The details of the metal complexes are described intable.16and its further details are discussed in the following sections.

Table.16. Molecular formulae, colours, elemental analysis data, conductivity and magnetic moments of the complexes

Compound	Molecular Weight	Melting point	Colour	yield	Ω^{-1}	μ_{eff}	M%
$C_{20}H_{19}N_3O_4$ (HBH)	365.4	292^0	Pale yellow	80	2.6	-	-
$Cr(BH)(CH_3COO)_4$	639.99	$>300^0$	Dark green	60	3.8	1.62	8.12 (8.23)
$Mn(BH)(CH_3COO)_4$	642.94	$>300^0$	Light brown	70	3.5	5.56	8.54 (8.82)
$Fe(BH)(H_2O)_2Cl_2$	514.75	$>300^0$	Light brown	70	6.8	3.82	10.84 (10.56
$Co(BH)(H_2O)_4$	482.93	$>300^0$	Pink	60	5.6	4.26	12.20 (12.44)
$Ni(BH)_2(H_2O)_2$ $(CH_3COO)_2$	564.69	$>300^0$	Bluish green	60	4.9	2.98	10.39 (10.42)
$Cu(BH)(H_2O)_4$	487.55	$>300^0$	Brown	80	7.8	1.78	13.03 (12.92)
$Zn(BH)(H_2O)_4$	487.37	$>300^0$	White	70	8.1	DIA	13.002 (13.12)
$Cd(BH)(H_2O)_2$	500. 41	$>300^0$	White	60	5.6	DIA	22. 46 (23.19)

5.5.1.2 Infrared studies

The characteristic IR spectra of the metal complexes of the spectra are given in Table.17and IR sepctra is represented in fig.23-26.The IR band in the region 3400-3600 cm^{-1} due to υ (OH) remains in the metal complexes indicating that the hydrogen atom of the OH group of the water molecules which is further supported by the peaks at 800 cm^{-1} region[9,10].The C-O stretch at 1172 cm^{-1} is red shifted to 1170-1200 cm^{-1} suggests the participation of enolic –OH in the complexation. The bands at 1652 cm^{-1} and 1492 cm^{-1} assigned to the υ (COO_{asymm}) and υ (COO_{symm}) respectively, a shift to lower frequencies indicating the reduction of electron density in

the oxygen in carboxylate group when coordinate to the metal ion. The difference between υ (COO_{asymm}) and υ (COO_{symm}) is greater than 140 cm^{-1} suggesting unidentate nature of acetate group. New absorption bands in the region 500-700 cm^{-1} assigned to υ (M-O) stretching vibrations[11-13].

Table.16. IR spectral assignments of the metal complexes

No.	Compound	υ (O-H)	υ (N-H)	υ (COO_{asymm})	υ (COO_{symm})	υ (H_2O)	υ(M-O)
1.	$C_{20}H_{19}N_3O_5$	-	3367	1652	1402	-	-
2.	$Cr(BH)(CH_3COO)_4$	3606	3410	1794	1415	-	530
3.	$Mn(BH)(CH_3COO)_4$	-	3434	1639	1412	-	520
4.	$Fe(BH)(H_2O)_2Cl_2$	-	3433	1631	1496	853	434
5.	$Co(BH)(H_2O)_4$	3621	3497	1641	1446	821	545
6.	$Ni(BH)_2(H_2O)_2(CH_3COO)_2$	3640	3432	1591	1491	754	460
7.	$Cu(BH)(H_2O)_4$	-	3408	1592	1468	845	481
8.	$Zn(BH)(H_2O)_4$	-	3409	1598	1410	762	434
9.	$Cd(BH)(H_2O)_2$	3606	3410	1594	1415	858	447

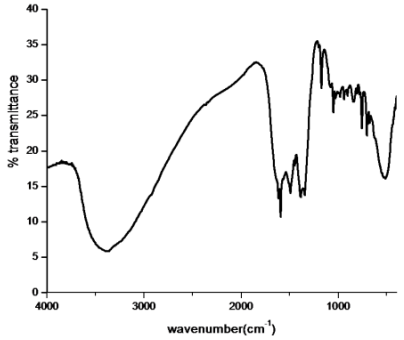

Fig.23. **IR spectrum of CrBH complex**

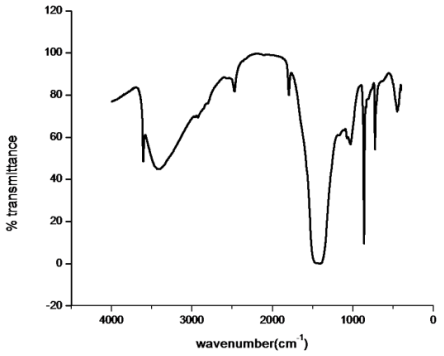

Fig.24. **IR spectrum of CdBH complex**

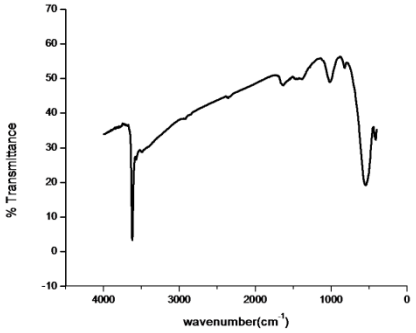

Fig. 25**. IR spectrum of CoBH complex**

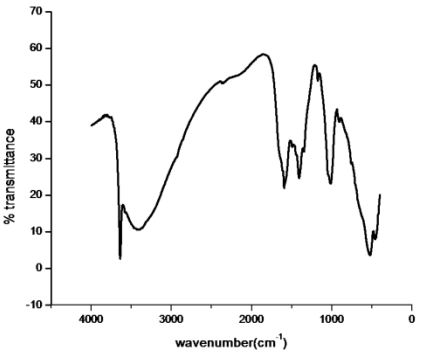

Fig.26. **IR spectrum of NiBH complex**

5.5.1.3 Electronic spectra

The electronic spectrum of the ligand exhibits bands at 254 nm attributed to the n→π* transition. The red shift in the value of the bands during complex formation indicates the involvement of ligand in metal coordination.The electronic spectra is tabulated in table 17.

Chromium (III) ion is having d^3 configuration. They exhibits three spin-allowed transitions i.e. ^4A_2g (F) → ^4T_2g (F) (v_1), ^4A_2g (F) → ^4T_1g (F) (v_2)at 365 nm and 497 nm respectively suggesting the octahedral stereochemistry of the chromium complexes. The electronic spectra of Mn (II) complexes show low intensity weak bands at 200 and 342nm due to n→π* and ^6A_1g →^4Eg (G) respectively, suggests an octahedral field of Mn (II) ion.

In the current work, absorption band of Fe (III) complex are in the range 336 and 388 nm assigned to ^6A_1g→^4A_1g (G) transition. From spectral data, an octahedral geometry is proposed for the Fe (III) chelate.

The electronic spectra Co (II) complexes are characterised by a band near 908-604 nm can be assigned to transition ^4T_1g→^4T2g (υ_1). In addition to this band, a multiple band is observed in the visible region near 426-412 nm can be assigned to ^4T_1g (F) → $^4T_1$ (P) (υ_3) transition[14,15]. The transition ^4T_1g (F) → ^4A_2g (υ_2) is two electron transition and observed at 686-534 nm. In the present work cobalt (II) metal complexes two bands present in electronic spectra of Co (II) at 478 and 660 nm. It is assignable to octahedral geometry. In the present work nickel chelate exhibits three bands in the region 336nm and 510 nm. Using energy level diagram these band are assigned to the transition ^3A_2g (F) → ^3T_2g (F) (υ_1), ^3A_2g (F) → ^3T_1g (F) (υ_2) and ^3A_2g (F) → ^3T_1g (P) (υ_3) respectively, for an octahedral stereochemistry[16].The octahedral geometry of the Cu

(II) complex shows a broad band at 276 nm and is assignable to d-d transition[17,18].

The electronic spectra of Zn (II) and Cd (II) complexes is not possible since there is no unpaired electrons and the'd' sub shell is completely filled. They show charge transfer transitions in the range of 200-340 nm and they are diamagnetic in nature. Most of the complexes are tetrahedral even though some octahedral complexes have also been reported.

Table.17. Electronic spectral bands and their assignments of the metal complexes

Sl.No	Compound	Wave number(nm)	Wavelength(cm^{-1})	Transitions
1	Cr complex	365 497	27397 20120	$^4A_2g(F)\rightarrow {}^4T_2g$ (F) $^4A_2g(F)\rightarrow {}^4T_1g$ (F)
2	Mn complex	200 342	50000 29239	$n\rightarrow\pi^*$ $^6A_1g\rightarrow {}^4A_1g$ (G)
3	Fe complex	336 388	29762 25773	$n\rightarrow\pi^*$ $^6A_1g\rightarrow {}^4A_1g$ (G)
4	Co complex	478 660	20920 15151	$^4T_1g\rightarrow {}^4T_2g$ $^4T_1g\rightarrow {}^4A_2g$
5	Ni complex	336 510	29761 19607	$^3A_2g\rightarrow {}^3T_1g(F)$ $^3A_2g\rightarrow {}^3T_1g(P)$
6	Cu complex	276	36231	$^2E_2g\rightarrow {}^2T_1g$
7	Zn complex	229 262 344	43668 38167 29069	$n\rightarrow\pi^*$ $\pi\rightarrow\pi^*$ $\pi\rightarrow\pi^*$
8	Cd complex	235 340	42553 29411	$n\rightarrow\pi^*$ $\pi\rightarrow\pi^*$

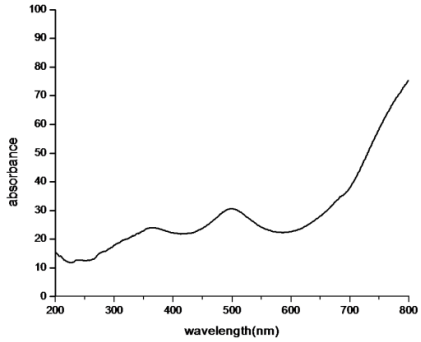

Fig.27. Electronic spectrum of CrBH

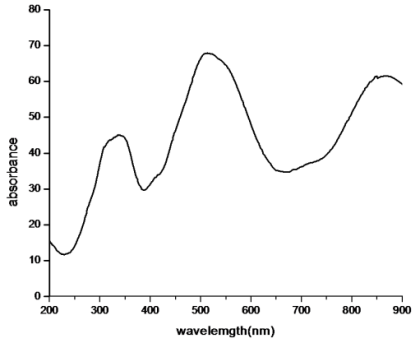

Fig.28. Electronic spectrum of NiBH

5.5.1.4Molar conductance

The molar conductance measurements in DMSO were carried out at a concentration of 10^{-3} solution at 28° C. The HBH ligand and its metal complexes in were observed to be in the range of 4-20ohm^{-1}cm^{2}mol^{-1} and their lower values suggests the non-electrolytic nature[19].

5.5.1.5Magnetic measurements

The magnetic moment values of the complexes helps in the prediction of their structure along with their electronic spectra. The Cr (III) complex possesses magnetic moment of 1.52 BM. It is suggested that if the measured value of the metal complex is in the range of 1.2- 2.5 BM, they possess to have an octahedral geometry. Magnetic moment values of an low spin Mn (II) complex having octahedral geometry are nearly 2.5 BM and that of an high spin Octahedral Mn (II) complex is between 5.64 and 6.15 BM. In the current case the complex possess a value of 4.64 BM which

suggests the octahedral nature of the complex. Fe (III) complex have a magnetic moment value of 3.82 BM which corresponds to three unpaired electrons and they possess to have an octahedral geometry. Co(II) complexes with one unpaired electron can either form octahedral as well as square planar complexes but complexes with three unpaired electrons may form either tetrahedral or octahedral complexes. In the present case Co (II) complex have a magnetic moment value of 4.32 BM suggesting their octahedral geometry[20]. Octahedral Ni (II) complexes have a magnetic moment values in the range of 2.60-3.30BM, due to spin-orbit coupling or higher state mixing with ground state. The Ni (II) complex with a magnetic moment value of 3.38 BM indicates its octahedral geometry[21]. The magnetic moment value of copper complex is 1.25 BM corresponding to their one unpaired electron suggesting their octahedral geometry[22]. Zn (II) complex and Cd (II) complexes are diamagnetic in nature.

5.5.1.6Thermal analysis

The metal complexes were subjected to thermal studies with the aid of TG-DTA, DTG data. The data provides information about the kinetic parameters, mechanism of decomposition and probable assignments in the decomposition curve. The kinetic parameters studied by non isothermal method and discussed in part II.

5.5.1.7X-ray diffraction

The XRD pattern of the ligand and metal complexes gives a brief account of crystal lattice structure, interplanar distance, crystalline size etc. PXRD studies were discussed in part III.

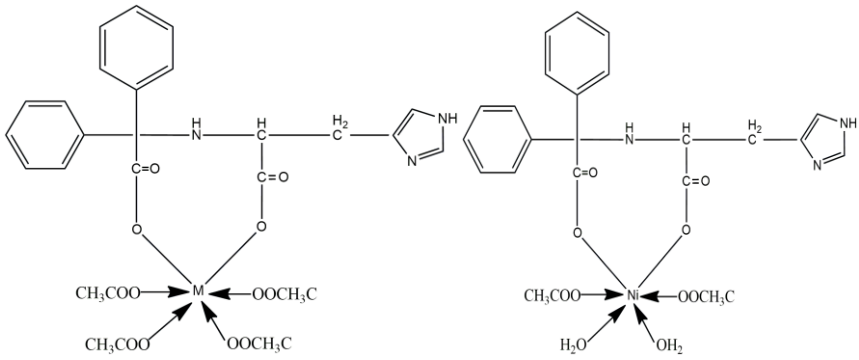

M=Mn

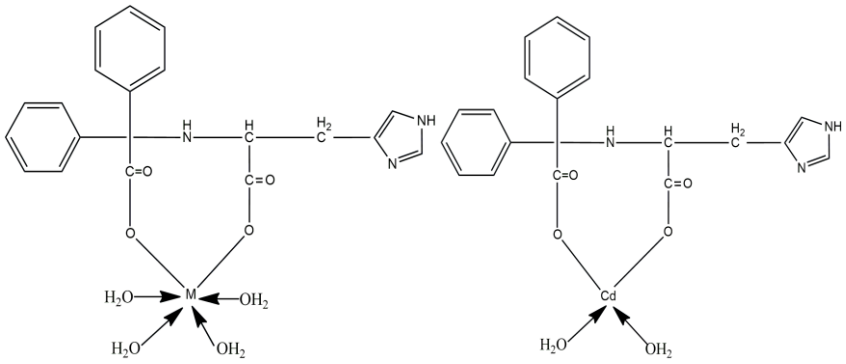

M=Co, Cu, Zn

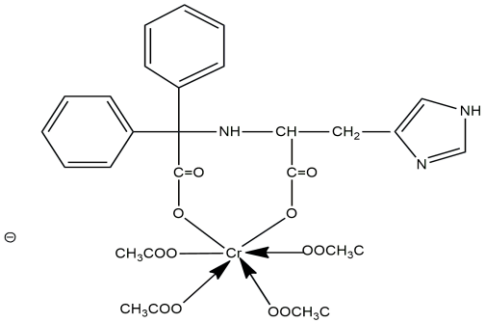

Fig.29. Structure of metal complexes of the ligand HBH

CHAPTER 6

STUDIES ON Cr (III), Mn (II), Fe (III), Co (II), Ni (II), Cu (II), Zn (II), Cd (II) COMPLEXES OF HBV

6.1Introduction

Valine or 2-Amino-3-methylbutanoic acid is an essential amino acid which helps in the biosynthesis of proteins. Valine is a branched chain amino acid which is provided to the body through foods containing protein, such as meats, dairy products, soy products, beans and legumes. Valine was named from valeric acid which is found in the roots of the plant valerian. It was first isolated from casein by the German Chemist Emil Fischer in 1901.Valine is an aliphatic and hydrophobic amino acid in nature. The valine is an insulin resistant and maintains mental vigor, muscle coordination and emotional calm.

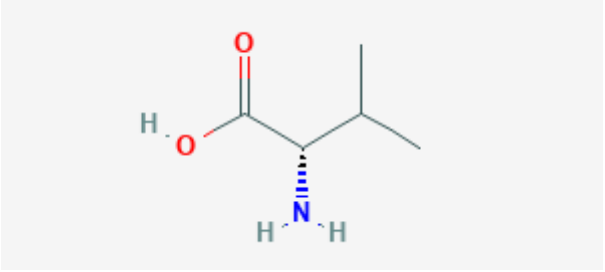

Fig.30. Valine

A tritentate Schiff base ligand derived from o-vanilin and L-valine is complexed with vanadium metal ion in a distorted octahedral

environment and the binding properties of the complex binds to calf thymus DNA have been investigated[31]. N-(salicylidine)-L-valine and its copper complex have been prepared and were characterized by the single crystal XRD, UV-Vis and FTIR[32]. Thermal study and antibacterial activity of the schiff base formed by condensing 4-chlorobenzaldehyde and some amino acid (DL-Alanine, DL-Phenyalalinane and DL-valine) have been reported by Salami et al[33]. One-step synthesis and structural assignment of five new chiral dialkyltin complexes of N-salicylidene-L-valine and its potential to act as a chiral Lewis acid catalyst have been reported by Tian et al[34]. Bencela et al synthesized Ni (II) and Zn (II) meal complexes of schiff base derived from Citral and Valine and the antimicrobial activity was investigated[35].

HBV is a potential bidentate ligand which has been prepared and eight transition metal complexes have also been synthesized. The elucidation of the structure of the HBV ligand and its complexes studied using various spectral and physicochemical methods.

6.2 Experimental

6.2.1 Preparation of HBV

0.1 M solution of diphenyl glycolic acid in aqueous ethanol was mixed with 0.1 M ethanolic solution of valine potassium salt and refluxed for 3 hours on water bath. The resulting solution concentrated for few minutes and the ligand crystallizes out and

washed with ethanol and dried over anhydrous $CaCl_2$. The melting point was found to be 249^0 C.

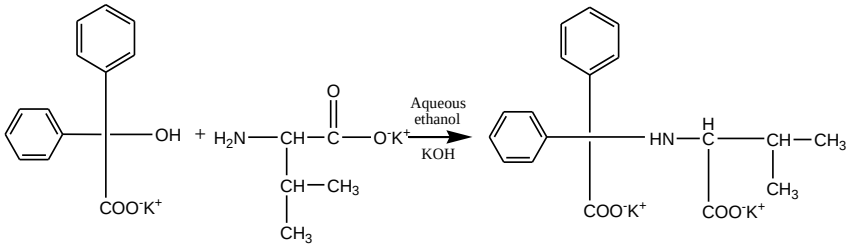

Scheme 4. The reaction pathway of the ligand HBV

6.3 Results and Discussion

6.3.1 Characterization of the ligand

The ligand is characterized by CHN analysis, IR, UV, ^{1}HNMR studies. The description of the ligand is discussed in the following sections.

6.3.1.1 Micro analytical data

The newly synthesized ligand having the molecular formula $C_{19}H_{19}NO_4$ is white crystalline powder. Elemental analysis data is in good agreement with the suggested molecular formula(Table 18).The ligand is soluble in all common solvents such as methanol, ethanol, DMSO, DMF etc.

Table 18 Analytical data of ligand (HBV)

Compound	Molecular Weight	Melting point	Colour	yield	Elemental Analysis Found(Calculated)		
					C	H	N
$C_{19}H_{19}NO_4$	327.39	249^0 C	Pale yellow	80	(70.95)	(4.88)	(3.59)

6.3.1.2. IR spectrum

Table.19 IR spectral data

No.	Compound	υ(O-H)	υ(N-H)	υ(COO_{asymm})	υ(COO_{symm})	υ(C=O)	υ(C-O)
1.	$C_{19}H_{19}NO_4$	3368	3207	1592	1382	1832	1200

The FT-IR spectrum of the ligand was recorded in the range 4000-400 cm^{-1} and presented in fig.31and the IR spectral values are tabulated in table 19. The sharp peak at 3368 cm^{-1} may be attributed to N-H stretching vibration. The bands at 1592 and 1382 cm^{-1} are assigned to υ (COO_{asymm}) and υ (COO_{symm}) respectively. The υ (C=O) band is at 1832 cm^{-1} and the υ (C-O) band is at 1200 cm^{-1}.[6]

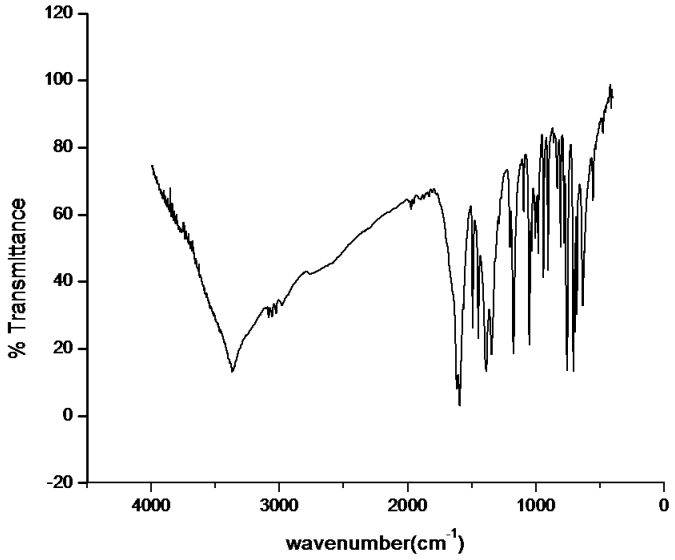

Fig.31. IR spectrum of the HBV ligand

6.3.1.3. Electronic spectrum

The solid state UV-visible spectrum of the ligand was recorded in the region 200-900 nm (fig.32) and values are tabulated in table 20. The compound gives peaks at 260 and 343 nm in which former peak indicates the π→π* transition and the latter may be due to n→π* transition[7].

Table 20. Electronic spectral data

No.	Compound	Band nm	cm^{-1}	Assignments
1.	$C_{19}H_{19}NO_4$	260	38461	π→π*
		343	29154	n→π*

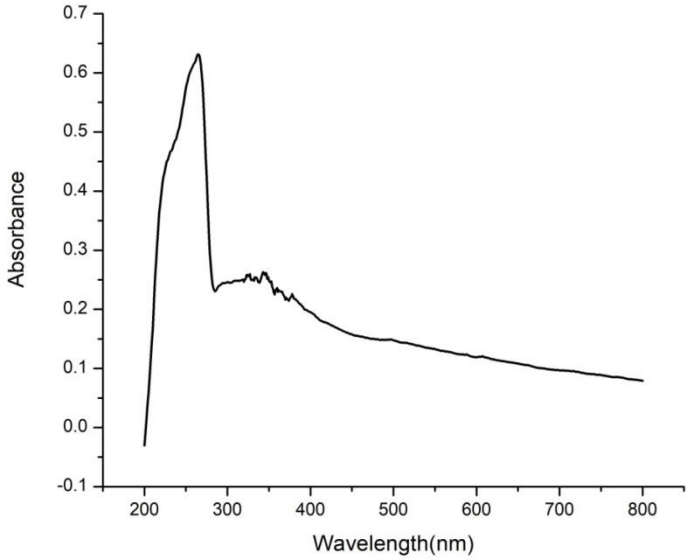

Fig.32. Electronic spectra of ligand

6.2.2 Preparation of the transition metal complexes

The metal complexes were prepared by adding the metal acetate/chloride solution drop wise to the hot ethanolic solution of HBV solution. A pinch of sodium acetate trihydrate was added and was refluxed for 1 hour, and cooled to room temperature. The crystalline precipitate was collected and washed several times with water and dried in dessicator.

6.3.2 Characterization of the transition metal complexes

The metal complexes were found to be insoluble in water and soluble in dilute hydrochloric acid and partially soluble in organic solvents like alcohol, DMF, DMSO, etc. The complexes have undergone elemental analysis, magnetic measurements, electronic

and infrared spectral studies, molar conductance measurements and thermal analysis. The data obtained helped to predict the properties, structure and geometries of the complexes.

6.3.2.1. Elemental Analysis

The elemental analysis of the metal complexes was conducted by the standard methods[8]. CHN analysis carried out to found the percentage of carbon, hydrogen and nitrogen. Ligand act as both bidentate and tridentate in some metal complexes. The metal complexes are formed in both 1:1 and 1:2 ratios. The details of the metal complexes are tabulated in table 21 and further details are tabulated in table 21 and further details aredescribed in the following sections.

Table 21. Molecular formulae, colours, elemental analysis data, conductivity and magnetic moments of the complexes

Compound	**Molecular Weight**	**Melting point**	**Colour**	**yield**	Ω^{-1}	μ_{eff}	**M%**
$C_{19}H_{19}NO_4$(HBV)	327.39	249^0	Pale yellow	80	4.5	-	-
$Cr(BV)(H_2O)_2(CH_3COO)_2$	533.38	$>300^0$	Dark green	60	6.5	1.38	10.32 (10.28)
$Mn(BV)(H_2O)_4$	454.32	$>300^0$	Brown	70	8.3	4.52	10.86 (10.78)
$Fe(BV)(H_2O)_2Cl_2$	554.27	$>300^0$	Reddish brown	70	10.2	3.28	13.38 (13.32)
$Co(BV)_2(H_2O)_2$	749.71	$>300^0$	Pink	60	6.7	4.16	6.82 (6.29)
$Ni(BV)_2(H_2O)_2$	877.69	$>300^0$	Bluish green	60	5.9	3.21	16.96 (16.40)
$Cu(BV)(CH_3COO)_4$	626.93	$>300^0$	Brown	80	7.3	1.29	9.26 (9.58)
$Zn(BV)(CH_3COO)_4$	628.77	$>300^0$	White	70	6.9	DIA	9.82 (9.63)
$Cd(BV)(H_2O)_2$	475.80	$>300^0$	White	60	8.9	DIA	24.02 (23.69)

6.3.2.2. Infrared studies

The characteristic IR spectra of the metal complexes of the spectra are given in Table 22. The IR band in the region 3500-3100 cm^{-1} may be due to υ (NH) stretching vibration of the ligand.The IR band in the region 3400-3600 cm^{-1} due to υ (OH) remains in the metal complexes indicating that the hydrogen atom of the OH group of the water molecules which is further supported by the peaks at 800 cm^{-1} region[9,10]. The C-O stretch at 1200 cm^{-1} is red shifted to 1170-1200 cm^{-1} suggests the participation of enolic –OH in the complexation. The bands at 1590 cm^{-1} and 1344 cm^{-1} assigned to the υ (COO_{asymm}) and υ (COO_{symm}) respectively, a shift to lower frequencies indicating the reduction of electron density in the oxygen in carboxylate group when coordinate to the metal ion. The difference between υ (COO_{asymm}) and υ (COO_{symm}) is greater than 140 cm^{-1} suggesting unidentate nature of acetate group. New absorption bands in the region 500-700 cm^{-1} assigned to υ (M-O) stretching vibrations[11-13] .

Table 22.IR spectral bands and their assignments of the metal complexes

No.	Compound	υ(O-H)	υ (N-H)	$\upsilon(COO_{asymm})$	$\upsilon(COO_{symm})$	$\upsilon(H_2O)$	υ (M-O)
1.	$C_{19}H_{19}NO_4$(HBV)	-	3368	1592	1382	-	552
2.	$Cr(BV)(H_2O)_2(CH_3COO)_2$	3406	-	1492	1346	847	510
3.	$Mn(BV)(H_2O)_4$	3434	-	1653	1447	806	522
4.	$Fe(BV)(H_2O)_2Cl_2$	3428	-	1628	1384	858	428
5.	$Co(BV)_2(H_2O)_2$	3631	3389	1545	1357	837	499
6.	$Ni(BV)_2(H_2O)_2$	3642	3391	1584	1413	804	522
7.	$Cu(BV)(CH_3COO)_4$	-	3328	1559	1374	-	528
8.	$Zn(BV)(CH_3COO)_4$	-	3398	1558	1384	-	425
9.	$Cd(BV)(H_2O)_2$	-	3389	1559	1423	857	418

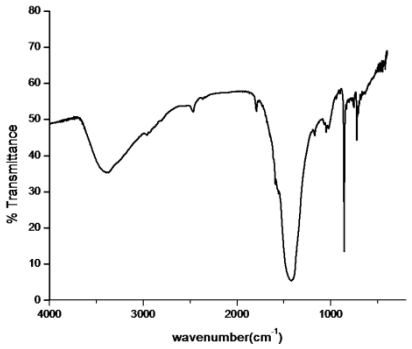

Fig.33. IR spectrum of CdBV ligand

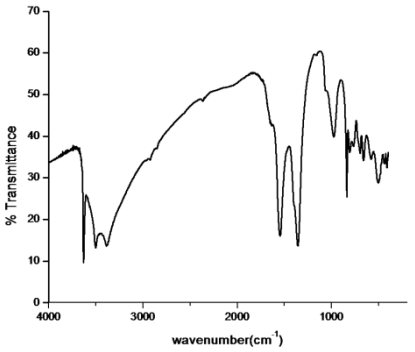

Fig.34. IR spectrum of CoBV ligand

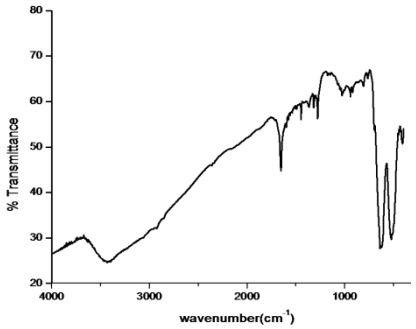

Fig.35. IR spectrum of MnBV ligand

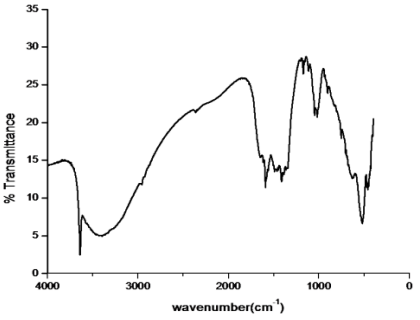

Fig.36. IR spectrum of NiBV ligand

6.3.2.3 Electronic spectra

Electronic spectra of the ligand were recorded in the range 200-900 nm and it exhibits bands at 260 and 343 nm which is attributed to the $\pi \rightarrow \pi^*$ and $n \rightarrow \pi^*$ transitions respectively. The coordination of the metal ion with the ligand is detected by the red shift of these bands.

The bands appearing around 264 nm, 428 nm and 590 nm in the spectra of Chromium (III) complex suggests the octahedral geometry. Here Mn (II) complexes show low intensity weak bands at 432 nm due to $^6A_1g \rightarrow {}^4T_1g$ (G) and 314nm due to $\pi \rightarrow \pi^*$ transitions, and respectively, in an octahedral field of Mn (II) ion.

The absorption band of Fe (III) complex In the range 480 nm assigned to $^5T_2g \rightarrow {}^5Eg$ transition. Two bands observed at 398 and 336 nm due to $^6A_1g \rightarrow {}^4A_1g$ (G) and $\pi \rightarrow \pi^*$ From spectral data, an octahedral geometry is proposed for the Fe (III) chelate.

The electronic spectra of cobalt (II) metal complex give three bands at 252, 331 and 361 nm. It is assignable to octahedral geometry.[14-15] The nickel(II) complexes exhibit two d-d transitions in the electronic spectra at about 674,394 nm and 252 nm due to ^3A_2g (F) $\rightarrow {}^3T_2g$ (P) (υ_1), ^3A_2g (F) $\rightarrow {}^3T_1g$ (F) (υ_2) and $n \rightarrow \pi^*$ transitions respectively[16]. The Cu (II) complex electronic spectrum shows a broad band in the region 478-700 nm and is assignable to d-d transition.[17, 18] The electronic spectra of Zn (II) and Cd (II)

complexes do not show any characteristic d-d transition bands and they are diamagnetic in nature.

Table 23. Electronic spectral bands and their assignments of the metal complexes

Sl.No	Compound	Wave number (nm)	Wavelength (cm^{-1})	Transitions
1	Cr complex	264 428 590	37879 23364 16949	$^4A_2g(F) \rightarrow {}^4T_2g$ (F) $^4A_2g(F) \rightarrow {}^4T_1g$ (F) $^4A_2g(F) \rightarrow {}^4T_1g$ (P)
2	Mn complex	314 432	31847 23148	$n \rightarrow \pi^*$ $^6A_1g \rightarrow {}^4A_1g$ (G)
3	Fe complex	336 398 480	29762 25125 20833	$n \rightarrow \pi^*$ $^6A_1g \rightarrow {}^4A_1g$ (G)
4	Co complex	252 331 361	39682 30211 27700	$^4T_1g \rightarrow {}^4T_2g$ $^4T_1g \rightarrow {}^4A_2g$
5	Ni complex	252 394 674	39682 25380 14836	$n \rightarrow \pi^*$ $^3A_2g \rightarrow {}^3T_1g$(F) $^3A_2g \rightarrow {}^3T_1g$(P)
6	Cu complex	331 356 531	30211 28089 18832	$n \rightarrow \pi^*$ $\pi \rightarrow \pi^*$ $^2E_2g \rightarrow {}^2T_1g$
7	Zn complex	330 347 358	30303 28818 27932	$n \rightarrow \pi^*$ $\pi \rightarrow \pi^*$ $\pi \rightarrow \pi^*$
8	Cd complex	235 341	42553 29325	$n \rightarrow \pi^*$ $\pi \rightarrow \pi^*$

6.3.2.4 Molar conductance

The low molar conductance values of the 10^{-3} solution of the HBV ligand and its metal complexes in DMSO suggest that the complexes behave as non-electrolytes and are neutral in nature.[19]

6.3.2.5Magnetic measurements

The magnetic moment values of the complexes helps in the prediction of their structure along with their electronic spectra. The Cr (III) complex possesses magnetic moment of 1.38 BM. It is suggested that if the measured value of the metal complex is in the range of 1.2- 2.5 BM, they possess to have an octahedral geometry. Magnetic moment values of a low spin Mn (II) complex having octahedral geometry are nearly 2.5 BM and that of a high spin Octahedral Mn (II) complex is between 5.64 and 6.15 BM. In the current case the complex possess a value of 4.52 BM which suggests the octahedral nature of the complex. Fe (III) complex have a magnetic moment value of 3.28 BM which corresponds to three unpaired electrons and they possess to have an octahedral geometry. Co(II) complexes with one unpaired electron can either form octahedral as well as square planar complexes but complexes with three unpaired electrons may form either tetrahedral or octahedral complexes. In the present case Co(II) complex have a magnetic moment value of 4.16 BM suggesting their octahedral geometry.[20] Octahedral Ni(II) complexes have a magnetic moment values in the range of 2.60-3.30BM, due to spin-orbit coupling or higher state mixing with ground state. The Ni(II) complex with a magnetic moment value of 3.21BM indicates its octahedral geometry.[21] The magnetic moment value of copper complex is 1.29 BM corresponding to their one unpaired electron suggesting their octahedral geometry.[22]Zn(II) complex and Cd(II) complexes are diamagnetic in nature.

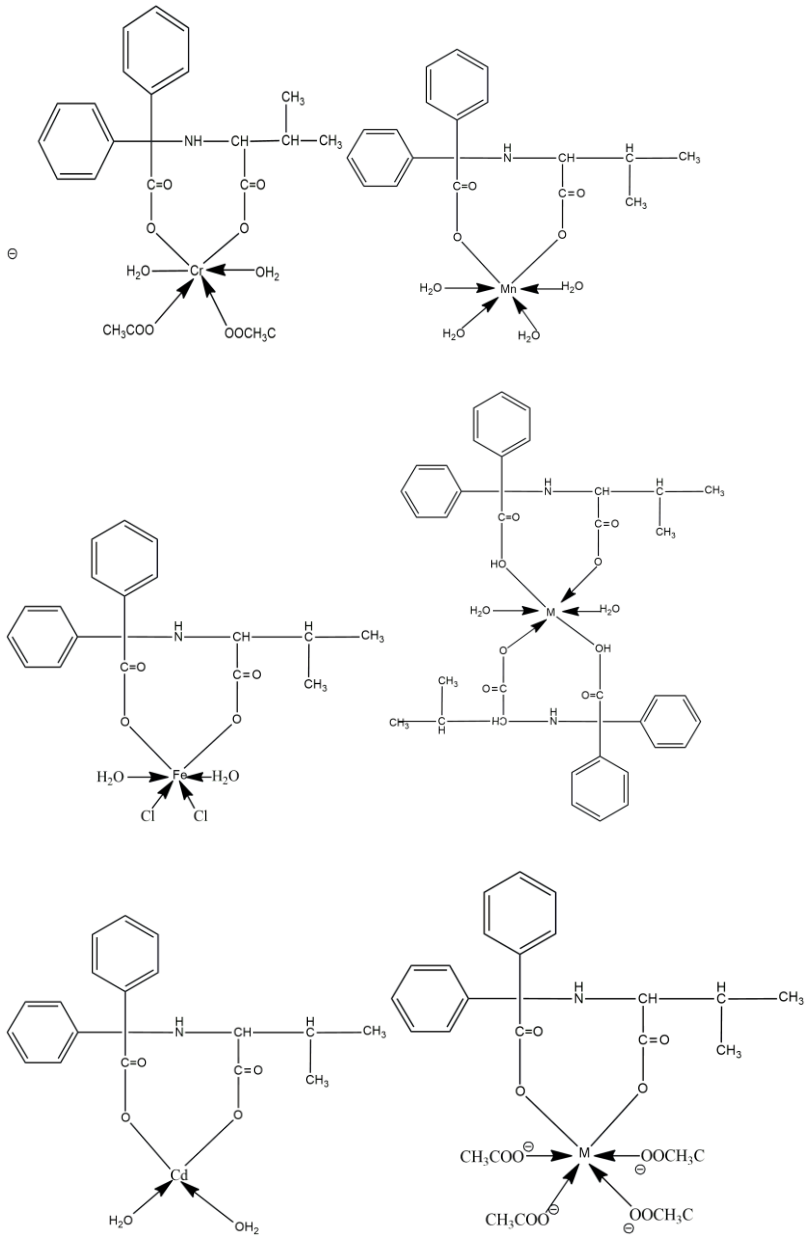

Fig.37. Structure of metal complexes of the ligand HBV

CHAPTER 7

STUDIES ON Cr (III), Mn (II), Fe (III), Co (II),Ni (II), Cu (II), Zn (II), Cd (II) COMPLEXES OF HBL

7.1 Introduction

Leucine or 2-Amino-4-methylpentanoic acid is an essential amino acid which is used in the biosynthesis of proteins. In humans it cannot be synthesized in our body it must be provided through our diet by taking the food such as meats, dairy products, soy products and beans. Leucine exhibit pharmacological activity in humans and shows the ability to stimulate the myofibrillar muscle protein synthesis. This pyruvate family amino acid is important for the blood sugar level regulation, wound healing and growth hormone production.

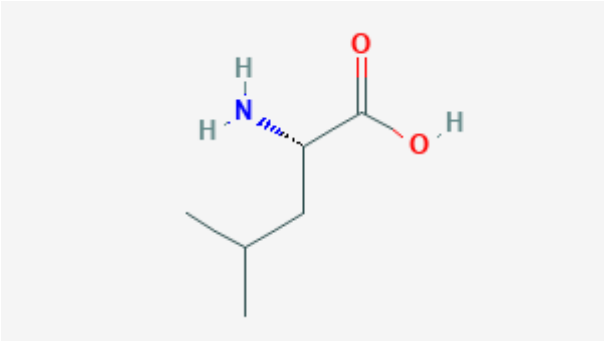

Fig.38. Leucine

The Schiff base ligand derived from the condensation of leucine and 2-acetylpyridine and their metal complexes were synthesized

and characterized by Hosny et al[21]. The antimicrobial study of the leucine derivative with salicyldehyde was studied by Pervaiz[22] and coworkers with different bacterial (Escheria coli, Staphylococcus aureus, Bacillus subbtilis) and fungal strains (Alternaria alternate, Aspergillus flavus and Aspergillus niger). The Fe(II) and Cu(II) complexes of leucine were synthesized and characterized by Asemave[23]. The antibacterial study of these complexes was evaluated by the agar diffusion method. The synthesis and characterization of a series of nickel (II) complexes of Schiff bases obtained by the condensation of 2-hydroxy-3-methylbenzaldehyde and 2, 4-dihydroxy-benzaldehyde with glycine, DL-alanine, DL-valine, DL-methionine, L-leucine, and DL-phenylalanine were reported[24].The theranostic potential of binuclear amino acid Schiff base derived by condensing Leucine and Salicyladehyde was reported[25].

HBL is a potential bidentate ligand which has been prepared and eight transition metal complexes have also been synthesized. The elucidation of the structure of the BT-LEU ligand and its complexes studied using various spectral and physicochemical methods.

7.2 Experimental

7.2.1 Preparation of HBL

0.1 M solution of diphenyl glycolic acid in aqueous ethanol was mixed with 0.1 M ethanolic solution of Leucine potassium salt and

refluxed for 3 hours on water bath. The resulting solution concentrated for few minutes and the ligand crystallizes out and washed with ethanol and dried over anhydrous $CaCl_2$. The melting point was found to be 260^0C .

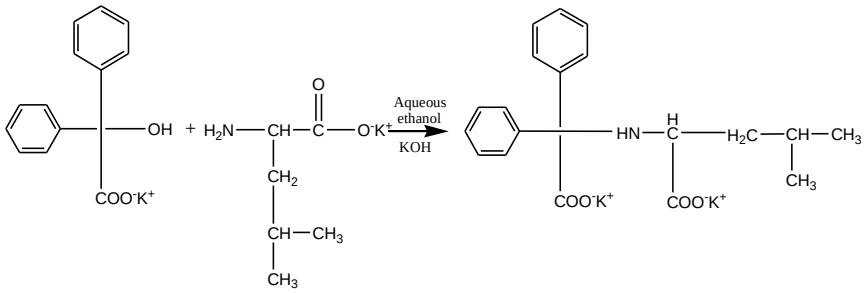

Scheme 5.The reaction pathway of the ligand HBL

7.3 Results and Discussion

7.3.1 Characterization of the ligand

The ligand is characterized by CHN analysis, IR, UV studies. The description of the ligand is discussed in the following sections.

7.3.1.1 Micro analytical data

The newly synthesized ligand having the molecular formula $C_{23}H_{19}NO_5$ is pale yellow in colour. Elemental analysis data is in good agreement with the suggested molecular formula. (Table 25). The ligand is soluble in all common solvents such as methanol, ethanol, DMSO, DMF etc.

Table 25. Analytical data of ligand (HBL)

Compound	Molecular Weight	Melting Point	Colour	yield	Elemental Analysis Found(Calculated)		
					C	H	N
$C_{20}H_{21}NO_4$	341.41	260^0	Pale yellow	80	71.02 (70.29)	6.89 (6.73)	4.23 (4.1)

7.3.1.2 IR spectrum

Table 26.IR spectral data

No.	Compound	υ (O-H)	υ (N-H)	υ (COO_{asymm})	υ (COO_{symm})	υ (C=O)	υ (C-O)
1.	$C_{20}H_{21}NO_4$	3398	-	1617	1388	1732	1174

The FT-IR spectrum of the ligand was recorded in the range 4000-400 cm^{-1} and presented in fig.39. The broad band at 3398cm^{-1} is assigned to the O-H stretching vibration of phenolic oxygen. The N-H stretching bands were overlapped by the O-H stretching vibration. The bands at 1617 and 1388 cm^{-1} are assigned to υ (COO_{asymm}) and υ (COO_{symm}) respectively. The υ (C=O) band is at 1732 cm^{-1} and the υ (C-O) band is at 1174 cm^{-1}.[6]

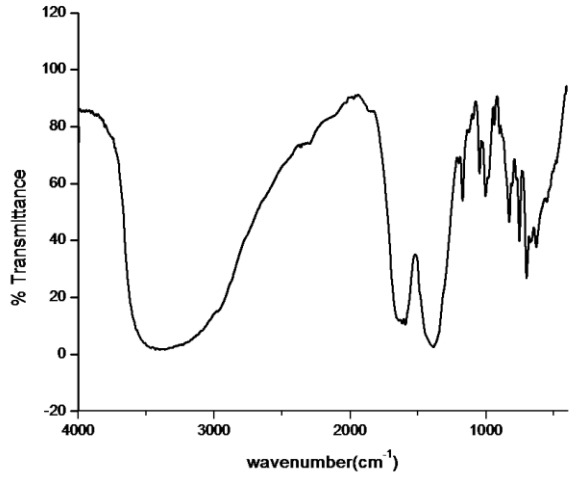

Fig.39. IR spectrum of the ligand

7.3.1.3 Electronic spectrum

The solid state uv-visible spectrum of the ligand was recorded in the region 200-900 nm (fig.40) and spectral data are tabulated in table 27.The compound gives peaks at 260 and 867 nm in which former peak indicates the π→π* transition and the latter may be due to n→π* transition.[7]

Table 27. Electronic spectral data

No.	Compound	Band nm	cm^{-1}	Assignments
1.	$C_{20}H_{21}NO_4$	264	38461	π→π*
		325	11534	n→π*
		361	30303	n→π*

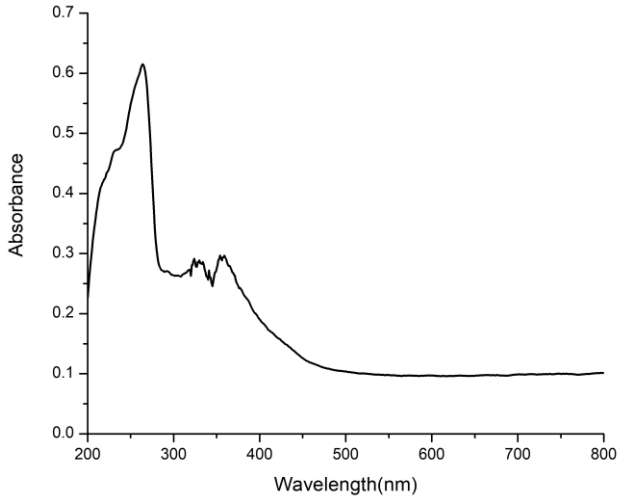

Fig.40. UV spectrum of the ligand

7.3.2Preparation of the transition metal complexes

The metal complexes were prepared by adding the metal acetate/chloride solution dropwise to the hot ethanolic solution of HBL solution. A pinch of sodium acetate trihydrate was added and was refluxed for 1 hour, and cooled to room temperature. The crystalline precipitate was collected and washed several times with water and dried in dessicator.

7.3.3 Characterization of the transition metal complexes

The metal complexes were found to be insoluble in water and soluble in dilute hydrochloric acid and partially soluble in organic solvents like alcohol, DMF, DMSO, etc. The complexes have

undergone elemental analysis, magnetic measurements, electronic and infrared spectral studies, molar conductance measurements and thermal analysis. The data obtained helped to predict the properties, structure and geometries of the complexes.

7.3.3.1 Elemental Analysis

The elemental analysis of the metal complexes was conducted by the standard methods.[8]. CHN analysis carried out to found the percentage of carbon, hydrogen and nitrogen. Ligand act as both bidentate and tridentate in some metal complexes. The metal complexes are formed in both 1:1 and 1:2 ratios. The details of the metal complexes are tabulated in table 28 and further details are described in the following sections.

Table.28. Molecular formulae, colours, elemental analysis data, conductivity and magnetic moments of the complexes

Compound	Molecular Weight	Melting point	Colour	yield	Ω^{-1}	μ_{eff}	M%
$C_{20}H_{23}NO_4$ (HBL)	341.41	260^0	White	80	2.8	-	-
$Cr(BL)(H_2O)_2)(CH_3COO)_2$	487.99	$>300^0$	Dark green	70	6.5	1.56	10.69 (10.65)
$Mn(BL)(H_2O)_4$	467.94	$>300^0$	Brown	60	6.8	5.08	11.74
$Fe(BL)(H_2O)_2Cl_2$	554.27	$>300^0$	Light brown	70	8.9	3.76	11.07 (11.92)
$Co(BL)_2(H_2O)_2$	776.93	$>300^0$	Pink brown	60	7.8	4.38	7.58 (7.62)
$Ni(BL)_2(H_2O)_2$	776.69	$>300^0$	Bluish green	60	8.5	3.27	7.55
$Cu(BL)(H_2O)_2)(CH_3COO)_2$	558.55	$>300^0$	Grey	70	7.2	1.42	11.37
$Zn(BL)(H_2O)_4$	476.37	$>300^0$	White	60	16.4	DIA	13.3026
$Cd(BL)(H_2O)_2$	489. 41	$>300^0$	White	60	12.7	DIA	22.9686

7.3.3.2Infrared studies

The characteristic IR spectra of the metal complexes of the spectra are given in Table 29 and the IR spectrum shown in figure 41-46. The IR band in the region 3500-3100 cm^{-1} due to υ (OH) of coordinated in the metal complexes indicating that the hydrogen atom of the H_2O group is attached to the metal.[9,10] The C-O stretch at 1174 cm^{-1} is red shifted to 1100-1150 cm^{-1} suggests the participation of enolic –OH in the complexation. The bands at 1617 cm^{-1} and 1388 cm^{-1} assigned to the υ (COO_{asymm}) and υ (COO_{symm}) respectively, a shift from the values indicates the binding of oxygen in carboxylate group when coordinate to the metal ion. The difference between υ (COO_{asymm}) and υ (COO_{symm}) is greater than 140 cm^{-1} suggesting unidentate nature of acetate group. New absorption bands in the region 460-560 cm^{-1} assigned to υ (M-O) stretching vibrations.[11-13]

Table 29. IR spectral assignments of the metal complexes

No.	Compound	υ(O-H)	υ (N-H)	υ(COO_{asymm})	υ(COO_{symm})	υ(H_2O)	υ (M-O)
1.	$C_{20}H_{23}NO_4$ (HBL)	3398	-	1617	1388	-	-
2.	$Cr(BL)(H_2O)_2)(CH_3COO)_2$	-	3411	1629	1385	835	543
3.	$Mn(BL)(H_2O)_4$	-	3359	1598	1318	812	498
4.	$Fe(BL)(H_2O)_2Cl_2$	-	3418	1624	1384	798	432
5.	$Co(BL)_2(H_2O)_2$	3631	3501	1546	1360	837	504
6.	$Ni(BL)_2(H_2O)_2$	3641	3357	1636	1409	828	547
7.	$Cu(BL)(H_2O)_2)(CH_3COO)_2$	-	3318	1610	1396	853	571
8.	$Zn(BL)(H_2O)_4$	-	3325	1653	1367	810	561
9.	$Cd(BL)(H_2O)_2$	3407	-	1796	1416	857	458

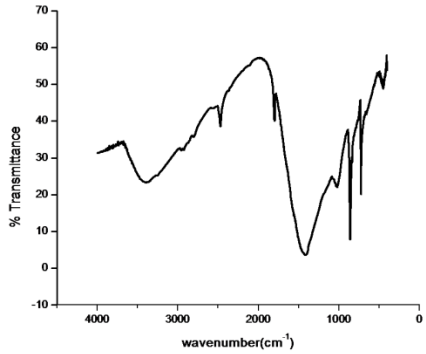

Fig.41. IR spectrum of the CdBL complex

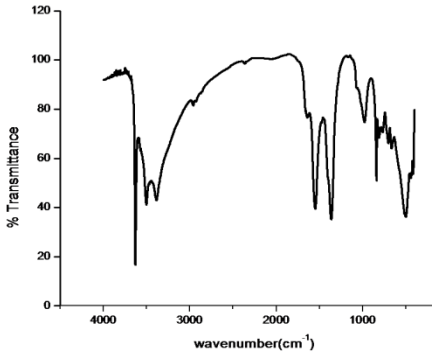

Fig.42. IR spectrum of the CoBL complex

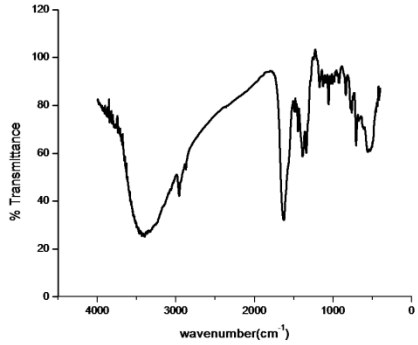

Fig.43. IR spectrum of the CrBL complex

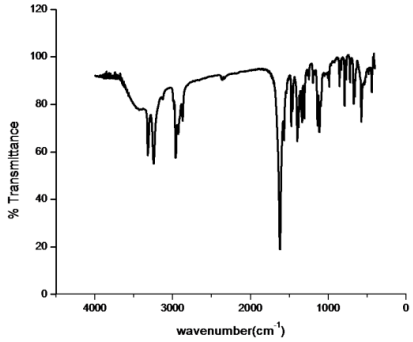

Fig.44. IR spectrum of the CuBL complex

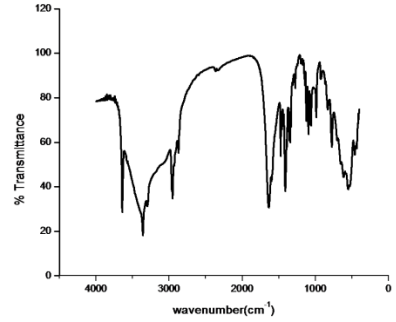

Fig.45. IR spectrum of the NiBL complex

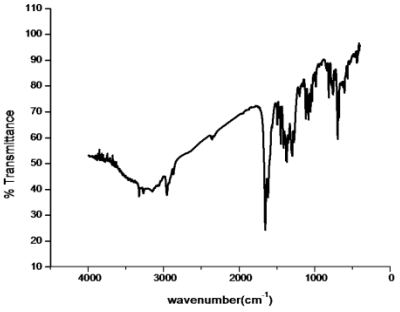

Fig.46. IR spectrum of the ZnBL complex

7.3.3.3 Electronic spectra

The electronic spectrum of the ligand was recorded in the range 200-900 nm and it exhibits bands at 264,325 and 361 nm. The bands attributed to the $\pi \rightarrow \pi^*$ and $n \rightarrow \pi^*$ transitions respectively. The shift in the value of the bands from the ligand to the complexes explains the metal coordination with the ligand and is tabulated in table 30.

Chromium (III) ion is having d^3 configuration and they exhibits three spin-allowed transitions i.e. ^4A_2g (F) $\rightarrow$ ^4T_2g (F) (v_1), ^4A_2g (F) $\rightarrow$ ^4T_1g (F) (v_2), ^4A_2g (F) $\rightarrow$ ^4T_1g (P) (v_3) at 251 nm, 430 nm and 575 nm respectively suggesting the octahedral stereochemistry of the chromium complexes. In the study Mn (II) complexes show low intensity weak bands at 265 nm due to the $\pi \rightarrow \pi^*$ transition and other band at 342 nm due to $^6A_1g \rightarrow ^4A_1g$ (G) transition in an octahedral field of Mn (II) ion.

The Fe (III) complex spectra consists of three bands at in the range 507 nm assigned to $^5T_2g \rightarrow ^5Eg$ transition. From spectral data, an octahedral geometry is proposed for the Fe (III) chelate. In the present work cobalt (II) metal complexes exhibits two bands in electronic spectra of Co (II) at 400 and 507 nm. It is assignable to octahedral geometry.[16]

In this study nickel(II) complexes having bands in the region 66 nm, 392 nm and 329 nm assigned to the transition ^3A_2g (F) $\rightarrow$ ^3T_2g (F) (υ_1), ^3A_2g (F) $\rightarrow$ ^3T_1g (F) (υ_2) and $n \rightarrow \pi^*$ respectively suggesting the octahedral stereochemistry of the Ni(II) chelates.[17]

The broad band at 504 nm is assignable to d-d transition which is in agreement with an octahedral geometry of the Cu (II) complex.[18] The Zn (II) and Cd (II) complexes showed bands almost similar to ligands and they are diamagnetic in nature

Table.30. Electronic spectral bands and their assignments of the metal complexes

Sl.No	Compound	Wave number (nm)	Wavelength (cm^{-1})	Transitions
1	Cr complex	251 430 575	39840 23255 17391	$^4A_2g(F)\rightarrow {}^4T_2g$ (F) $^4A_2g(F)\rightarrow {}^4T_1g$ (F) $^4A_2g(F)\rightarrow {}^4T_1g$ (P)
2	Mn complex	265 342 408 492	37735 29239 24510 20325	$n\rightarrow\pi^*$ $^6A_1g\rightarrow {}^4A_1g$ (G)
3	Fe complex	330 371 507	30303 26954 19723	$n\rightarrow\pi^*$ $^6A_1g\rightarrow {}^4A_1g$ (G)
4	Co complex	255 331 400 533	39215 30211 25000 18761	$n\rightarrow\pi^*$ $\pi\rightarrow\pi^*$ $^4T_1g\rightarrow {}^4T_2g$ $^4T_1g\rightarrow {}^4A_2g$
5	Ni complex	225 329 392 666	44444 30395 25510 15015	$n\rightarrow\pi^*$ $\pi\rightarrow\pi^*$ $^3A_2g\rightarrow {}^3T_1g(F)$ $^3A_2g\rightarrow {}^3T_1g(P)$
6	Cu complex	267 365 504	37453 27397 19841	$n\rightarrow\pi^*$ $\pi\rightarrow\pi^*$ $^2E_2g\rightarrow {}^2T_1g$
7	Zn complex	226 259 344	44247 38610 29069	$n\rightarrow\pi^*$ $\pi\rightarrow\pi^*$ $\pi\rightarrow\pi^*$
8	Cd complex	272	36764	$\pi\rightarrow\pi^*$

7.3.3.4 Molar conductance

The molar conductance values of the 10^{-3} solution of the HBL ligand and its metal complexes in DMSO were observed are in the range of 4-20ohm^{-1}cm^{2}mol^{-1} and the low values of conductance suggest that the complexes behave as non-electrolytes and are neutral in nature.[19]

7.3.3.5 Magnetic measurements

The magnetic moment values of the complexes helps in the prediction of their structure along with their electronic spectra. The Cr (III) complex possesses magnetic moment of 1.56 BM. It is suggested that if the measured value of the metal complex is in the range of 1.2- 2.5 BM, they possess to have an octahedral geometry. Magnetic moment values of an low spin Mn (II) complex having octahedral geometry are nearly 2.5 BM and that of an high spin Octahedral Mn (II) complex is between 5.64 and 6.15 BM. In the current case the complex possess a value of 5.08 BM which suggests the octahedral nature of the complex. Fe (III) complex have a magnetic moment value of 3.76 BM which corresponds to three unpaired electrons and they possess to have an octahedral geometry. Co(II) complexes with one unpaired electron can either form octahedral as well as square planar complexes but complexes with three unpaired electrons may form either tetrahedral or octahedral complexes. In the present case Co (II) complex have a magnetic moment value of 4.38 BM suggesting their octahedral

geometry.[20] Octahedral Ni (II) complexes have a magnetic moment values in the range of 2.60-3.30BM, due to spin-orbit coupling or higher state mixing with ground state. The Ni (II) complex with a magnetic moment value of 3.27 BM indicates its octahedral geometry.[21] The magnetic moment value of copper complex is 1.42 BM corresponding to their one unpaired electron suggesting their octahedral geometry.[22]Zn(II) complex and Cd(II) complexes are diamagnetic in nature.

7.3.3.6 Thermal analysis

The metal complexes were subjected to thermal studies with the aid of TG-DTA, DTG data. The data provides information about the kinetic parameters, mechanism of decomposition and probable assignments in the decomposition curve. The kinetic parameters studied by non isothermal method and discussed in Part II.

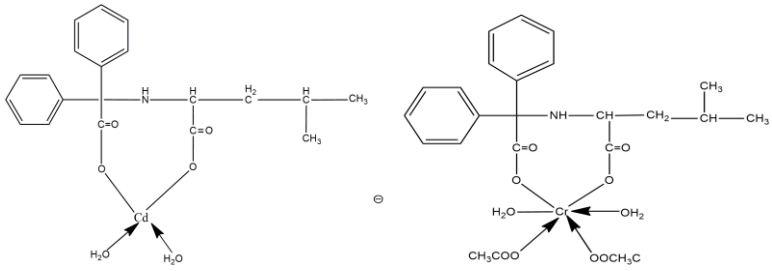

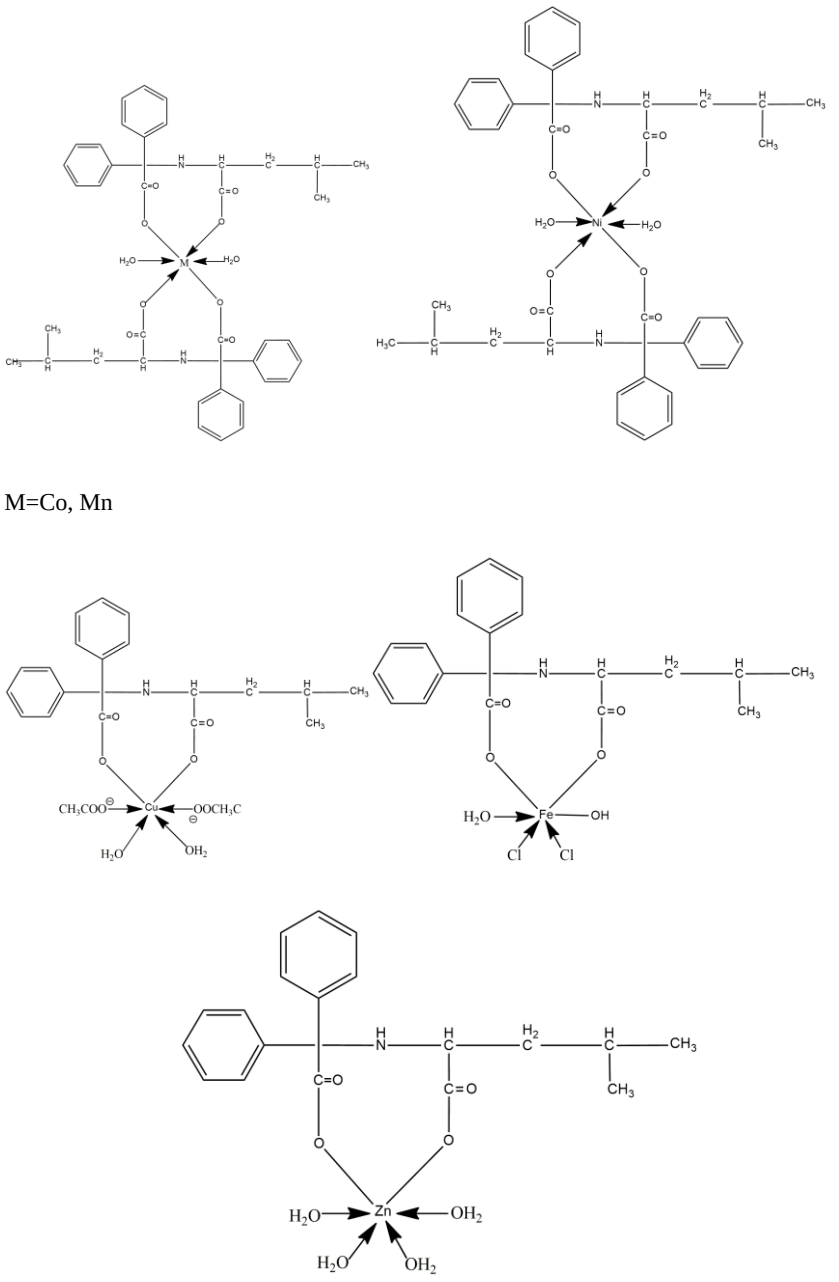

Fig.47. Structure of metal complexes of the ligand HBL

References

1. Wojciechowska, A., Daszkiewicz, M., Staszak, Z., Zdybek, A. T., Bienko, A., & Ozarowski, A., (2011). *Inorg. Chem.,* 50, 11532.

2. Baul, T. S.B., Kehie, P., Duthie, A., Wang, R., Englert, U., & Hopfl, H. (2017). *J. Organomet. Chem*., 828, 96.

3. Rathgeb, A., Bohm, A., Novak, M. S., Gavriluta, A., Domotor, O., Tommasino, J.B., Enyedy, E. A., Shova, S., Meier, S., Jakupec, M. A., Luneau, D., & Arion, V. B. (2014). *Inorg. Chem*., 53, 2718.

4. Reddy, P. R., & Shilpa, A. (2011). *Polyhedron*, 30, 565.

5. Chen, L., Wang, L., An, W., Wang, R., &Tian, L. (2020). *Inorg. Nano-Met. Chem.,* 50, 872.

6. Soliman, A. A., & Linert, W. (1999).*Thermochim.Acta.,* 338, 67.

7. Sutton,D. (1968). "Electronic spectra of metal complexes", McGraw Hill, London.

8. Vogel, A. I. (1961). A Text book of Quantitative Inorganic Analysis", ELBS & Longman, London.

9. Ferrare, J. R. (1971). Low Frequency Vibration of Inorganic & Coordination Compounds", Plenum press, New York .

10. Biradar, N.S., & Kulkurni, V.H. Z. (1971). *Inorg. Ally. Chem*., 33, 3847.

11. Sharma, B. C. & Patel, C. C. (1970). *Indian J. Chem.,* 8 , 747.

12. Nakamato, K. (1966). "Infrared spectra of Inorganic and Coordination compound". John Wiley, New York .

13. Bellamy, L. J. (1978). "The Infrared Spectra of Complex Molecule", Chapman and Hall London.

14. Jorgensen, C.K., Cox, R. A., & Peacocke, A. R. (1956). *Acta.Chem. Scand*.,10, 887.

15. Saaco, A., & Cotton, F. A., (1962). *J. Am. Soc*., 84, 2043.

16. Lever, P. A. B. (1968). "Inorganic Electronic Spectroscopy", Elsevier, London.

17. Geary, W.J. (1971). *Coord. Chem.Rev*.,7, 81.

18. Lewis, J., & Wilkins, R.G. (1969). "The Magneto chemistry of Complex Compounds in Coordination Chemistry," Interscience, New York .

19. Earnshow, A. (2013). " Introduction to Magneto Chemistry." Academic Press, London.

20. Figgis, B. N., & Ngholm, R. S. (1958). *J. Amer. Chem. Soc*., 41.

21. Xometl, O. O., Likhanova, N.V., Aguilar, M.A.D., Arce, E., Dorantes, H. & Lozad, P. A. (2008). *Mater. Chem. Phys*, 110, 344.

22. Zhang, X., Zhang, Y., Yang, L., Yang, R., & Jin, D. (2000). *Synth. React. Inorg. Met.-Org. Chem*, 30,45.

23. Singh, H. L. & Singh, J. (2014). *Bioinorg. Chem. Appl*., 2014.

24. Hamza, U., Uzairu, A., Sallau, M.S., & Abechi, E.S. (2015). *Der Chemica Sinica*, 6, 25.

25. Amira, A. J., & Miaa, A. A. (2014). *Res. J. Chem. Sci.,* 4, 25.

26. Al-Saadawy, N. H., Alyassin, F. F., & Faraj, H. R. (2016). *Global J. Pure Appl. Chem.* Res., 4, 13.

27. Ariadna, G. O., Carlos, C. C., Teresita, S. E., Irma, R. O., Raul, G. L.L., Carrillo, A. G., & Ramirez, M. A. V. (2013). *Bioinorg. Chem. Appl*.

28. El-Baradie, K. Y., El-Wakiel, N. A., & El-Ghamry, H. A. (2014). *Appl. Organometal. Chem.,* 29,117.

29. Sebastian, M. , Arun, V., Robinson, P. P., Leeju, P., Varsha, G., Varghese. D., & Yusuff, K. K. M. (2011). *J. Coord. Chem.*, 64, 525.

30. Neelofar, N., Ali, N., Khan, A., Amir, S., Khan, N. A. & Bilal, M. (2017). *Bull. Chem. Soc. Ethiop.*,31, 445.

31. Guo, Q., Li, L., Dong, J., Liu, H., Xu, T., & Li, J. (2013). *Spectrochim Acta A Mol Biomol Spectrosc*.,106, 155.

32. Lakshmi, S. S., & Geetha, K. (2016).*J. Crystallography*.

33. Bushra, K.A.S., Raghed, A.G., & Kahtan, A.A. (2017). *Adv. Appl Sci Res*., 8, 4.

34. Tian, L., Wang, R., Zhang, J., & Qiu, F. Z. Y. (2018). *Main Group Met. Chem.*, 43, 138.

35. Bencela, M., Kumari, S. S. & Parmila, T.S. (2019). *Spectroscopic Analysis*, 6, 12.

36. Nasser, M. H., & Farid, I. E. D. (2008). *J. Chem. Eng. Data*, 53, 2567.

37. Pervaiz, M., Ahmad, I., Yousaf, M., Kirn, S., Munawar, A., Saeed, Z., Adnan, A., Gulzar, T., Kamal, T., Ahmad, A. & Rashid, A. (2019).*Spectrochim Acta A Mol Biomol Spectrosc*., 206, 642.

38. Asemave, K., Anhwange, B. A., & Anom, T.J. (2015). *Int. J. Sci. Res.*, 4, 1527.

39. Wang, G., & Chang, J. C. (1994). *Synth React Inorg MetOrg Chem.*, 24, 1091.

40. Thamaraikannan, T., Rubiga, M., Jayalakshmi, R., & Rajavel, R. (2017). *IOSR-J.Appl. Chem*.,10,01.

PART II

THERMAL STUDIES OF THE SELECTED DIPHENYL GLYCOLIC ACID -AMINO ACID METAL COMPLEXES

CHAPTER 1

INTRODUCTION

The human era began with the mesmerizing effect of heat on materials. The physical changes that occurred to the materials during heating are unique to that specific material. So the analysis of the thermal property of the materials provides information regarding them. The history of thermal analytical studies dates back to the 19^{th} century. Thermal data impart the details of the changes in the macroscopic properties such as temperature (T), pressure (P), enthalpy (H), entropy (S) and Gibb's energy (G). Techniques that monitor any specific property of the materials as a function of temperature are the thermal analysis method and the most important techniques are: Thermogravimetry (TG), Differential thermal analysis (DTA) and Differential scanning calorimetry (DSC) [1-7]. The progress in the thermal analysis begins from the last half of the 20^{th} century[8]. The application in the field of catalysis, hazards evaluation and measuring important physical properties quickly with enhanced precision made the technique more relevant.

Recent thermal analysis techniques such as micro thermal analysis, pulsed thermal analysis and fast scanning calorimetry have become popular nowadays. In addition sample controlled thermal analysis (SCTA) or controlled rate thermal analysis (CRTA) have been reported in which the rate of sample property changes is controlled

in some modes by controlling the sample temperature which is a reverse concept of conventional method[9-14]. A highly sensitive quartz crystal microbalance/heat conduction calorimeter has recently emerged. The combination of IR, Raman, XPS, dispersive X-ray with the thermal properties helps in detecting changes in composition and molecular structure in more precise manner. '3D thermal analysis' by Ozawa convey the results in three dimensions. Duval[15], Smoothers and Yao Chiang[16], Mackenzic[17, 18], Schulze[19] and Garn[20] describe about the thermal analytical methods and their instrumentation procedures in detail in their books. TG and DTA which are used in the current study are outlined in the section.

1.1 Thermogravimetry

Thermogravimetry is one of the most important thermal analysis methods that monitors the sample mass against time or temperature on a controlled environmental furnace[21]. The sample is analyzed at an increasing temperature at a constant rate or as a function of time. The TGA unit consists of a furnace, microbalance, temperature controller and a data acquisition system. The sample weight is monitored on the microbalance while heating or cooling the sample in the furnace according to a predetermined system. TGA is a low cost technique and needs a small amount of sample. TGA is a destructive analysis and it may not be accurate due to the presence of volatile components. TGA can be employed to determine the thermal stability, oxidative stability, chemical composition and

water content.TGA can provide information about chemical phenomena such as second-order phase transitions, including vaporization, sublimation, absorption, and adsorption and desorption. TGA is commonly used for characterizing the compound through characteristic decomposition patterns, studies of the degradation mechanisms and reaction kinetics, determination of organic content in a sample and the determination of inorganic content in a sample which can be used for predicting material structures.

The sample size can affect the shape of TG curve i.e, a large sample may develop thermal gradients within the sample so finely ground samples are preferred for the analysis. The TG curve provides the details about the temperature at which the complexes lose moisture or ignites into their oxide form. The DTG curve records the difference in temperature between the sample and reference as a function of time or temperature by keeping the material under study and the inert reference in similar thermal cycles. Nowadays synchronized TG-DTA apparatus are available since both TG-DTA need identical sample and experimental conditions and the data can be rapidly obtained.

The structure of the chelating agents and their metal chelates shows relationship with their thermal stability. The thermal stability of the metal chelates can be predicted from the initial decomposition temperature. The studies reported that the thermal decomposition

of the compounds helps to interpret the structure of the compounds. The kinetic study can be done with the help of isothermal or non-isothermal methods[22-24].The kinetic parameters viz., energy of activation, entropy and order of reaction can be evaluated based on the differential method employing the Freeman-Carroll equation, the integral method using Coats-Redfern equation[25,26] and the approximation method using the Horowitz-Metzger equation[27].

Thermogravimetry is used in various aspects to solve the problems in chemistry. One is the phenomenological aspect in which the temperature of initiation, maximum decomposition and completion of the decomposition is evaluated. Another one is the kinetic aspect in which the kinetic parameters such as the energy of activation, pre-exponential factor and entropy of activation are determined. There are two approaches used for the kinetic study of the weight change viz., isothermal (static) and non isothermal (dynamic heating) approaches.

1.2 Dynamic or Non-isothermal Approach

The non isothermal method is the clarification of the degree of transformation as function of time during a linear increase of temperature in comparison with the isothermal method. There are two modes under non-isothermal conditions to evaluate the kinetic parameters of the thermal decomposition reaction.

1. A kinetic study that extends the simple homogeneous kinetics to heterogeneous solid kinetics.

2. A mechanism based study that provides a physicochemical description of the process.

The origin of the calculation of kinetic data from a TG curve is based on the kinetic equation

$$-dx/dt = kx^n \quad (1)$$

Where x is the amount of sample undergoing reaction, n is the order of reaction and k is the specific rate constant. The temperature dependence of the specific rate constant k is expressed by the Arrhenius equation.

$$K = Ae^{-\frac{E}{RT}} \quad (2)$$

where A is the pre exponential factor, E is the activation energy, R is the universal gas constant and T is the absolute temperature.

The kinetic equation

$$dx/dt = (A/\phi)\ e^{-E/RT}(1-\alpha)^n \quad (3)$$

may be considered as a general equation relating the parameters A, E and n where A is the pre-exponential factor, E is the energy of activation, ϕ is the linear heating rate, R is the universal gas constant and n is the order parameter.

For the thermal decomposition of solid state reaction as the following type:

$$A_{(solid)} \rightarrow B_{(solid)} + C_{(gas)}$$

Several simpler and practically useful forms of equations for calculating the kinetic parameters are given. The mass loss of the reaction at time t, is monitored using a dimensionless quantity, the fractional decomposition α, which can be defined as the fraction of the sample decomposed. Therefore

$$\alpha = \frac{W_t}{W_\alpha} = (m_o - m_t)/(m_o - m_\infty)$$

in which

W_t = mass loss at time t

Wα = maximum mass loss in the TG experiment for the reaction under investigation

m_0 = initial mass of the sample

m_t= the mass at time t

m_α = the mass at the end of the reaction

The calculation of the kinetic parameters is generally made use the equation (2) in some form or other.

The mathematical treatment of kinetic equations makes use of one of the following three method of evaluation i) differential method ii) integral method iii) approximation method

The temperature integral on the right hand side of the equation cannot be integrated in a closed form and different techniques have been employed for the evaluation of the temperature integral.

1.3 Coats-Redfern method

The temperature integral is calculated by Coats and Redfern with the aid of the Rainville function.

$$ln\,[g\,(\alpha)/\,T^2]\;=\;ln\,[\,(AR/\,\phi E)\;\;(1-(2RT/\,E))]\;-\;\;(E/\,RT)\;(3)$$

This is the Coat-Redfern equation. For the usual value of E and temperature range in which the reaction generally occurs, the term

$$ln\,[\,(AR/\phi E)\;\;(1-\;\;(2RT/\,E))]$$

is sensibly constant, since 2RT/E << 1. A plot of ln [g(α)/T^2] against 1/T would be linear. E and A can be evaluated from the slope and the intercept of the linear plot. The authors have suggested a trial and error method for evaluating the form of g (α), i.e., the value of n is calculated by trial and error method. The entropy of activation, ΔS, is determined from pre-exponential factor, A, using the equation

$$A\;=\;\frac{KT_S}{h}\;exp.\left(\frac{\Delta S}{R}\right) \qquad (4)$$

where k is the Boltzmann constant, h is the Planck constant, T_s is the peak temperaturefrom DTG/DTA and R is the universal gas constant.

1.4 Approximation method using the Horowitz-Metzger equation

Horowitz and Metzger evaluated the approximate value for the exp(-E/RT) by integrating it in the closed form. The equation defines the term θ, which is related to the peak temperature, T_S and temperature under consideration T, as $\theta = T - T_s$. Therefore, the Horowitz- Metzger equation for n = 1 is

$$log\ g(\alpha) = E\theta/2303\ RT_s^2 \quad ;$$

$$\text{where} g(\alpha) = 1 - (1 - \alpha)(1 - n)/(1 - n) \quad (8)$$

Where n=1, the left hand side of the equation (8) would be log [-ln(1-α)].

A plot of log g(α) against θ was drawn and found to be linear, from the slope of which E was calculated. The pre-exponential factor was evaluated using the equation

$$E/RT_s^2 = A/\phi\ exp.(E/RT_s)$$

where Ts is the peak temperature. The entropy of activation, ΔS, was calculated as earlier from equation (6). The disadvantage of

this method is that T_s is dependent onprocedural factors such as sample mass and heating rate.

1.5 Mechanism of reaction from non-isothermal TG traces

Sestak and Satava[28] and Redfern[29] have developed a procedure for deducing the mechanism of the reaction using non-isothermal kinetic methods. Satava reveals that a non-isothermal reaction proceeds in an infinitesimal time interval isothermally, where the rate can be expressed by an Arrhenius type equation.

$$d\alpha/dt = A\, exp.(E/RT)\, f(\alpha) \qquad (9)$$

A is the pre-exponential factor, t is the time and f(α) depends on the mechanism of the process.

For a linear heating rate, ϕ = dT/ dt

Substitution into eqn(10) gives

$$d\alpha/f(\alpha) = \int_0^t (A/\phi)\ e^{-E/RT}\, dT \qquad (10)$$

integration of the LHS of the eqn.(11) gives

$$\int_0^0 d\alpha/f(\alpha) = g(\alpha) = \int_0^t (A/\phi)\, e^{-E/RT} dT \qquad (11)$$

where g(α) is the integrated form of f(α). A series of f(α) forms are proposed and the mechanism is obtained from that which gives the best representation of the experimental data. Nine probable equation mechanism given by Satava are given in Table 1.Several authors recommended that kinetic parameters can be evaluated from the mechanistic equations, using the temperature integral,

which is an incomplete gamma function in the form given by Coats and Redfern. The equation used is the following:

$$ln\,[g\,(\alpha)/\,T^2] = ln\,[\,AR/\phi E - E/\,RT]$$

the linear plots for the nine forms of $ln[\,g(\alpha)\,/T^2]$ versus 1/T were drawn with the aid of origin software and by the method of least squares E, A, ΔS and the corresponding correlation coefficient ,r, for the linear plots were calculated.

Table1.1 Nine mechanistic equations

Function	Equation	Rate-Controlling Process
$D1$	$\alpha^2 = kt$	one-dimensional diffusion
$D2$	$(1-\alpha)\,ln\,(1-\alpha) + \alpha =$ kt	Two-dimensional diffusion, Cylindrical symmetry
$D3$	$[1-(1-\alpha)^{1/3}]^2 = kt$	Three-dimensional diffusion, Spherical symmetry, Jander equation
$D4$	$(1-2/3\,\alpha) - (1-\alpha)^{2/3} = kt$	Three-dimensional diffusion, Sphericalsymmetry, Ginsling-Brounshtein equation
$F1$	$-ln(1-\alpha) = kt$	Random nucleation, one nucleus at each particle, Mampel equation
$A2$	$-ln(1-\alpha)^{1/2} = kt$	Random nucleation; Avrami equation I
$A3$	$-ln(1-\alpha)^{1/3} = kt$	Random nucleation; Avrami equation II
$R2$	$1-(1-\alpha)^{1/2} = kt$	Phase boundary reaction; Cylindrical symmetry
$R3$	$1-(1-\alpha)^{1/3} = kt$	Phase boundary reaction; Spherical symmetry

1.6 Differential thermal analysis

Differential thermal analysis is a comparative analytical method in which the temperature of a sample and a thermally inert reference material are compared as the sample is heated or cooled at a uniform rate. It is the plot between the temperature differential ΔT, difference between the reference material and sample, i.e., $\Delta T = T_{(sample)} - T_{(reference)}$, and the temperature. The reference substance should not undergo any decomposition or phase transition in the temperature range of observation and here α- Alumina is often used as the reference material which that satisfies the condition up to 1950^0C.

1.7 Scope of the investigation

The thermal study of the diphenyl glycolic acid-amino acid metal complexes was discussed in the current section. Thermal decomposition of Mn (II),Fe (III), Cu (II) and Zn (II) complexes of HBG, Cu (II) and Cr (III) complexes of HBH, Cu (II), Ni (II) and Cr (III) complexes of HBL complexes using the TG, DTG and DTA techniques has been discussed in the chapter.

The TG plot gives the temperature regions of stability, the temperature of inception and the maximum rate of decomposition. The TG curves discuss about thermal stability and decomposition stages of complexes. Comparative studies of these data with DTA have been carried out.

The TG curves undergo non isothermal and isothermal analysis with the aid of the integral method of the Coats-Redfern equation, the approximation method of Horowitz-Metzger and nine equations. The activation parameters have been determined for all the metal complexes. The mechanistic equations recognized the mechanism of the decomposition from the TG data.

CHAPTER 2

MATERIALS, METHODS AND INSTRUMENTS

2.1 Materials

The amino acid ligands and their metal complexes were prepared from the analytical grade chemicals supplied by Sigma Aldrich and E-Merck. Commercial solvents were used as they were obtained. A detailed description of the reagents and their purity is described in Part 1.

2.2 Methods

The preparation of the amino acid ligand and their metal complexes was given in detail in the part 1 section. The thermogravimetric information was recorded using 2-5 mg of samples at a constant heating rate of 10^0C/min in the flowing air atmosphere using the thermal analyzer. Computational work was done on a personal computer with the help of the Microsoft Excel program and Origin software.

2.3 Instruments

Perkin Elmer make Pyris Diamond model thermal analyzer were used for the thermogravimetric study of the compounds.

CHAPTER 3

THERMAL DECOMPOSITION KINETICS OF METAL COMPLEXES OF DIPHENYL GLYCOLIC ACID-GLYCINE, HISTIDINE AND LEUCINE

The thermal study of the complexes provides structural information from the thermal behavior of the complexes. Thermal properties are related to the molecular structure of the complexes in such a manner that thermal decomposition data give details about each substituent bonded to the metal ion. The literature survey by Donia[30] et al gives a brief detail about large number of transition metal complexes and relation between their structural properties and thermal stability. A thermal decomposition study of Schiff base complexes of Co (II) and Cu (II) was reported by Bhaskare[31] et al. Thermal decomposition kinetics of transition metal complexes of Schiff bases and related ligands were reported by Geetha Parameswaran[32-35] et al. Emin[36] et al carried out the thermal analysis of the Ni (II) Complex of 3, 4-Methylenedioxaphenylaminoglyoxime and the thermodynamic parameters of decomposition was calculated. Refat[37] studied the thermogravimetric analysis of metal complexes of a new thiophene derivative containing an o-aminobenzoic acid ligand and their kinetic and thermodynamic parameters were calculated using the Coats-Redfern and Horowitz and Metzger approximation method. Kavitha and Anantha Lakshmi[38] carried out the thermal study of the metal complexes of hydrazine benzoxazine. Thermal studies of transition metal complexes of thiosemicarbazide were carried out

and kinetic parameters were also estimated[39]. The thermal behavior of Cr (III) complexes of hydroxycarboxylic acids was studied using their decomposition patterns and DSC curves[40]. Using the Broido method activation parameters were calculated by Pravin[41] et al. Thermal decomposition study of the 1, 10-phenanthroline derivatives was investigated during their heating in inert and N_2 atmosphere[42]. Soliman and co-workers carried out the thermal study of Schiff base, 3-methoxy-salicylidene-2-aminothiophenol and their kinetics study was also carried out[43].

The thermal decomposition studies of selected metal complexes of diphenyl glycolic acid-glycine, diphenyl glycolic acid-histidine and diphenyl glycolic acid- leucine have been described in this chapter. The kinetic parameters of the decomposition reaction such as activation energy E, pre exponent factor A and entropy of activation ΔS of the decomposition reactions were calculated by the Coats-Redfern kinetic equation and nine equations.

3.1 Treatment of data

Mn (II), Fe (III), Cu (II) and Zn (II) complexes of HBG, Cu (II) and Cr (III) complexes of HBH and Cu (II), Ni (II) and Cr (III) complexes of HBL

The TG plots from the instrument were redrawn as weight percentage versus temperature as the axis. The plots of the thermal data are given in figures 3.1 to 3.9. The temperature ranges, peak temperature, probable assignments and total mass from TG curves of the Mn (II), Fe (III), Cu (II) and Zn (II) complexes of HBG, Cu

(II) and Cr (III) complexes of HBH and Cu (II), Ni (II) and Cr (III) complexes of HBL are summarized in the tables 3.1 to 3.4 respectively. The kinetic parameters data from the Coats-Redfern kinetic equation and nine equations are given in the table 3.5-3.10.

3.2 Results and Discussion

The metal percentage of the metal complexes from the pyrolytic studies and also from the thermal studies was found as agreeable with the calculated values. The thermal study data helps to confirm the structure of the metal complexes. The final product of the decomposition was identified to be the oxides of the corresponding metals. The TG traces of the complexes do not show any detectable change up to 100^0C suggesting the absence of water of hydration and mass loss around 150^0C attributed to the loss of coordinated water molecule suggested by Nikolaev[44, 45].

Two step decomposition patterns was observed for Cu (II) complex of HBG among which first stage of decomposition stands for the removal of four coordinated acetate molecules. The second stage corresponds to the removal of Diphenyl glycolic acidic part of ligand moiety and histidine part of the HBG ligand. From the thermal data an overall weight loss of 74.27% while the theoretical weight loss during decomposition of the complex is 73.98%. Their DTA pattern suggests an exothermic curve for the decomposition.

Two step decomposition patterns was observed for Zn(II) complex of HBG among which first stage of decomposition stands for the removal of four coordinated water and glycine part of the HBG

ligand. The second stage corresponds to the removal of the Diphenyl glycolic acidic part and glycine part of the HBG ligand. From the thermal data an overall weight loss of 69.84%, while the theoretical weight loss during decomposition of the complex is 66.99%. Their DTA pattern suggests an endothermic curve for the decomposition.

Two step decomposition patterns was observed for Fe (III) complex of HBG ligand among which first stage of decomposition stands for the removal of two coordinated water and coordinated chlorine atom. The second stage corresponds to the removal of the Diphenyl glycolic acidic part and glycine part of HBG ligand. From the thermal data an overall weight loss of 79.93%, while the theoretical weight loss during decomposition of the complex is 79.19%. Their DTA pattern suggests an exothermic curve for the decomposition.

Single step decomposition patterns was observed for Mn (II) complex of HBG ligand among which first stage of decomposition stands for the removal of coordinated water and Diphenyl glycolic acidic part of HBG ligand. From the thermal data an overall weight loss of 58.65%, while the theoretical weight loss during decomposition of the complex is 58.27%. Their DTA pattern suggests an exothermic curve for the decomposition and the decomposition pattern of the above discussed complexes are depicted in table 3.1.and their TG-DTA curve was shown in fig.3.1-3.4.

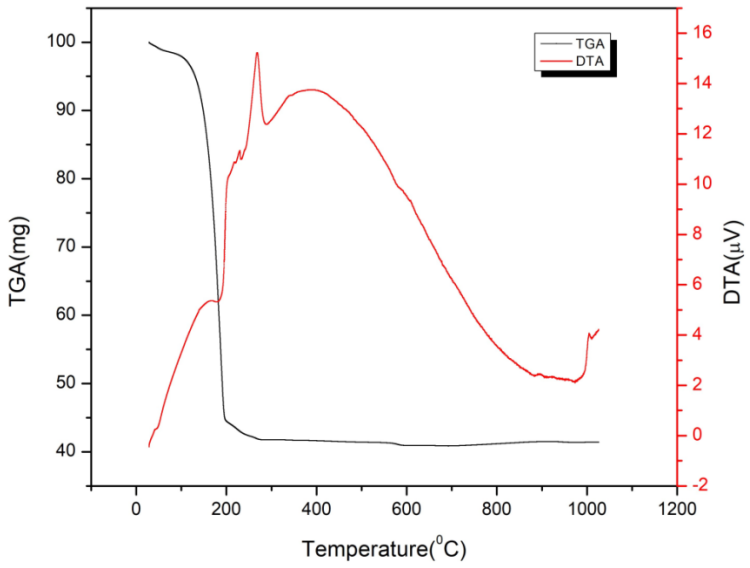

Fig.3.1.TG-DTA curve of MnBG

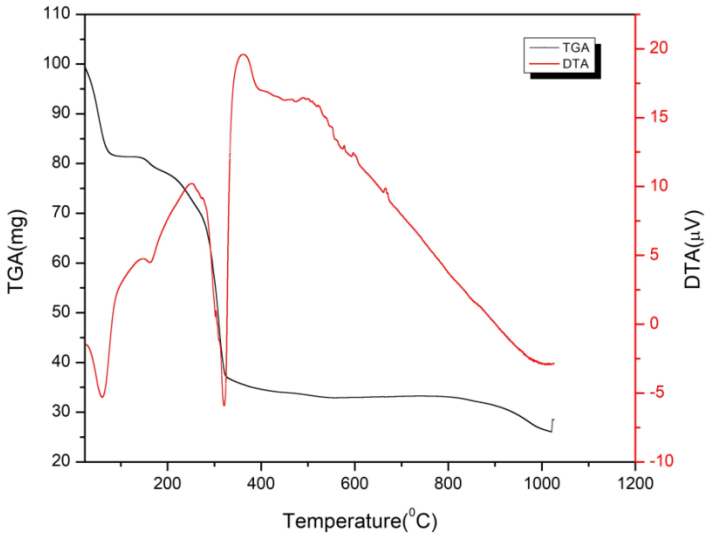

Fig.3.2.TG-DTA curve of ZnBG

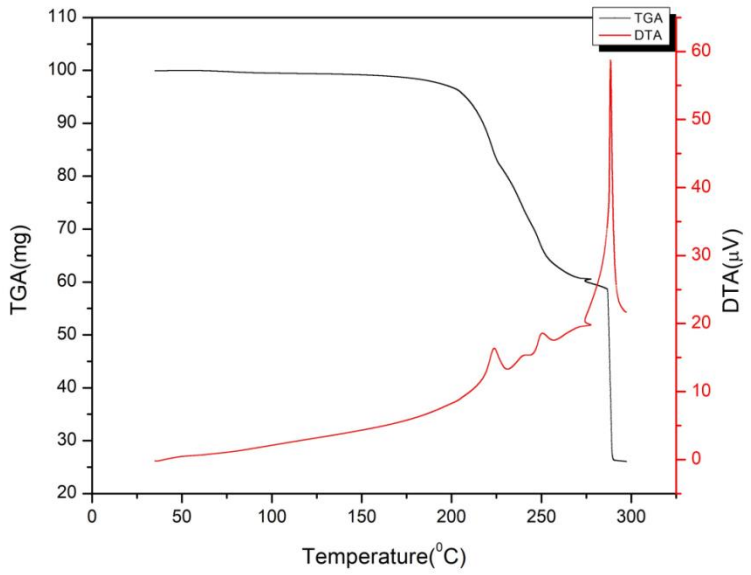

Fig.3.3.TG-DTA curve of CuBG

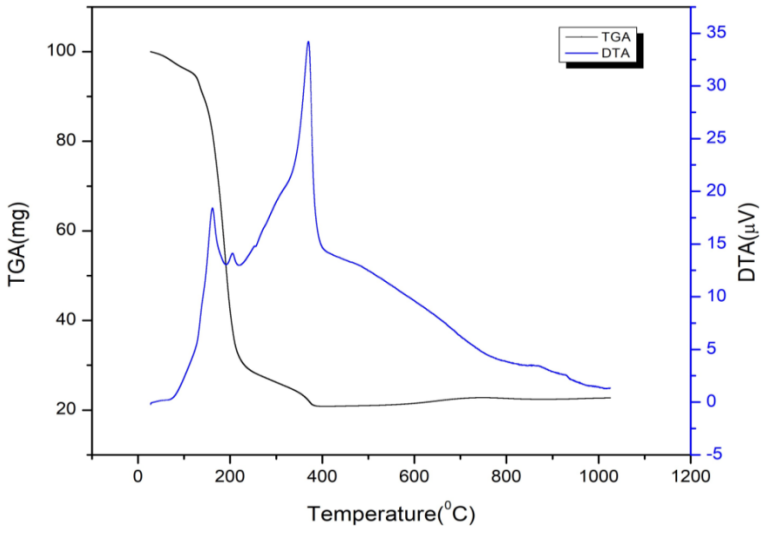

Fig.3.4.TG-DTA curve of FeBG

Table 3.1. Thermal decomposition data of Zn (II), Fe (III) Ni (II) and Cu (II) complexes of diphenyl glycolic acid - L – Glycine

Complex	stage	Temp range	Peak temp	Loss of mass %		Probable assignment
				From TG	theoretical	
$[CuBG(CH_3COO)_4]$	I	55.18-255.18	205.18	40.85	40.51	Loss of $4CH_3COO$
	II	255.18-295.18	275.18	33.42	33.64	Loss of DAA part + loss of Glycine part
				74.27	73.98	$[CuBG(CH_3COO)_4] \rightarrow Cu_2O$
$[ZnBG(H_2O)_4]$ (422.37)	I	33.41-203.41	53.41	23.91	22.10	Loss of $4H_2O$+ loss of glycine part
	II	203.41-553.41	313.41	45.93	44.89	Loss of DAA part
				69.84	66.99	$[ZnBG(H_2O)_4] \rightarrow ZnO$ +impurities
$[FeBG(H_2O)_2Cl2]$ (447.74)	I	37.46-167.46	167.46	23.87	22.49	Loss of $2H_2O$+2Cl
	II	167.46-407.46	197.46	56.05	56.70	Loss of DAA part + loss of Glycine part
				79.93	79.19	$[FeBG(H_2O)_2Cl2] \rightarrow Fe_2O_3$
$[MnBG_2(H_2O)_2]$ (656.94)	I	38.75-278.75	188.75	58.65	58.27	Loss of $2H_2O$+ Loss of $C_{13}H_{12}N$
				58.65	58.27	$[MnBG_2(H_2O)_2] \rightarrow Mn_2O_3$ + impurities

Two step decomposition patterns was observed for Cr (III) complex of HBH ligand among which first stage of decomposition stands for the removal of four coordinated acetate and Diphenyl glycolic acidic part of HBH ligand. The second stage corresponds to the removal of the Diphenyl glycolic acidic part and histidine part of HBH ligand. From the thermal data an overall weight loss of 69.3%, while the theoretical weight loss during decomposition of the complex is 71.04%. Their DTA pattern suggests an endothermic curve for the decomposition.

Two step decomposition patterns was observed for Cu (II) complex of HBH ligand among which first stage of decomposition stands for the removal of four coordinated water and Diphenyl glycolic acidic part of HBH ligand. The second stage corresponds to the removal of the Diphenyl glycolic acidic part and histidine part of HBH ligand. From the thermal data an overall weight loss of 79.81%, while the theoretical weight loss during decomposition of the complex is 77.73%.Their DTA pattern suggests an endothermic curve for the decomposition and the decomposition pattern of the above discussed complexes are depicted in table 3.2.and their TG-DTA curve was shown in fig.3.5-3.6.

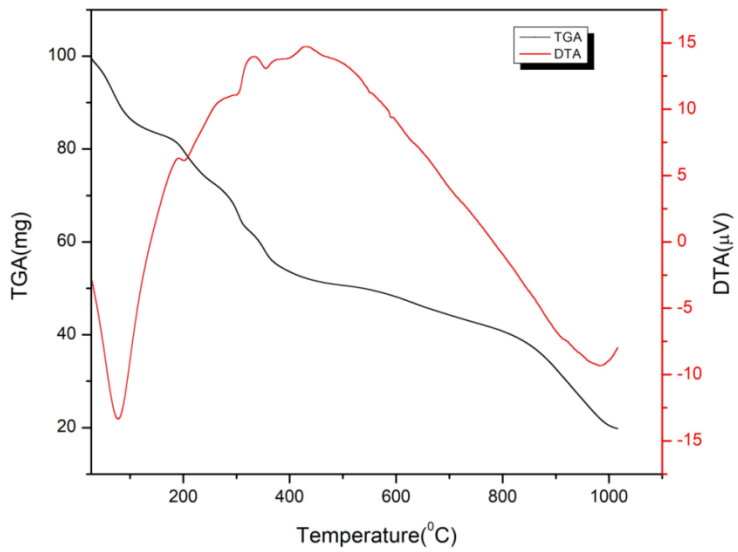

Fig.3.5.TG-DTA curve of CuBH

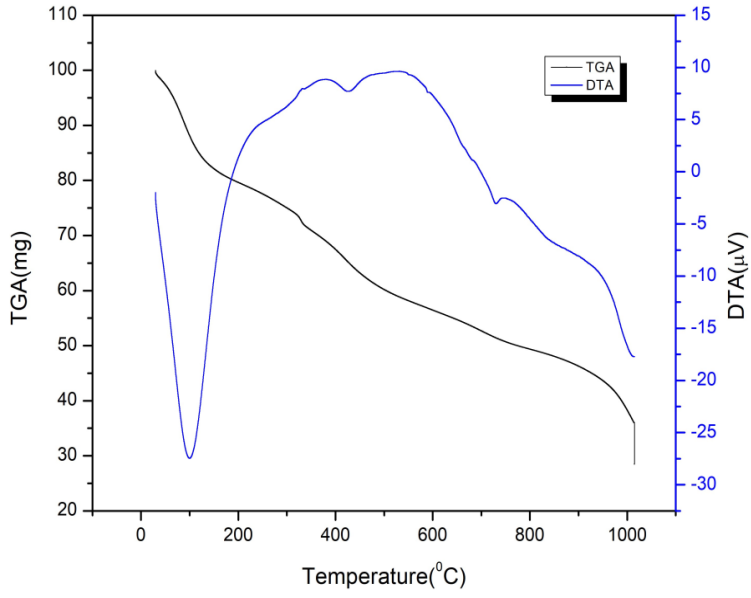

Fig.3.6.TG-DTA curve of CrBH

Table 3.3 Thermal Decomposition Data of Cr (III) and Cu (II) Complexes of Diphenyl Glycolic Acid - L - Histidine

Complex	**stage**	**Temp range**	**Peak temp**	**Loss of mass %**		**Probable assignment**
				From TG	**theoretical**	
$[CrBH(CH_3COO)_4]$ (639.99)	I	40.09-810.09	90.09	50.42	48.90	Loss of 4 CH_3COO+C6H5
	II	810.09-1020.09	1020.09	20.62	21.40	Loss of C3N2H3+CH2+CH+NH+CO
				71.04	69.3	$[CrBH(CH_3COO)_4]$ $\rightarrow Cr_2O_3$+ impurities
$[CuBH(H_2O)_4]$ (487.55)	I	37.19-717.19	717.19	56.25	54.55	Loss of $4H_2O$+2C6H5+C+CO
	II	255.18-295.18	275.18	23.55	22.35	Loss of C3N2H3+CH2+CH+NH
				79.81	77.73	$[CuBH(H_2O)_4]\rightarrow$CuO+ impurities

Two step decomposition patterns was observed for Cr (III) complex of HBL ligand among which first stage of decomposition stands for the removal of two coordinated acetate molecule and one coordinated water. The second stage corresponds to the removal of the one coordinated water and Diphenyl glycolic acidic part and leucine part of HBL ligand. From the thermal data an overall weight loss of 69.37%, while the theoretical weight loss during decomposition of the complex is 71.1%.Their DTA pattern suggests an endothermic curve for the decomposition.

Two step decomposition patterns was observed for Cu (II) complex of HBL ligand among which first stage of decomposition stands for the removal of one coordinated water. The second stage corresponds to the removal of the one coordinated water and Diphenyl glycolic acidic part and leucine part of HBL ligand. From the thermal data an overall weight loss of 69.24 %, while the theoretical weight loss during decomposition of the complex is 72.50 %. Their DTA pattern suggests an endothermic curve for the decomposition.

Three step decomposition patterns was observed for Ni (II) complex of HBL ligand among which first stage of decomposition stands for the removal of two coordinated water molecule and one coordinated water and leucine part of HBL ligand. The second stage corresponds to the removal of the one coordinated water and

Diphenyl glycolic acidic part and Leuine part of HBL ligand. From the thermal data an overall weight loss of 59.92%, while the theoretical weight loss during decomposition of the complex is 62.18%.Their DTA pattern suggests an endothermic curve for the decomposition.The decomposition pattern of the above discussed complexes is depicted in table 3.3. and their TG-DTA curve was shown in fig 3.7-3.9.

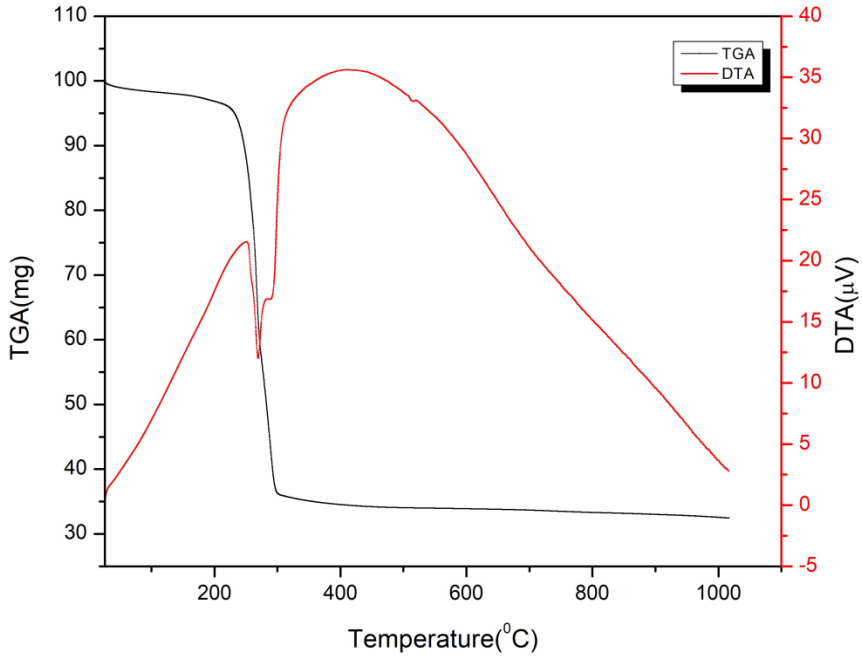

Fig. 3.7TG-DTA curve of CuBL

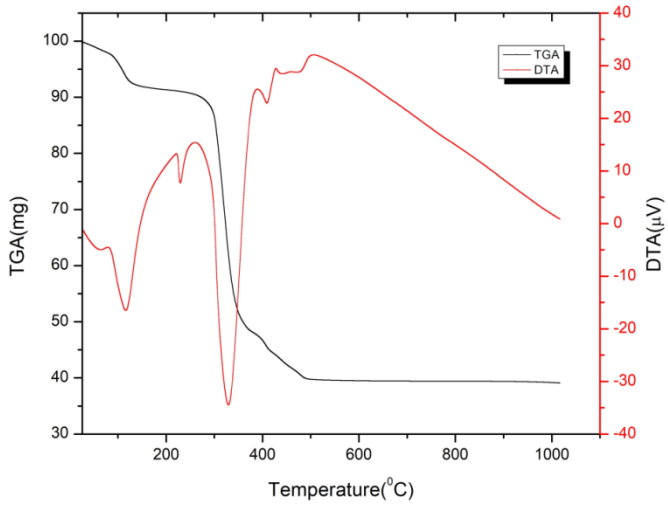

Fig. 3.8TG-DTA curve of NiBL

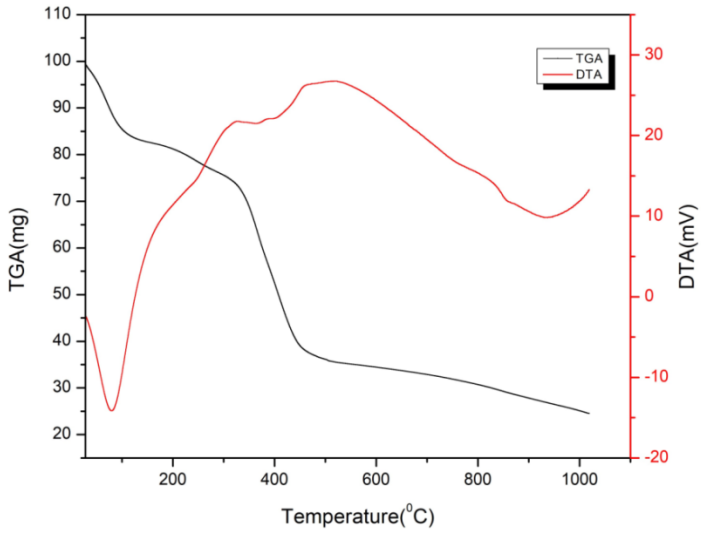

Fig. 3.9TG-DTA curve of CrBL

Table 3.4. Thermal Decomposition Data of Cr (III), Ni (II) and Cu (II) Complexes of Diphenyl Glycolic Acid - L - Leucine

Complex	stage	Temp range	Peak temp	Loss of mass %		Probable assignment
				From TG	theoretical	
$[CrBL(H_2O)_2(CH_3COO)_2]$ (487.99)	I	38-288	78	23.67	27.86	Loss of $2CH_3COO+1H2O$
	II	288-798	368	45.70	46.92	Loss of 1H2O + 2C6H6+2CH3+CH+CH2
				69.37	71.1	$[CrBL(H_2O)_2(CH_3COO)_2]\rightarrow Cr_2O_3$
$[CuBL(H_2O)_2(CH_3COO)_2]$ (558.55)	I	36.75-186.75	46.75	2.75	3.22	Loss of $1H_2O$
	II	186.75-1016.75	266.75	67.49	69.28	Loss of $1H_2O+ 2CH_3COO$ 2C6H5+C++CO+2CH3+2CH+CH2
				69.24	72.50	$[CuBL(H_2O)_2(CH_3COO)_2]\rightarrow Cu_2O+$ impurities
$[Ni(BL)_2(H_2O)_2]$ (487.55)	I	36.41-266.41	266.41	9.701798	10.1713	Loss of $2H_2O$+2CH3+CH
	II	266.41-326.41	326.41	25.547	26.7803	Loss of 2C6H5+C+NH+CH+CH2
	III	326.41-486.41	336.41	24.68386	25.2352	Loss of 2C6H5+C+2CH3
				59.92	62.18	$[Ni(BL)_2(H_2O)_2]\rightarrow NiO+$ impurities

3.3 Decomposition Kinetics

The thermal decomposition kinetic parameters viz activation energy E, Arrhenius factor A, entropy of activation ΔS and order parameters n for the thermal decomposition of the three complexes were calculated. The values of E and A from the thermal data and from the equations are nearly the same. The highly stable metal complexes have larger activation energy for decomposition and a negative ΔS value. The decomposition mechanism of these metal complexes was deduced by the use of non-isothermal kinetic methods given by the Sestak and Berggren and Satava. The figured out values of E and A from the mechanistic equation are in good agreement with the values obtained from the non-mechanistic equation(Coats Redfern) and also with Horowitz Metzger equation of the same order.

The values of kinetic parameters obtained for first stage decomposition of Mn (II), Fe (III), Cu (II) and Zn (II) complexes of HBG, Cu (II) and Cr (III) complexes of HBH and Cu (II), Ni (II) and Cr (III) complexes of HBL calculated from Coats Redfern equation with n = ½ agree well with those values obtained for equation 8. R_2 mechanismbased on phase boundary reaction, cylindrical symmetry gives the maximum correlation for the first stage decomposition of Mn (II), Fe (III), Cu (II) and Zn (II) complexes of HBG, Cu (II) and Cr (III) complexes of HBH and Cu (II), Ni (II) and Cr (III) complexes of HBL. Kinetic parameters for

the decomposition of Co (II), Ni (II) and Cu (II) complexes of Diphenyl Glycolic Acid - L – Glycine, Diphenyl Glycolic Acid - L – Histidine and Diphenyl Glycolic Acid - L – Leucine from TG using mechanistic equations and non-mechanistic equations are tabulated in table 3.5-3.10. In the current study the order of thermal stability was given on the basis of observation made by Naidu and co-workers[46, 47]:

$$MnBG_2(H_2O)_2] < [ZnBG(H_2O)_4] < [FeBG(H_2O)_2Cl_2] < [CuBG(CH_3COO)_4]$$

$$[CuBH(H_2O)_4] < [CrBH(CH_3COO)_4]$$

$$[CrBL_2(H_2O)_2(CH_3COO)_2] < [CuBL_2(H_2O)_2\,(CH_3COO)_2] < [NiBL_2(H_2O)_2]$$

Table 3.6. Kinetic parameters for the decomposition of Zn (II), Fe (III) Ni (II) and Cu (II) complexes of Diphenyl Glycolic Acid - L - Glycine from TG using mechanistic equations

Complex		mechanistic equations								
		1	2	3	4	5	6	7	8	9
$[CuBG(CH_3COO)_4]$	E	19690.33717	25106.16944	32971.7988	27661.30629	19834.73702	19834.73702	19834.73702	13469.95511	15397.74137
	A	4.681552016	9.31014066	15.45591318	10.29299107	5.823432311	5.13028513	4.724820022	-1.04806537	0.422007718
	ΔS	-74.3494005	-64.6695825	-51.916397	-62.5240768	-72.0659658	-73.4432493	-74.2489084	-86.4885473	-83.3017326
	r	-0.94081701	-0.94481792	-0.94742916	-0.94601896	-0.94277771	-0.94277771	-0.94277771	-0.93836097	-0.94041584
$[ZnBG(H_2O)_4]$	E	3017.744	3743.275	4635.23626	4038.062948	1550.690303	1550.690303	1550.690303	857.6012449	1076.887658
	A	-11.6841494	-11.5257577	-12.0057285	-12.6910136	-11.8138282	-12.5069754	-12.9124405	-13.2997923	-13.4531163
	ΔS	-110.728858	-109.986032	-110.515059	-112.150772	-112.309493	-113.686776	-114.492435	-116.439036	-116.291268
	r	-0.73401013	-0.77101883	-0.80220079	-0.78280821	-0.61505717	-0.61505717	-0.61505717	-0.44799987	-0.51356421
$[FeBG(H_2O)_2Cl2]$	E	14760.15804	14952.77341	15152.6378	15141.63977	6936.872559	6936.872559	6936.872559	6786.208701	6835.96484
	A	1.724659486	1.321524015	0.118057353	0.065947199	-5.617752221	-6.310899401	-6.71636451	-6.537476	-6.8681
	ΔS	-80.49359449	-81.26886269	-83.63376789	-83.73875349	-96.5833115	-97.96059494	-98.76625411	-98.45443456	-99.09686017
	r	-0.98433774	-0.984029133	-0.983611411	-0.983529196	-0.97952324	-0.97952324	-0.97952324	-0.980237424	-0.980027166
$[MnBG_2(H_2O)_2]$	E	14069.21	14634.41	15273.72	14901.46	7149.113	7149.113	7149.113	6659.96	6817.964
	A	0.534321	0.653235	0.065656	-0.48936	-5.430251	-6.123398	-6.528863	-6.82439	-7.0033
	ΔS	-82.91693	-82.60238	-83.68494	-84.83679	-96.11373	-97.49101	-98.29667	-99.02471	-99.33362
	r	-0.970750849	-0.970741963	-0.970517888	-0.970946952	-0.9633605	-0.9633605	-0.9633605	-0.963435052	-0.96349553

Table 3.7. Kinetic parameters for the decomposition of Cr(III) and Cu (II) complexes of Diphenyl Glycolic Acid - L – Histidine from TG using mechanistic equations

Complex		mechanistic equations								
		1	**2**	**3**	**4**	**5**	**6**	**7**	**8**	**9**
$[CrBH(CH_3COO)_4]$	E	2114.62575	3441.47363	5154.250105	4005.849233	1139.074974	1139.074974	1139.074974	-203.787239	216.2050732
	A	-14.2812678	-14.2812678	-14.6320704	-15.3153739	-13.7558799	-14.4490271	-14.8544922	-15.2428803	-15.3975106
	ΔS	-118.167234	-117.199521	-117.093973	-118.952552	-118.352568	-119.729852	-120.535511		-124.916374
	r	-0.5410699	-0.5410699	-0.69635156	-0.66300414	-0.32973525	-0.32973525	-0.32973525	0.08723266	-0.08240695
$[CuBH(H_2O)_4]$	E	2362.174742	2602.063356	2867.963843	2690.485775	488.4600268	488.4600268	488.4600268	285.9059171	351.6965569
	A	-13.1151217	-13.4497171	-14.5613762	-14.823252	-13.3397165	-14.0328637	-14.4383288	-14.3312137	-14.6394721
	ΔS	-114.037681	-114.510335	-116.525872	-117.173149	-117.615622	-118.992906	-119.798565	-120.649954	-120.850944
	r	-0.82121044	-0.84909182	-0.87450043	-0.85819435	-0.4697543	-0.4697543	-0.4697543	-0.29041528	-0.35228382

Table 3.8. Kinetic parameters for the decomposition of Co (II), Ni (II) and Cu (II) complexes of Diphenyl Glycolic Acid - L – Leucine from TG using mechanistic equations

Complex		mechanistic equations								
		1	**2**	**3**	**4**	**5**	**6**	**7**	**8**	**9**
$[CrBL(H_2O)_2(CH_3COO)_2]$	E	3130.939669	3231.645846	3336.069921	3266.443603	896.2404862	896.2404862	896.2404862	817.5410375	843.5372805
	A	-12.2065042	-12.7199732	-14.0385101	-14.1622192	-12.8710073	-13.5641545	-13.9696196	-13.7039088	-14.0631624
	ΔS	-111.870472	-112.827829	-115.384572	-115.672291	-115.676337	-117.053621	-117.85928	-117.513933	-118.165571
	r	-0.74481107	-0.75277369	-0.76067151	-0.75545573	-0.51590595	-0.51590595	-0.51590595	-0.4853985	-0.49574246
$[CuBL(H_2O)_2(CH_3COO)_2]$	E	2935.325342	2948.625848	2961.984923	2953.078854	740.8011639	740.8011639	740.8011639	730.7763085	734.1142586
	A	-15.9504689	-16.6192797	-18.0989264	-18.1152136	-14.8752939	-15.5684411	-15.9739062	-15.586773	-15.9861334
	ΔS	-119.096309	-120.416253	-123.347329	-123.385675	-119.69572	-121.073003	-121.878662	-121.136501	-121.920975
	r	-0.95126108	-0.95161358	-0.9519636	-0.95173076	-0.82709369	-0.82709369	-0.82709369	-0.82368975	-0.82483377
$[Ni(BL)_2(H_2O)_2]$	E	25923.98	27058.73038	28267.12578	27461.1777	13618.61704	13618.61704	13618.61704	12704.28413	13004.29866
	A	6.716571142	7.097722766	6.735509367	5.973946899	-2.29673548	-2.98988267	-3.39534777	-3.85364631	-3.97555924
	ΔS	-69.9368354	-69.0943612	-69.7272676	-71.2979686	-89.1253682	-90.5026516	-91.3083108	-92.3570435	-92.5529065
	r	-.93147842	-0.9299758	-.92836158	-.92942902	-0.9161077	-0.9161077	-0.9161077	-.91801556	0.91738586

Table 3.9. Kinetic parameters for the decomposition of Zn (II), Fe (III) Ni (II) and Cu (II) complexes of Diphenyl Glycolic Acid - L – Glycine using non mechanistic equations

Complex	**parameter**	**Coats Redfern**	**Horowitz Metziger**	**Mechanistic equation followed**	**Order of reaction**
$[CuBG(CH_3COO)_4]$	E	15397.74137	17596.14315	Phase boundary reaction; Spherical symmetry	2/3
	A	1.52062	-0.01256		
	ΔS	-81.1188	-111.05		
	r	-0.9404	0.95319		
$[ZnBG(H_2O)_4]$	E	1076.89	2859.15	Phase boundary reaction; Spherical symmetry	2/3
	A	-12.355	-0.47544		
	ΔS	-114.108	-115.315		
	r	-0.5136	0.84868		
$[FeBG(H_2O)_2Cl2]$	E	6835.96484	13044.36316	Phase boundary reaction; Spherical symmetry	2/3
	A	-5.769483	-0.3923853		
	ΔS	-96.913917	-111.210702		
	r	-0.98002	-0.98311		
$[MnBG_2(H_2O)_2]$	E	6817.964	10202.37	Phase boundary reaction; Spherical symmetry	2/3
	A	-5.90469	-1.25616		
	ΔS	-97.15068	-112.4388		
	r	-0.96349	0.96571		

Table 3.10. Kinetic parameters for the decomposition of Cr (III) and Cu (II) complexes of Diphenyl Glycolic Acid - L – Histidine using non mechanistic equations

Complex	parameter	Coats Redfern	Horowitz Metziger	Mechanistic equation followed	Order of reaction
$[CrBH(CH_3COO)_4]$	E	216.2050732	5941.86397	Phase boundary reaction; Spherical symmetry	2/3
	A	-14.2988983	-0.04547138		
	ΔS	-122.733432	-108.957174		
	r	-0.08240695	0.893864715		
$[CuBH(H_2O)_4]$	E	351.6965569	2294.344833	Phase boundary reaction; Spherical symmetry	2/3
	A	-13.5408598	-1.23266875		
	ΔS	-118.668001	-109.426596		
	r	-0.35228382	0.871606858		

Table.3.11. Kinetic parameters for the decomposition of Cr (III), Ni (II), and Cu (II) complexes of Diphenyl Glycolic Acid – L – Leucine using non mechanistic equations

Complex	parameter	Coats Redfern	Horowitz Metziger	Mechanistic equation followed	Order of reaction
$[CrBL(H_2O)_2(CH_3COO)_2]$	E	843.5372805	5307.167734	Phase boundary reaction; Spherical symmetry	2/3
	A	-12.9645501	-0.5112037		
	ΔS	-58.3707238	-55.1882997		
	r	-0.49574246	0.806760129		
$[CuBL(H_2O)_2(CH_3COO)_2]$	E	734.1142586	4445.665138	Phase boundary reaction; Spherical symmetry	2/3
	A	-14.8875211	-2.780904		
	ΔS	-119.738032	-113.817473		
	r	-0.82483377	0.962451011		
$[Ni(BL)_2(H_2O)_2]$	E	13004.29866	17136.67431	Phase boundary reaction; Spherical symmetry	2/3
	A	-2.87694695	-0.976885		
	ΔS	-90.3699639	-112.913689		
	r	-0.91738586	0.947180588		

References :

1. Donia, A. M., & El-Boraey, H. A. (1993). *Transition Met.Chem*., 18, 315.
2. Wendlandt, W. W., & Smith, J. P. (1963). *J. Inorg. Nucl. Chem*., 25, 843.
3. Wendlandt, W. W., & Funes, L. A. (1964). *J. Inorg. Nucl. Chem*., 26, 1879.
4. Smith, J. P., & Wendlandt, W. W. (1964). *J. Inorg. Nucl. Chem*., 26, 1157.
5. Wendlandt, W. W. & George, T.D. (1961). *Texas. J. Sci*. 13, 316.
6. Wendlandt, W. W. (1963). *J. Inorg. Nucl. Chem*., 25, 545.
7. Wendlandt, W. W. & Smith, J. P. (1963). *Inorg. J. Nucl. Chem*., 25, 985.
8. Liptay, G. (1989). *Thermochim.Acta*., 150, 93.
9. Donia, A. M., & Ebeid, E. M. (1998). *Thermochim. Acta*., 131, 1.
10. Donia, A. M. (1989). *Thermochim. Acta*., 162, 335.
11. Donia, A. M., El-Shereafy, E., & El-Ries, M. A. (1990). *Reactivity of Solids*, 8, 1.
12. Donia, A. M., & El-Boraey, H. A. (1992). *Transition Met. Chem*., 18, 303.
13. Donia, A. M., & El-Boraey, H. A. (1993). *Transition Met. Chem*., 18, 315.
14. Mackenzie, R. C., ed. (1957) *The Differential Thermal Investigation of Clays*. Mineralogical Society (Clay Minerals Group), London.
15. Duval, C. (1962). "Inorganic Thermogravimetric Analysis" Elsevier, New York.
16. Smoothers, W. J., & Yaochiang, M.S. (1996). "Handbook of Differential Thermal Analysis", New York Chemical Publishing Co., New York.

17. Mackenzic, R. C. (1970). "Differential Thermal Analysis", Academic press, London,1, 17.

18. Mackenzie, R. C. (1984). *Thermochim*, 73, 307.

19. Schulze, D. (1969). "Differential Thermo Analyzer", VEB Verlangder Wissenchaften, Berlin.

20. Garn, P. D. (1964). "Thermo Analytical Methods of Investigation", Academic Press, New York.

21. Wendlandt, W. W. (1985). "Thermal Analysis", 3rd Ed., Wiley, New York.

22. Skavara, F., & Satava, J. (1970). *J. Thermal Anal*., 2, 325.

23. Carrol, B., & Masche, E. P. (1972). *ThermoChim., Acta*, 3, 442.

24. Ninan, K. N., & Nair, C. G. R. (1978). *ThermoChim. Acta*, 23, 161.

25. Sestak J. & Berggren G. (1971)*ThermoChim. Acta*, 3.

26. Coats, A. W. & Redfern, J. P. (1964). *Nature London*, 68, 201.

27. Horowitz, H. H., & Metzger, G. (1963). *Anal. Chem.*, 36, 1464.

28. Sestak, J. (1973). *Thermochim. Acta*., 7, 333.

29. Redfern, J. P. (1970). "Differential Thermal Analysis", Academic Press, New York.

30. Donia, A. M. (1998). *Thermochim. Acta*., 320, 187.

31. Bhaskare, C. K., More, P. G., & Hankare, P. F. (1981). "Proceedings of the National Symposium on Thermal Analysis", India.

32. Rehina, K., & Parameswaran G. (1999). *J. of Ther. Anal. and Calorimetry*, 55, 817.

33. Indira, V., & Parameswaran, G. (1986). *Thermochim. Acta*., 101, 145.

34. Laly, S., & Parameswaran,G., (1991). *React. Kinet. Cal. Lett*., 43, 169.

35. Mary, N. L., & Parameswaran, G. (1991).*Thermochim. Acta*., 185, 345.

36. KarapInar, E., Gubbuk, I. H., Taner, B., Deveci, P., & Ozcan, E. (2013). *J. Chem.,2013*.

37. Refat, M. S., Altalhi, T. A., Al-Hazmi, G. H., & Al-Humaidi, J. Y. (2021). *Bull. Chem. Soc. Ethiop*., 35, 129.

38. Kavitha, N., & Anantha Lakshmi, P.V. (2017). *J. Saudi Chem.Soc*., 21, 457.

39. Refat, M. S., El-Deen, I. M., Zein, M. A., Adam, A. M. A., & Kobeasy, M. I., (2013). *Int. J. Electrochem. Sci.*, 8, 9894.

40. Baranwal, B.P., Fatma, T., & Varma, A. (2009). *J. Mol. Struct.*, 920, 472.

41. Prajapati, K. N., Brahmbhatt, M.P., Vora, J.J., & Prajapati, P.B. (2019). *RJLBPCS*, 5, 763.

42. Zapała, L., Kosinska, M., Woznicka, E., Byczynski, L., Ciszkowicz, E., Lecka-Szlachta, K., Zapała, W., & Chutkowski, M. (2018). *Thermochem. Acta*, 671, 134.

43. Soliman, A. A. & Linert, W. (1999). *Thermochim. Acta*., 338, 67.

44. Nikolaev, A. V., Logvinenko, V. A., & Myachina, L. I. (1969) . "Thermal Analysis", Academic Press, New York,779.

45. Vatsala, S., & Parameswaran, G. (1986). *J. Therm. Anal*., 31, 883.

46. Naidu, R. S., & Naidu, R. R. (1997). *Indian J. Chem*., 15A, 65.

47. Naidu, R. S., Rao, E. N., Ruby, R., & Mallikarjun, K. G. (1988). *Thermochim. Acta*., 131, 299.

PART III

X-RAY DIFFRACTION STUDIES OF THE DIPHENYL GLYCOLIC ACID -AMINO ACID METAL COMPLEXES

CHAPTER 1

INTRODUCTION

X-ray diffraction method is a significant tool for the elucidation of the crystal structure of the compounds. Diffraction patterns are used as the fingerprint for the compounds, as they can be described in terms of the three-dimensional arrangement of lattice points. It is possible to diffract X-rays by means of crystals. The inter-atomic distances in a crystal have the same order as the wavelength of the X-rays used. Hence X-rays can interact with the inner electrons in the atoms and can predict the internal arrangement of the atoms in the crystal. X-ray diffraction is an effective method for the characterization of compounds because it is a non-destructive, fast, and sensitive method.

X-ray diffraction technique was discovered by Von Laue in 1912; the X-rays diffracted on traversing through the crystal and the manner of the diffraction reveals the structure of the crystal. Diffraction patterns are unique for each compound; hence, it is considered a significant method for structure elucidation. This technique gives important information about the arrangement and spacing of atoms in crystalline materials. XRD is a unique method that provides both qualitative and quantitative information about the compounds present in a solid sample. For the analytical study, a finely powdered sample is used. When the X-ray beam passes through the material, a significant number of particles can be

oriented in such a way as to fulfill the Bragg condition for reflection. The automatic scanning gives various diffraction patterns, which help in the identification of species depending upon the position of lines and their relative intensities. The lattice type of the complexes is determined by the powder XRD method.

The study of coordination compounds with the help of XRD began during the last decade. Hull and Davey[3], Bjurstorm4, and Bunn[5] have used several graphical methods for indexing the powder photographs during the crystallographic studies. Much easier methods for the interpretation of crystallographic patterns were introduced by Hesse[6] and Lipson[7]. Henry[8] et al. derived equations for analyzing the powder crystallographs. X-ray diffraction studies depend on the nature of crystals, and it is one of the most appropriate methods for the complete determination of the molecular structure. The crystals can be classified into seven crystal systems, with particular axial lengths and axial angles for each system. The crystal system can be classified as cubic, tetragonal, orthorhombic, trigonal, hexagonal, monoclinic, and triclinic. Several studies were reported by Bhagavntam[9], Hearmon[10], Krishnan[11], and Suryanarayana[12] on the elastic constants of crystalline compounds. Unit cell dimensions, lattice type of crystal, interplanar spacing of lattice planes, and miller indices of the reflection planes are determined with the help of crystallographic studies[13–15].

A particular wavelength of X-rays is allowed to fall on the crystal, which produces an interference pattern because of the scattering of these rays from the neighboring atoms. The diffraction obeys Bragg's law.

$$n\lambda = 2dSin\theta$$

where n is an integer, λ is the wavelength of the incident light, d is the interplanar distance, and θ is the angle of diffraction. The X-ray crystallographic pattern between twice the angles of diffraction (2θ) against the intensity of diffraction is very helpful for the analysis.

1.1 Determination of the crystal system

The relationship between the interplanar space d and the Miller indices h, k, and l is used in the study of crystal systems. Crystals belonging to a regular or cubic system have equal axial lengths (a=b=c), and axial angles are at right angles (α=β=γ=90°). Here, the relation d and miller indices (h, k, l) are given as

$$1/d^2 = (h^2 + k^2 + l^2)/a^2 and$$

$$d^2 = \lambda^2/4\, Sin^2\theta$$

$$Sin^2\theta = \lambda^2(h^2 + k^2 + l^2)/4a^2 \quad (1)$$

$(h^2 + k^2 + l^2)$will be constant, and other than 7, 15, 23, etc.

With the help of Bragg's angles, the values of $Sin^2\theta$ are obtained, and the integral multiple of $\lambda^2/4a^2$ is a constant.

For a tetragonal system, all axial angles are 90°,where a = b ≠ c.

The equation (1) changes as

$$Sin^2\theta = \lambda^2(h^2 + k^2)/4a^2 + (\lambda^2 l^2)/4c^2 \quad (2)$$

An orthorhombic system with the same axial angles but different axial lengths satisfies the equation.

$$Sin^2\theta = (\lambda^2 h^2)/4a^2 + (\lambda^2 k^2)/4b^2 + (\lambda^2 l^2)/4c^2 \quad (3)$$

$d_{(h,\ k,\ l)}$ represents the distance between adjacent planes. For an orthorhombic lattice, the interplanar distance is given by the equation.

$$1/d_{hkl}^2 = (h/a)^2 + (k/b)^2 + (l/c)^2 \quad (4)$$

For a cubic lattice, a = b = c.

Hence,

$$1/d_{hkl}^2 = (h/a)^2 + (k/a)^2 + (l/a)^2 = (h^2 + k^2 + l^2)/a^2 \quad (5)$$

$$d_{(h\,k\,l)} = a/(h^2 + k^2 + l^2)^{1/2}$$

For a hexagonal system a=b=c and $\alpha = \beta \neq 90^0$, $\gamma = 120^0$, $\sin^2\theta$ in this case is

$$Sin^2\theta = \lambda^2/3a^2(h^2 + hk + k^2) + (\lambda^2 l^2)/4c^2 \quad (7)$$

For rhombohedral or trigonal, a = b = c, $\alpha = \beta = \gamma \neq 90^0$; for a monoclinic system, a = b ≠c, and

$\alpha = \gamma = 90^0$, $\beta \neq 90^0$, and for the triclinic system, a ≠b≠ c, $\alpha \neq \beta \neq \gamma \neq 90^0$.

The density and number of molecules per unit cell of the complex have been calculated using the formula

$$D = nM/VN \qquad (8)$$

Where D is the density of the complex, n is the number of molecules in the unit cell, N is the Avogadro number, V is the volume of the unit cell, and M is the molecular mass of the complex. The relative intensity of the peak in the pattern can be calculated using the equation 100 (I/I_0), where I is the intensity of the diffracted beam and I_0 is the intensity of the incident beam.

Doman[16] et al. reported the crystal structure of the Cu(II) complexes of the Schiff base. The synthesis and XRD analysis of the Ni(II) complexes of Schiff base obtained by the condensation of o-vanillin and diamines have been reported by Dexin[17] et al. Nathmala[18] studied the X-ray analysis of Cu(II) complexes derived from salicyaldehyde and glycine. X-ray analysis of mononuclear and binuclear Cu(II) complexes of Schiff bases has been reported[19]. Garcia-Raso[20] et al. carried out the X-ray diffraction study of two N-salicylidenetryptophanatodiaquoCu(II) complexes (erythro and thero isomers). The crystal structure of the salicyaldehydevaniline

copper was found using the X-ray diffraction technique[21]. Saleem[22] et al. synthesized and carried out the X-ray diffraction study of the Schiff base derived from salicylaldehyde and diamine acids. Using the XRD analytical method, the structure of N-salicylidine amino acidate complexes of oxovanadium IV dissolved in pyridine complexes (glycine and alanine) was detected, and the octahedral geometry was suggested for both complexes.

The structural elucidation of coordination compounds using the XRD technique has increased during the last few years. Various crystalline systems of coordination compounds have been reported so far[23–28]. The crystal structure determination of Cd(II) complexes of anthranilic acid and 5-bromo-anthranilic acid-derived Schiff bases has been carried out[29]. X-ray diffraction studies of Fe(II), Ni(II), and Cu(II) complexes of o-vanillin L-histidine have been reported[30]. Indiradevi[31] et al. detected the crystal structure of the metal complexes of amino acid Schiff bases of anthracene carboxaldehyde. The crystal and molecular structure of neutral Cu (II) complexes of Schiff bases from 2-aminopyridine and substituted salicylaldehydes were carried out by the X-ray diffraction method by Casrineiras[32]. et al. 32. X-ray crystallographic studies of the β-alanine Schiff-base complex were carried out by Kumar[33] et al. Stanley et al. carried out the X-ray crystallographic studies of the metal complexes Schiff bases derived from Furoin[34].

1.2 Scope of the investigation

The current section deals with the determination of the crystal system of some of the synthesized transition metal complexes of Diphenyl glycolic acid-tyrosine (HBT), Diphenyl glycolic acid-histidine (HBH), and Diphenyl glycolic acid -glycine (HBG). The unit cell dimensions a, b, c, number of molecules per unit cell, and density D has been found from crystallographic data. Also, the crystallinity and interplanar spacing were calculated from the diffraction studies.

CHAPTER 2

MATERIALS, METHODS AND INSTRUMENTATION

2.1 Materials

Analar-grade chemicals, purchased from Sigma Aldrich and Nice, were utilized for the synthesis of the metal complexes. Commercial solvents were used without further purification.

2.2 Instrumentation

The synthesis of the ligands HBT, HBG, and HBH and their metal complexes was described in Section I. The compounds are dried well and powdered homogeneously into a very nice powder. X-ray diffraction patterns of the ligands and their metal complexes were recorded using an AXS Bruker Germany D5005 model X-ray diffractometer. The X-ray generator was operated at 40 KV and 30 mA. Cu K_α (λ = 1.54056 A^0) radiation was used with a Ni filter. The estimations were done for 2θ values from 10^0 to 90^0 at a scan rate of 2^0/min. The densities of the compounds were calculated from their mass and volume.

The instruments utilized for the study of the ligands and their metal complexes are

1) Aeris research benchtop X-ray diffractometer

CHAPTER 3

X-RAY DIFFRACTION STUDIES OF SELECTED METAL COMPLEXES OF HBT, HBG AND HBH

The X-ray diffraction study is the most important technique used for structural determination. Single crystals of the compounds give the complete details of the structure directly, but if appropriate crystals cannot be obtained, there is a necessity to tackle the powder XRD data. Since the discovery of the XRD technique, several developments have been made in its data collection, instrumentation, and data reduction methods. The discovery of synchondron radiation sources, area detector-based data collection instruments, and high-speed computers has dramatically improved the efficiency of crystallographic structural elucidation. Single crystal X-ray diffraction is sufficient for the complete prediction of the compound, but developing a single crystal of sufficient size, quality, and stability is very difficult. The X-ray diffraction method is applicable for the determination of the complexes in the solid state[35–37]. The study of X-ray diffraction patterns with the help of equations was developed by Lipson[7] et al. Different crystallographic systems can be predicted with the help of mathematical expressions.

The diffraction pattern of the selected complexes of HBT, HBG, and HBH was recorded between 2θ values of 10° and 90°. Using the peaks obtained, determine the nature of the crystalline systems and the constants A, B, and C. $A = \lambda^2/4a^2$, $B = \lambda^2/4b^2$, $C = \lambda^2/4c^2$) were calculated, and also the lattice constants a, b, and c and the

volume were obtained. Using equation 8 in Chapter 1, the density and number of molecules were also calculated.

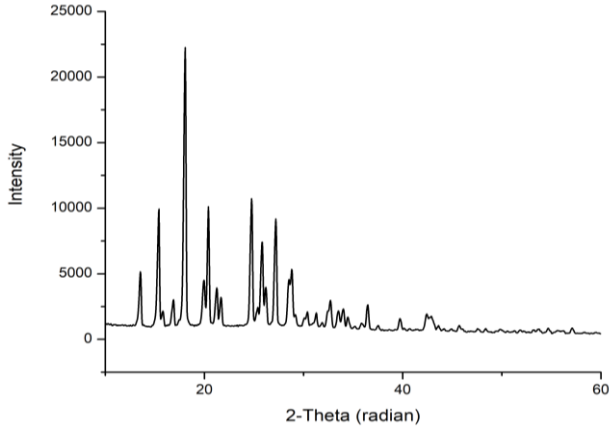

Fig 3.1: Crystallographic pattern of HBT

Table 3.1: XRD data of HBT

Crystal system: Orthorhombic

A=0.01395	B=0.003671	C=0.00279
a=6.52145	b=12.71275	c=14.58242

Cell volume: 1208.96498A^3
Density: 1.013gm/cm^3
No of molecules per unit cell: 2

Peak No.	2θ	$Sin^2\theta$		d-spacing	Relative intensiy	h	k	l
		Calculated	Observed					
1.	13.5464		0.01395	6.5314	23.55			
2.	15.3720	.017885	0.0179	5.7610	44.88	0	2	1
3.	16.8498	.021498	0.0215	5.2573	14.23	1	1	1
4.	18.0234	.024547	0.02455	4.9176	100	1	1	1
5.	20.3705	.031283	0.0313	2.2133	45.37	0	1	3

6.	24.7606	.046006	0.046	1.8390	48.79	1	2	2
7.	25.8038	.049899	0.0499	1.7698	35.08	0	2	1
8	27.1512	.055107	0.0551	1.6880	41.69	0	3	1
9.	28.8029	.061893	0.0619	1.5990	25.49	0	3	2
10.	32.7148	.079315	0.0793	1.4253	14.26	2	2	1
11	36.4529	.097796	0.0978	1.2963	12.58	1	4	3

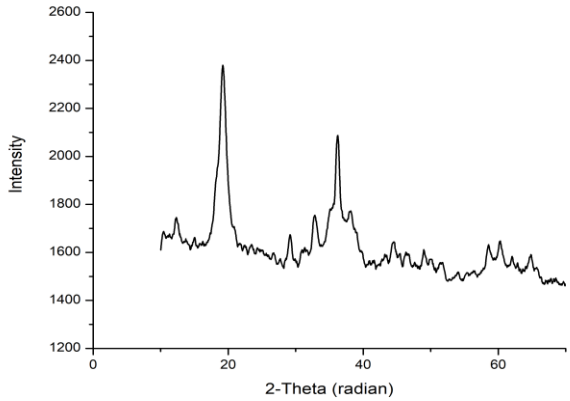

Fig 3.2: Crystallographic pattern of of $Mn(BT)_2(H_2O)_2$

Table 3.2: XRD data of $Mn(BT)_2(H_2O)_2$

Crystal system: Orthorhombic

A=0.01395	B=0.003671	C=0.00279
a=6.52145	b=12.71275	c=14.58242

Cell volume: 1208.96498A^3
Density: 1.013gm/cm^3
No of molecules per unit cell: 2

PEAK NO	2θ	$Sin^2\theta$		d-spacing	Relative intensiy	h	k	l
		calculated	observed					
1.	12.3728		0.0116	5.7610	73.94			
2.	19.1535	.0276	0.0276	4.6316	100	1	0	2
3.	29.1506	.0633	0.0633	3.0614	71.21	1	2	4

4.	32.6713	.079102	0.0791	2.7391	73.90	1	1	5
5.	36.1921	.096398	0.0964	2.4798	90.92	2	2	3
6.	44.49	.143351	0.14335	2.035007	70.10661	3	1	3
7.	48.92	.171453	0.17145	1.860507	68.27292	3	4	1
8.	58.49	.238698	0.2387	1.576766	69.29638	2	5	2
9.	60.35	.252650	0.25265	1.534363	69.72281	0	5	5
10.	62.09	.26555	0.26555	1.493601	67.33475	4	1	5
11.	64.92	.288088	0.2881	1.435159	67.3774	3	4	2

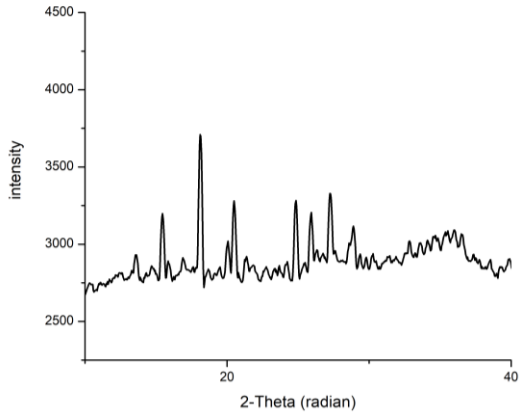

Fig 3.3. Crystallographic pattern of $Fe(BT)(H_2O)_2Cl_2$

Table 3.3.XRD data of $Fe(BT)(H_2O)_2Cl_2$

Crystal system: Orthorhombic

A=0.014 B=0.004242 C=0.002979
a=6.509800647 b=11.82623147 c=14.116226
Cell volume: 1089.289429A^3
Density: 1.6177gm/cm^3
No of molecules per unit cell: 2

PEAK NO	2θ	$Sin^2\theta$		d-spacing	Relative intensiy	h	k	l
		calculated	observed					
1.	13.5899		0.014	6.510989	79.30295			
2.	15.4154	.017902	0.0179	5.7438	85.17	0	1	2
3.	18.1103	.024701	0.0247	4.8966	100	1	1	1
4.	20.06	.030352	0.03035	4.424182	80.67024	0	2	1
5.	20.5009	.031608	0.0316	4.3296	87.66	0	2	2

6.	24.8475	.0462	0.0462	3.5808	87.85	0	2	2
7.	25.8907	.050094	0.0501	3.4386	85.38	0	3	2
8.	27.2816	.0556	0.0556	3.2665	89.49	1	1	3
9.	28.9333	.0624	0.0624	3.0834	83.45	0	2	2
10.	32.84	.079948	0.07995	2.725584	81.3941	0	3	1

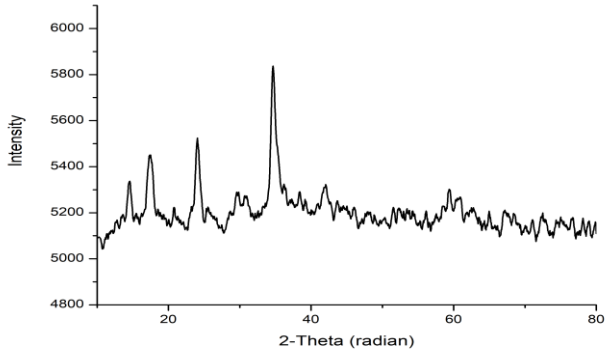

Fig 3.4: Crystallographic pattern of $Co(BT)(H_2O)_4$

Table 3.4: XRD data of $Co(BT)(H_2O)_4$

Crystal system: Orthorhombic

A=0.0157	B=0.003829	C=0.00314
a=6.14726	b=12.44769	c=13.7457

Cell volume: 1051.81119A^3
Density: 1.5346 gm/cm^3
No of molecules per unit cell: 2

PEAK NO	2θ	$Sin^2\theta$		d-spacing	Relative intensiy	h	k	l
		calculated	observed					
1.	14.4157		0.0157	6.1423	91.04			
2.	17.3279	.022702	0.0227	5.1145	92.98	0	1	2
3.	20.7617	.032503	0.0325	4.276791	90.01208	1	1	2
4.	24.0651	.043496	0.0435	3.6960	94.72	0	2	2
5.	29.5418	.065043	0.06505	3.021773	91.06434	0	3	3
6.	34.6708	.088799	0.0888	2.5855	100	1	3	1
7.	41.9296	.128054	0.12805	2.153341	91.6681	2	3	2
8.	59.3593	.245193	0.2452	1.555746	91.44385	3	4	1
9.	62.967	.270232	0.27275	1.47501	89.85682	4	0	2
10.	65.0099	.288801	0.2888	1.433557	89.61532	4	3	1
11.	72.3556	.348436	0.34845	2.541241	89.56357	2	4	1

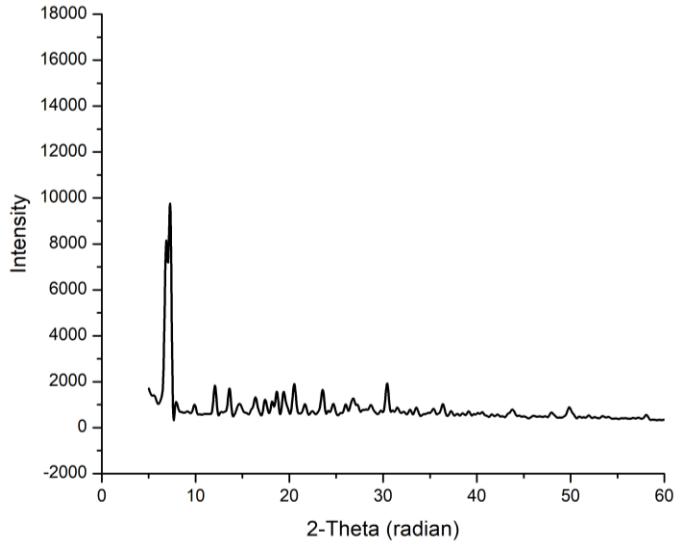

Fig 3.5. Crystallographic pattern of HBG

Table 3.5.XRD data of HBG
Crystal system: Orthorhombic

A=0.0035	B=0.0014	C=0.001
a=13.031	b=20.6037	c=24.37

Cell volume: 6545.3042A^3
Density: 1.006 gm/cm^3
No of molecules per unit cell: 14

PEAK NO	2θ	$Sin^2\theta$		d-spacing	Relative intensiy	h	k	l
		Calculated	Observed					
1.	11.9762	0.0108	.0108	7.3833	5.16	1	1	3
2.	13.4540	0.0138	.013797	6.7705	2.81	1	3	2
3.	21.3648	0.0346	.034603	4.1387	5.87	2	3	2
4.	22.5384	0.0384	.0384	3.9266	8.77	0	4	4
5.	33.4483	0.0828	.0828	2.6766	4.08	2	3	5

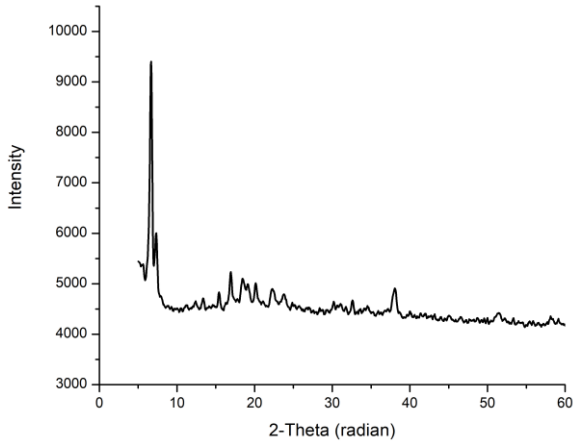

Fig 3.6. Crystallographic pattern of $Co(BG)_2(CH_3COO)H_2O$

Table 3.6.XRD data of $Co(BG)_2(CH_3COO)H_2O$

Crystal system: Orthorhombic

A=0.0033 B=0.001375 C=0.003
a=13.40833145 b=20.7902 c=14.075
Cell volume: 3926.9822A^3
Density: 2.7012 gm/cm^3
No of molecules per unit cell: 9

PEAK NO	2θ	Sin2θ		d-spacing	Relative intensiy	h	k	l
		Calculated	Observed					
1	15.4535	0.018	.018	5.7289	51.78	0	1	1
2	16.9313	0.0216	.0216	5.232	56.12	2	2	2
3	18.4961	0.0258	.0258	4.7928	54.81	2	2	1
4	20.1043	0.0304	.0304	4.4129	53.87	2	2	2
5	22.2776	0.0373	.0373	3.987	52.63	1	4	2
6	23.7120	0.0422	.04218	3.749	51.57	3	1	3
7	38.0991	0.1065	.1065	2.3599	52.69	5	0	4
8	51.4431	0.1883	.1883	1.7747	47.57	1	4	3

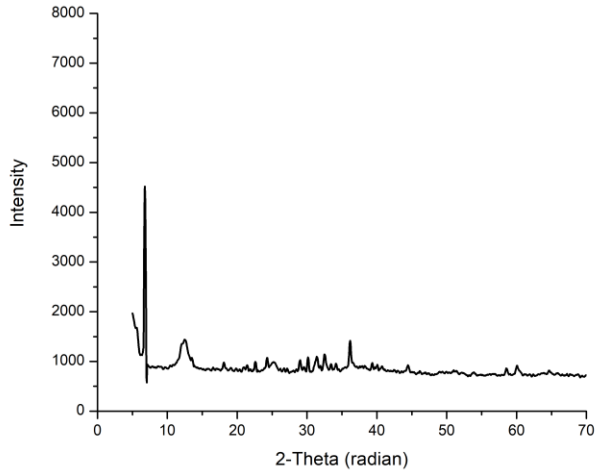

Fig 3.7. Crystallographic pattern of $CuBG)(CH_3COO)_4$

Table 3.7.XRD data of $Cu(BG)(CH_3COO)_4$

Crystal system: Orthorhombic

A=0.0034	B=0.002	C=0.001
a=13.2212	b=17.2383	c=24.3786

Cell volume: 5556.1436A^3
Density: 1.5692 gm/cm^3
No of molecules per unit cell: 9

PEAK NO	2θ	Sin2θ		d-spacing	Relative intensiy	h	k	l
		Calculated	Observed					
1	12.4543	0.0117	.011699	7.101	31.5631	0	3	2
2	18.1483	0.0249	.0249	4.8839	21.3958	1	2	5
3	22.6253	0.0384	.0384	3.9266	22.0563	1	3	1
4	30.1449	0.0676	.0676	2.962	23.9448	2	5	2
5	31.3619	0.073	0.073	2.8498	23.9013	4	4	3
6	32.5355	0.0784	.0784	2.7496	25.0374	1	5	5
7	36.1432	0.0962	.0962	2.483	30.8718	5	3	1
8	44.4886	0.1433	.143299	2.0347	20.3126	2	5	3
9	58.5715	0.2392	.239214	1.5746	18.7582	5	3	4
10	60.0493	0.2503	.250305	1.5393	20	4	5	4

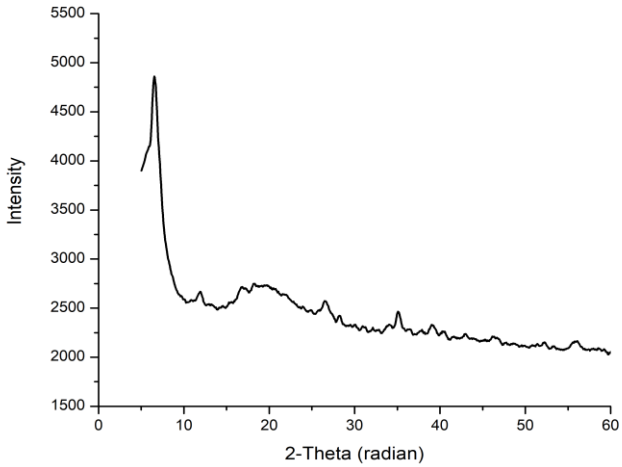

Fig 3.8. Crystallographic pattern of $Fe(BG)(H_2O)_2Cl_2$

Table 3.8.XRD data of $Fe(BG)(H_2O)_2Cl_2$
Crystal system: Orthorhombic

A=0.0032 B=0.001778 C=0.001
a=13.628 b=18.284 c=24.379
Cell volume: 6074.551A^3
Density: 1.5104 gm/cm^3
No. of molecules per unit cell: 12

PEAK NO	2θ	Sin2θ		d-spacing	Relative intensiy	h	k	l
		Calculated	Observed					
1	11.9327	0.0108	0.010801	7.4102	53.81	1	1	3
2	19.3654	0.0282	.0282	4.5795	54.84	1	3	3
3	26.5372	0.0526	.052598	3.3559	51.46	3	1	5
4	28.2324	0.0594	.0594	3.1581	49.39	4	1	3
5	34.1003	0.0859	.0859	2.6269	46.68	5	2	1
6	35.1435	0.0911	.0911	2.5513	49.89	3	5	1
7	38.9684	0.1112	.1112	2.3092	46.83	1	3	3

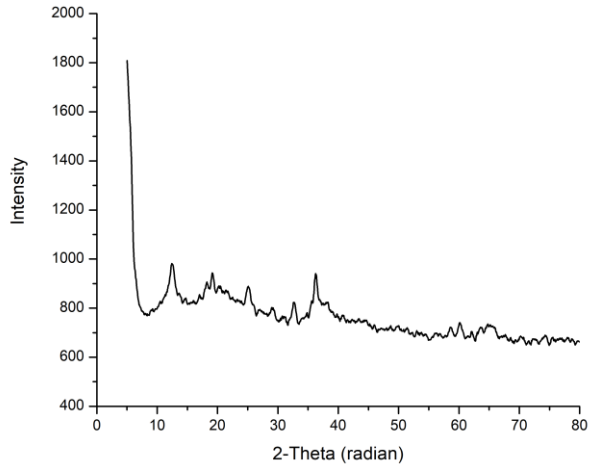

Fig. 3.9. Crystallographic pattern of $Mn(BG)_2(H_2O)_2$

Table 3.9.XRD data of $Mn(BG)_2(H_2O)_2$

Crystal system: Orthorhombic

A=0.0018 B=0.006 C=0.0006
a=18.171 b=9.95 c=31.47

Cell volume: 5691.68A^3
Density: 2.5913 gm/cm^3
No of molecules per unit cell: 14

PEAK NO	2θ	Sin2θ		d-spacing	Relative intensiy	h	k	l
		Calculated	Observed					
1	12.5413	0.0119	.01119	7.052	52.86	1	3	2
2	19.1915	0.0277	.0277	4.6207	50.61	2	4	3
3	25.1463	0.0473	.0473	3.5383	47.6	4	1	1
4	29.1452	0.0633	.0633	3.0613	43.04	1	4	3
5	32.5790	0.0786	.0778	2.746	44.16	1	2	2
6	36.2301	0.0966	.0966	2.4772	51.02	0	4	1
7	60.1363	0.251	.25095	1.5373	39.75	2	5	5

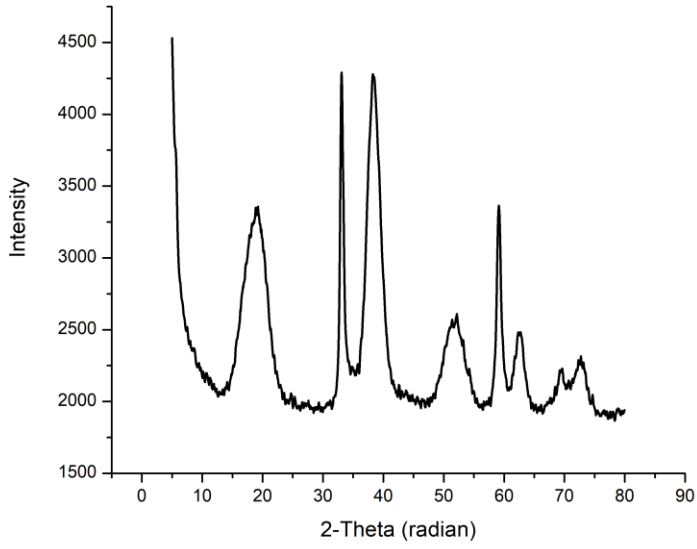

Fig.3.10. Crystallographic pattern of $Ni(BG)(H_2O)_2(CH_3COO)_2$

Table 3.10.XRD data of $Ni(BG)(H_2O)_2(CH_3COO)_2$

Crystal system: Orthorhombic

A=0.0019 B=0.0038 C=0.001
a=17.686 b=12.506 c=24.379
Cell volume: 5392.117 A^3
Density: 2.3292 gm/cm^3
No of molecules per unit cell: 15

PEAK NO	2θ	Sin2θ		d-spacing	Relative intensiy	h	k	l
		Calculated	Observed					
1	18.8438	0.0267	.0267	4.7051	74.22	2	3	2
2	33.1006	0.0811	.0811	2.7039	93.54	3	5	3
3	38.2295	0.1072	.1072	2.3521	94.56	4	4	4
4	52.1386	0.1931	.193088	1.7221	57.5	4	4	3
5	59.1366	0.2435	.2435	1.5609	73.82	5	3	5
6	62.6573	0.2703	.270275	1.4814	54.65	4	5	1
7	69.4814	0.3247	.324719	1.3516	48.9	3	4	2
8	72.7848	0.352	.352	1.2982	50.97	5	4	1

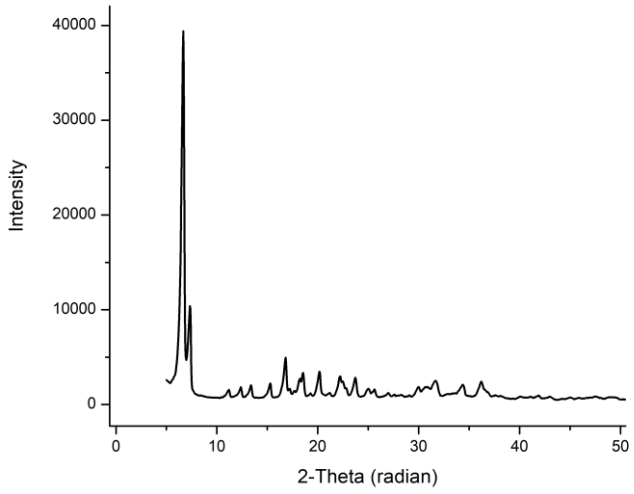

Fig.3.11. Crystallographic pattern of $Zn(BG)(H_2O)_4$

Table 3.11.XRD data of $Zn(BG)(H_2O)_4$

Crystal system: Orthorhombic

A=0.003388 B=0.002125 C=0.000919
a=13.2211 b=16.69 c=25.385
Cell volume: 5602.934 A^3
Density: 2.349 gm/cm^3
No of molecules per unit cell: 19

PEAK NO	2θ	Sin2θ		d-spacing	Relative intensiy	h	k	l
		Calculated	Observed					
1	7.3254	0.0041	.004094	12.0596	26	0	2	1
2	16.8009	0.0213	.0213	5.2734	12.57	2	2	2
3	18.4961	0.0258	.0258	4.7937	8.35	2	1	3
4	20.1478	0.0321	.032099	4.40434	8.72	2	4	2
5	22.2341	0.0372	.037201	3.99556	7.5	2	4	3
6	23.7120	0.0422	.0422	3.7497	7.35	0	4	3
7	31.7097	0.0747	.0747	2.8198	6.37	4	2	1
8	34.4045	0.0875	.087501	2.6049	5.29	4	5	1
9	36.1866	0.0965	.096498	2.4806	6.12	4	3	5

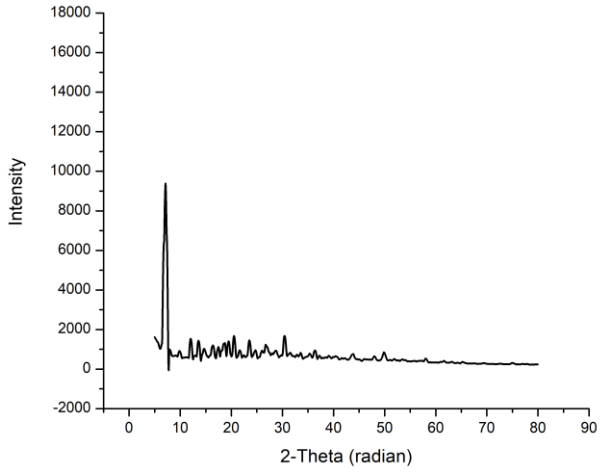

Fig.3.12: Crystallographic pattern of $Cd(BG)(H_2O)_2$

Table 3.12: XRD data of $Cd(BG)(H_2O)_2$

Crystal system: Orthorhombic

A=0.0036 B=0.004 C=0.0018
a=12.849 b=12.189 c=18.17

Cell volume: 2845.839 A^3
Density: 1.2981 gm/cm^3
No of molecules per unit cell: 5

PEAK NO	2θ	Sin2θ		d-spacing	Relative intensiy	h	k	l
		Calculated	Observed					
1	7.32	0.0041	.0041	12.0601	100	0	1	2
2	12.11	0.0111	.0111	7.3092	17.25	1	1	1
3	16.36	0.0202	.0202	5.4177	11.37	2	1	1
4	18.19	0.025	.025	4.8759	10.13	0	4	1
5	19.40	0.0284	.0284	4.5721	14.2	2	1	1
6	21.71	0.0355	.0355	4.0935	7.8	1	3	3
7	24.71	0.0458	.0458	3.6033	8.18	0	5	1
8	30.44	0.0689	.0689	2.9348	13.96	3	4	1
9	36.40	0.0976	.0976	2.4668	6.86	4	1	1
10	49.79	0.1772	.1772	1.8307	5.51	2	3	1

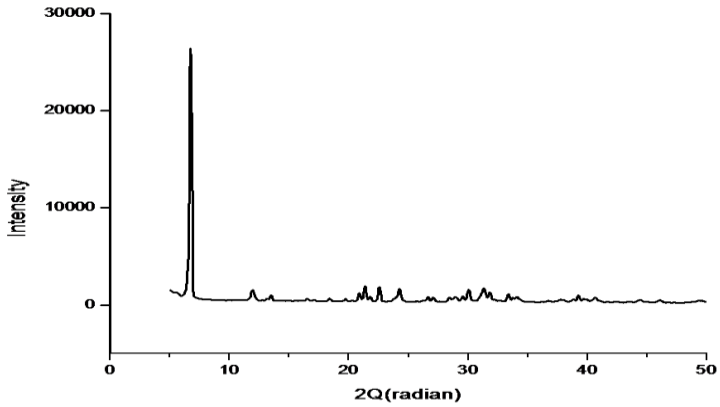

Fig.3.13.Crystallographic pattern of HBH

Table3.13.XRD data of HBH

Crystal system: Orthorhombic

A=0.0034	B=0.002	C=0.0017
a=13.20967852	b=17.2233136	c=18.68130652

Cell volume: 4250.26691A^3
Density: 1.134
No of molecules per unit cell: 8

PEAK NO	2θ	Sin2θ		d-spacing	Relative intensiy	h	k	l
		Calculated	Observed					
1.	11.9762	0.0108	.0108	7.3833	5.92	1	1	2
2.	13.4540	0.0137	.0128	6.5755	3.79	1	2	2
3.	21.3648	0.0343	.0343	4.1553	7.4	3	1	1
4.	22.5384	0.0381	.0381	3.9415	7.05	2	1	4
5.	24.2335	0.044	.044003	3.6695	6.28	3	2	3
6.	30.0580	0.0672	.06722	2.9704	6.14	4	3	1
7.	31.3185	0.0728	.0728	2.8536	6.43	2	2	4
8	33.4048	0.0825	.082529	2.68	4.298	4	3	4

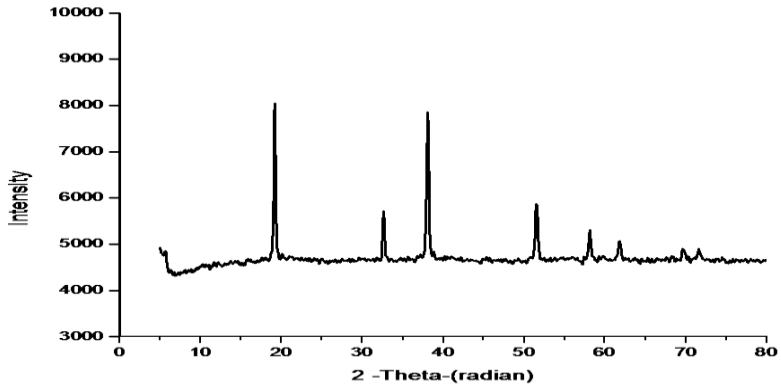

Fig. 3.14. Crystallographic pattern of $Co(BH)(H_2O)_4$

Table 3.14.XRD data of $Co(BH)(H_2O)_4$

Crystal system: Orthorhombic

A=0.0019 B=0.0095 C=0.001
a=17.7 b=7.909 c=24.38
Cell volume: 3410.274 A^3
Density: 1.6845 gm/cm^3
No of molecules per unit cell: 7

PEAK NO	2θ	Sin2θ		d-spacing	Relative intensiy	h	k	l
		Calculated	Observed					
1.	32.6224	.078798	0.0788	2.7425	71.07	1	1	2
2.	38.0991	.106123	0.1065	2.3599	97.66	1	2	2
3.	51.5300	.1889	0.1889	1.7719	73.02	3	1	1
4.	58.1368	.236038	0.236	1.5853	66.07	2	1	4
5.	61.7880	.2636	0.2636	1.5001	63.06	3	2	3
6.	69.7422	.3268	0.3268	1.3472	60.73	4	3	1
7.	71.6982	.34295	0.3429	1.3151	60.43	2	2	4

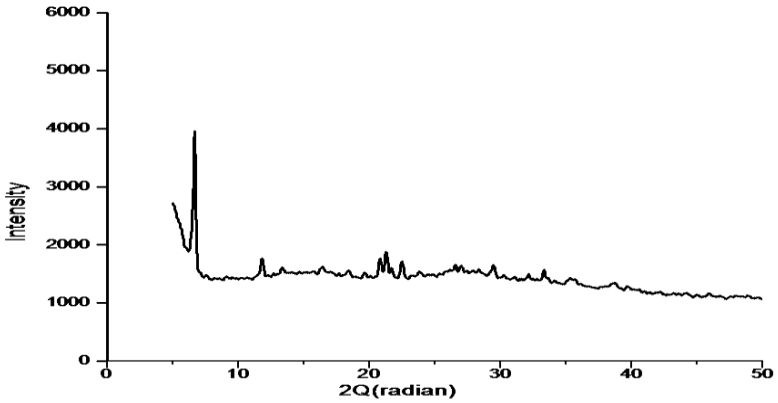

Fig.3.15. Crystallographic pattern of $Cu(BH)(H_2O)_4$

Table 3.15.XRD data of $Cu(BH)(H_2O)_4$

Crystal system: Orthorhombic

A=0.0033 B=0.0055 C=0.0015
a=13.40833145 b=10.38604888 c=19.88776948
Cell volume: 2769.562542 A^3
Density: 1.1438 gm/cm^3
No of molecules per unit cell: 4

PEAK NO	2θ	Sin2θ		d-spacing	Relative intensiy	h	k	l
		Calculated	Observed					
1.	11.8458	.010648	0.0106	7.4643	44.77	1	1	2
2.	21.2779	.034083	0.034	4.1721	47.55	0	1	1
3.	22.4949	.038008	0.038	3.949	43.29	0	3	4
4.	29.4494	.0646	0.0646	3.0303	41.78	4	1	2
5.	33.3614	.0823	0.0823	2.6834	39.66	4	1	4

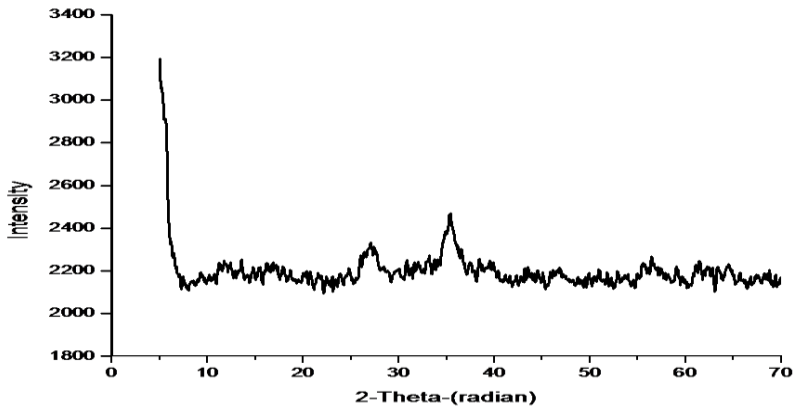

Fig.3.16. Crystallographic pattern of $Fe(BH)(H_2O)_2Cl_2$

Table 3.16.XRD data of $Fe(BH)(H_2O)_2Cl_2$

Crystal system: Orthorhombic

A=0.0019 B=0.0095 C=0.00043
a=17.6707469 b=7.902598257 c=37.14475338
Cell volume: 5187.072164 A^3
Density: 1.9356 gm/cm^3
No of molecules per unit cell: 12

PEAK NO	2θ	Sin2θ		d-spacing	Relative intensiy	h	k	l
		Calculated	Observed					
1.	11.8458	.0547	0.0547	3.2924	73.04	5	2	3
2.	21.2779	.092545	0.0924	2.5331	77.3	4	5	2
3.	22.4949	.15777	0.1578	1.9389	69.08	1	4	3
4.	29.4494	.184842	0.1848	1.7913	68.82	2	3	4
5.	33.3614	.223247	0.2241	1.6269	70.64	5	5	5

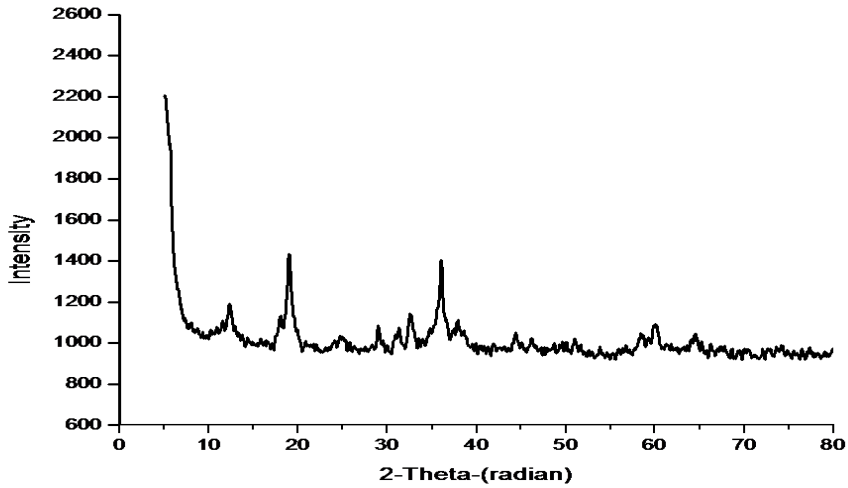

Fig.3.17. Crystallographic pattern of $Mn(BH)_2(CH3COO)_4$

Table 3.17.XRD data of $Mn(BH)_2(CH3COO)_4$

Crystal system: Orthorhombic

A=0.00191 B=0.002375 C=0.000613
a=17.7 b=15.86 c=31.2189
Cell volume: 8665.954273 A^3
Density: 1.3084 gm/cm^3
No of molecules per unit cell: 11

PEAK NO	2θ	Sin2θ		d-spacing	Relative intensiy	h	k	l
		calculated	observed					
1.	12.2805	.0114	0.0114	7.2011	53.32	2	0	1
2.	17.3279	.02399	0.0244	4.9316	50.89	0	3	5
3.	24.7551	.0459	0.0459	3.5933	46.4	1	5	5
4.	24.0651	.062498	0.0625	3.0793	48.6	4	5	1
5.	29.5418	.07281	0.0728	2.8536	48.02	3	5	2
6.	34.6708	.07861	0.0786	2.7466	51.25	3	3	3
7.	41.9296	.0957	0.0957	2.4888	63.11	4	3	3
8.	59.3593	.1051	0.1051	2.3756	49.37	4	5	5
9.	62.967	.142694	0.1427	2.0384	46.76	5	3	5
10.	65.0099	.239189	0.2392	1.5749	46.67	0	5	2
11.	72.3556	.250694	0.2507	1.5383	48.78	0	5	5

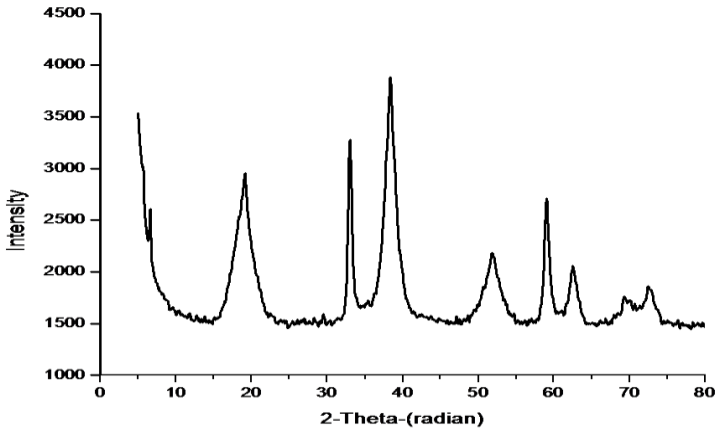

Fig.3.18. Crystallographic pattern of $Ni(BH)(H_2O)_2(CH3COO)_2$

Table 3.18.XRD data of $Ni(BH)(H_2O)_2(CH3COO)_2$
Crystal system: Orthorhombic

A=0.0019 B=0.0095 C=0.000864
a=17.7 b=7.909 c=26.227
Cell volume: 3659.313742 A^3
Density: 1.2553 gm/cm^3
No of molecules per unit cell: 5

PEAK NO	2θ	Sin2θ		d-spacing	Relative intensiy	h	k	l
		calculated	observed					
1.	19.1481	0.0276	0.0276	4.631	76.1	2	1	1
2.	33.0136	0.08123	0.0807	2.7109	84.31	3	5	2
3.	38.3599	0.107905	0.1079	2.3444	100	5	4	5
4.	51.7908	0.190701	0.1907	1.7636	56.22	3	4	5
5.	59.0496	0.24282	0.2428	1.563	69.83	1	5	3
6.	62.5269	0.2689	0.2693	1.4841	53.01	4	3	5
7.	72.4805	0.3491	0.3494	1.3029	47.97	1	4	4

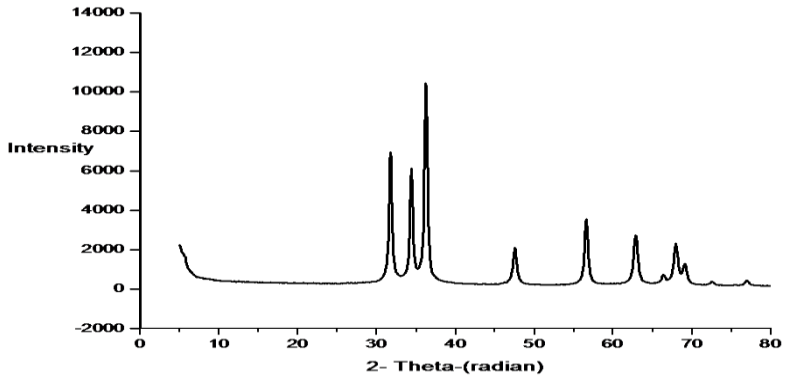

Fig.3.19. Crystallographic pattern of $Zn(BH)(H_2O)_4$

Table 3.19.XRD data of $Zn(BH)(H_2O)_4$
Crystal system: Orthorhombic

A=0.00191 B=0.00475 C=0.000413
a=17.686 b=11.215 c=38.0342
Cell volume: 7465.460582 A^3
Density: 1.1194 gm/cm^3
No of molecules per unit cell: 10

PEAK NO	2θ	Sin2θ		d-spacing	Relative intensiy	h	k	l
		calculated	observed					
1.	31.7531	.07457	0.0748	2.1861	66.46	4	3	2
2.	34.4045	.08741	0.0874	2.6044	58.69	0	3	2
3.	36.2301	.0966	0.0966	2.4772	100	5	4	5
4.	47.5312	.162405	0.1624	1.9113	20.07	1	5	2
5.	56.5721	.223744	0.2245	1.6254	34.06	5	4	5
6.	66.3953	.2997	0.2997	1.4067	7.14	4	5	5
7.	67.9601	.312799	0.3123	1.3781	22.14	2	4	2

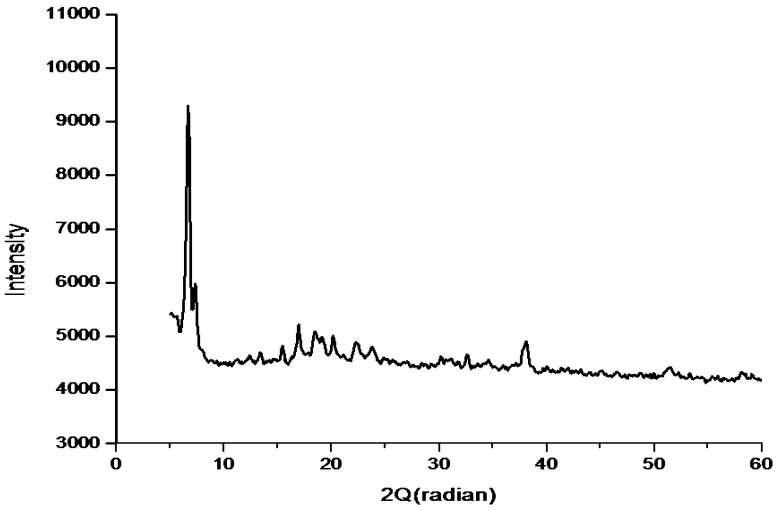

Fig.3.20. Crystallographic pattern of $Cd(BH)(H_2O)_2$

Table 3.20.XRD data of $Cd(BH)(H_2O)_2$

Crystal system: Orthorhombic

A=0.001865 B=0.0038 C=0.000487
a=17.7 b=12.3903 c=34.611
Cell volume: 7778.563904 A^3
Density: 1.6177 gm/cm^3
No of molecules per unit cell: 15

PEAK NO	2θ	Sin2θ		d-spacing	Relative intensiy	h	k	l
		calculated	observed					
1.	23.84	.041908	0.0427	3.7299	69	4	3	1
2.	30.66	.070373	0.0699	2.914	100	3	5	4
3.	36.75	.0994	0.0994	2.4438	33	0	5	3
4.	44.05	.1406	0.1406	2.0543	25	2	2	3
5.	50.18	.18006	0.1798	1.8168	37	1	3	3
6.	58.45	.238032	0.2385	1.5781	16	6	3	9
7.	62.04	.265558	0.2653	1.4949	13	3	5	3

References:

1. Cullity B. D. (1978). "Elements of X-ray Diffraction", 2nd Edition, Addison-Wesley Publishing Company Inc., London.

2. Klug, H. P., & Alexander, L. E. (1955). "X-ray Diffraction Procedures for Poly Crystalline and Amorphous Materials", 2nd Edition, John Wiley & Sons, New York.

3. Hull, A. W., & Davey, W. P. (1921). *Phys. Rev*., 17, 549.

4. Bjurstrom, T. (1931). *Phys. Z*., 69,346.

5. Bunn, C. W. (1945) . "Chemical Crystallographic Physics", Oxford University Press, 133.

6. R. Hesse. (1948). *Acta Crystallogr*., 1, 200.

7. Lipson, H. (1949). *Acta Crystallogr*., 2,43.

8. Hentry, N. F. M., Lipton, H., & Wooster, W. A. (1951). "Interpretation of X-ray Diffraction Photographs", 81.

9. Bhagavantam, S. (1955). In *Proceedings of the Indian Academy of Sciences-Section A*, 41, 72.

10. Hearmon, R. F. S. (1956). The elasic constants of anisotropic materials II. Phil. Mag.,5, 323.

11. Krishnan, R. S. (1958). "Progress in Crystal Physics".

12. Krishnamurty, M., & Narayana, M. S. (1969). "Physics of Solid State", Academic Press, London, 487.

13. Azaroff, L.V., & Buerger, M. J. (1958). "The Powder Method in X-ray Crystallography", McGraw Hill, New York.

14. d'Eye, R. W. M., & Wait, E. (1960). "X-ray Powder Photography in Inorganic Chemistry", Academic Press, New York.

15. Lipson, H., & Steeple, H. (1970). "Interpretation of X-ray Powder Diffraction Pattern", Macmillan, London.

16. Doman, T. N., Williams, D. E., Banks, J. F., Buchanan, R. M., Chang, H. R., Webb, R. J., & Hendrickson, D. N.(1990). *Inorg. Chem*., 29, 1058.

17. Dexin, L., Shulan, L., Xuegue, C., Xiaoyan, L., Xuexiao, G., & Xuehao, H. (1993).14, 879.

18. Nath, M., (1991). *Thermochimica Acta*, 185, 11.

19. Dhamwaskar, S., & Salvi, S. V. (1995). *Asian J. Chem*., 7, 289.

20. Garcia-Raso, A., Fiol, J. J., Badenas, F., & Quiros, M. (1996). *Polyhedron*, 15, 4407.

21. Shuilan, L., De-xin, L., Hai-wei, X., Zhao-He, Y., & Huaxue, J. (1997). 16, 159.

22. Mahmood, S., Malik, M. A., Molevalli, M., Nunn, P. B., & O'Brien, P. (1998). *Tetrahedron*, 54, 5721.

23. Cavaco, I., Pessoa, J.C., Costa, D., Duarte, M.T., Gillard, R.D., & Matias, P. (1994). *J. Chem. Soc. Dalton Trans*., 2, 149.

24. Mahesh, K. K., & Goutam, R. K. (1991). *Asian J. Chem*., 4, 417.

25. Chourasia, P., Suryesh, K. K. & Mihra, A. P. (1993). *Proc. Indian. Acad. Sci*., 105, 173.

26. Singh, R., & Gautam, R. K. (1987). *J. Indian. Chem. Soc*., 14,631.

27. Cherayath, S. R., Alice, J., & Prabhakaran, C. P. (1990). *Trans. Met. Chem*., 15, 449.

28. Caric, S., Petrovic, D., Lazar, D., & Leovaz, V. M. (1978). *Z. Kristallogr*., 148, 153.

29. Lali, K. T. (1994). Ph. D Thesis, Calicut University, Kerala 206-227.

30. Sleema, B., & Parameswaran, G. (2002). *Asian J.Chem*., 14, 961.

31. Indiradevi, G., (2002). Ph. D Thesis, Calicut University, Kerala 144-151.

32. Casrineiras, A., Castro, J. A., Duran, M. L., Vazquez, J. A. G., Macias, A., Romero, J., & Sousa, A. (1989). *Polyhedron,* 89, 2543.

33. Kumar, C. S., Ray, B. P., Samudranil, D. P., Chakravarthy, & Anemesh, (1990). *Inorg. Chem*., 29, 2428.

34. Jacob, K. S. (2008). Ph. D Thesis, Calicut University, Kerala, 144-151.

35. Harris, K. D. M. (2002). Curr. Opin. *Solid. St. M*., 6, 125.

36. Harris, K. D. M., Tremayne, M., & Kariuki, B. M. (2001). *Angew .Chem. Int. Ed.,* 40, 1626.

37. Langford, J. I., & Louer, D. (1996). *Rep. Prog. Phys*., 59, 131.

PART IV

CORROSION INHIBITION STUDIES OF DIPHENYL GLYCOLIC ACID (BENZILIC ACID) –AMINO ACID LIGANDS ON MILD STEEL

CHAPTER 1

INTRODUCTION

Corrosion is a natural phenomenon in which the pure metals are transformed to undesirable substances on reaction with water, air and sulfates. In other words it can be explained as an electrochemical phenomenon that converts the refined metal to its chemically stable form on reaction with an oxidant such as oxygen and sulfates. During corrosion all the atoms of the metal surface get oxidized and the oxidant gets reduced. Metals easily oxidize by losing the electrons and the oxidant is reduced by gaining electrons and transforms to oxide. This reaction gets accelerated by warm temperatures and by acids and salts. Corrosion is a dangerous cause faced by the developing as well as developed countries. A huge amount of money is used for the replacement of corroded materials every year. Corrosion is proving to be a big threat in both social as well as economic ways. Corrosion emerged as a social issue because of the hazardous byproducts expelled during the process and the cost for the replacement of metals corroded during each time interval is very huge. Corrosion products itself can act as a corrosion inhibitor by staying on the surface and protect the metal beneath from further corrosion. It is a diffusion controlled process thus it occurs only on the exposed surfaces. Combative acid solutions are frequently used in industries for applications like acid pickling, acid cleaning, acid de-scaling and oil well cleaning.

Hydrochloric acid is the most common acid used for the industrial processes and acidification of oil wells. In the acidifying procedure of petroleum oil wells in order to increase the flow of oil 15% of hydrochloric acid is enforced to the well through the steel tubing to open up near-bore canals in the formation. The aggressive nature of hydrochloric acid leads to the corrosion of steel tubing. The consequence of the process is the dreadful loss of resources and money. Corrosion engineering is one of the major fields dedicated for controlling and preventing corrosion. Normal techniques used for the reduction of corrosion involve coating, painting, galvanizing and anodizing. Nowadays electropolishing, hot dip galvanizing, cathodic protection, anodic protection and use of adsorption inhibitors are the new methods improved for the surface treatment. Great efforts are carrying out by scientific community to prevent the corrosion or to diminish the rate of corrosion every year. A lot of remedies have been already described and the research world is in a hurry to develop an immediate solution to reduce corrosion. Out of the numerous techniques, employing of corrosion inhibitors is one of the most important techniques for controlling the corrosion.

An inhibitor is a compound, when coated in small concentrations to an situation they can decrease the rate of corrosion. In other words it is regarded as the retarding catalysts. They get adsorbed on the surface of the metal and suppress the metal dissolution and reduction reactions. Major class of these compounds was organic

amines and its derivatives. One of the cost efficient techniques to protect metal against corrosion is the use of organic inhibitors. The adsorption of organic inhibitors on the metal surface occurs via the formation of a coordinate covalent bond (chemical adsorption) or the electrostatic interaction between the metal and inhibitor. Organic compounds containing hetero atoms with electronic lone pair (N, O, S and P), or p systems, or conjugated bonds, or aromatic rings, are generally considered to be effective corrosion inhibitors. Corrosion inhibitors are heterocyclic compounds containing N, S and O atoms and can prevent the rate of corrosion. The inhibitor contains various functional groups which are capable of donating lone pair of electrons which can contribute towards the adsorption on the metal surface, bonds with the vacant metal orbital. There is an electrostatic interaction between the alkyl/aryl groups with the vacant d-orbital of the metal surface. Therefore Schiff bases and their metal complexes are proved to serve as potential inhibitors nowadays. The inhibitor is adsorbed on the metal surface can be described mainly due to three reasons: (1) due to the interaction of non-bonding, lone/ unpaired electron or may be (2) the interaction of π-bonds or may be (3) due to the electrostatic interaction of the alkyl or aryl group with metal's vacant d-orbital.

Corrosion is considered to be an electrochemical reaction and the inhibitors slow down the velocity of the electrochemical reaction. The inhibitors are classified into anionic, cathodic and mixed type depending upon their mechanism. Anodic inhibitors diminish the

anodic part by acting on the anodic spots and polarize the anodic reaction and displace the corrosion potential in the positive direction whereas the cathodic inhibitors reduce the cathode part by acting on the cathodic spots and polarize the cathode reaction and displace the corrosion potential in negative direction. But there are few organic compounds which affect both cathodic and anodic reaction by adsorbing on the metal surface and repress the metal dissolution and reduction reaction.

Zhang[1] et al investigated the inhibition efficiency of arginine self-assembled monolayers on copper surface in 0.5 M hydrochloric acid (HCl) solution at room temperature and the synergic effect of iodide ions on the Arg SAMs was also studied. The EIS and polarization techniques show that Arg SAMs have limited protection effect but the addition of iodide ions improves the efficiency of Arg SAMs.Aouniti[2] et al have studied the inhibition efficiency of (*E*)-2-methyl-N-(thiophen-2-ylmethylidene)aniline (**T**) on steel in1M HCl using gravimetric and electrochemical methods. The outcome showed that thiophene derivative perform as a mixed type inhibitor and could inhibit both anodic metal dissolution and cathodic hydrogen evolution reactions and it obeys Langmuir adsorption isotherm. Density functional theory (DFT) methods have been used to evaluate the quantum mechanical study of the compound and also to correlate between the theoretical and experimental results.

Amino acids and hydroxy carboxylic acids can compete with the inhibition effect of CrO^{2-}_4 was investigated by Bereket[3] et al. They also studied the inhibition effect in NaCl at different pH values and also the effect of addition of $NaNO_3$ at different pH values. The electrochemical nature of 1-(2-ethylamino)-2-methylimidazoline (imidazoline), its precursor N-[3-(2-amino-ethylaminoethyl)]-acetamide (amide) and its derivative 1-(2-ethylamino)-2-methylimidazolidine (imidazolidine is studied using the potentiodynamic polarization curves and electrochemical impedance spectroscopy, EIS techniques by Cruz[4] and coworkers. Imidazoline act as efficient inhibitor at different concentrations but amides have low efficiency.DFTcalculations done to explain the corrosion inhibition efficiencies of the compounds. Lateef[5] et al synthesized Ni (II), Cu(II), Zn(II) complexes of salicylidine anthranilate sodium salt ligand and the inhibition study of the ligand and their complexes on the carbon steel in HCl investigated using the electrochemical study. They predicted that the inhibitor obeys the Langmuir adsorption isotherms which are in agreement with DFT calculations.

Inhibition efficiency of novel Co (II) and Cu (II) complexes of pyridinylimino phenolate sodium sulfonate (HPSS) have been examined by Adam[6] et al and they prove to be mixed type inhibiting agents and they prove to obey the Langmuir chemisorption. Copper complex exhibits the high potency which is greater than the ligand itself.Shaker[7] et al derived three anionic

oxide vanadium Schiff base N-salicylidene amino acid complexes and the inhibition studies against the carbon steel in chloride acid solution were carried out using EIS and PDP studies. The study reveals it as mixed type inhibitors with an maximum efficiency of 94% and theoretical calculations were in good agreement with experimental datas. The anticorrosive study of the *N′*-phenylbenzohydrazide and their Cu, Mn and Co metal complexes were carried out by electrochemical techniques and the theoretical studies were in agreement with the experimental studies[8].

Lateef[9] studied the corrosion inhibition studies and their computational calculations which provide the relationship between the inhibition efficiencies of studied inhibitors and their molecular structure. The polarization studies show that the compounds were acting as mixed-type inhibitors. The enhancement of inhibition efficiency with the increase in concentration was noted. The corrosion inhibition efficiency of novel eco-friendly azelaic acid dihydrazide has been studied by Amiery[10] et al. The maximum efficiency is 93% at 5×10^{-3} M and the potentiodynamic polarization studies reveals it to be a mixed- type inhibitor. The inhibitor obeys the Langmuir adsorption isotherm. Theoretical evaluation of some amino acid for corrosion inhibition of copper in acidic medium conducted by Ibrahimi[11] et al using DFT calculations, Monte Carlo simulations and QSPR studies. Aby[12] et al synthesized new Schiff base derived from 3-formylindole and 2-aminobenzoic acid and its Mn(II),Ni(II) and Cu(II) transition metal

complexes and their corrosion inhibition capacity screened by Electronic Impedance Spectroscopy and they were proved to be good corrosion inhibitor which obeying the Langmuir adsorption isotherm. Behpour [13] studied the corrosion inhibition effect of three Schiff bases 2-{[(2-sulfanylphenyl)imino]methyl}]phenol (A), 2-{[(2)-1-(4-methylphenyl)methylidene]amino}-1-benznethiol (B), and 2-[(2-sulfanylphen-yl)ethanimidoyl)]phenol (C) of mild steel using weight loss measurements, polarization and electrochemical impedance spectroscopy and the result shows it behave as a mixed type inhibitor wih high inhibiting potential. The DFT calculations were also done for the theoretical data and the compounds adsorption isotherm. Inhibition efficiency order is A ≈B > C in all methods employed with small differences in their numerical values.

The inhibition ability of a new class of Schiff bases of 2-({-1-methyl-3-[(2-sulfanylphenyl)imino]butylidene}-amino)-1-benzenethiol and 2-({-1,2-diphenyl-2-[(2-sulfanylphenyl)imino]ethylidene}amino)-1-benzenthiol were investigated using weight loss and electrochemical measurements. They were found to be mixed inhibitors following Langmuir adsorption isotherm. Results shows that compound 2 shows better inhibiton compared to that of compound 1. The morphological studies carried out by SEM micrographs[14].Bentiss[15] et al studied the corrosion inhibition efficiency of 2,5-bis(2-aminophenyl)–1,3,4-oxadiazole [2-APOX]) on the mild steel in HCl. Potentiodynamic studies clearly revealed that 2-APOX is a mixed

type inhibitor and it also obeys the Langmuir adsorption isotherm model. Jia[16] et al investigated the computational and electrochemical studies of amino acid compounds as corrosion inhibitors in acidic media. The PDP and EIS measurements shows the efficiency increasing order as follows: L-Ser\ L-Cys \L-His\L-Try wich are in agrrement with theoretical values. The inhibition effect of new S-heterocyclic Schiff base (SB) and the corresponding amine (DBTDA) on mild steel in HCl solution was investigated by Daoud[17] et al using various weight loss, electrochemical and morphological studies. They found to be a mixed type inhibitor and obeys Langmuir isotherm. Quantum mechanical parameters calculated using DFT method.

The inhibition ability of L-tryptophan in HCl solution was studied by Mobin[18] and co-workers using weight loss measurements which shows a maximum efficiency of 83% at 50° C at 500 ppm concentration. The Potentiodynamic results similar to that of weight loss method and the compound act as an anodic inhibitor. Saurav[19] et al investigated corrosion inhibition performance of 2-(2-hydroxybenzylideneamino)phenol (L1), 2-(5-chloro-2-hydroxybenzylideneamino)phenol (L2) and 2-(2-hydroxy-5-nitrobenzylideneamino)phenol (L3) of mild steel in 1 M HCl. The PDP studies showed that compounds behave as a mixed-type inhibitor and adsorption obeys the Langmuir adsorption isotherm. Surface studies using SEM technique which confirms the existence of an adsorbed film. Density functional theory and Molecular

Dynamics simulation used to establish the relationship between molecular configuration and their inhibition efficiencies.Mahendra[20] et al synthesized new amino acid derivatives namely, 2-(2-oxo-2-phenothiazin-10-yl)ethylamino)-3-mercaptopropanoic acid (OPEM) and 2-(2-oxo-2-phenothiazin-10-yl)ethylamino)acetic acid (OPEA) and corrosion study have been carried out. The inhibitors OPEM and OPEA shows efficiency of 97.5 and 95.8% respectively in 200 ppm and obeys Langmuir adsorption isotherm .Surface analysis carried out by SEM and the polarization studies reveals to be mixed type inhibitor. The Quantum mechanical results obtained from semiempirical AMI method were in good agreement with experimental studies and the higher value of E_{HOMO} and lower value $E_{LUMO,}$ and smaller value of ΔE, predicts the good corrosion inhibition efficiency of the mild steel in hydrochloric acid.

Simonovic[21] et al aimed to study a green non-toxic biodegradable copper corrosion inhibitor in an acidic sodium sulphate solution using potentiodynamic measurements, open circuit potential measurements, and chronoamperometric measurements. Langmuir adsorption data suggests that cysteine is chemisorbed onto the electrode surface. The corrosion inhibition efficiency of three triazine derivatives namely 4-((2-(5,6-diphenyl- 1,2,4-triazin-3-yl)hydrazineylidene)methyl)-N,N-dimethylaniline (HT-1), 3-(2-(4 methoxybenzylidene) hydrazineyl)-5,6-diphenyl-1,2,4-triazine (HT-2) and 2-(2-(5,6-diphenyl-1,2,4-triazin-3-yl)hydrazineylidene)

methyl)phenol (HT-3) on mild steel in 1 M HCl has been studied using electrochemical, morphological and quantum mechanical studies by Ambrish[22]. At optimum concentration (80 mg L^{-1}) HT-1 exhibits an efficiency of 98.6% , HT-2 97.1% and HT-3 94.3% respectively at 308 K. Mixed type inhibitor with cathodic predominance was confirmed by potentiometric studies and they obey Langmuir adsorption isotherm. The smoothness of the metal surface in presence of inhibitors was confirmed by the SEM analysis. The experimental findings were confirmed by the Quantum chemical calculation and Molecular dynamics simulation.

Sorkhabi[23] et al studied the corrosion inhibition ability of benzylidene-pyridine-2-yl-amine (A), (4-benzylidene)-pyridine-2-ylamine (B) and (4-chloro-benzylidene)-pyridine-2-yl-amine (C) on mild steel in 1M HCl. The studies reveal the efficiency changes with the type of functional groups substituted on benzene ring. The interaction between compound and mild steel surface obeys Langmuir isotherm. Polarization data indicates the mixed type behavior of the compound. Theoretical studies using linear and non-linear QSAR models found correlation with the experimental results. The inhibition study of Schiff base 4-Chloro-2-(2-oxo-1, 2-dihydro-indol-3-ylidene amino)-benzoic acid (ACBAI) and their Titanium (IV), Zirconium (IV), Cadmium (II) and Mercury (II) metal complexes in 0.1 M HNO_3 on mild steel were studied using weight loss measurement. The studies by Suraj[24] et al reveal that the compound inhibits the oxidation of metal ion in acidic medium.

The inhibitive properties of *N*-(2-methylphenyl)salicyaldimine,*N*-(2-hydroxyphenyl)salicyaldimine(Salhp), *N*-(2-methoxyphenyl)-Salicyaldimine(Salmop) and *N*-(2-nitrophenyl)salicyaldimine· HCl(Salnp.HCl) on mild steel in 1M HCl was examined using electrochemical calculations. Emergul and Atakol[25] explained that all of these compounds act as both anodic and cathodic inhibitors but their efficiencies are better when they act as anodic inhibitor.Salhp obeys the Langmuir adsorption isotherm and Salmp and Salmop follows the Temkin adsorption isotherm and the inhibition efficiencies follow the order Salmp >Salhp >Salmop. The effect of changing the functional groups of several amides and thiosemicarbazone derivatives on their inhibitory abilities were investigated by Ebenso[26] et al using the weight loss and hydrogen evolution methods. Results indicate the order of efficiency as follows: TSC > TU > TA where as the thiosemicarbazone derivatives having the order BZOTSC> BZITSC > MBTSC > 2AP4MTSC < 2AP4PTSC. The structure of the inhibitor, nature and spatial relationship of the different functional groups are the major factors influencing the mechanism of the corrosion inhibition.

Herrag[27] et al investigated the inhibition ability of the new diamine derivatives, namely 2-[{2-[bis-(2-hydroxyethyl)amino]ethyl}(2-hydroxyethyl)amino]ethanol (DAME) and 2-[{2-[bis-(2-hydroxyethyl)amino]ethyl}(2-hydroxyethyl)amino]propanol (DAMP) using gravimetric measurements and polarization curves

method. At 10^{-3}M , DAME exhibits an efficiency of 91.7% and the compounds are mixed-type inhibitor. The inhibitor obeys the Langmuir adsorption on the surface of the mild steel. Both the experimental as well as quantum mechanical results show both the compounds exhibits better inhibiting ability. The anti-corrosive study of the (3-phenylallylidene) amino-5-(pyridine-4-yl)-4H-1,2,4-triazole-3-thiol (SB-1), 3-mercapto-5 (pyridine-4-yl)-4H-1,2,4-triazole-4-yl) imino) methyl) phenol (SB-2) and (4-nitrobenzylidene) amino)-5-(pyridine-4-yl)-4H-1,2,4-triazole-3-thiol (SB-3) were done by Ansari[28] et al. Among the three, SB-1 exhibits high performance and all of them obey Langmuir isotherm. The potentiodynamic polarization data reveals the mixed-mode of inhibitors. DFT used for the theoretical calculations.

Lebrini[29] et al synthesized new macrocyclic polyether(n- MCTH) compounds containing a 1,3,4-thia diazole and studied the inhibitive effect of mild steel in HCL solutions using weight loss and EIS studies. The result shows an increase in the inhibition efficiencies with the extent of the polyethylene glycol unit that forms a cavity. Their inhibition efficiency increases in the order: 5-MCTH > 4-MCTH > 3-MCTH > 2-MCTH > 1-MCTH and the maximum inhibition value of 99.5% at 10^{-4} M for 5-MCTH.Shokry et al studied the corrosive effect of Schiff base derived from diamines and o-hydroxy, o-methoxy aromatic aldehydes in various aqueous solutions such as tap water, concentrated tap water and HCl solutions. Singh and Mukharjee[32] investigated the inhibition

efficiency of mild steel in acetic acid over a broad variety of concentration and test immersion periods. Maximium efficiency observed at 25% acetic acid solution and the surface studies agree with the weight loss method. Both the anodic and cathodic polarization techniques are in good agreement.

The corrosion inhibition efficiency of four double Schiff bases of mild steel in 2 M HCl is conducted by gravimetric, polarization and electrochemical impedence spectroscopy methods. The study also investigate the effects of substituents such as methoxy, hydroxyl and chloride groups on the N,N'-bis(salicylidene)-phenylmethanediamine. Adsorption studies obeys Langmuir isotherm and all the results were in agreement with quantum echanical studies.The quantum studies reveals that inhibition of Schiff bases involve both physisorption and chemisorption interaction[33].The anticorrosive study of furoin thiosemicarbazone in hydrochloric acid towards mild steel was carried out by Stanly[34] et al and reported that they exhibit better inhibition efficiency. Comparative study of Schiff base and their parent amine and the effect of temperature on inhibition efficiency were also carried out. In an effort to establish a suitable adsorption isotherm for the process we obtained that they obeys Langmuir isotherm.

Inhibition study of Cu(II) complexes containing amino acids such as glutamine cysteine and aspartic acid with pyridine or triphenylphosphine on mild steel in 1 M HCl were conducted. The best inhibitor among them reported as $[CuCl(SCys)PPh_3H_2O]$ at 3 mmol concentration. Corrosion inhibition increases with increase in

concentration and the interaction between metal surface with inhibitor found to obey Langmuir adsorption isotherm model[35]. The nitrogen-containing heterocyclic compounds such as triazole –type were considered to be good corrosion inhibitors[36-41]. Hui-Long[42] Wang et al synthesized mercapto-triazole compound, namely 4-salicylideneamino-3-phenyl-5-mercapto-1,2,4-triazole (SAPMT) and investigated the corrosion ability of the compound using gravimetric and electrochemical studies. Thermodynamic parameters evaluated in the basis of statistical model. Zhang[43] et al reported inhibition efficiency in the order BTA >alanine >cysteine for copper corrosion in 0.5 mol l^{-1} HCl.

Inhibitory action of four amino acids aspartic acid (Asp), glutamic acid (Glu), asparagine (Asn), glutamine (Gln) on copper corrosion studied and reports reveals that inhibition efficiency of these compounds increases in the order Gln > Asn > Glu > Asp[44].The corrosion protection of copper by various amino acids such as glutamic acid, cysteine, glycine and their derivative (glutathione) in 0.5 M hydrochloric acid has been studied with the aid of EIS, PDP and cyclic voltammetry. The efficiency increases in the order: glutathione >cysteine>cysteine+glutamic acid+glycine>glutamic acid>glycine. The intramolecular synergistic effect of glutamic acid, glycine,cysteine and glutathione shows an lower LUMO energy level and excess adsorption centers and the bigger molecular volume gives better inhibition properties against copper corrosion[45]. The inhibition effect of amino acids and hydroxyl carboxylic acid in NaCl solution has investigated by Bereket et al

[46]. Anticorrosive effect of cysteine on the corrosion of low carbon steel in sulphuric acid solution was studied using electrochemical and SEM techniques. Cys shows an accelerating effect on LCS corrosion process because of the catalytic effect of the Fe-cys complex on anodic metal dissolution reaction[47]. A combined theoretical and experimental inhibition studies of amino acid, L-methionine and its derivatives for copper surface in 1.0 M nitric acid was conducted by Khaled and co-workers[48].

The electrochemical measurement used to characterize the inhibition efficiency of the aminoacid complexes reveals the efficiency in the order, L-Ser>L-Cys>L-His>L-Try. The molecular dynamics simulation results show that amino acid complexes adsorb on the iron surface through the heteroatoms and heterocyclic ring in their structures[29]. Cruz[30] et al evaluated the electrochemical behaviour of 1-(2-ethylamino)-2-methylimidazoline (imidazoline), its precursor N-[3-(2-amino-ethylaminoethyl)]-acetamide (amide) and its derivative 1-(2-ethylamino)-2-methylimidazolidine (imidazolidine) using potentiodynamic polarization curves and electrochemical impedence spectroscopy. The results indicate that imidazoline is a good inhibitor compared to amide which is also supported by the theoretical calculations which indicate imidazoline is the more efficient corrosion inhibitor because of its two very active sites (two nitrogen atoms) and the plane geometry of the heterocyclic ring, thus promoting coordination with the metal surface.

CHAPTER 2

MATERIALS, METHODS AND INSTRUMENTATION

The inhibition studies of the amino acid complexes were carried out by weigh loss method. Immersion of the metal coupons in the corrosive environment is one of the best methods to monitor the inhibition study of the compounds. It provides very fruitful information about the compound's inhibitive action.

2.1. Preparation of inhibitor solution

Preparation of the Diphenyl glycolic acid- Amino acid ligands HBT, HBV, HBH, HBL, HBG and their molecular structures of the compounds are well explained in the Part I. Inhibitorsolutionswithdifferentconcentrationswerepreparedbyusing 0.5 M HCl solution as the test solution and dissolving the required amount of inhibitor in 50 ml of test solution. The blank solution for the study is the 50 ml of 0.5 M HCl without inhibitor.

2.2.Preparation of test specimens

Mild steel coupons having 99.22% Fe, 0.019% Mn, 0.28 % Ni and 0.30% carbon with dimension 1cm × 1 cm × 0.1 cm was selected as test sample for corrosion studies. The mild steel coupons was washed with methanol, acetone, and distilled water, dried, and

thenweighed withanaccuracyof0.0001g using an electronic balance. The area of the MS coupon was determined using Vernier calipers.

2.3 Weight loss method

Weight loss method one of the effective methods to measure the inhibition efficiency of the compounds in which the weight loss before exposing to the test solutions and after exposing was calculated. It is a very easy, precise and trustworthy method for scrutinizing the corrosion efficiency. From the weight loss data inhibition efficiency and corrosion rate can be calculated using the following equations.

$$CR = W / (A \times t) \quad (1)$$

$$IE = (W_0 - W_i/W_0) \times 100 \quad (2)$$

where W is the weight loss before and after immersion in the test solution, W_0 and W_i are the weight loss in the absence and presence of inhibitor respectively. A is the area of the mild steel coupon and t is the time(hours). The surface examination of the mild steel coupons conducted with the help of Olympus Japan make BX 51 model optical microscope. The keen observation of the data reveals the direct rapport of inhibition efficiency with inhibitor concentration and the inverse rapport with the corrosion rate.

2.4Adsorption isotherm studies

The action of corrosion inhibitors in the corrosion reaction is assumed to be an adsorption process. The inhibitors are being adsorbed on the metal surface preventing the aggressive solutions to act on the surface thereby reducing the metal-environment interaction. The adsorption process is regarded as the substitution between organic compound in aggressive media and the water molecules on the metallic surface. Organic inhibitors mainly act as adsorption inhibitor due to the presence of lone pairs and aromatic system in it. Adsorption isotherm studies are used to evaluate the adsorption of inhibitorsonto metal surfaces. Theadsorptionbehavior of corrosion inhibitorsprovidesimportantevidenceofmetal-corrosion inhibitor interactions. At constant temperature; surface coverage can be evaluated as a function of inhibitor efficiency for organic compounds. Adsorption isotherms gives relationship between surface coverage and concentration are the following:

Langmuir adsorption isotherm which obeys the equation

$$C/\theta = 1/K + C$$

The plot for testing the fitting of this isotherm is drawn as a plot of C/θ vs C.

2.5 Calculation of thermodynamic parameters

Arrhenius equation is used to obtain the activation energy (E_a) value for the steel corrosion reaction. The plot between the log (corrosion rate) vs 1/T will provide the activation energy value from the slope of the plot. The equilibrium constant (K_{ads}) of the adsorption process is obtained from the intercept of adsorption isotherm from the relationship

$$K_{ads} = 1/(intercept)$$

The free energy of the adsorption process is related to the equilibrium constant by the equation

$$\Delta G = -RT\ ln\ (55.5K_{ads})$$

where R is the universal gas constant, T is the temperature on an absolute scale, K is the equilibrium constant for the adsorption process and 55.5 concentration of water in the solution[5, 41].

CHAPTER 3

INHIBITIVE ACTION STUDIES OF DIPHENYL GLYCOLIC ACID- AMINO ACID LIGANDS ON MILD STEEL IN 0.5 M HCl

The chapter comprise of results and discussion of the various types of experiments we conducted to study the corrosion inhibition nature of the Diphenyl glycolic acid-amino acid ligands (HBT, HBG, HBV, HBH and HBL) and some of its complexes on mild steel in HCl.

3.1Effect of concentration of inhibitors on mild steel coupons

3.1.1 Weight loss method

The weight loss occurred for the MS coupons immersed in 50ppm, 100ppm, 150 ppm and 200 ppm of the compounds (HBT, HBG, HBV, HBH and HBL in 0.5 HCl solution after 24 hours was given in Table 3.1. The weight loss study depicts HBL as corrosion accelerator and the weight loss trend of HBT, HBG was increasing after 200ppm. But the weight loss of the HBV and HBH continue to decrease up to 800 ppm and 1000 ppm respectively and afterwards it also shows an increasing trend. The MS coupons in inhibitor solution was least corroded as compared to the blank solution. The naked eye observation itself confirms the inhibitive nature of the HBH ligand because of the smooth and polished surface obtained after the corrosion reaction whereas the MS coupons in the blank solution become rough and the weight loss

was visible. A protective film layer was formed on the surface of the MS coupons in the inhibitor solution. The weight loss,corrosion rate and inhibition efiiciency plot of HBT, HBG,HBH,HBV and HBL for 24 hours time interval at different concentration was plotted in fig 3.1, 3.2 and3.3respectively**.**

Table 3.1 Weight loss occurred for MS in 24 hours time with and without inhibitor

Concentration [M]	**Weight loss**				
	HBT	**HBG**	**HBL**	**HBV**	**HBH**
Blank	0.4624	0.2229	0.2603	0.4557	0.623
50 ppm	0.3584	0.2088	0.2731	0.3489	0.1752
100ppm	0.32	0.1794	0.2937	0.2785	0.1129
150ppm	0.2440	0.1507	0.3058	0.2026	0.0931
200ppm	0.1692	0.1325	0.3527	0.1549	0.0745

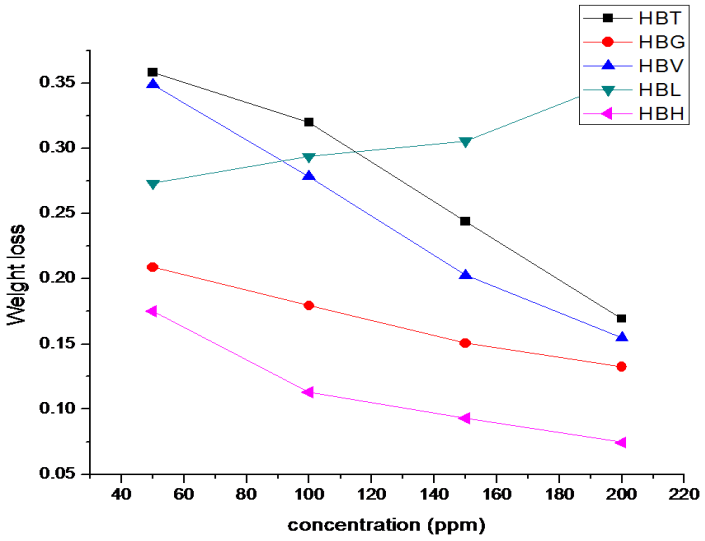

Fig. 3.1 Weight loss occurred for MS in 24 hours time with and without inhibitor

The weight loss of the MS coupons is inversely proportional to the concentration of the inhibitor. As the concentration of the inhibitor increases the weight loss decreases and after an optimum concentration, when the surface of adsorption is at its maximum the weight loss tend to increase. The loss of weight of coupons in HBG is high whereas in HBH is least. The decreasing order of weight loss of different Benzilic acid-amino acid ligands are the following: HBG >HBT >HBV >HBH. The weight loss of the Benzilic acid-amino acid ligands is decreasing indicates the inhibitive properties of the compounds.

3.1.2Corrosion rate and inhibition efficiency

The variation of corrosion rate expressed in mm/yr of the MS specimens in 0.5 M HCl is calculated and tabulated in this section.The table 3.2 gives the corrosion rate for HBT, HBG, HBH, HBV and HBL inhibitor and represented in fig.3.2

Table 3.2. Corrosion rate occurred for MS in 24 hours time with and without inhibitor

Concentration [M]	**Corrosion rate**				
	HBT	**HBG**	**HBL**	**HBV**	**HBH**
50 ppm	41.6065	24.2395	31.7041	40.5037	20.3389
100ppm	37.1487	20.8264	34.0955	32.3309	13.1065
150ppm	28.3258	17.4947	35.5002	23.5197	10.8079
200ppm	19.6423	15.3818	40.9448	17.9822	8.6486

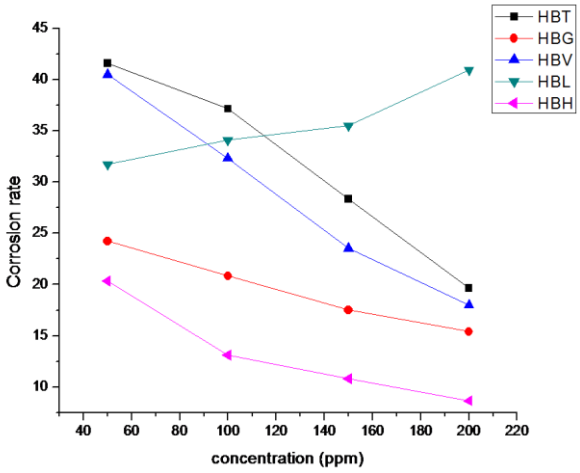

Fig. 3.2 Corrosion rate occurred for MS in 24 hours time with and without inhibitor

The corrosion rate and concentration of inhibitor shows an inverse relationship, i.e, a decreasing trend for corrosion rate is observed with the increase of inhibitor concentration. At the highest concentration the corrosion rate for HBG is maximumand HBH shows the least corrosion rate. The efficiency of the Benzilic acid-amino acid ligands against corrosion towards MS was observed in 0.5 M HCl for 24 hours and the efficiency values are tabulated in the table 3.3.

Table 3.3 Inhibition efficiency occurred for MS in 24 hours time with and without inhibitor

Concentration [M]	**Inhibition efficiency**			
	HBT	**HBG**	**HBV**	**HBH**
50 ppm	22.4913	6.3257	23.4364	71.8780
100ppm	30.7958	19.5154	38.8852	81.8780
150ppm	47.2318	32.3912	55.5409	85.0561
200ppm	63.4018	40.5563	66.0083	88.041

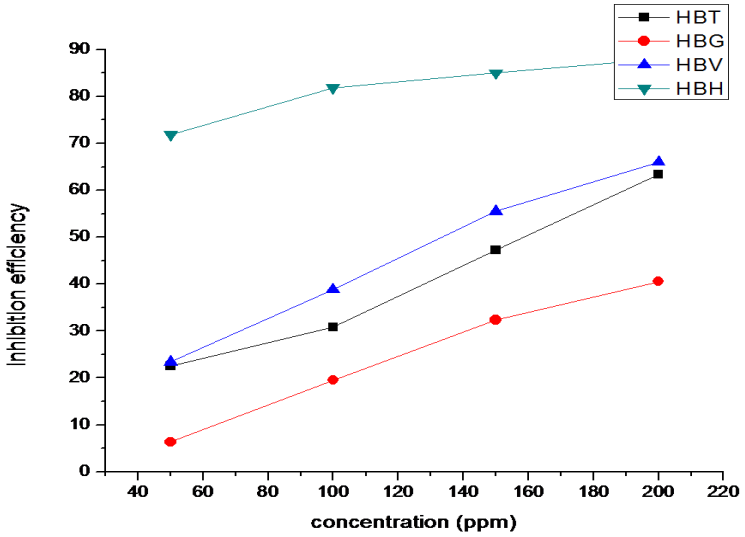

Fig. 3.3 Inhibition efficiency of ligands occurred for MS in 24 hours time with and without inhibitor

The weight loss, corrosion rate and Corrosion inhibition efficiency of the HBH and HBV after 200ppm was studied at various time intervals 24,48 and 72 hours and the efficiency seems to be increasing upto 800 ppm for HBV ligand and 1000ppm for HBH ligand.The weight loss corrosion rate and inhibition efiiciency plot of HBV and HBH for 24, 48 and 72 hours at different concentration were plotted and the weight loss,corrosion rate and inhibition efficiency of HBH was also depicted in fig. 3.4,3.6 and 3.8 respectively.Also the weight loss,corrosion rate and inhibition efficiency of HBH was also depicted in fig. 3.5, 3.7and3.9 respectively The rate of corrosion in presence of inhibitors at different concentrations was recorded at room temperature for 24, 48 and 72 hours for HBV and HBH inhibitor and 24 hours for HBT and HBG inhibitor The effect of temperature, effect of concentration of inhibitor, effect of concentration of acid solution, comparative study with their parent compounds and their different metal complexes have also been studied. Adsorption studies of the ligands on the mild steel surface have also been carried out and the thermodynamic parameters and kinetic parameters have calculated.

Table 3.4 Weight loss occurred for MS in 24, 48, 72 hours time with and without inhibitor of HBH ligand

Concentration [M]	**Weight loss**		
	24	**48**	**72**
50 ppm	0.1752	0.2753	0.3357
100 ppm	0.1129	0.1621	0.1928
150 ppm	0.0931	0.1316	0.1569
200 ppm	0.0745	0.114	0.1373
300 ppm	0.0636	0.1008	0.1207
500 ppm	0.0268	0.0316	0.0428
800 ppm	0.0242	0.0312	0.0381
1000 ppm	0.0164	0.0237	0.0252
1500 ppm	0.0236	0.307	0.0342

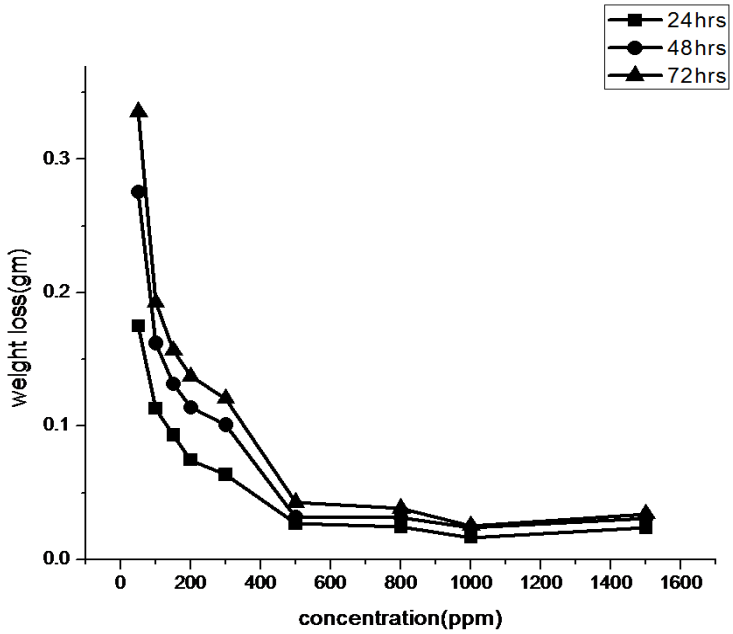

Fig. 3.4. Weight loss occurred for MS in 24, 48, 72 hours time with and without inhibitor of HBH ligand

Table 3.5. Weight loss occurred for MS in 24, 48, 72 hours time with and without inhibitor of HBV ligand

Concentration [M]	Weight loss		
	24	48	72
50 ppm	0.3489	0.5085	0.5293
100 ppm	0.2785	0.4156	0.4365
150 ppm	0.2026	0.3124	0.3714
200 ppm	0.1549	0.2213	0.2698
300 ppm	0.1002	0.1632	0.2146
500 ppm	0.0427	0.0803	0.1102
800 ppm	0.0313	0.0528	0.0709
1000 ppm	0.0843	0.0697	0.0986

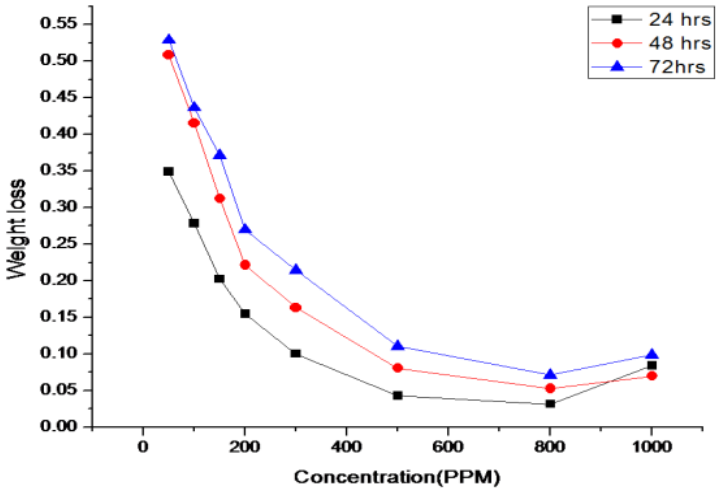

Fig. 3.5. Weight loss occurred for MS in 24, 48, 72 hours time with and without inhibitor of HBV ligand.

Table 3.6. Corrosion Rate occurred for MS in 24, 48, 72 hours time with and without inhibitor of HBH ligand

Concentration [M]	Corrosion rate		
	24	48	72
50 ppm	20.3384	15.9797	12.9904
100 ppm	13.1065	9.4090	7.4606
150 ppm	10.8079	7.6387	6.0714
200 ppm	8.6486	6.6171	5.3130
300 ppm	7.3833	5.8509	4.6706
500 ppm	3.1112	1.8342	1.6562
800 ppm	2.8093	1.8109	1.4743
1000 ppm	1.9038	1.3756	0.9751
1500 ppm	2.7397	1.7819	1.3234

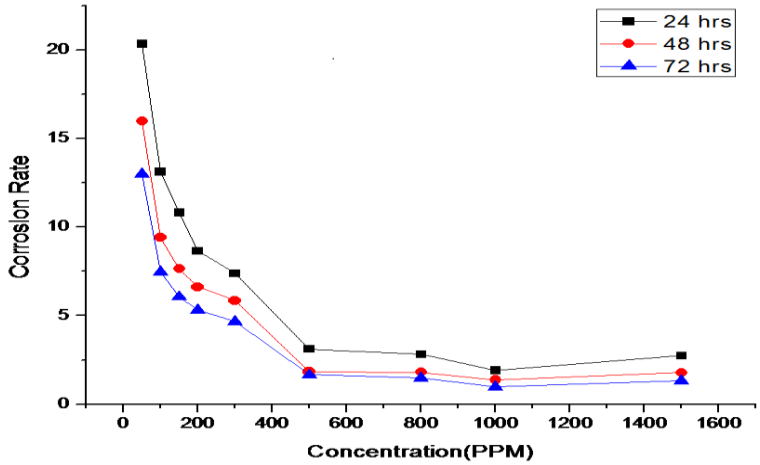

Fig. 3.6 Corrosion rate occurred for MS in 24, 48, 72 hours time with and without inhibitor of HBH ligand

Table 3.7 Corrosion rate occurred for MS in 24, 48, 72 hours time with and without inhibitor of HBV ligand

Concentration [M]	**Corrosion rate**		
	24	**48**	**72**
50 ppm	40.5037	29.5158	20.4820
100 ppm	32.3309	24.1234	16.8910
150 ppm	23.5081	18.1332	14.3719
200 ppm	17.9822	12.8453	10.4403
300 ppm	11.6321	9.4729	8.3042
500 ppm	4.9570	4.6610	4.2643
800 ppm	3.6336	3.0647	2.7435
1000 ppm	9.786	4.0457	3.8154

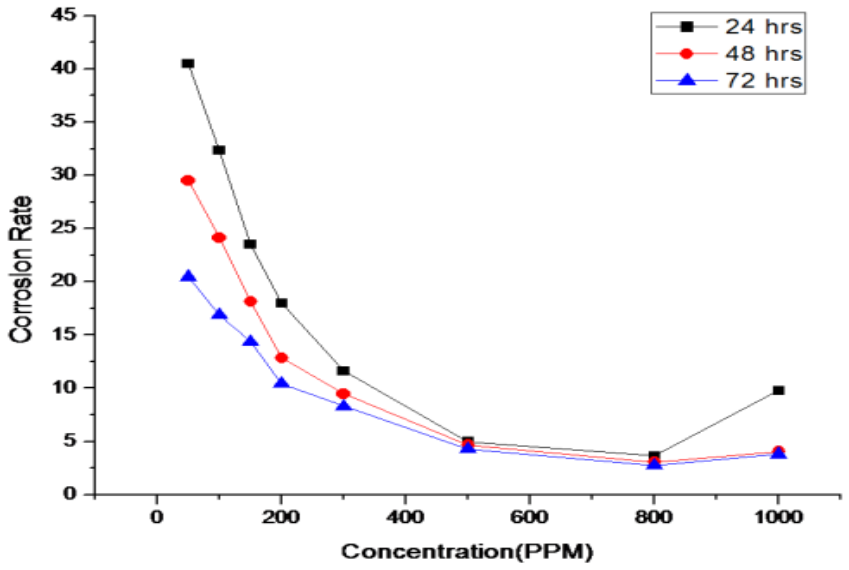

Fig.3.7. Corrosion rate occurred for MS in 24, 48, 72 hours time with and without inhibitor of HBV ligand

Table 3.8 Inhibition efficiency occurred for MS in 24, 48, 72 hours time with and without inhibitor of HBH ligand

Concentration [M]	Inhibition Efficiency		
	24	48	72
50 ppm	71.8780	70.4867	70.3576
100 ppm	81.8780	82.6222	82.9757
150 ppm	85.0561	85.8919	86.1456
200 ppm	88.041	87.7787	87.8763
300 ppm	89.7913	89.1938	89.3421
500 ppm	95.07	96.0450	96.2207
800 ppm	95.5535	96.0951	96.6357
1000 ppm	96.98	97.0337	97.7748
1500 ppm	95.6641	96.1576	96.9801

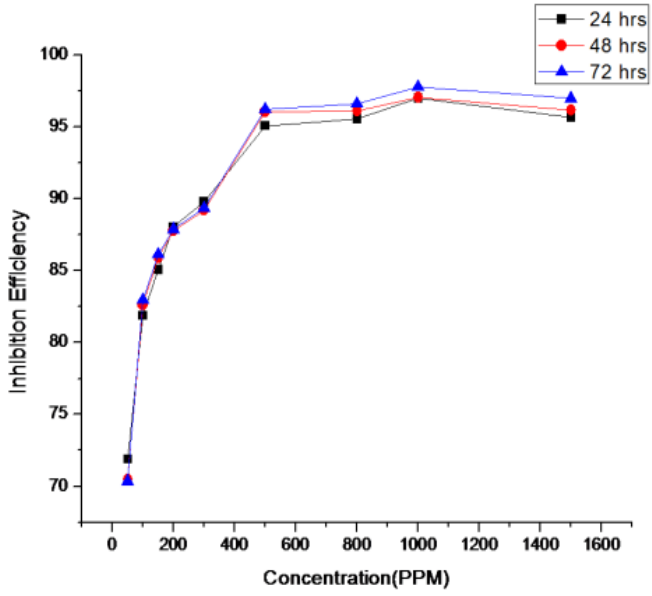

Fig.3.8. Inhibition efficiency occurred for MS in 24, 48, 72 hours time with and without inhibitor of HBH ligand

Table.3.9. Inhibition efficiency occurred for MS in 24, 48, 72 hours time with and without inhibitor of HBV ligand

Concentration [M]	Inhibition Efficiency		
	24	48	72
50 ppm	23.4364	21.0281	18.9185
100 ppm	38.8852	35.4558	33.1341
150 ppm	55.5409	51.4831	43.1066
200 ppm	66.0083	65.6313	58.6703
300 ppm	78.0118	74.6544	67.1262
500 ppm	90.6298	87.5291	83.1188
800 ppm	93.1314	91.7996	89.1390
1000 ppm	81.5009	89.1753	84.8958

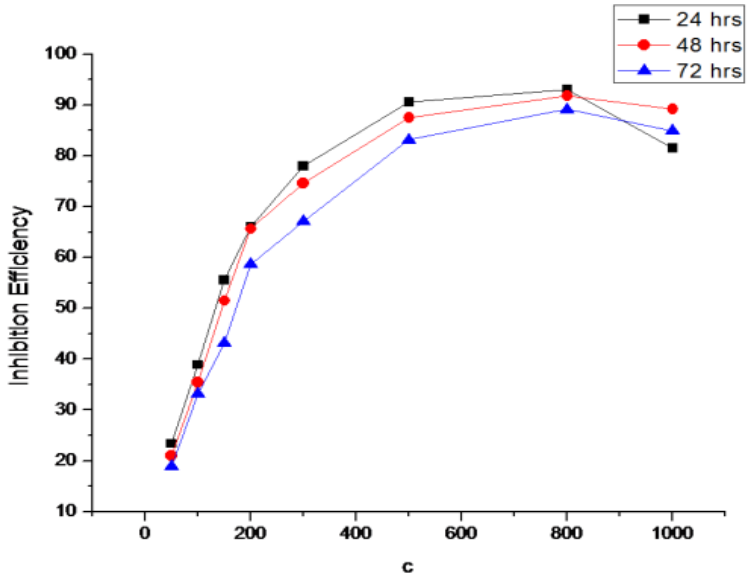

Fig. 3.9. Inhibition efficiency occurred for MS in 24, 48, 72 hours time with and without inhibitor of HBV ligand

The corrosion inhibition efficiency of Diphenyl glycolic acid-amino acid ligands is discussed in the portion. HBG ligand is the inhibitor with least efficiency of only 40% at 200 ppm. HBT ligand has an efficiency of 22.49% at lower concentration of 50 ppm and it seems to increase up to 66% at 200 ppm. HBL ligand seems to accelerate the corrosion reaction. The HBV and HBH ligand are the two ligands exhibiting high inhibition efficiency. HBV shows a maximum efficiency of 93% at 800 ppm .In the case of HBH 71% for 50 ppm and the efficiency tend to increase with the increase in concentration to a maximum of 97% at 1000 ppm. The comparative study of the % inhibition efficiency of inhibitors at different concentration was plotted and shown in fig 3.3.The study reveals the fact that HBH and HBV are found to be potent inhibitors against corrosion and they act as effective inhibitor at 1000 and 800 ppm respectively. The increasing efficiency order of the inhibitors follows the order HBG <HBT <HBV <HBH.

3.2. Effect of Temperature on the Action of Diphenyl glycolic acid-amino acidinhibitors

The effect of temperature on the weight loss measurements, inhibition efficiency, and corrosion rate was conducted at different temperatures (303-333K) with 1000 ppm of HBH ligand and 800 ppm of HBV ligand at an interval of 3 hours. The percentage inhibition efficiencies plotted against different temperatures was shown in fig. 3.10.The inhibition efficiencies tend to decrease with

an increase in temperature due to the increase in hydrogen evolution on the metal surface at high temperature which leads to the desorption of adsorbed inhibitor layer from the metal surface. The Arrhenius equation is used for calculating the activation energy of the HBH inhibitor. The graphical representation of logarithmic values of corrosion rate at different temperatures for the blank and 1000ppm HBH ligand against 1000/T provides the activation energy from the slope of the plot. The fig. 3.11 and 3.12 depicts the Arrhenius plot of the blank and 1000ppm HBH ligand and 800 ppm HBV ligand and the calculated values of corrosion rate, surface coverage, and inhibition efficiency occurred for MS in 3 hrs of HBH ligand and HBV ligand at different temperatures is given in Table 3.10 and 3.11.

Table 3.10 Weight loss, Corrosion rate and inhibition efficiency occurred for MS in 24 hrs of HBH ligand at different temperature

Temp (^{0}C)	**Weight loss**	**Inhibition efficiency**	**Corrosion rate**
30	0.0081	87.8923	7.5140
40	0.0123	91.3319	11.4101
50	0.0294	84.1423	27.2731
60	0.0991	67.6033	92.0359

Table 3.11 Weight loss, Corrosion rate and inhibition efficiency occurred for MS in 24 hrs of HBV ligand at different temperature

Temp (^{0}C)	Weight loss	Inhibition efficiency	Corrosion rate
30	0.0176	73.6920	16.3267
40	0.0386	72.7977	35.8075
50	0.0789	57.44	73.1921
60	0.2095	31.5135	194.3442

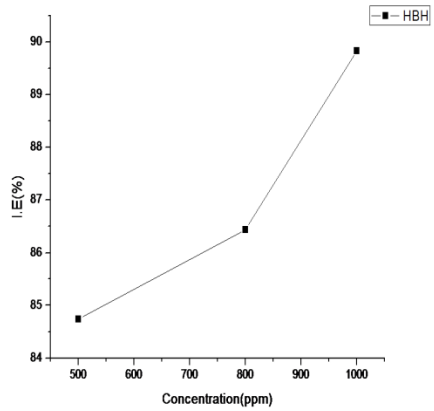

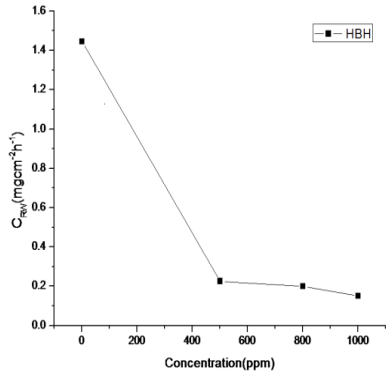

Fig. 3.10.(a) Relationship between inhibition efficiency (I.E) and concentration of inhibitor(C) in 0.5M HCl at 30˚C obtained by weight loss measurement.**(b)**Relationship between corrosion rate (C_{RW}) and concentration of inhibitor(C) in 0.5 M HCl at 30˚C obtained by weight loss measurement.(HBH)

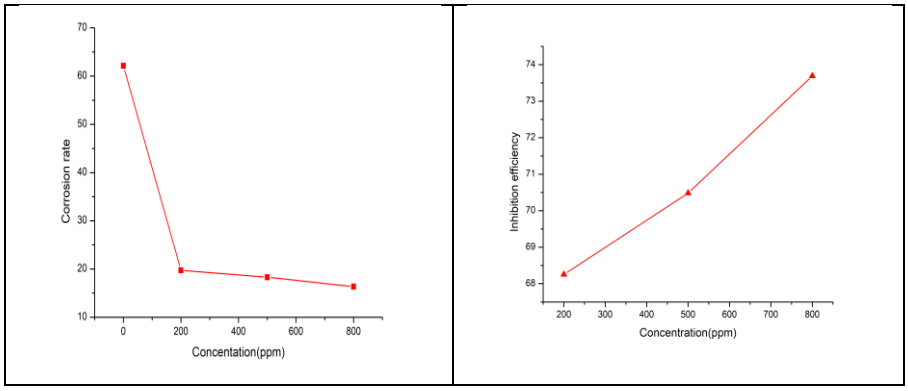

Fig. 3.11.(a) Relationship between inhibition efficiency (I.E) and concentration of inhibitor(C) in 0.5M HCl at 30˚C obtained by weight loss measurement.**(b)**Relationship between corrosion rate (C_{RW}) and concentration of inhibitor(C) in 0.5 M HCl at 30˚C obtained by weight loss measurement.(HBV)

Table 3.10 Corrosion rate, Surface coverage, and Inhibition efficiency occurred for MS in 3 hrs of HBH ligand at different temperatures

Temperature (˚C)	**Concentration(ppm)**	**C_{RW}(mgcm^{-2}h^{-1})**	**θ**	**η_w(%)**
30	Blank	1.445	-	-
	500	0.2255	0.8474	84.74
	800	0.2005	0.8644	86.44
	1000	0.1503	0.8983	89.83
40	Blank	3.3166	-	-
	500	0.5597	0.6196	61.96
	800	0.5263	0.8413	84.13
	1000	0.5179	0.8438	84.38
50	Blank	13.2414	-	-
	500	1.3533	0.8997	89.97
	800	1.261	0.9047	90.47
	1000	1.1946	0.9097	90.97
60	Blank	21.2364	-	-
	500	2.7318	0.8713	87.13
	800	2.5563	0.8796	87.96
	1000	2.3893	0.8874	88.74

Table 3.11 Corrosion rate, Surface coverage, and Inhibition efficiency occurred for MS in 3 hrs of HBV ligand at different temperatures

Temperature (˚C)	**Concentration (ppm)**	**C_{RW}(mgc $m^{-2}h^{-1}$)**	**θ**	**η_w(%)**
30	Blank	1.445	-	-
	200	0.2255	0.8474	84.74
	500	0.2005	87.8923	87.8923
	800	0.1503	0.8983	89.83
40	Blank	3.3166	-	-
	200	0.5597	0.6196	61.96
	500	0.5263	0.9133	91.3319
	800	0.5179	0.8438	84.38
50	Blank	13.2414	-	-
	200	1.3533	0.8997	89.97
	500	1.261	0.8414	84.1423
	800	1.1946	0.9097	90.97
60	Blank	21.2364	-	-
	200	2.7318	0.8713	87.13
	500	2.5563	0.6760	67.6033
	800	2.3893	0.8874	88.74

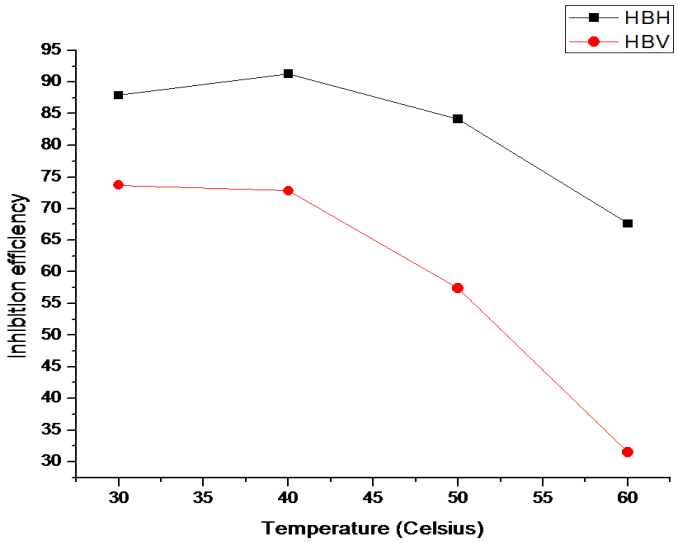

Fig. 3.12. Weight loss, Corrosion rate and inhibition efficiency occurred for MS in 24 hrs of HBV ligand at different temperature

3.3 Effect of Concentration of acid on the Action of Diphenyl glycolic acid-amino acidinhibitors

The study of the effect of concentration of acid solution at room temperature was carried out. The weight loss, inhibition efficiency, corrosion rate of the inhibitor at 0.1 N and 1 N HCl was studied. The results show as the concentration of the acid solution increases the efficiency of the inhibitor tends to decrease but at all concentration of acid solution, the maximum efficiency shown by the same concentration of the inhibitor.

Table 3.13 Weight loss, Corrosion rate and inhibition efficiency occurred for MS in 0.1 M HCl in 24 hrs of HBV ligand

Concentration [M]	Weight loss	Corrosion rate	Inhibition efficiency
50 ppm	0.026	87.8776	3.0183
100 ppm	0.0173	91.7343	2.0083
150 ppm	0.0133	93.6454	1.5439
200 ppm	0.0088	94.1284	1.0215
300 ppm	0.0084	94.0969	0.9751
500 ppm	0.0067	95.2916	0.7778
800 ppm	0.0064	95.5024	0.7429
1000 ppm	0.0066	95.3619	0.7661

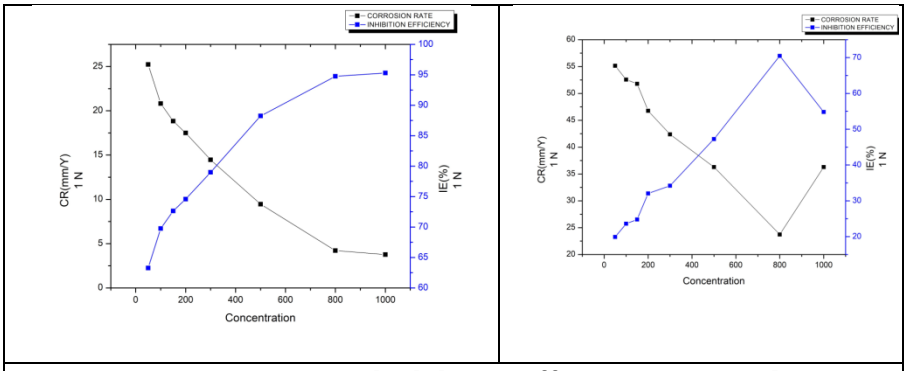

Fig. 3.13 Corrosion rate and inhibition efficiency HBH and HBV in 1 N HCl solution

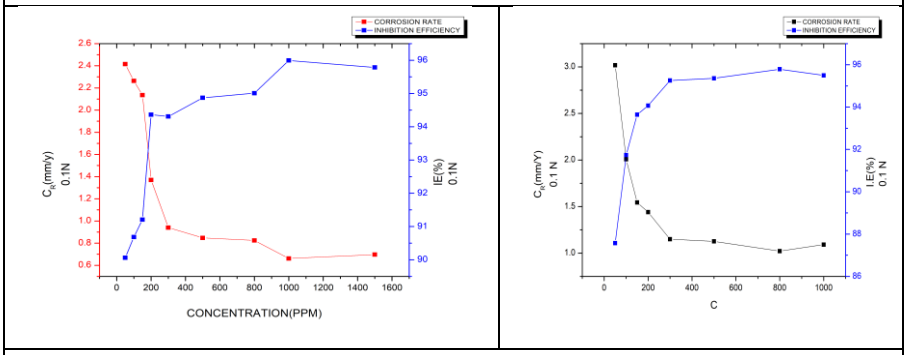

Fig. 3.14 Corrosion rate and inhibition efficiency HBH and HBV in 0.1 N HCl solution

Table 3.14 Weight loss, Corrosion rate and inhibition efficiency occurred for MS in 1M HCl in 24 hrs of HBV ligand

Concentration [M]	**Weight loss**	**Inhibition efficiency**	**Corrosion rate**
50 ppm	0.208	90.0621	2.4146
100 ppm	0.0195	90.6832	2.2637
150 ppm	0.0184	91.2087	2.1360
200 ppm	0.0118	94.3621	1.3698
300 ppm	0.0081	94.3078	0.9403
500 ppm	0.0073	94.8699	0.8474
800 ppm	0.0071	95.0105	0.8242
1000 ppm	0.0057	95.9943	0.6617
1500 ppm	0.006	95.7835	0.6965

Table 3.15 Weight loss, Corrosion rate, and inhibition efficiency occurred for MS in 0.1 N, 0.5 N, and 1 N HCl concentration in presence of HBH ligand

Concentration [M]	**0.1 N**			**0.5 N**			**1N**		
	Wt.loss	**%IE**	**CR**	**Wt.loss**	**%IE**	**CR**	**Wt.loss**	**%IE**	**CR**
50 ppm	0.208	90.0621	2.4146	0.1752	71.8780	20.3384	0.2173	63.2715	25.2262
100 ppm	0.0195	90.6832	2.2637	0.1129	81.8780	13.1065	0.1793	69.7639	20.8148
150 ppm	0.0184	91.2087	2.1360	0.0931	85.0561	10.8079	0.1623	72.6306	18.8413
200 ppm	0.0118	94.3621	1.3698	0.0745	88.041	8.6486	0.1507	74.6306	17.4947
300 ppm	0.0081	94.3078	0.9403	0.0636	89.7913	7.3833	0.1246	78.9881	14.4647
500 ppm	0.0073	94.8699	0.8474	0.0268	95.07	3.1112	0.0814	88.24	9.4497
800 ppm	0.0071	95.0105	0.8242	0.0242	95.5535	2.8093	0.0363	94.75	4.2140
1000 ppm	0.0057	95.9943	0.6617	0.0164	96.98	1.9038	0.0324	95.31	3.7613
1500 ppm	0.006	95.7835	0.6965	0.0236	95.6641	2.7397	0.0626	90.52	7.2672

3.4 Comparative study of Diphenyl glycolic acid- Histidine/Valineinhibitors and their parent compounds

The comparative study of the Diphenyl glycolic acid- Histidine and Diphenyl glycolic acidValine inhibitors conducted with its parent compounds Diphenyl glycolic acid, Histidine and Valine in 0.5 N HCl at room temperature (25^0 C). The weight loss, corrosion rate and inhibition efficiency of the compounds were studied and are tabulated in the table 3.16. The plots of weight loss, corrosion rate and corrosion inhibition efficiency was given in the fig. 3.14. The study shows that the ligands are more potent than its parent compounds.

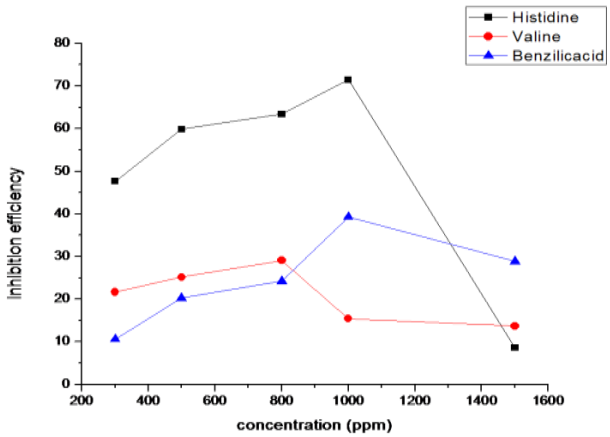

Fig. 3.15 Comparison of Weight loss, Corrosion rate and inhibition efficiency of parent compounds occurred for MS in 24 hours

Table 3.16 Comparison of Weight loss, Corrosion rate and inhibition efficiency of parent compounds occurred for MS in 24 hours.

Concentration [M] (in ppm)	**Histidine**			**Valine**			**Diphenyl glycolic acid**		
	Wt.loss	%IE	CR	Wt.loss	%IE	CR	Wt.loss	%IE	CR
300	0.3081	47.6643	35.7672	0.461	21.6918	53.5173	0.5259	10.6675	61.0515
500	0.2364	59.8437	27.4436	0.4405	25.1741	51.1375	0.4693	20.2819	54.4809
800	0.2185	63.3939	25.3656	0.4174	29.0980	48.4558	0.446	24.2398	51.7760
1000	0.1682	71.4285	19.5262	0.5082	15.4068	58.9967	0.3571	39.3409	41.4556
1500	0.538	8.612	62.4562	0.498	13.6741	57.8126	0.4188	28.8602	48.6183

3.5 Comparative study of Diphenyl glycolic acid-Histidineinhibitor and their metal complexes

The comparative study of the Diphenyl glycolic acid- Histidine inhibitor is conducted with its metal complexes of Diphenyl glycolic acid-Histidine in 0.5 N HCl at room temperature (25^0 C). The weight loss, corrosion rate and inhibition efficiency of the compounds were studied and are tabulated in the table 3.17. The plots of weight loss, corrosion rate and corrosion inhibition efficiency was given in the fig.3.17. The study shows that the metal complexes are more potent than its parent ligand.

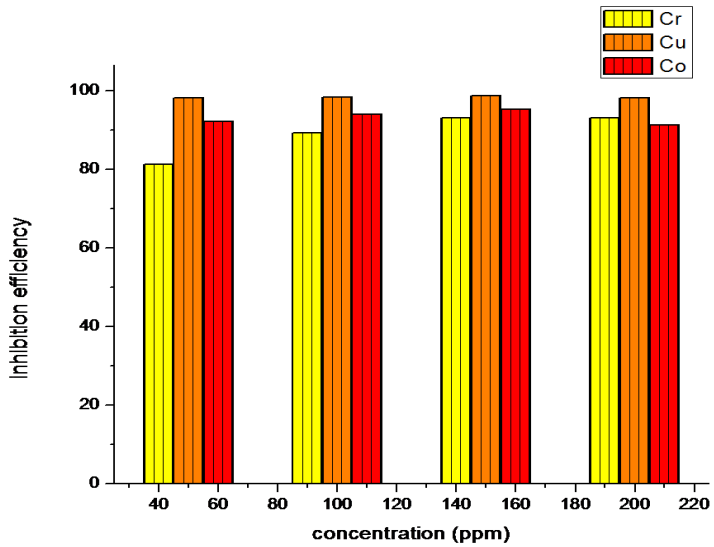

Fig.3.17. Comparison of Weight loss, Corrosion rate and inhibition efficiency of metal complexes of HBH occurred for MS in 24 hours.

Table.3.17. Comparison of Weight loss, Corrosion rate and inhibition efficiency of metal complexes of HBH occurred for MS in 24 hours.

Concentration in ppm	Cu complex			Cr complex			Co complex		
	WL	**IE**	**CR**	**WL**	**IE**	**CR**	**WL**	**IE**	**CR**
500	0.006	98.32	62.16	0.0666	81.38	7.731	0.0276	92.28	3.204
800	0.0055	98.46	61.341	0.0383	89.29	4.446	0.0215	93.98	2.495
1000	0.0045	98.74	44.822	0.0246	93.12	2.855	0.0171	95.21	1.985
1500	0.0063	98.23	43.208	0.247	93.09	2.867	0.0307	91.41	3.563

3.6 Adsorption isotherm studies

Corrosion is a surface phenomenon in which the inhibitors act on the surface of the metal to reduce the corrosion. The mechanism of corrosion inhibition is considered to be the adsorption of the inhibitor on the metal surface thereby suppressing the active sites on the surface to react with environment. This mechanism helps to reduce the corrosion to a great extent. The degree of surface coverage (θ) is calculated from the weight loss measurement results if MS in 0.5 M HCl, with the help of eqn (16) of the chapter 2. The surface coverage (θ) values of the four inhibitors are given in the table and the data fit with the Langmuir isotherm. The Temkin and Frumkin isotherm do not yield a satisfactory description about the mechanism of corrosion process but the Langmuir isotherm provide the best description of the inhibitors adsorption behaviour. The plot of C/ θ vs θ gives a straight line and obeys Langmuir adsorption isotherm.

Table 3.18. Weight loss occurred for MS in 24 hours time with and without inhibitor

Compound	R^2 value	Intercept	K_{ads}	ΔG	Types of Adsorption	Slope
HBH	0.93504	3.26897	0.3059	-7.06×10^3	Physisorption	0.73566
HBV	0.9804	2.64729	0.3777	-7.59×10^3	Physisorption	0.1122

Table 3.19. Weight loss occurred for MS in 24 hours time with and without inhibitor

Compound	Slope	E_a
HBH	-5.2710	43.8236
HBV	-3.5615	29.6108

The Arrhenius equation is used for calculating the activation energy of the HBH and HBV inhibitor. The graphical representation of logarithmic values of corrosion rate at different temperatures for the blank and 800ppm HBV ligand and 1000ppm HBH ligand against 1000/T provides the activation energy from the slope of the plot. The Arrhenius plot of the blank, 800ppm HBV ligand and 1000ppm HBH ligand is given in the fig 3.18(a) and 3.19(a) and the activation energy values for the inhibitors are tabulated in the table 3.21 and 3.23. The activation parameters like enthalpy of activation, ΔH_a, and the entropy activation, ΔS_a were obtained by the transition state equation.

$$CR = (RT/Nh)\, exp(S/R)\, exp\,(-H/RT) \qquad (8)$$

Where N is Avogadro's number, h is Planck's constant; ΔS_a is the entropy of activation, and ΔH_a and the enthalpy of activation. From the plot of ln (C_{RW}/T) versus 1/T, fig. 3.20(b) and 3.21(b) slope of the straight line obtained and the intercept, values give the ΔH_a and ΔS_a values.

Table 3.20. Adsoprtion parameters $-K_{ads}$ and ΔG^0 values for HBH on mild steel in 0.5N HCl at various temperatures as obtained from Langmuir adsorption isotherm.

Sl.No	Temperature	$K_{ads}\times10^4(M^{-1})$	ΔG^0_{ads} (kJ/mol)
1.	303K	5.72	-31.92
2.	313 K	0.84	-27.08
3.	323K	27.84	-35.90
4.	333K	16.51	-34.59

Table 3.21. Activation parameters obtained from Arrhenius plot

Inhibitor	C(ppm)	E_a (KJ/mol)	ΔH_a (KJ/mol)	ΔS_a ($Jmol^1K^1$)
HBH	500	161.78	165.43	-20.8508
	800	164.72	168.51	-17.3141
	1000	177.04	180.68	-1.5468

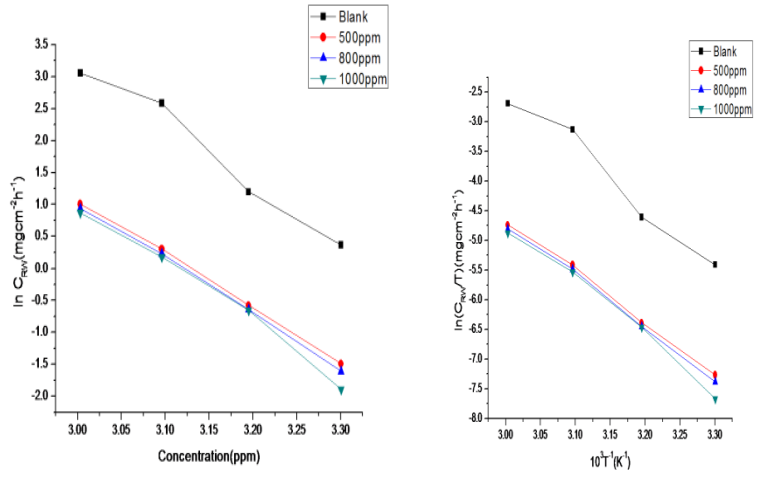

Fig. 3.18(a) Arrhenius plots for mild steel in 0.5 M HCl in the absence and presence of different concentrations of HBH. (b)Alternative Arrhenius plots for mild steel in 0.5 M HCl in the absence and presence of different concentrations of HBH.

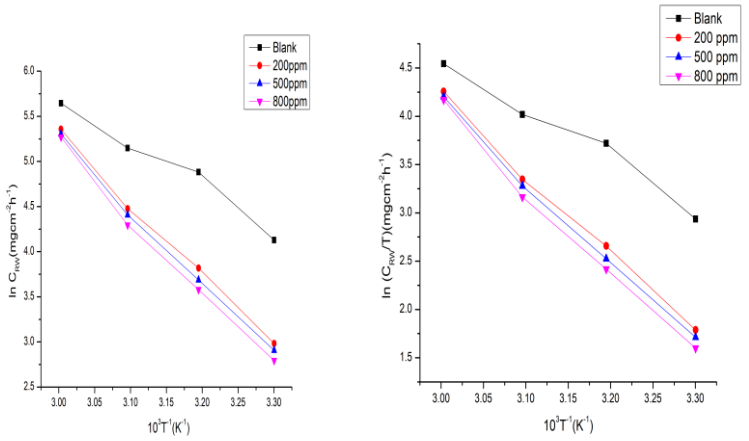

Fig. 3.19(a) Arrhenius plots for mild steel in 0.5 M HCl in the absence and presence of different concentrations of HBV. (b)Alternative Arrhenius plots for mild steel in 0.5 M HCl in the absence and presence of different concentrations of HBV.

Table 3.22. Adsoprtion parameters –$K_{ads}$and ΔG^0 values for HBV on mild steel in 0.5N HCl at various temperatures as obtained from Langmuir adsorption isotherm.

Sl.No	Temperature	$K_{ads}\times10^4(M^{-1})$	ΔG^0_{ads} (kJ/mol)
1.	303K	9.11	-14.63
2.	313 K	6.85	-15.42
3.	323K	3.01	-17.70
4.	333K	1.45	-19.71

Table 3.23. Activation parameters obtained from Arrhenius plot of HBV

Inhibitor	C(ppm)	E_a (KJ/mol)	ΔH_a (KJ/mol)	ΔS_a ($Jmol^1K^1$)
HBV	200	150.2317	156.30	-41.1860
	500	152.6525	158.72	-43.8176
	800	157.0494	163.12	-49.0742

3.7Surface morphological studies

Surface morphological studies of the HBH and HBV ligands were carried out to understand the interaction between metal surface and inhibitor. The study was carried out by immersing the mild steel coupon for 6 h and the mild steel specimens were washed thoroughly with double distilled water, dried and undergo SEM analysis. Fig. 3.20(A) shows SEM images of mild steel coupon without inhibitor at 303K whereas fig.3.20(B) depicts the SEM images of polished mild steel surface. The SEM images indicates that the mild steel surface immersed in 0.5 N HCl without HBH and HBV is damaged severely in comparison with that of mild

steel surface immersed in 0.5 N HCl with HBH and HBV. Fig. 3.21(A) & (B) shows the MAP data of HBH and HBV respectively. The MAP data along with SEM data helps to explain the interaction between metal surface and inhibitor molecule.

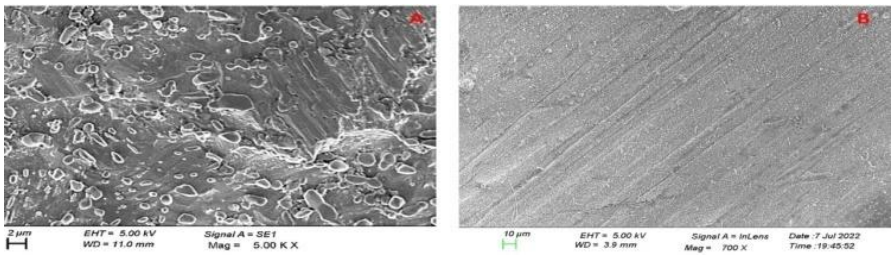

Fig.3.20.SEM images of (A) mild steel immersed in 0.5 M HCl (B) polished mild steel of HBH

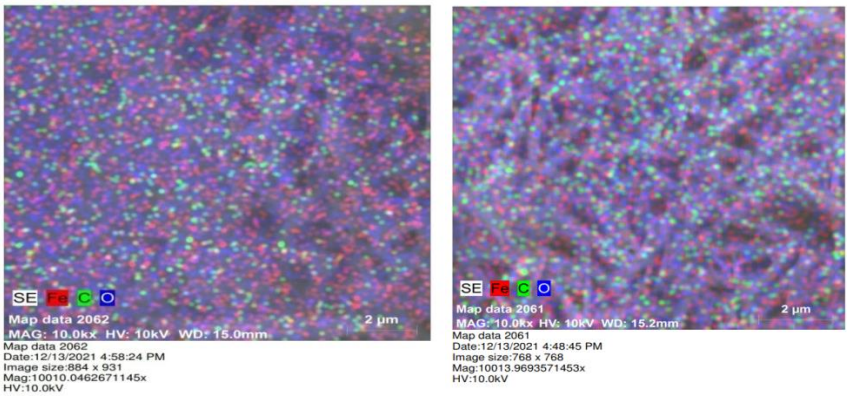

Fig.3.21. Map data of (a) HBH (b) HBV ligands

Conclusion

The corrosion inhibition efficiency of the Diphenyl Glycolic acid-amino acid ligands have been carried out. From the observations the Diphenyl Glycolic acid-Histidine and Diphenyl Glycolic acid-

Valine ligand shows maximum efficiency of 97%and 93 % respectively. The observation was confirmed by the SEM morphological study and MAP data. The inhibitors obey the Langmuir Adsorption isotherm and various thermodynamic parameters have been calculated using Adsorption studies. The efficiency of the investigated compounds varied depending upon their chemical structure and constituents present in them. The adsorption isotherm analysis and thermodynamic parameters calculated indicate that the newly synthesized ligands inhibit corrosion through the physical adsorption process and follow Langmuir adsorption isotherm. Relevant references are given at the end of Part IV.

References:

1) Zhang, D. Q., He, X. M., Cai, Q. R., Gao, L. X., & Kim, G. S. (2009). *J Appl Electrochem.,* 39, 1193.

2) Aouniti, A., Elmsellem, H., Tighadouini, S., Elazzouzi, M., Radi, S., Chetouanic, A., Hammouti, B.and Zarrouk, A. (2016). *J. Taibah Univ. Sci*., 10, 774.

3) Bereket, G., & Yurt, A.Y.S.E.L., (2001). *Corros. sci.*, 43, 1179.

4) Cruz, J., Martinez, R., Genesca, J., & Garcia-Ochoa, E. (2004). *J. Electroanal. Chem.*, 566, 111.

5) El-Lateef, H. M. A., Adam, M. S. S., & Khalaf, M. M. (2018). *J. Taiwan Inst. Chem. Eng.*, 88, 286.

6) Adam. M. S. S., & Mohamad, A. D. M. (2018). *Polyhedron*, 151, 118.

7) Adam, M. S. S., Abd El-Lateef, H. M., & Soliman, K. A. (2018). *J. Mol. Liq.*, 250, 307.

8) Mahross, M. H., Efil, K., El-Nasr, T. A. S., & Abbas, O. A. (2019). *Z. Phys. Chem*., 233 ,949.

9) Abd El-Lateef, H M. (2015). *Corros. Sci*, 92, 104.

10) Al-Amiery, A. A., Kassi, F. A.B., Kadhum, A. A. H., & Mohamad, A. B. (2016). Scientific reports,6, 19890.

11) El Ibrahimi, B., Jmiai, A., El Mouaden, K., Oukhrib, R., Soumoue, A., El Issami. S., & Bazzi, L. (2020). *J. King Saud Univ. Sci.*,32, 163.

12) Paul, A., Thomas, K. J., Raphael, V. P., & Shaju, K.S. (2012). *Orient. J. Chem.*, 28, 1501.

13) Behpour, M., Ghoreishi, S.M., Soltani, N., Salavati-Niasari, M., Hamadanian, M., & Gandomi, A. (2008). *Corros. Sci.*, 50, 2172.

14) Behpour, M., Ghoreishi, S. M., Gandomi-Niasar, A., Soltani, N., & Salavati-Niasari, M. (2009). *J Mater Sci* 44, 2444.

15) Bentiss, F., Lagrenee, M., Traisnel, M., & Hornez, J.C. (1999). *Corrosion*, 55, 968.

16) Fu, J. J., Li, S.N., Wang, Y., Cao, L. H., & Lu, L. D. (2010). *J Mater Sci*, 45, 6255.

17) Daoud, D., Douadi, T., Hamani, H., Chafaa, S., & Al-Noaimi, M., (2015). *Corros. Sci.*, 94, 21.

18) Mobin, M., Parveen, M., & Khan, M. A. (2011). *Recent Research in Science and Technology* 3, 40.

19) Saha, S. K., Dutta, A., Ghosh, P., Sukul, D., & Banerjeeb, P. (2012). *PCCP RSCPublishing*, 00, 1.

20) Yadav, M., Kumar, S., & Gope, L., (2014). *JAST*, 28, 1072.

21) Simonovic, A. T., Petrovic, M. B., Radovanovic, M. B., Milic, S. M., & Antonijevic, M. M. (2014). *Chemical Papers* 68, 362.

22) Singh, A., Ansari, K.R., Haque, J., Dohare, P., Lgaz, H., Salghi, R., & Quraishi, M.A. (2018). *J. Taiwan Inst. Chem. Eng.*,82, 233.

23) Ashassi-Sorkhabi, H., Shaabani, B., & Seifzadeh, D. (2005). *Appl. Surf. Sci*.,239, 154.

24) Ade, S. B., Deshpande, M. N., & Kolhatkar, D. G. (2012). *J.Chem. Pharm. Res* 4, 1033.

25) Emregul, K. C., & Atakol, O.R.H.A.N., (2003). *Mater. Chem. Phys.*, 82, 188.

26) Ebenso, E.E., Ekpe,U.J., Ita, B.I., Offiong, O.E., & Ibok, U.J. (1999). *Mater. Chem. Phys.*, 60, 79.

27) Herrag, L., Hammouti, B., Elkadiri, S., Aouniti, A., Jama, C., Vezin, H., & Bentiss, F. (2010). *Corros. Sci.*,52, 3042.

28) Ansari, K.R., Quraishi, M.A., & Singh, A. (2014). *Corros. Sci.*, 79, 5.

31) Lebrini, M., Lagrenee, M., Vezin, H., Traisnel, M., & Bentiss, F. (2007). *Corros. Sci*., 49, 2254.

32) Singh, S.K., & Mukherjee, A.K. (2010). *J. Mater. Sci. Technol*., 26, 264.

33) Soltani, N., Behpour, M., Ghoreishi. S.M., & Naeimi, H. (2010). *Corros. Sci*, 52, 1351.

34) Jacob, K. S., & Parameswaran, G. (2010). *Corros. Sci*., 52, 224.

35) Kiruthikajothi, K., Chandramohan, G. & Jayabharathi, G. (2014). *Chem Sci Rev Lett.,* 3, 603.

36 Quraishi, M.A., Ahmad. S., & Ansari, M.Q. (1997). *Br. Corros. J*. 32, 297.

37) Quraishi. M.A., & Jamal, D. (2001). *Mater. Chem. Phys*. 68, 283.

38) Bentiss, F., Lagrenée, M., Traisnel, M., & Hornez, J.C. (1999). *Corros. Sci*., 41, 789.

39) Bentiss, F., Traisnel, M., Gengembre, L., & Lagrenée, M., (2000). *Appl. Surf. Sci*. 161,194.

40) El Hajjaji, S., Lgamri, A., Aziane, D., Guenbour, A., Essassi, E.M., Akssira, M., Bachir, A.B. (2000). *Progr. Org. Coat*. 38, 207.

41) Bentiss, F., Traisnel, M., Gengembre, L., & Lagrenée, M. (1999). *Appl. Surf.Sci*.,152, 237.

42) Wang, H. L., Fan, H. B., & Zheng, J. S. (2003). *Mater. Chem. Phys.*, 77, 655.

43) Zhang, D. Q., Gao. L. X., & Zhou, G. D. (2005). *J. Appl. Electrochem.*, 35, 1081.

44) Zhang, D. Q., Cai, Q. R., He, X. M. Gao, L. X., & Zhou, G. D., (2008). *Mater. Chem. Phys*., 112, 353.

45) Zhang, D. Q., Xie, B., Gao, L. X., Cai, Q. R., Joo, H. G.,& Lee, K. Y.(2011).*Thin Solid Films*, 520, 356.

46) Bereket, G., Sarac, A.S., & Kose, M. (2001). *Corros. Sci*., 43, 1179.

47) Oguzie, E.E., Li, Y., & Wang, F.H. (2007).*Electrochim. Acta*, 53, 909.

48) Khaled, K.F. (2010). *Corros. Sci*., 52, 3225.

PART V

ANTIFUNGAL STUDIES OF DIPHENYL GLYCOLIC ACID-AMINO ACID METAL COMPLEXES

CHAPTER 1

INTRODUCTION

Amino acid complexes play an important role in the history of medicines. They have high potential to act as antimicrobial agents. On complexation with the metal atom they seem to raise the ability to act against microbes such as bacteria and fungus. The reviews such as "The effects of chelating agents on organisms"[1], "Chelation in medicine"[2]"Metal binding in medicine"[3],"Metal chelates in biological systems"[4] and "Structure and bonding in biochemistry"[5] gives an basic idea about the concept. The role of Schiff base in diverse biological and pharmaceutical activities[6, 7] and their wide range of applications in clinical[8], biochemical[9, 10] and physiological[11, 12] activities are a leading part of research nowadays. Mechanism of the action of antifungal agents has been reported by Frank[13] et al. The review describes about the various amino acid transition metal complexes having wide range of applications in the field of pharmaceutical, clinical and physiological areas.

Schiff base and its metal complexes of sulphametrole and varelaldehyde showed a higher effect on E. coli (Gram-negative bacteria) and S. aureus[14] (Gram-positive bacteria). It is known that the membrane of Gram-negative bacteria is surrounded by an outer membrane containing lipopolysaccharides. The synthesized Schiff base and its metal complexes combine with the lipophilic layer in order to increase the membrane permeability of the Gram-negative

bacteria. The lipid membrane surrounding the cell felicitate the passage of only lipid soluble materials thus the lipophilicity can be considered as an important factor that controls the antimicrobial activity. Also the lipophilicity of the compounds enhances the penetration of Schiff base and its metal complexes into the lipid membranes and thus restricts further growth of the organism[15, 16, 17].

Andreea[18] et al have studied the antifungal and antibacterial properties of various copper and cobalt amino acid complexes using the agar method and evaluated against three bacterial strains (*Escherichia coli, Bacillus cereus, and Micrococcus luteu*s). Studies already revealed that amino acid complexes are active against gram-positive bacteria and in the current study complexes with leucine and histidine are more active than parent free ligand. Moderate activity showed formethionine and phenylalanine where as the lysine and valine complexes are less efficient. The copper and cobalt complexes are proved to be a potential antibacterial agent.Barnabas[19]et al synthesized the new Sulfamerazine Schiff base ligand complexed with Co (II) and Cu (II) ions which is intercalated between Mg/Al-layered double hydroxide. They showed excellent antibacterial potency against both gram negative (Escherichia coli, E. coli) and gram positive (Staphylococcus aureus, S. aureus) bacteria. This study suggest that intercalation of the metal complex enhanced their activity and Cu complex (Cu-SS-LDH) exhibits higher activity than Co complex (Co-SS-LDH). microwave assisted synthesis of some Schiff base and their

antimicrobial activities conducted by Sandeep Miglani[20] et al. The method produce compounds in excellent yield with short reaction times and without any undesirable side products. They suggest Microwave assisted synthesis to be an effective method for the synthesis of various important drugs. The excellent antimicrobial properties of copper and Cobalt complexes were studied by Jian[21] et al. These valine derived Schiff base are proved to be an efficient antimicrobial agent against gram positive as well as gram negative bacteria and also against different fungal species.

α-methyl trans cinnamaldehyde, a less irritating derivative of cinnamaldehyde with comparatively less MIC have been synthesized and also they complexed with Co(II) and Ni(II) metal ions. Their inhibition efficiency were studied and the results indicates that even though the ligand does not possess any inhibition efficiency their metal complexes produced an 19% cellular toxicity[22]. The *in vitro* antifungal activity of Sn(IV) complexes conducted against the *Rhizoctonia solani* and *Bortrytis cinera* by the poisoned food test and they exhibited activities comparable with fungicides manzate and ziram[23]. The antifungal activity of few new N-R-sulfonyldithiocarbimate metal complexes were tested and they are found to be active inhibitant against the Collectotrichum gloeosporioides[24]. The Ni(II), Cu(II) and Cd(II) complexes of thiophene-2,3-dicarboxaldehyde bis(thiosemicarbazone) tested for their antifungal activity and cytotoxicity and among them Cd(II) complexes found to exhibit

highest antifungal activity[25]. Chitosan based metal complexes showed an excellent inhibiting power against Phytophthora capsici, Verticilium alboatrum, Botrytis cineraa and Rhizoctonia solani which was confirmed by the pot experiment[26].

The antimicrobial activities of the semicarbazones and their organitin(IV) complexes were evaluated against various Candida species and their MICs also calculated. SAR calculations also performed to evaluate the physico-chemical properties related to the antimicrobial action[27]. Mohapatra[28] et al screened the antimicrobial behavior of the complexes of Cu(II), Co(II), Ni(II) and Zn(II) with some hydrazone derivatives containing benzimidazole moiety and they found to possess excellent inhibitors against bacteria as well as fungal strains.

CHAPTER 2

MATERIALS AND METHODS

The fungal strains used for the analysis of antifungal study of the prepared Diphenyl glycolic acid- amino acid ligands and their metal complexes are Pencillium sp., Fusarium sp.,Pythium sp., Lasiodiplodia theobromae and Aspergillus sp. These strains were obtained from the Department of Botany, The Zamorin's Guruvayurappan College, Calicut. Potato-dextrose agar medium was used for the culturing of the fungal strains.

2.1 Preparation of Potato dextrose agar medium

1. Potato - 200 g
2. Dextrose -20 g
3. Agar-agar -20 g
4. Distilled water -1000mL

2.2 Procedure

Antifungal activities of the prepared Diphenyl glycolic acid- amino acid complexes were examined using the disc method using potato dextrose agar medium, which have been prepared from potato, dextrose, agar-agar and distilled water. Various concentrations of prepared complexes was prepared by dissolving it in DMSO and poured it into the potato dextrose agar medium in appropriate

quantities. The studies involves the pouring of the medium to the petriplates, cutting the solidified mycelia discs of 5 mm in diameter from the periphery of the 48 hours old culture have been carried out under aseptic conditions in a laminar flow hood. The disc was inoculated upside down within the middle of the petriplates and these were incubated at room temperature until fungal growth in the controlled plates was almost complete. The estimation of the mycelial development of fungi in each petriplates was conducted and growth inhibition (I) was calculated with the help of the following equation:

$$\text{Percentage inhibition} = C - T/C \times 100$$

where c and T are diameters of the fungal colony in the control and test plate respectively.

CHAPTER 3

RESULTS AND DISCUSSION

The results of the study at 24, 48 and 72 hours were tabulated in the tables 3.1-3.5 and their graphical representations are shown in fig.3.1-3.5. The antifungal activity of the ligand and its complexes were shown in fig 3.6-3.10. The studies reveal that the new amino acid complexes act as efficient inhibitor against all the five fungal strains even at the lower concentration. The metal complexes were more efficient than their corresponding ligands suggesting the increase of inhibition activity due to the complexation with the metal ion suggested by Tweedy's Chelation theory. The complexes show to be highly efficient inhibitor against the various fungal strains such as Aspergillus sp., Pythium sp., Pencillium sp., Lasiodiplodia sp. and Fusarium sp. Pythium sp. and Lasiodiplodia sp. had completed its growth within 48 hours whereas others Aspergillus sp., Pencillium sp., and Fusarium sp needs 72 hours of incubation. Zn complexes of certain ligands shows high inhibition against phythium sp compared to other complexes and its parent ligand. All the complexes exhibit a moderate activity against the tested samples when compared with the standard drugs available.

Table.3.1. Preliminary *In vitro* antifungal activity of HBT ligands and its Co(II),Cu(II) and Zn(II) complexes against various fungal strains at 24, 48 and 72 hours.

Tyrosine ligand and its complexes(24 hrs)

Fungi	**Percentage of inhibition**							
	L1		**CoL1**		**CuL1**		**ZnL1**	
Conc. (ppm)	1000	1500	1000	1500	1000	1500	1000	1500
Aspergillus niger	17	30	29	36	34	39	25	35
Phythium	-	2.22	5.55	10	4.44	6.66	-	12.32
Pencillium	3.7	11	25	29	22	25	18	25
Lasiodiplodia theobromae	26	30	34	36	39	60	30	34
Fusarium sp.	4	8	16	20	8	16	12	20

Tyrosine ligand and its complexes(48 hrs)

Fungi	**Percentage of inhibition**							
	L1		**CoL1**		**CuL1**		**ZnL1**	
Conc. (ppm)	1000	1500	1000	1500	1000	1500	1000	1500
Aspergillus niger	21	35	26	38	35	41	28	37
Pythium	-	14.28	17.46	23.8	14.28	20.63	-	20.63
Pencillium	13	22	36	50	27	40	31	50
Lasiodiplodia theobromae	6	12	21	23	44	55	13	22
Fusarium sp.	8.6	11.4	20	22	14.2	20	14.2	22

Tyrosine ligand and its complexes(72 hrs)

Fungi	**Percentage of inhibition**							
	L1		**CoL1**		**CuL1**		**ZnL1**	
Conc. (ppm)	1000	1500	1000	1500	1000	1500	1000	1500
Aspergillus niger	29	37	38	46	39	48	34	42
Pencillium sp.	19	31	40	56	38	50	32	50
Fusarium sp.	13.3	20	33.3	40	26	33.3	26	33.3

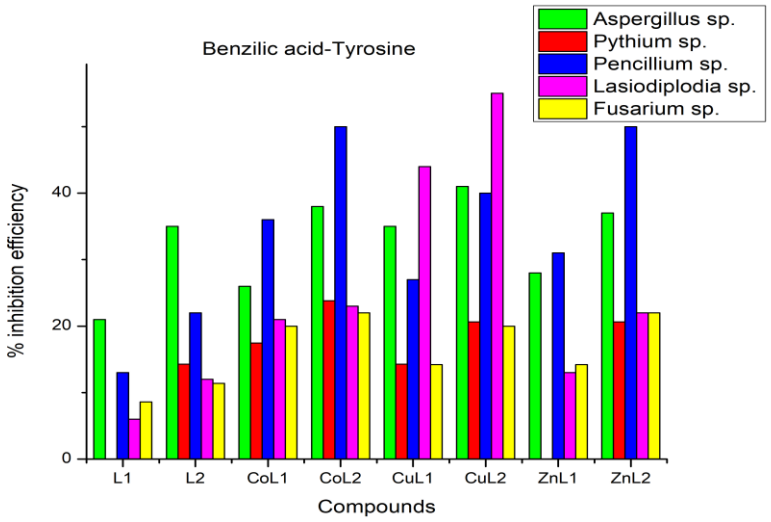

Fig.3.1. Fungal Inhibition efficiency of Diphenyl glycolic acid - tyrosine ligand and its metal complexes at L1 (1000ppm) and L2 (1500ppm) concentrations

Among the Diphenyl glycolic acid-tyrosine complexes, Cobalt complex shows higher inhibition efficiency against the Pencillium sp., Fusarium sp. and Pythium sp. Copper complexes exhibits maximum efficiency for Lasiodiplodia theobromae and Aspergillus sp. All the other complexes exhibit better efficiency when compared with that of their parent ligand which clearly indicates that their inhibition efficiency has been increased upon complexation. For Pythium species the ligand and complexes show the following order: $CoL_1 > CuL_1 > ZnL_1 > L_1$. But in the case of Lasiodiplodia theobromae and Aspergillus sp. it exhibits an order of $CuL_1 > CoL_1 > ZnL_1 > L_1$. In the case of Pencillium sp. and

Fusarium sp. the order of inhibition efficiency is CoL_1 > ZnL_1 >CuL_1 > L_1.

Table.3.2. Preliminary *In vitro* antifungal activity of HBG ligands and its Co(II),Cu(II) and Zn(II) complexes against various fungal strains at 24, 48 and 72 hours.

Glycine ligand and its complexes (24hrs)

Fungi	**Percentage of inhibition**							
	L2		**CoL2**		**CuL2**		**ZnL2**	
Conc. (ppm)	1000	1500	1000	1500	1000	1500	1000	1500
Aspergillus niger	7	13	18	23	21	31	32	40
Phythium	10.25	20.51	16.66	23.07	35.55	38.46	60	71.11
Pencillium	20	22	24	26	25	30	25	29
Lasiodiplodia theobromae	25	44	58	64	53	56	42	46
Fusarium sp.	6.6	11	12	26	12	14	20	28

Glycine ligand and its complexes (48 hrs)

Fungi	**Percentage of inhibition**							
	L2		**CoL2**		**CuL2**		**ZnL2**	
Conc. (ppm)	1000	1500	1000	1500	1000	1500	1000	1500
Aspergillus niger	13	21	25	39	29	43	39	47
Phythium	-	-	-	30.76	-	55.12	65.38	76.92
Pencillium	20	24	28	30	36	38	26	36
Lasiodiplodia theobromae	31	51	60	65	58	63	45	50
Fusarium sp.	8.57	13.3	20	28	16	24	28.5	34

Glycine ligand and its complexes (72 hrs)

Fungi	**Percentage of inhibition**							
	L2		**CoL2**		**CuL2**		**ZnL2**	
Conc. (ppm)	1000	1500	1000	1500	1000	1500	1000	1500
Aspergillus niger	21	25	30	43	35	46	42	55
Pencillium	23	26	28	34	40	50	27	36
Fusarium sp.	12	16	24	29	26	33.3	33.3	40

Among the glycine complexes Zinc complexes shows higher inhibition efficiency against the Aspergillus sp., Pythium sp. and Fusarium sp. For Pencillium sp. Copper complexes exhibits better inhibition whereas in the case of Lasiodiplodia theobromae Cobalt

complexes shows better inhibition efficiency. All the other complexes exhibit better efficiency when compared with that of their parent ligand which clearly indicates that their inhibition efficiency has been increased upon complexation. For Lasiodiplodia theobromae, Copper complex exhibits better efficiency. For pythium species the ligand and complexes shows the following order: $ZnL_2 > CuL_2 > CoL_2 > L_2$. But in the case of Lasiodiplodia theobromae, the order is $CoL_2 > CuL_2 > ZnL_2 > L_2$ and for Aspergillus sp. it exhibits an order of $ZnL_2 > CuL_2 > CoL_2 > L_2$. In the case of Pencillium the order of inhibition efficiency is $CuL_2 > ZnL_2 > CoL_2 > L_2$ and Fusarium sp. the order of inhibition efficiency is $ZnL_2 > CuL_2 > CoL_2 > L_2$.

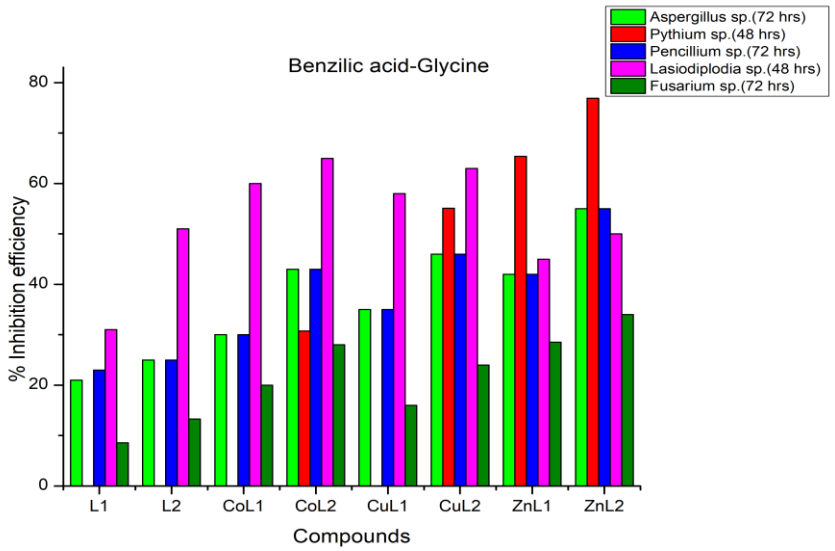

Fig.3.2. Fungal Inhibition efficiency of Benzilic acid-Glycine ligand and its metal complexes at L1 (1000ppm) and L2 (1500ppm) concentrations

Table.3.3. Preliminary *In vitro* antifungal activity of HBH ligands and its Co(II),Cu(II) and Zn(II) complexes against various fungal strains at 24, 48 and 72 hours.

Histidine ligand and its complexes(24 hrs)

Fungi	**Percentage of inhibition**							
	L3		**CoL3**		**CuL3**		**ZnL3**	
Conc. (ppm)	1000	1500	1000	1500	1000	1500	1000	1500
Aspergillus niger	13	21	28	32	18	23	23	25
Pythium	-	25	28	30	29	30	33	43
Pencillium	6	10	33	48	11	13	24	26
Lasiodiplodia theobromae	31	44	45	52	49	56	41	50
Fusarium sp.	14	19	24	29	24	38	19	24

Histidine ligand and its complexes(48 hrs)

Fungi	**Percentage of inhibition**							
	L3		**CoL3**		**CuL3**		**ZnL3**	
Conc. (ppm)	1000	1500	1000	1500	1000	1500	1000	1500
Aspergillus niger	21	25	30	35	28	33	38	43
Pythium	-	28	30	32	30	33	35	50
Pencillium	16	19	37	44	25	28	38	43
Lasiodiplodia theobromae	10	13	19	25	23	30	15	20
Fusarium sp.	17	23	33	40	43	47	33	40

Histidine ligand and its complexes(72 hrs)

Fungi	Percentage of inhibition							
	L3		CoL3		CuL3		ZnL3	
Conc. (ppm)	1000	1500	1000	1500	1000	1500	1000	1500
Aspergillus niger	25	28	31	39	34	40	43	52
Pencillium	20	23	40	53	34	40	50	60
Fusarium sp.	24	35	47	64	47	59	41	53

Among the histidine complexes Copper complex shows higher inhibition efficiency against the Lasiodiplodia theobromae and Zinc complexes show maximum potential against Fusarium sp. Aspergillus sp. and Pythium sp. In the case of Pencillium sp. Copper complex exhibits maximum inhition efficiency. All the other complexes exhibit better efficiency when compared with that of their parent ligand which clearly indicates that their inhibition efficiency has been increased upon complexation. For Lasiodiplodia theobromae, Copper complex exhibits better efficiency. For pythium species the ligand and complexes shows the following order: $ZnL_3 > CuL_3 > CoL_3 > L_3$. But in the case of Lasiodiplodia theobromae it exhibits an order of $CuL_3 > CoL_3 > ZnL_3 > L_3$ and Aspergillus sp. it exhibits an order of $ZnL_3 > CoL_3 > CuL_3 > L_3$. In the case of Pencillium the order of inhibition efficiency is $CoL_3 > ZnL_3 > CuL_3 > L_3$ and Fusarium sp. the order of inhibition efficiency is $CuL_3 > ZnL_3 > CoL_3 > L_3$.

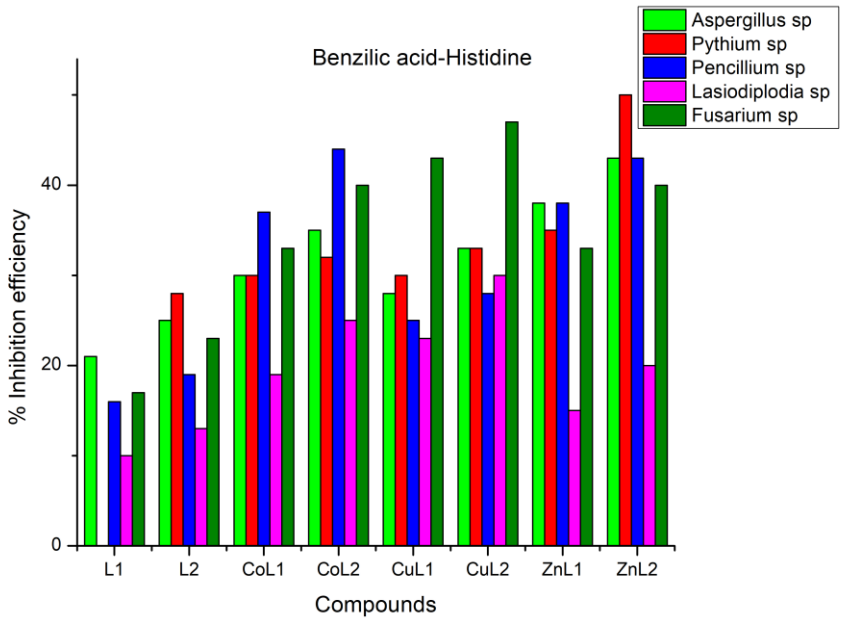

Fig.3.3. Fungal Inhibition efficiency of Benzilic acid-Histidine ligand and its metal complexes at L1 (1000ppm) and L2 (1500ppm) concentrations

Table.3.4. Preliminary *In vitro* antifungal activity of HBV ligands and its Co(II),Cu(II) and Zn(II) complexes against various fungal strains at 24, 48 and 72 hours.

Valine ligand and its complexes(24hrs)

Fungi	**Percentage of inhibition**							
	L4		**CoL4**		**CuL4**		**ZnL4**	
Conc. (ppm)	1000	1500	1000	1500	1000	1500	1000	1500
Aspergillus niger	11	16	15	26	19	25	18	25
Phythium	-	-	-	-	-	3.33	-	-
Pencillium	7	12	23	36	12	24	22	32
Lasiodiplodia theobromae	24	29	30	34	35	40	29	34
Fusarium sp.	12.5	15	20	22.5	20	30	17.5	25

Valine ligand and its complexes(48 hrs)

Fungi	Percentage of inhibition							
	L4		CoL4		CuL4		ZnL4	
Conc. (ppm)	1000	1500	1000	1500	1000	1500	1000	1500
Aspergillus niger	20	28	28	33	31	37	26	31
Phythium	-	-	-	-	-	42.22	-	-
Pencillium	9	15	27	38	22	33	23	34
Lasiodiplodia theobromae	8	11	14	18	20	23	12	15
Fusarium sp.	13.3	20	26.6	30	26	33	20	27

Valine ligand and its complexes(72 hrs)

Fungi	Percentage of inhibition							
	L4		CoL4		CuL4		ZnL4	
Conc. (ppm)	1000	1500	1000	1500	1000	1500	1000	1500
Aspergillus niger	23	29	35	41	42	47	32	38
Pencillium	16	22	28	39	30	38	46	61
Fusarium sp.	16.6	23.3	33.3	40	27	34	21	34

Among the valine complexes Cobalt complexes shows higher inhibition efficiency against the Fusarium sp. Copper complexes have a high potential activity against the fungi Aspergillus sp., Pythium sp., Lasiodiplodia theobromae whereas for Pencillium sp. Zinc complexes show maximum inhibition efficiency. All the other complexes exhibit better efficiency when compared with that of their parent ligand which clearly indicates that their inhibition efficiency has been increased upon complexation. For Lasiodiplodia theobromae, Copper complex exhibits better

efficiency. For pythium species the ligand and complexes shows the following order: $CuL_4 > L_4$. But in the case of Lasiodiplodia theobromae and Aspergillus sp. it exhibits an order of $CuL_4 > CoL_4 > ZnL_4 > L_4$. In the case of Pencillium exhibits the order of inhibition efficiency of $CoL_4 > ZnL_4 > CuL_4 > L_4$ and Fusarium sp. exhibits the order of inhibition efficiency of $CoL_4 > CuL_4 > ZnL4 > L_4$.

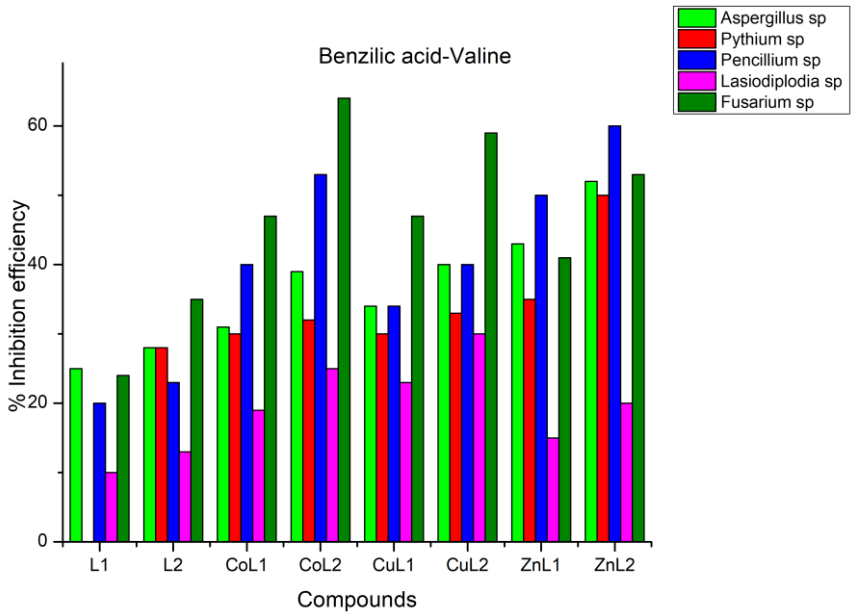

Fig.3.4. Fungal Inhibition efficiency of Diphenyl glycolic acid-Valine ligand and its metal complexes at L1 (1000ppm) and L2 (1500ppm) concentrations

Table 3.5. Preliminary *In vitro* antifungal activity of HBL ligands and its Co(II),Cu(II) and Zn(II) complexes against various fungal strains at 24, 48 and 72 hours.

Leucine ligand and its complexes(24 hrs)

Fungi	**Percentage of inhibition**							
	L5		**CoL5**		**CuL5**		**ZnL5**	
Conc. (ppm)	1000	1500	1000	1500	1000	1500	1000	1500
Aspergillus niger	-	-	-	-	-	-	-	-
Pythium	12	18	26	29	19	34	31	57
Pencillium	5	16	27	38	22	33	27	38
Lasiodiplodia theobromae	36	45	39	50	40	52	45	50
Fusarium sp.	13.3	20	26	40	26	40	40	46.6

Leucine ligand and its complexes(48 hrs)

Fungi	**Percentage of inhibition**							
	L5		**CoL5**		**CuL5**		**ZnL5**	
Conc. (ppm)	1000	1500	1000	1500	1000	1500	1000	1500
Aspergillus niger	-	-	-	-	-	-	-	-
Pythium	-	-	38	42	37	49	49	62
Pencillium	20	28	40	48	28	36	32	40
Lasiodiplodia theobromae	8	12	18	23	10	17	45	50
Fusarium sp.	26.6	30	38.75	42.5	35	45	40	47.5

Leucine ligand and its complexes(72 hrs)

Fungi	**Percentage of inhibition**							
	L5		**CoL5**		**CuL5**		**ZnL5**	
Conc. (ppm)	1000	1500	1000	1500	1000	1500	1000	1500
Aspergillus niger	-	-	-	-	-	-	-	-
Pencillium	30	38	42	50	30	38	46	53
Fusarium sp.	32.5	35	40	46	46	51	45	50

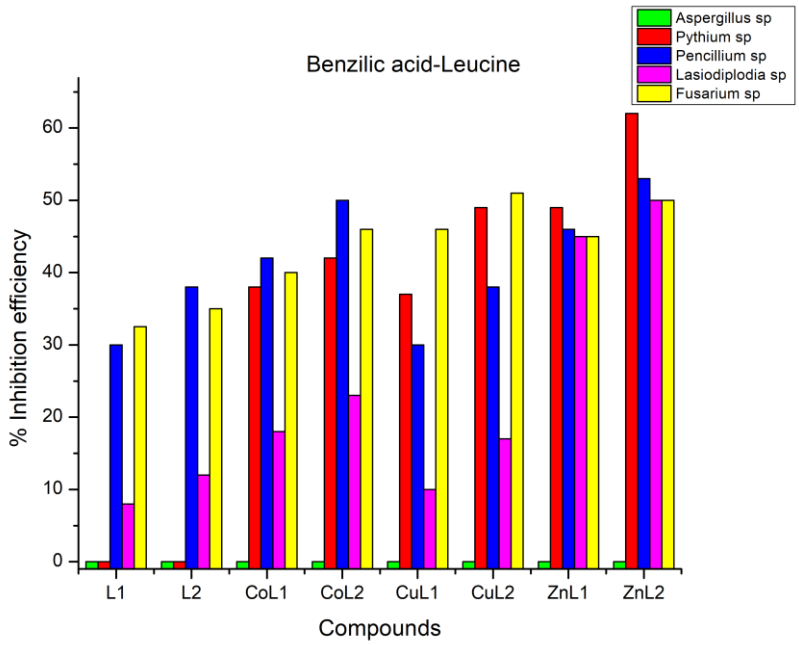

Fig.3.5. Fungal Inhibition efficiency of Diphenyl glycolic acid-Leucine ligand and its metal complexes at L1 (1000ppm) and L2 (1500ppm) concentrations

Among the leucine complexes Zinc complexes shows higher inhibition efficiency against the Pencillium sp., Lasiodiplodia theobromae, and Pythium sp. Copper complexes exhibits an maximum inhibition against the Fusarium sp. All the other complexes exhibit better efficiency when compared with that of their parent ligand which clearly indicates that their inhibition efficiency has been increased upon complexation. For Lasiodiplodia theobromae, Copper complex exhibits better efficiency. For pythium species the ligand and complexes shows the following order: $ZnL_5 > CuL_5 > CoL_5 > L_5$. But in the case of

Lasiodiplodia theobromae and Pencillium sp. it exhibits an order of $ZnL_5 > CoL_5 > CuL_5 > L_5$. In the case of and Fusarium sp. the order of inhibition efficiency is $CuL_5 > ZnL_5 > CoL_5 > L_5$.

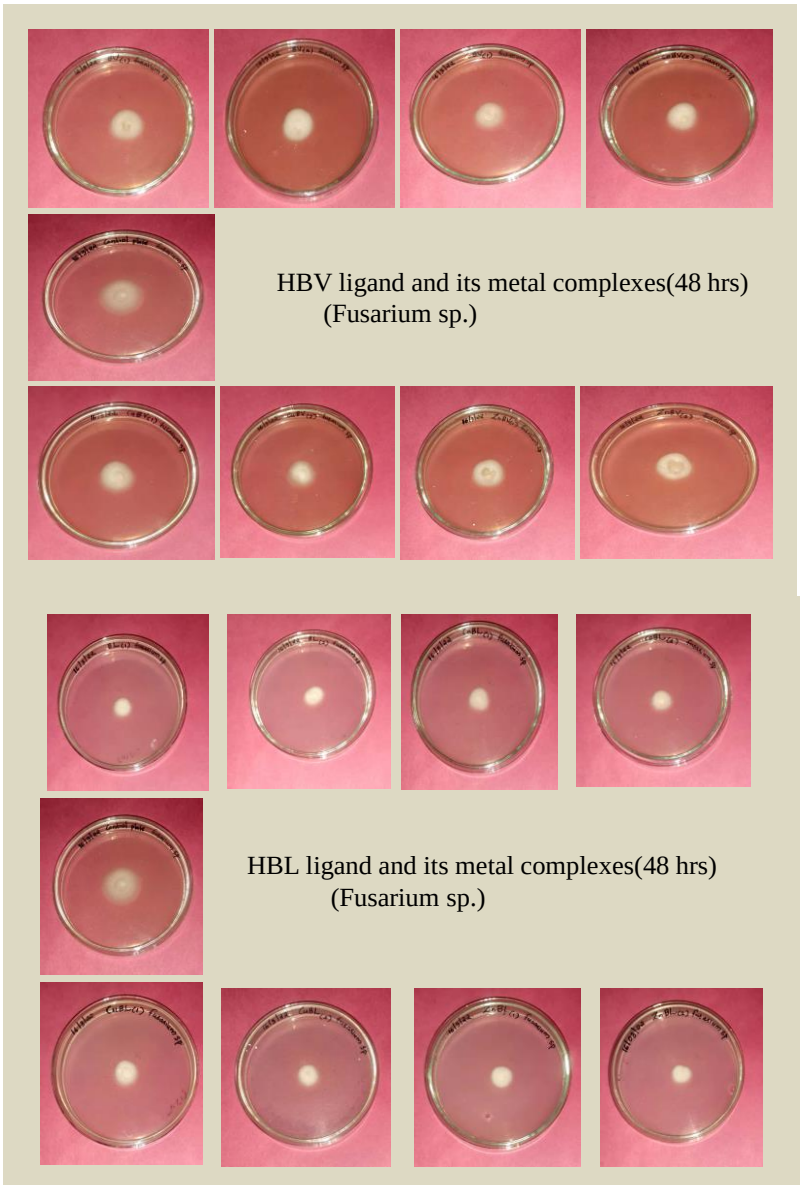

HBV ligand and its metal complexes(48 hrs) (Fusarium sp.)

HBL ligand and its metal complexes(48 hrs) (Fusarium sp.)

HBT and its metal complexes(48 hrs)
(Fusarium sp.)

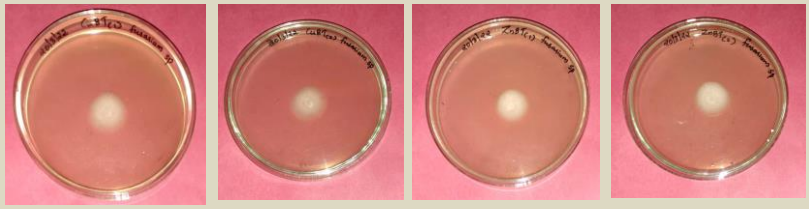

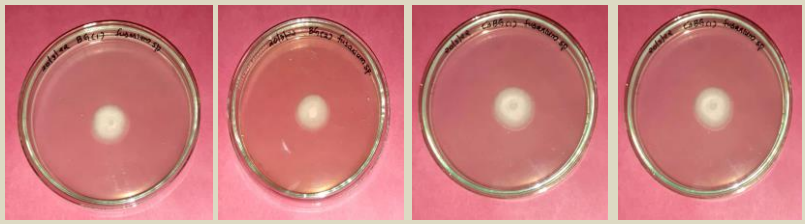

HBG and its metal complexes(48 hrs)
(Fusarium sp.)

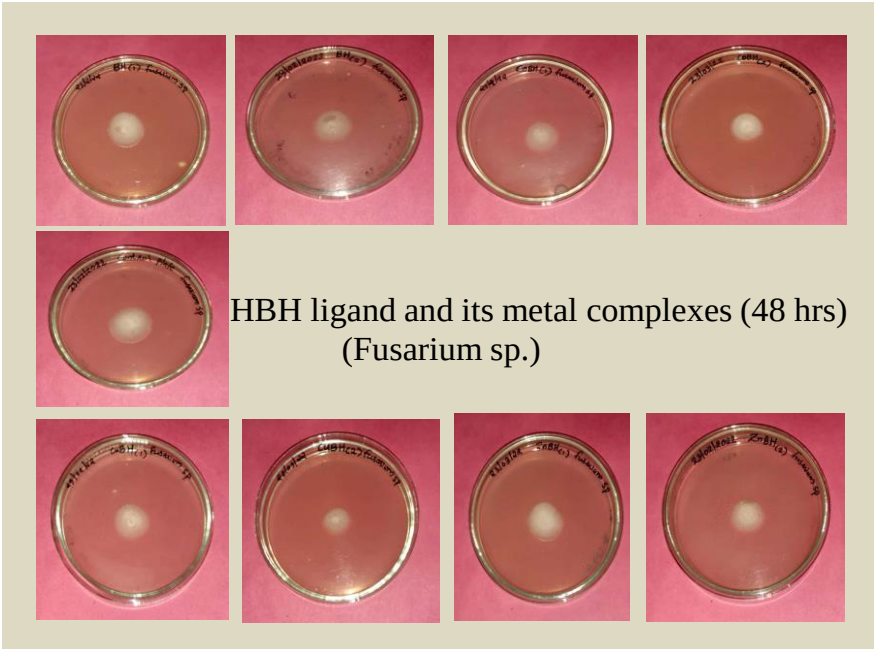

Fig.3.6. *In vitro* antifungal activity of HBT,HBG,HBH,HBV and HBL ligands and its Co(II),Cu(II) and Zn(II) complexes against Fusarium sp.

HBL and its metal complexes(48hrs)
(Pencillium sp.)

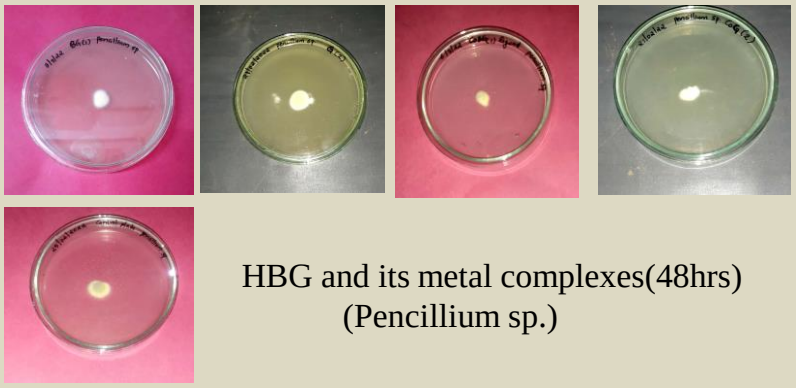

HBG and its metal complexes(48hrs)
(Pencillium sp.)

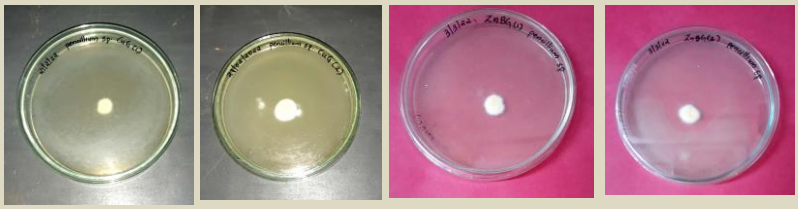

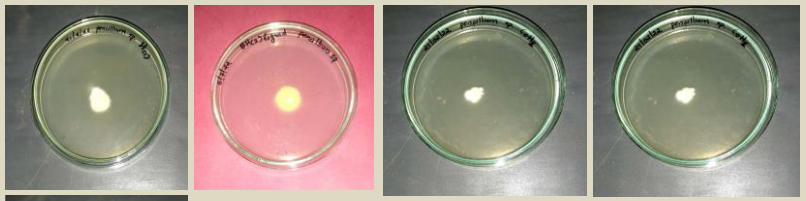

HBH and its metal complexes(48hrs)
(Pencillium sp.)

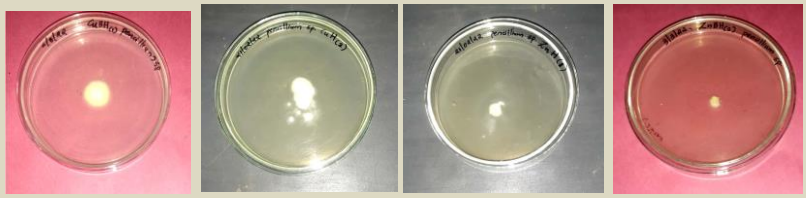

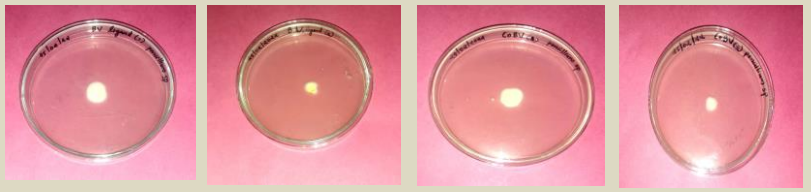

HBV and its metal complexes(48hrs)
(Pencillium sp.)

Fig.3.7. *In vitro* antifungal activity of HBT,HBG,HBH,HBV and HBL ligands and its Co(II),Cu(II) and Zn(II) complexes against Penciliium sp.

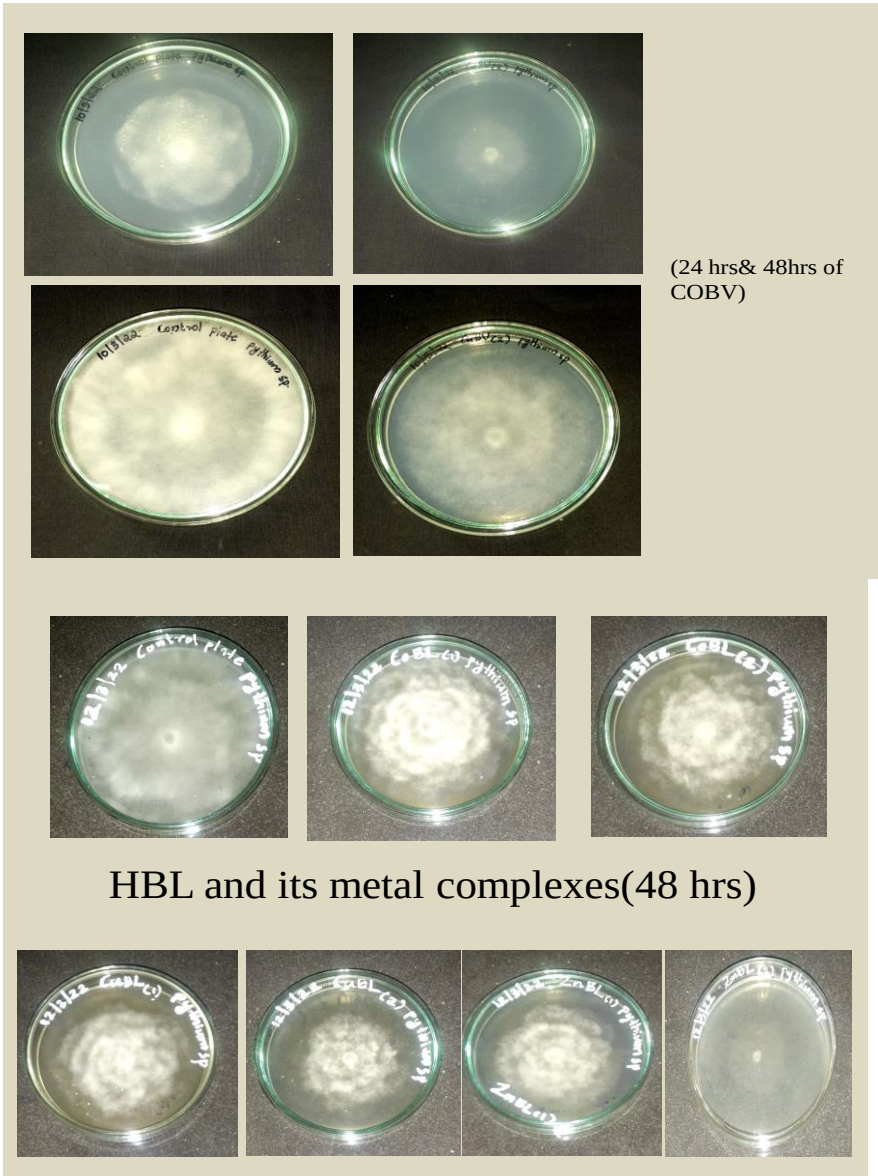

HBH and its metal complexes(48 hrs)

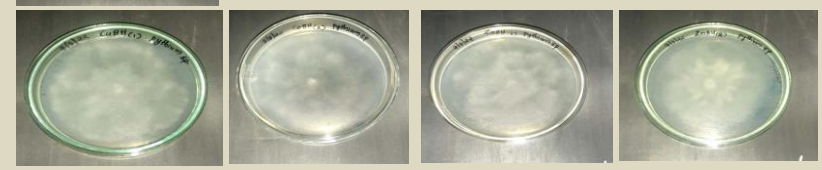

HBG and its metal complexes(48 hrs)

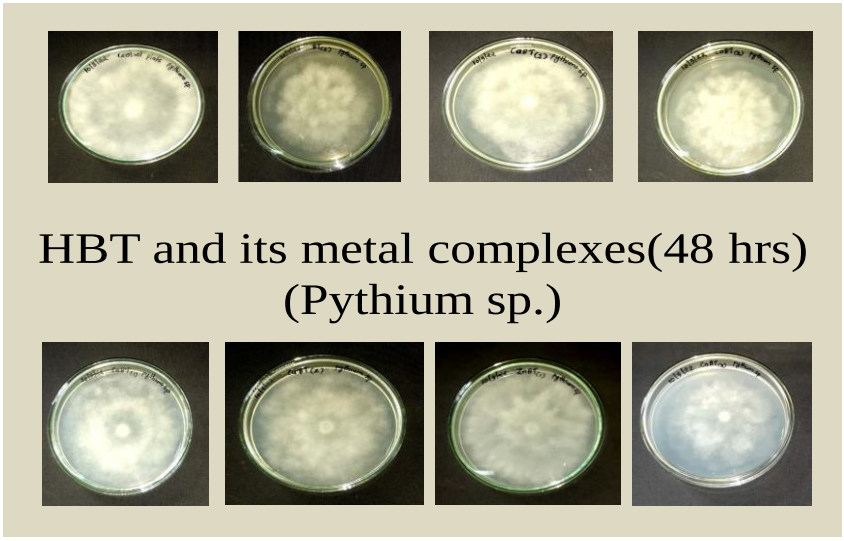

Fig.3.8. *In vitro* antifungal activity of HBT,HBG,HBH,HBV and HBL ligands and its Co(II),Cu(II) and Zn(II) complexes against Pythium sp.

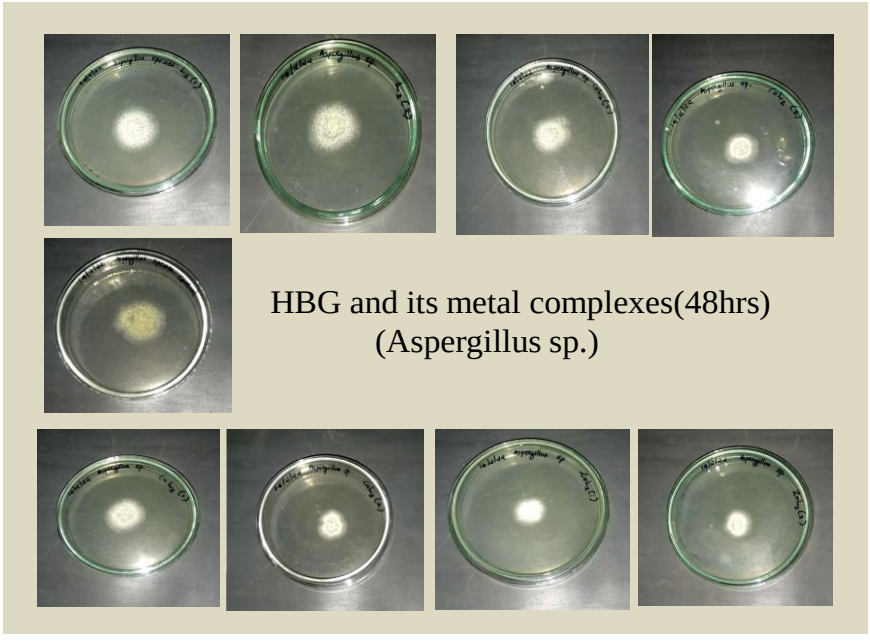

HBH and its metal complexes(48hrs)
(Aspergillus sp.)

HBT and its metal complexes(48hrs)
(Aspergillus sp.)

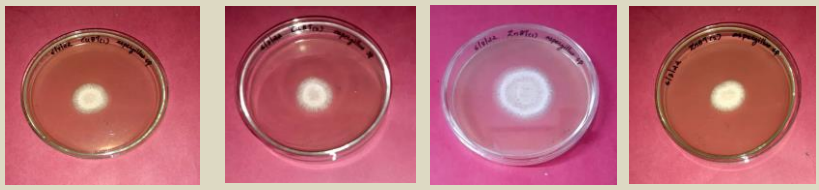

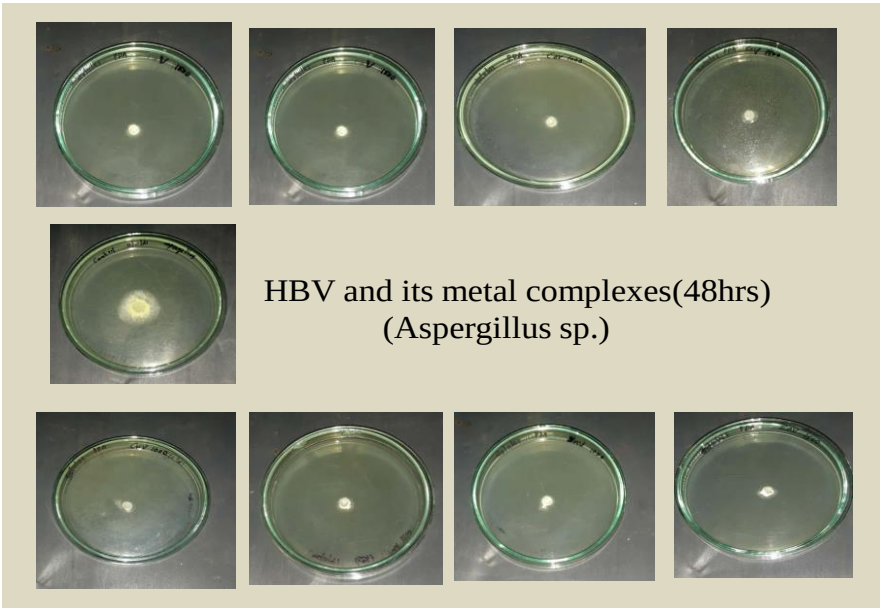

Fig.3.9. *In vitro* antifungal activity of HBT,HBG,HBH,HBV and HBL ligands and its Co(II),Cu(II) and Zn(II) complexes against Aspergillus sp.

HBH and its metal complexes(48hrs)
(Lasiodiplodia sp.)

HBT and its metal complexes(48hrs)
(Lasiodiplodia sp.)

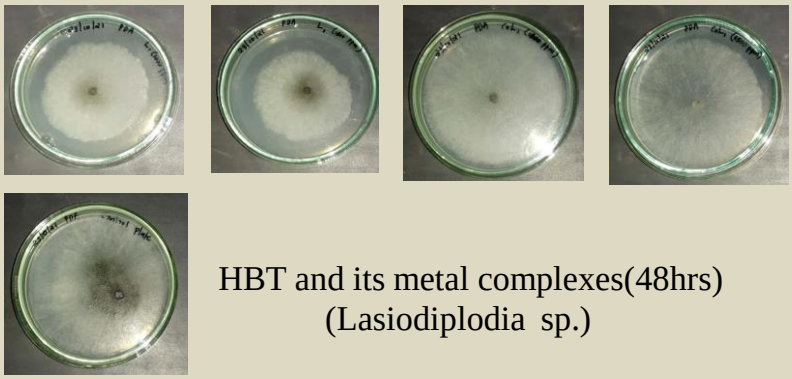

HBT and its metal complexes(48hrs)
(Lasiodiplodia sp.)

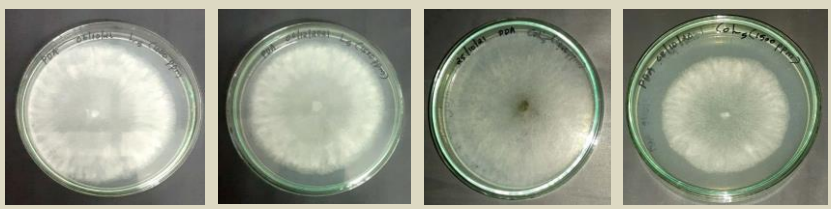

HBL and its metal complexes(48hrs)
(Lasiodiplodia sp.)

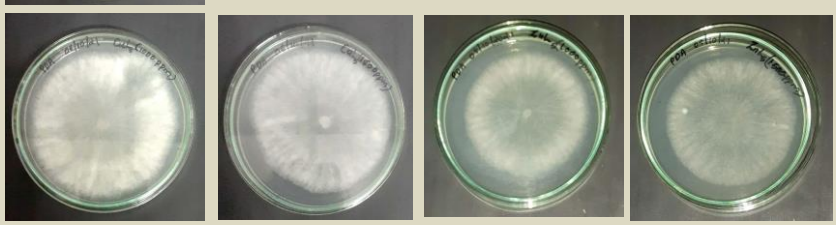

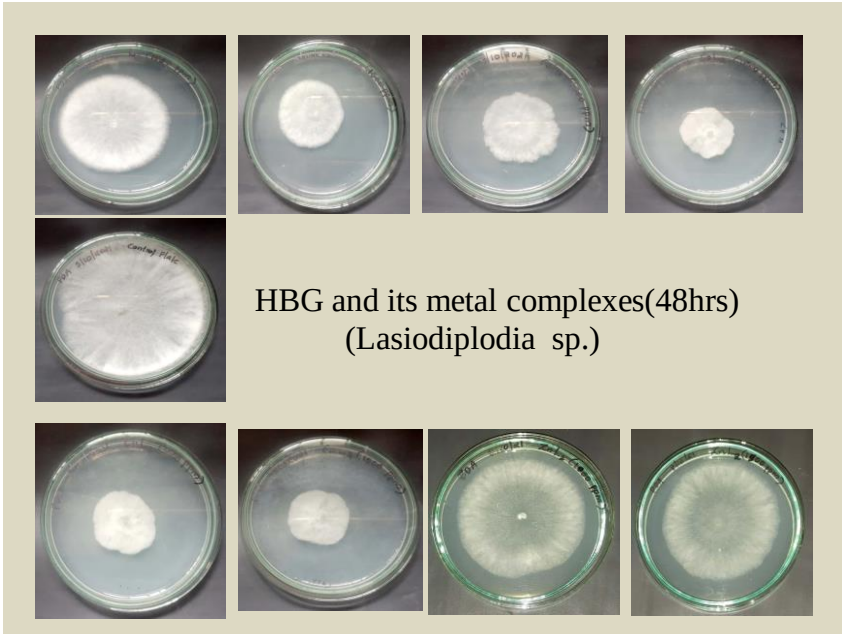

Fig.3.10. *In vitro* antifungal activity of HBT,HBG,HBH,HBV and HBL ligands and its Co(II),Cu(II) and Zn(II) complexes against Lasiodiplodia sp.

Conclusion

The observation of the study reveals that the tested compounds were showing activity against the fungal strains. The metal complexes shows higher activity compared to the free ligand. The Zn (II) metal complexes show high inhibition against Pythium sp than compared to that of other metal complexes. All metal complexes show moderate activity against the tested fungal strains. The graphical representations of the tested samples against the fungal strains have been represented in the Graph.no.1-5. Among the tyrosine complexes Cobalt complexes show better efficiency

against Pythium sp., Pencillium sp. and Fusarium sp. Copper complexes shows high inhibition against Lasiodiplodia sp.and Aspergillus sp. In the case of Glycine complexes Zn complexes inhibits Pythium sp., Aspergillus sp. and Fusarium sp. most effectively and Copper complex inhibits Pencillium sp and Cobalt complex inhibits Lasiodiplodia sp. The Histidine complexes are also active inhibitors against the fungal strains. Zinc complexes are efficient inhibitors against the Pythium sp., Aspergillus sp. and Pencillium sp., whereas Copper complex inhibits Lasiodiplodia sp. and Cobalt complexes inhibits Fusarium sp. Copper complexes of Valine ligand are active inhibitors against Pythium sp., Aspergillus sp. and Lasiodiplodia sp. and Zn complexes of the Valine ligand inhibits Pencillium sp. and Fusarium sp. The Zinc complex of Leucine is active against Pythium sp., Aspergillus sp. and Pencillium sp. and Copper complexes inhibit Fusarium sp. effectively. From the above study we can conclude that Zinc complexes are much active inhibitor against fungal strains. The graphical comparison of the antifungal activity of various metal complexes against various fungal strains are represented in Fig.3.11.

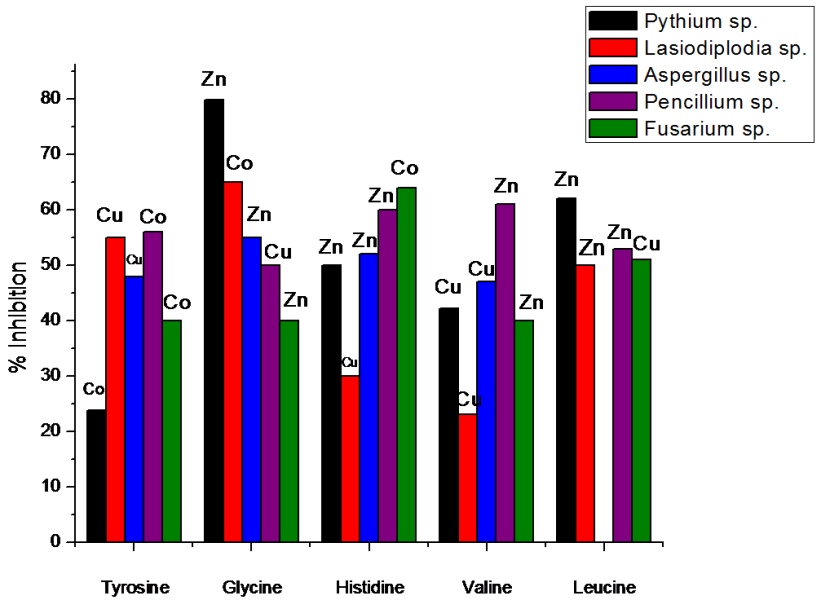

Fig.3.11. Graphical representation of antifungal activity of the complexes

References :

1. Albert, A., (1967). *Aus. J. Sci.*, 30, 1.
2. Schubert, J. (1966). *Sci. Amer*., 214, 40.
3. Seven, M. J. and Johnson, L. A. (1960). Metal-binding in medicine: proceedings of a symposium sponsored by Hahnemann Medical College and Hospital, Philadelphia.
4. Dwyer, F. (Ed.). (2012). *Chelating agents and metal chelates*. Elsevier.
5. Lehmann, G., JD Dunitz et al.(Eds.), (1975). Structure and Bonding, Chemical Bonding in Solids, Springer- Verlag, Berlin- Heidelberg- New York 1974, 165 Seiten, Preis: DM 64.19.
6. Padhye, S., & Kauffman, G. B. (1985).*Coord. Chem. Rev.*, 63, 127.
7. Wang, L. F., Zhu, Y., Yang, Z. Y., Wu, J. G., & Wang, Q. (1991). *Polyhedron*, 10, 2477.
8. Kovelskaya, T., Ganusevich, I., Osinsky, S. P., Levitin, I., Bubnovskaya, L., Sigan, A., & Michailenko, V. (2000). Poster 33, 6th Internet World Congress for Biomedical Sciences.
9. Bolos, C. A., Nikolov, G. S., Ekateriniadou, L., Kortsaris, A., & Kyriakidis, D. A. (1998). *Metal Based Drugs*, 5, 323.
10. Yıldırım, L. T., Kurtaran, R., Namli, H., Azaz, A. D., & Atakol, O. (2007).*Polyhedron*, 26, 4187.
11. Takeuchi, T., Bottcher, A., Quezada, C. M., Simon, M. I., Meade, T. J., & Gray, H.B. (1998). *J. Am. Chem. Soc*., 120, 8555.
12. Liu, W., Qing, C., Chen, X., Ye, Q., Yu, Y., & Hou, S. (2008). *Chem. Pharm. Bull*., 56, 659.
13. Odds, F. C., Brown, A. J., & Gow, N. A. (2003). *Trends Microbiol*., 11, 272.
14. Mohamed, G. G., Zayed, M. A., & Abdallah. S. M. (2010). *J Mol. Struct*., 979, 62.

15. Tumer, M., Koksal, H., Sener, M. K., & Serin, S. (1999). *Trans Met Chem*, 24, 414.

16. Wang, R. M., Mao, J. J., Song, J. F., Huo, C. X., & He, Y. F. (2007). *Chin Chem Lett*, 18, 1416.

17. Imran, M., Iqbal, J., Iqbal, S., & Ijaz, N. (2007). *Turk J Biol*, 31, 67.

18. Raman, N., Raja, S. J., & Sakthivel, A. (2009). *J Coord Chem*, 62, 691.

19. Stănilă, A., Braicu, C., & Stănilă, S. (2011). *Not Bot Horti Agrobo*, 39, 124.

20. Barnabas, M. J., Parambadath, S., Nagappan, S., & Ha, C. S. (2019). *Heliyon*, 5.

21. Miglani, S., Mishra, M., & Chawla, P. (2012). *Der Pharma Chemica*, 4, 2265.

22. Lv, J. , Liu, T., Cai, S., Wang, X., Liu, L. & Wang, Y. (2006) . *J. Inorg. Biochem*, 100, 1888.

23. Shreaz, S., Sheikh, R. A., Bhatia, R., Neelofar, K., Imran, S., Hashmi, A. A., & Khan, L. A. (2011). *Biometals*, 24, 923.

24. Bomfim Filho, L. F., Oliveira, M. R., Miranda, L. D., Vidigal, A. E., Guilardi, S., Souza, R. A., & Rubinger, M. M. (2017). *J. Mol. Struct.*, 1129, 60.

25. Alves, L. C., Rubinger, M. M., Lindemann, R. H., Perpétuo, G. J., Janczak, J., Miranda, L. D., & Oliveira, M. R. (2009). *J. Inorg. Biochem.*, 103, 1045.

26. Alomar, K., Landreau, A., Allain, M., Bouet, G., & Larcher, G. (2013). *J. Inorg. Biochem.*, 126, 76.

27. Liu, W., Qin, Y., Liu, S., Xing, R., Yu, H., Chen, X. & Li, K. (2018). *Sci. Rep.*,8, 4845.

28. Parrilha, G. L., da Silva, J. G., Gouveia, L. F., Gasparoto, A. K., Dias, R. P., Rocha, W. R., & Beraldo, H. (2011). *Eur. J. Med. Chem.*, 46, 1473.

29. Mohapatra, R. K., Mishra, U. K., Mishra, S. K., Mahapatra,A., & Dash, D. C. (2011). *Journal of the Korean Chem. Soc.*, 55, 926.

PART VI

CATALYTIC STUDIES OF DIPHENYL GLYCOLIC ACID-AMINO ACID METAL COMPLEXES

CHAPTER 1

INTRODUCTION

Catalysis is the enhancement in the rate of chemical reaction by the addition of foreign particle to the reaction which is not consumed in the reaction and functions to lower the activation barrier than the normal unanalyzed reaction. A fidgety effort by the scientific community leads to the development of efficient catalyst for the important chemical reactions. An extreme condition such as high temperature and high pressure leads to the development of effective catalysts, which can decrease the reaction conditions to a minimum with high yield of products. Transition metal complexes have wide range of applications among which the activity of complexes as catalyst is also having a significant role. A broad array of transition metal complexes are widely used as catalysts in the organic reactions. The nature of the environment of the metal ion and their conformational flexibility predicts the catalytic efficiency of the transition metal complexes. The electronic and steric effects of the metal complexes can be enhanced with the help small changes in the ligand frame work. Therefore art of designing the ligand is very crucial in the field of catalysis. Majority of the catalytic reactions are still using the homogeneous catalysts. But the ease of separation, recyclability of catalyst, high activity and selectivity makes the heterogeneous catalyst more attractive.

The oxidation reactions involving transformation of alcohols to their corresponding carbonyl compounds, oxidation of sulfides to sulfoxides, alkenes to epoxides and diols, oxidation of azodyes to

their corresponding non-hazardous products are widely using large scale reactions. Hundreds of various types of reagents and techniques are accessible for the oxidation of different organic compounds. The rate of the reaction and the amount of product produced can be supervised with the selection of solvent, oxidant, reaction conditions such as temperature, pressure and number of reaction steps. Schiff base transition metal complexes due to their cheap and easy synthesis and their chemical and thermal stability can be used as a family of prominent oxidation catalysts.

Organic dyes disposal is one of the serious environmental issue faced by our society for few decades. Environmental pollutants become one of the key hazardous substances which can affect the mankind as well as nature. Over 50 years back, dumping of organic pollutants to the river named Cooum experienced worst effect to the flora and fauna exploring in the bank of the river. Toxicity and the carcinogenic effect of these hazardous dyes need the proper treatment for its disposal. The disposal of these hazardous dyes to the aquatic system without proper treatment is one of the major causes for the water pollution. These dyes not only made the water bodies colored but also kill the aquatic living creature by decreasing the dissolved oxygen capacity of water and blocking the sunlight thereby disturbing the natural growth activity of aquatic animals and plants. Methylene blue and methyl orange are the important azodyes widely used in textiles, printing, rubber etc.

Methylene blue is a thiazine dye which can also act as a medication to treat methemoglobinemia by converting the ferric ion in

hemoglobin to ferrous ion. Methyl orange is an azodye which exhibit a color change from red to yellow with increasing basicity thereby act as an indicator and also used in several industries including textile, paper, printing and food industries. Not only these dyes are hazardous but some of their reduced products are very toxic to the environment. A number of azo-reductases can interrelate with body organ like kidney, brain, liver, lung, heart, spleen and muscle tissues. Several dyes are reported to be skin sensitizers and can cause allergic skin reactions. So decomposition of theses dyes to less hazardous product is also much important.

Hydrogen peroxide oxidation and exposure of UV light for the reaction are not found to be much concerning problem therefore these methods are widely used nowadays for the dye degradation. The oxidation reactions using aqueous hydrogen peroxide is very cheap, ecofriendly and easy to handle[1,2]. Hydrogen peroxide is a best choice for the degradative study due to their cheap, readily available nature and most importantly the only byproduct is the water. Numerous work using aqueous H_2O_2 as oxidant and ligand-based catalysts under catalytic conditions have been studied. The degradation of toxic dyes using photo catalyst was mainly focused absorption of light and separation of the charge. To overcome these toxic effects of these toxic dyes numerous research works have been carried out using nanoparticles and various transition metal complexes. The nano compounds also had some undesirable consequence on the environment. So, recent research works focuses to reduce the adverse effect of these nanoparticles and transition

metal complexes. In the same way the use of transition metal complexes for the dye removal is highly encouragable due to their cheap, environment friendly nature as well as their structural diversity and useful chemical and physical properties. Eventhough much effective and simple method for the dye degradation is needed to be developed. So our effort is to develop a simple transition metal complex which can be easily developed as well as can act as an efficient catalyst.

Pangkita[3] et al conducted the study of CuO nanostructures on the enhanced catalytic degradation of methylene blue and methyl orange. The catalytic oxygenation of 2, 6-di-tert-butylphenol by series of tetra-halogeno-dimethyl salen cobalt (II) complexes was reported by Aurel[4] et al. Samira[5] et al conducted the study of photocatalytic degradation of organic pollutant dyes by mononuclear copper(II) complexes of bis-(2-pyridylmethyl)amine NNN-derivative ligands. The reactions followed a zero-order model suggesting the independence of concentration in the photocatalytic reactions. The Ag-doped mesophorous TiO_2 modified with Zinc(II) tetrakis(4 carboxyphenyl)-porphyrin was evaluated for the photocatalytic degradation of p-nitrophenol and methylene blue under UV and visible light irradiation[6]. The photocatalytic bleaching of methylene blue dye upon the irradiation of UV light using Cu(II), Ni(II) and Co(II) complexes of (2E)-2-[(2E)-3-phenylprop-2-en-1-ylidene]hydrazinecarbothioamide were carried out by Murali[7] et al.

The photocatalytic activity of six novel Co (II) and Ni(II)- triazole

Schiff bases have been carried out by Mostafa[8] et al for the degradation of methylene blue under UV irradiation in presence of hydrogen peroxide. The degradation of methylene blue using copper(II) and cadmium (II) complexes of Schiff base ligand under visible light irradiation using sodium borohydride as reductant was carried out by Saikat[9] et al. Both the complexes are found to be efficient among which copper complexes shows better catalytic activity. Cobalt-beta hydroxyl benzoate complex was found to be an enhanced competitor in the catalytic world. The improved activity of these compounds against the methylene blue dye is a very promising result[10]. The complete decolorization of the methylene blue dye in Co^{2+}-HCO_3^- system with H_2O_2 was obtained in less than 50 minutes was studied by Aihua et al[11].Ni (II), Cu(II) and Zn(II) complexes of 2-aminophenol ligand has undergone degradative studies of methylene blue dye by visible light irradiation and the results reveals the Cu(II) complex have 100% activity after 30 min irradiation. Ni(II) and Zn(II) complexes exhibits an degradative percentage of 85 and 60% respectively[12].

The salicylaldimine-modified mesoporous silica was undergone the photocatalytic reduction of methyl orange under UV irradiation and the kinetics study was found to obey pseudo-first order kinetics[13]. The photocatalytic activity of Cu(II) complexes of chitosan modified Schiff bases was carried out and the results proved them to be efficient catalysts[14]. The enhanced activity of ZnO nanoparticles doped with Eu^{3+} ions have been studied by Trandafilovic[15] et al. Nauman[16] et al synthesized low-cost alkaline

earth and transition –metal ferrite photocatalysts and they found to enhanced with their catalytic activity. Photocatalytic degradation of methyl orange using zinc nitroprusside complex under sunlight irradiation was conducted by Djebli[17] et al and they are found to be efficient photocatalyst. Liu[18] et al studied degradation of Methyl orange under visible light irradiation using Copper(II) coordination polymers.

During their search for new metal catalysts containing salen-type ligands, they found that better catalytic behaviour can be molded out when the substrate molecule can be easily coordinated by the complex and this is favoured when the catalyst has either a vacancy in the coordination sphere or a labile ligand. Jun Takaya studied about the scope of main group metals or metalloids in the field of catalysis instead of usual transition metal complexes.Urmila[19] et al synthesized amino acid coordinated vanadium(IV) complex which can act as active biocatalyst and they mimics the VHPO activity by effecting in vitro bromination of olefinic alcohols to the corresponding brominated products with much higher efficiency. The conversion of p-nitrophenol to p-aminophenol with an efficiency of 97% was conducted by Nikhil[20] et al by using Ni nanoparticles synthesized using One-pot green synthesis.

CHAPTER 2

(A) DEGRADATION STUDY OF THE HAZARDOUS DYE METHYL ORANGE USING H_2O_2 AS OXIDANT

2.1. EXPERIMENTAL

2.1.1. Materials

Methyl orange, Hydrogen peroxide, Ultrasonicator, UV spectrophotometer etc.

2.1.2. Procedure: Catalytic activity measurements

The degradation of the Methyl orange carried out in a clean beaker (100 ml). Accurately measured 10 ml dye solution is poured to the beaker followed by the addition of preferred catalyst concentration. The mixture is sonicated for 2 minutes in order to maintain equilibrium between the reactant solution and the catalyst. The oxidant is introduced to the equilibrium solution and blended thoroughly by continuous mixing. The progress of the reaction was checked by taking the aliquots from the reaction mixture at regular intervals and undergoes their UV spectra analysis is shown in fig.8.1. The effect of catalyst concentration, effect of oxidant concentration and the recyclability of the catalyst were studied.

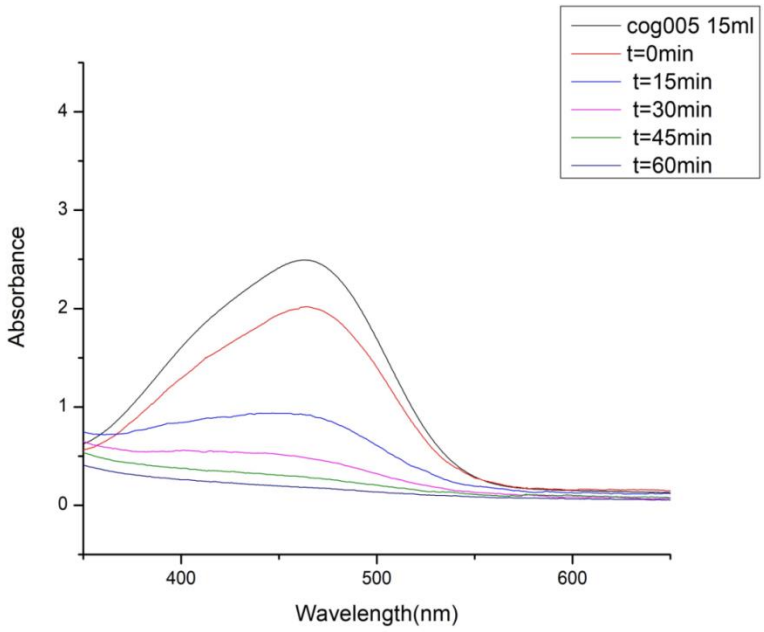

Fig.1.1. Time dependent UV-Visibleabsorption spectra of the MO solution and mixtures, viz ., MO + H_2O_2 + CoBG catalyst at various time intervals respectively. Condition:[dye=0.001g/L], volume of dye solution=10 ml, H_2O_2= 1ml and amount of catalyst= 0.005g

2.2 RESULTS AND DISCUSSION

The details of the spectral characterization ofthe catalysts used, i.e, the Cu (II), Co (II) and Ni (II) complexes of HBG, HBV and HBL ligands are described in the part I. The characteristic peaks obtained for the specific functional groups of the dye solution has been degraded to minimum, which indicates the removal of the toxic entity in the molecule thereby yield a non-hazardous products such as water, carbon dioxide etc. The degraded product was

compared with that of pure water which shows resemblance in the UV spectra. The heterogeneous study of the catalytic degradation of the toxic dyes made the study much easier and economically viable. The catalytic degradation of the hazardous dyes using H_2O_2 was catalyzed by the Cu (II), Co (II) and Ni (II) complexes of HBG, HBL and HBV ligand. The reaction was conducted in water as solvent which also reduces the chance of environmental pollution. The order of reactivity of the complexes in the catalytic degradation study may be given as CoBG >CoBV >CoBL >CuBG >CuBL >CuBV >NiBV >NiBL >NiBG. The catalytic degradation of the dyes was high for the cobalt complexes and they degrade the dyes within 15 minutes.

2.2.1. Blank run

The blank run was conducted in the absence of catalyst at room temperature keeping all the other conditions for the reaction as same for the screening experiments. The conversion rate was comparatively slow for the blank solution with that of the catalyzed solutions which shows that our catalysts are efficient for the degradation purposes.

2.2.2. Effect of various parameters on catalysis

The study of the degradation of dyes using various parameters has been conducted in order to understand the influence of various parameters. The reaction was carried out under different factors

such as: (1) type of catalyst (2) amount of catalyst, (3) reaction time and (4) amount of oxidant.

2.2.2.1 Effect of type of catalyst

The nature of catalyst is one of important factor depends on the degradation efficiency. Different catalyst has been employed in the study and each catalyst acts differently to the process. The Co (II), Cu (II) and Ni (II) catalysts have been used in the study and the efficiency was found to be maxima for Co (II) catalyst. The values are tabulated in Table 1.1 and the percentage degradation is shown in fig.1.2.

Table 1.1. Percentage degradation of methyl orange using Cu (II), Co (II) and Ni (II) complexes of HBG, HBV and HBL as catalysts.

Catalyst	**%D**
CoBG	91
CoBV	87
CoBL	82
CuBG	60
CuBV	52
CuBL	58
NiBG	16
NiBV	47
NiBL	28

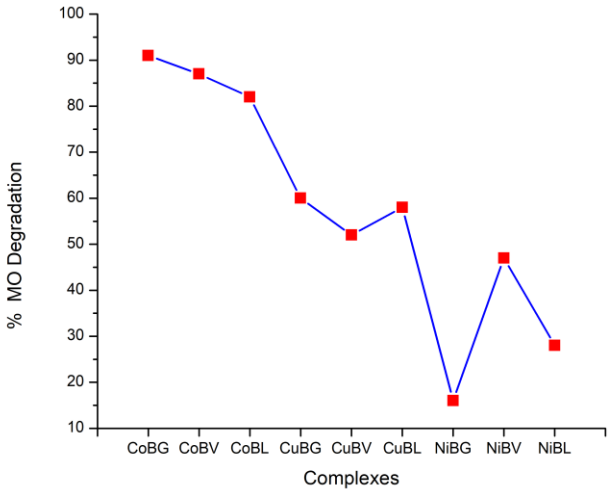

Fig. 1.2. Percentage degradation of methyl orange using Cu (II), Co (II) and Ni (II) complexes of HBG, HBV and HBL as catalysts.

2.2.2.2Effect of catalyst concentration

The effect of catalyst concentration on the degradation study of methyl orange using 0.001-0.005g under identical conditions is represented on the fig. 1.3. The degradation percentage is discussed in the table 1.2. The results shows that methyl orange degradation depends on the amount of catalyst in such a way that as the amount of catalyst increases the degradation efficiency also increases, which may due to the increase in number of active sites on the catalyst surface. The degradation efficiency increases with increase in the catalyst amount. This indicates the dependence of catalyst amount on the degradation process.

Table 1.2 Effect of amount of catalyst on the degradation of methyl orange

Catalyst Concentration	%C								
	Co BG	**Co BV**	**Co BL**	**Cu BG**	**Cu BV**	**Cu BL**	**Ni BG**	**Ni BV**	**Ni BL**
0.001	59	74	43	33	20	23	2	6	7
0.002	73	79	46	34	21	37	7	9	8
0.003	80	80	59	40	22	38	9	20	11
0.004	84	84	77	48	27	45	11	28	27
0.005	91	87	82	60	52	58	16	47	28

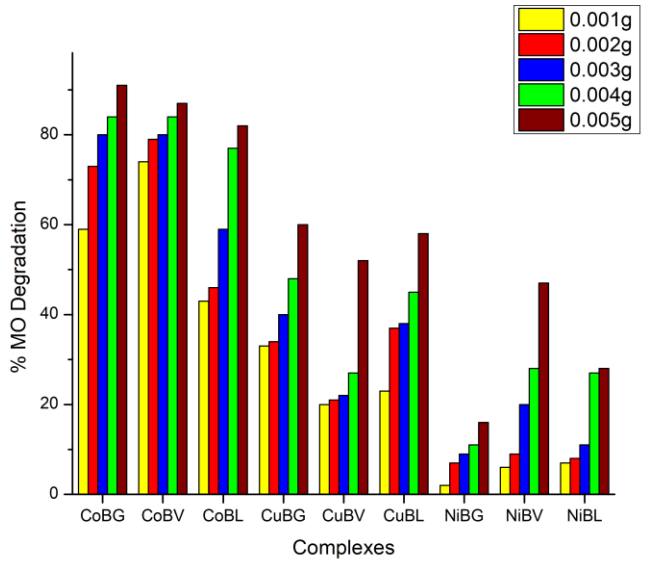

Fig. 1.3. Effect of amount of catalyst on the degradation of methyl orange

2.2.2.3Effect of reaction time

The effect of reaction time on the degradation of dyes with 0.005 mg of catalyst with an oxidant amount of 1ml is studied. The degradation percentage seems to be increasing with the increase of reaction time and it is represented graphically in fig.1.4.and the values are tabulated in Table. 1.3. The reaction time varied from 0 to 1 hour.

Table 1.3 Effect of reaction time on the degradation of methyl orange

Catalyst Concentration	**%C**			
	15	**30**	**45**	**60**
CoBG	45	83	88	91
CoBV	44	78	84	87
CoBL	46	71	80	81
CuBG	16	29	48	60
CuBV	9	19	24	52
CuBL	8	19	32	58
NiBG	6	10	13	16
NiBV	13	29	35	47
NiBL	4	12	21	28

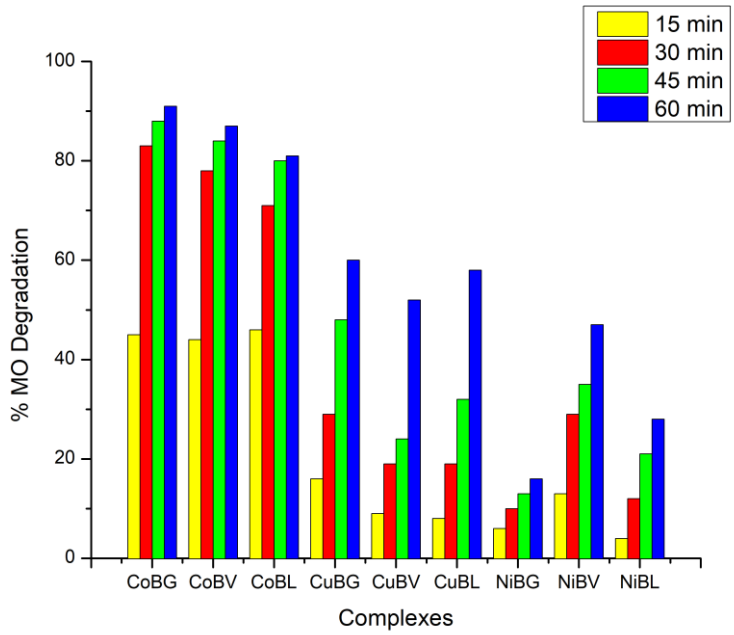

Fig. 1.4.Effect of reaction time on the degradation of methyl orange

2.2.2.4 Effect of oxidant concentration

The effect of concentration of the H_2O_2 oxidant on the methyl orange degradation study was studied by using different amount oxidant varying from 0.5-1.5 ml. The rate of degradation found to be increasing with the increase of H_2O_2 concentration due to the increase of $^{\cdot}OH$ radicals take part in the degradation process and it is represented graphically infig.1.5 and the values are tabulated in Table.1.4.

Table 1.4. Effect of oxidant concentration on the degradation of methyl orange

Catalyst Concentration	**%C**		
	0.5 ml	**1 ml**	**1.5 ml**
CoBG	86	91	90
CoBV	85	87	74
CoBL	64	82	55
CuBG	51	70	60
CuBV	20	35	32
CuBL	33	58	55
NiBG	12	16	13
NiBV	32	47	44
NiBL	13	16	9

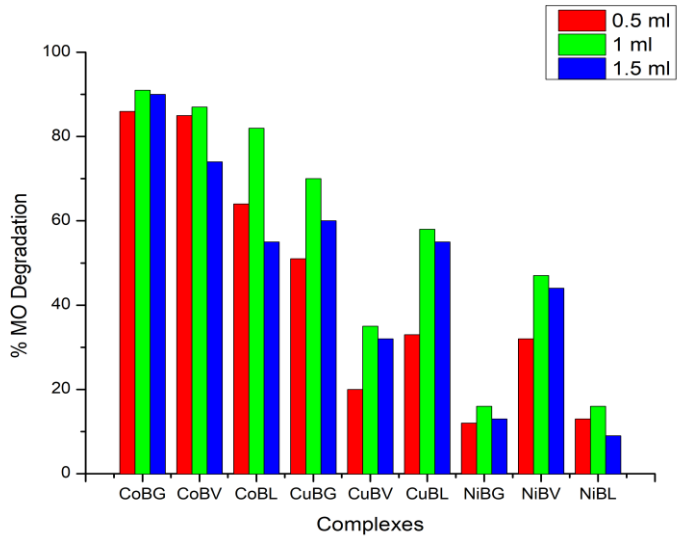

Fig. 1.5 Effect of oxidant concentration on the degradation of methyl orange

2.2.2.5 Kinetic study

The degradation kinetics of the methyl orange dye was studied by using the zero, first and second-order reaction kinetics formula. To study the kinetics of the degradation absorbance at 462 nm was measured as a function of time. The integrated equations for the reaction kinetics are presented below.

For Zero order reaction kinetics: $C_t = C_0 - k_0 t$ (1)

For First order reaction kinetics: $C_t = C_0 e^{-k0t}$ (2)

For Second order reaction kinetics: $1/C_t = 1/C_0 + k_2 t$ (3)

Where C_t is the concentration of MO at reaction time t

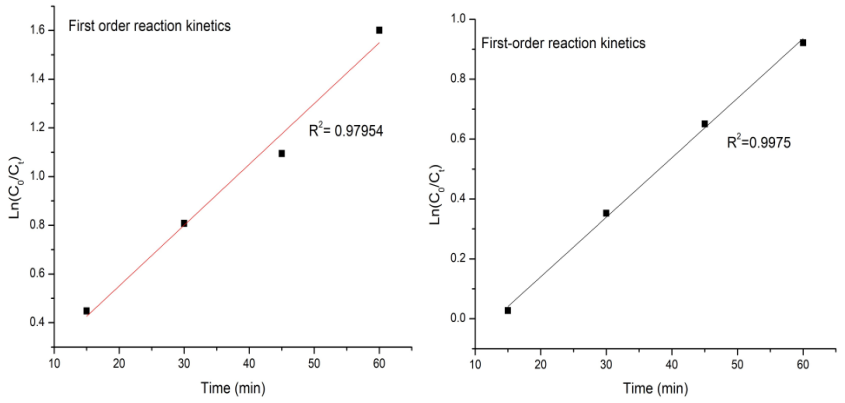

(a) (b)

Fig. 1.6. First order reaction kinetics for degradation of Methyl orange by (a) CoBG and (b) CuBG complexes.Condition:[dye=0.001g/L], volume of dye solution=10 ml, H_2O_2= 1ml and amount of catalyst= 0.005g

Regression analysis based on zero-, first- and second-order reaction kinetics for the degradation of MO using various complexes of HBG, HBV and HBL ligands was studied and on comparing the regression coefficient values, the results shows that the degradation kinetics of the MO followed the zero-order kinetics well and represented in fig.1.6.

(B) DEGRADATION STUDY OF THE HAZARDOUS DYE METHYLENE BLUE USING H_2O_2 AS OXIDANT

2.3.EXPERIMENTAL

2.3.1. Materials

Methylene blue, Hydrogen peroxide, Ultrasonicator, UV spectrophotometer etc.

2.3.2. Procedure: Catalytic activity measurements

The degradation of the Methylene blue carried out in a clean beaker (100 ml). Accurately measured 10 ml dye solution is poured to the beaker followed by the addition of preferred catalyst concentration. The mixture is sonicated for 2 minutes in order to maintain equilibrium between the reactant solution and the catalyst. The oxidant is inserted to the equilibrium solution and mixed thoroughly by constant mixing. The progress of the reaction was monitored by taking the aliquots from the reaction mixture at

regular intervals and undergoes their UV spectra analysis and is represented in fig.1.7.The effect of catalyst concentration, effect of oxidant concentration and the recyclability of the catalyst were studied.

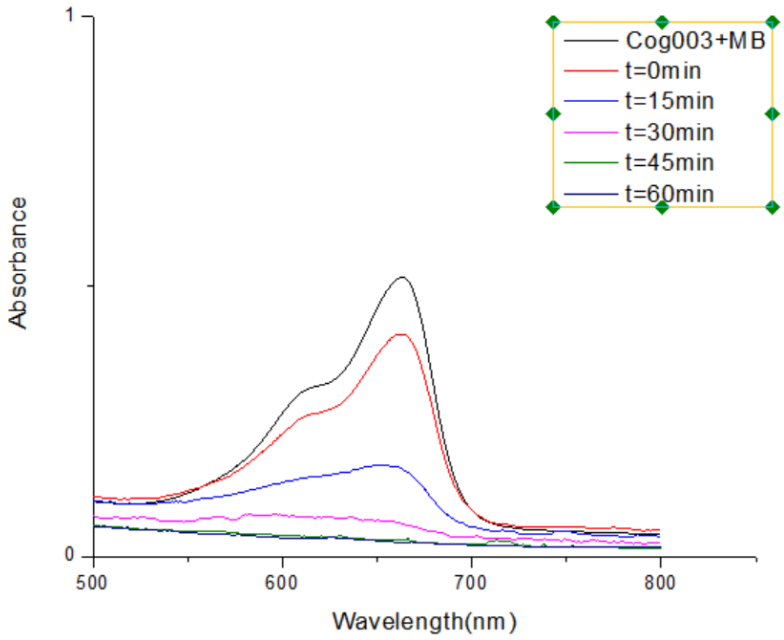

Fig. 1.7. Time dependent UV-Visibleabsorption spectra of the MB solution and mixtures, viz ., MO + H_2O_2 + CoBG catalyst at various time intervals respectively. Condition:[dye=0.001g/L], volume of dye solution=10 ml, H_2O_2= 1ml and amount of catalyst= 0.005g

2.4. RESULTS AND DISCUSSION

The details of the spectral characterization ofthe catalysts used, i.e, the Cu (II), Co (II) and Ni (II) complexes of HBG, HBV and HBL ligands are described in the Part 1. The characteristic peaks obtained for the specific functional groups of the dye solution has been degraded to minimum, which indicates the removal of the toxic entity in the molecule thereby yield a non-hazardous products such as water, carbon dioxide etc. The degraded product was compared with that of pure water which shows resemblance in the UV spectra. The heterogeneous study of the catalytic degradation of the toxic dyes made the study much easier and economically viable. The catalytic degradation of the hazardous dyes using H_2O_2 was catalyzed by the Cu (II), Co (II) and Ni (II) complexes of HBG, HBL and HBV ligand. The reaction was conducted in water as solvent which also reduces the chance of environmental pollution. The order of reactivity of the complexes in the catalytic degradation study may be given as CoBV >CoBG >CoBL >CuBG >CuBV >CuBL >NiBG >NiBV >NiBL. The catalytic degradation of the dyes was high for the cobalt complexes and they degrade the dyes within 15 minutes.

2.4.1. Blank run

The blank run was conducted in the absence of catalyst at room temperature keeping all the other conditions for the reaction as same for the screening experiments. The conversion rate was

comparatively slow for the blank solution with that of the catalyzed solutions which shows that our catalysts are efficient for the degradation purposes.

2.4.2. Effect of various parameters on catalysis

The study of the degradation of dyes using various parameters has been conducted in order to understand the influence of various parameters. The reaction was carried out under different factors such as: (1) type of catalyst (2) amount of catalyst, (3) reaction time and (4) amount of oxidant.

2.4.2.1Effect of type of catalyst

The nature of catalyst is one of important factor depends on the degradation efficiency. Different catalyst has been employed in the study and each catalyst acts differently to the process. The Co (II), Cu (II) and Ni (II) catalysts have been used in the study and the efficiency was found to be maxima for Co (II) catalyst. The values are tabulated in Table 1.5 and the percentage degradation is shown in fig. 1.8.

Table 1.5. Percentage degradation of MB using Cu (II), Co (II) and Ni (II) complexes of HBG, HBV and HBL as catalysts.

Catalyst	%C
CoBG	94
CoBV	97
CoBL	82
CuBG	75
CuBV	77
CuBL	80
NiBG	48
NiBV	47
NiBL	74

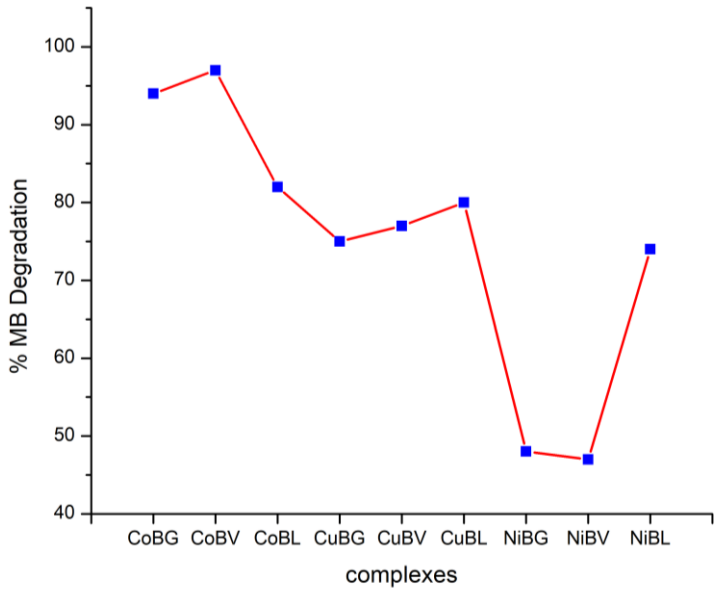

Fig. 1.8. Percentage degradation of MB using Cu (II), Co (II) and Ni (II) complexes of HBG, HBV and HBL as catalysts.

2.4.2.2Effect of catalyst concentration

The effect of catalyst concentration on the degradation study of methylene blue using 0.001-0.005g under identical conditions is represented on the fig.1. The degradation percentage is discussed in the table.1. The results shows that methyl orange degradation depends on the amount of catalyst in such a way that as the amount of catalyst increases the degradation efficiency also increases, which may due to the increase in number of active sites on the catalyst surface. The degradation efficiency increases with increase in the catalyst amount. This indicates the dependence of catalyst amount on the degradation process. The values are tabulated in Table 1.6 and the percentage degradation is shown infig. 1.9.

Table 1.6. Effect of amount of catalyst on the degradation of MB

Catalyst Concentration	**%C**								
	CoBG	**CoBV**	**CoBL**	**CuBG**	**CuBV**	**CuBL**	**NiBG**	**NiBV**	**NiBL**
0.001	76	85	40	41	35	29	22	16	13
0.002	91	92	45	60	41	63	34	21	20
0.003	92	93	58	65	51	65	39	24	55
0.004	93	95	71	69	72	73	45	42	71
0.005	94	97	82	75	77	80	48	47	74

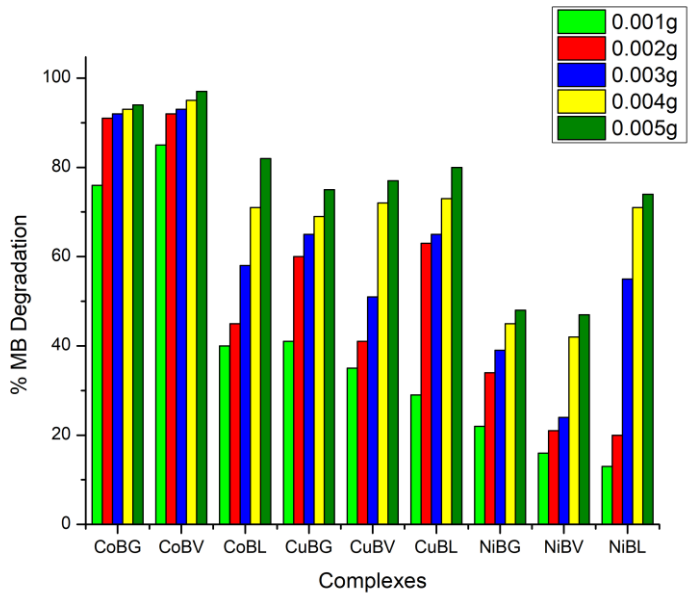

Fig. 1.9. Effect of amount of catalyst on the degradation of MB

2.4.2.3Effect of reaction time

The effect of reaction time on the degradation of dyes with 0.005 mg of catalyst with an oxidant amount of 1ml is studied. The degradation percentage seems to be increasing with the increase of reaction time and it is represented graphically in fig. 1.10 and tabulated inTable 1.7. The reaction time varied from 0 to 1 hour.

Table 1.7. Effect of reaction time on the degradation of MB

Catalyst Concentration	%C			
	15	**30**	**45**	**60**
CoBG	84	90	93	94
CoBV	60	87	94	97
CoBL	53	65	72	82
CuBG	38	57	65	75
CuBV	45	61	70	77
CuBL	29	51	74	80
NiBG	18	32	38	48
NiBV	17	31	36	47
NiBL	33	50	66	74

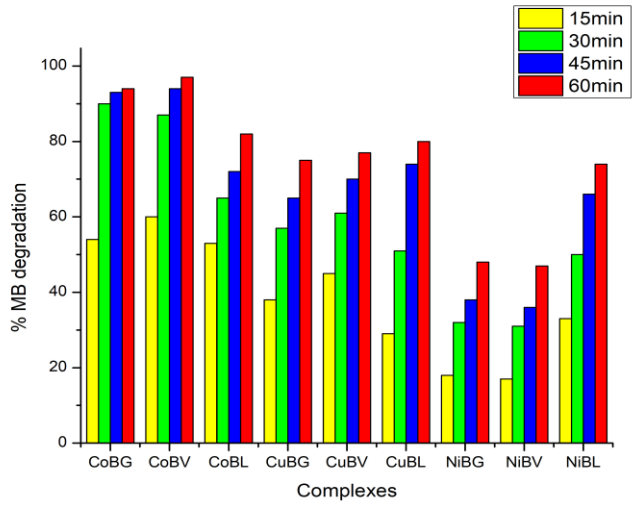

Fig. 1.10. Effect of reaction time on the degradation of MB

2.4.2.4Effect of oxidant concentration

The effect of concentration of the H_2O_2 oxidant on the methylene blue degradation study was studied by using different amount oxidant varying from 0.5-1.5 ml. The rate of degradation found to be increasing with the increase of H_2O_2 concentration due to the increase of $^{\cdot}OH$ radicals take part in the degradation process and it is represented graphically in fig.1.11. and tabulated in Table 1.8.

Table 1.8. Effect of oxidant concentration on the degradation of MB

Catalyst Concentration	**%C**		
	0.5 ml	**1 ml**	**1.5 ml**
CoBG	89	94	89
CoBV	85	97	80
CoBL	71	82	75
CuBG	51	75	63
CuBV	73	77	74
CuBL	77	80	75
NiBG	41	48	22
NiBV	35	47	46
NiBL	34	78	77

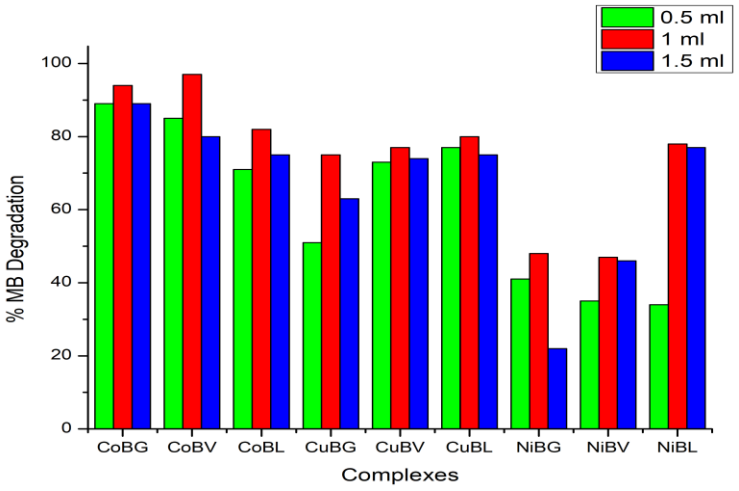

Fig. 1.11. Effect of oxidant concentration on the degradation of MB

2.4.2.5Kinetic study

The degradation kinetics of the methylene blue dye was studied by using the zero, first and second-order reaction kinetics formula. To study the kinetics of the degradation absorbance at 462 nm was measured as a function of time. The integrated equations for the reaction kinetics are presented below.

For Zero order reaction kinetics: $C_t = C_0 - k_0 t$ (1)

For First order reaction kinetics: $C_t = C_0 e^{-k0t}$ (2)

For Second order reaction kinetics: $1/C_t = 1/C_0 + k_2 t$ (3)

Where C_t is the concentration of MB at reaction time t

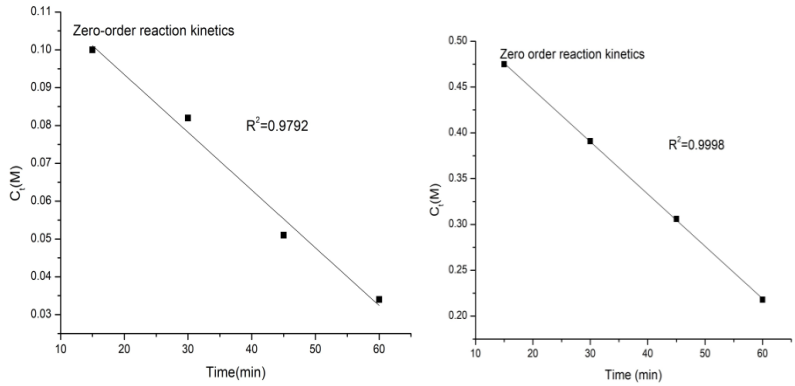

(a) (b)

Fig. 1.12. Zero order reaction kinetics for degradation of Methylene Blue by (a) CoBG and (b) CuBG complexes.Condition:[dye=0.001g/L], volume of dye solution=10 ml, H_2O_2= 1ml and amount of catalyst= 0.005g

Regression analysis based on zero-, first- and second-order reaction kinetics for the degradation of MB using various complexes of HBG, HBV and HBL ligands was studied and on comparing the regression coefficient values, the results shows that the degradation kinetics of the MB followed the zero-order kinetics well and is shown in fig. 1.12.

Conclusion

The catalytic activity of the newly synthesized complexes towards the degradation of methyl orange was also studied using H_2O_2 as an oxidant. The reactivity order is CoBG >CoBV >CoBL >CuBG >CuBL >CuBV >NiBV >NiBL >NiBG. Among these complexes, a

Cobalt complex shows the maximum degradation of the dye and among them Cobalt complex of the HBG is the highest with an efficiency of 91%. Optimum values were found to be the reaction time (1 hour), amount of catalyst (0.005g), amount of oxidant (1ml). Any further increase in the optimum values results in the lower yield of methyl orange dye. Among the nine catalysts Co-gly was found to be the efficient candidate for the degradation process.

The catalytic activity order of the newly synthesized complexes towards the degradation of methylene blue with the use of oxidizing agent H_2O_2 is CoBV >CoBG >CoBL >CuBG >CuBV >CuBL >NiBG >NiBV >NiBL. Among these complexes, Cobalt complexes exhibits high percentage conversion efficiency and among them Cobalt complex of the HBV is the highest with an efficiency of 97%. Hence these catalysts are found to be an efficient catalyst for the decomposition of methylene blue. Detailed study of the catalytic activity of the complexes was carried out by varying the parameters like catalyst amount, reaction time and amount of oxidant. At optimum conditions Co-Val complex gives high efficiency towards the degradation of the methylene blue dye. These complexes are environment friendly thereby reducing the environmental pollution.

References :

1. Ishii, Y., Yamawaki, K., Ura, T., Yamada, H., Yoshida, T., & Ogawa, M., (1988). *J. Org. Chem*. 53, 3587.

2. Limberg, C. (2007). Organometallic Oxidation Catalysis, *Springer*, New York, 79.

3. Deka, P., Hazarika, A., Deka, R. C., & Bharali, P., (2016). *RSC Adv*., 6 , 95292.

4. Pui, A., Policar C., & Mahy, J.P. (2007). *Inorganica Chim. Acta*, 360, 2139.

5. Carvalho, S.S., Rodrigues, A. C. C., Lima, J. F., & Carvalho, N. M. (2020). *Inorganica Chim. Acta*, 512, 119924.

6. Rabbani, M., Bathaee, H., Rahimi, R., & Maleki, A. (2016). *Desalin. Water Treat.*, 57, 25848.

7. Krishna, P. M., Reddy, N. B., Kottam, N., Yallur, B. C., & Katreddi, H. R. (2013). *Sci. World J*.,2013.

8. Nassar, M. Y., Aly, H. M., Abdelrahman E. A., & Moustafa, M. E. (2017). *J. Mol. Struct.*, 1143, 462.

9. Mirdya, S., Basak, T., & Chattopadhyay, S., (2019). *Polyhedron*, 170, 253.

10. Sangeetha, S., Krishnamurthya. G., & Raghavan, M. S. (2019). *Mater. Sci. Semicond.Process.*, 101, 164.

11. Xu, A., Li, X., Ye, S., Yin, G., & Zeng, Q. (2011). *Appl. Catal. B: Environ.*, 102, 37.

12. Mardani, H. R., Esmaeili, A., & Malekzadeh, A. (2018). *Res Chem Intermed*, 44, 6183.

13. Shen, Z., Zhou, H., Chen, H., Xu, H., Feng, C., & Zhou, X. (2018). *Nanomaterials*, 8, 317.

14. Manimohan, M., Pugalmani, S., Ravichandran, K., & Sithique, M. A. (2020). *RSC Adv*., 10, 18259.

15. Trandafilovic, L. V., Jovanovic, D. J., Zhang, X., Ptasinska, S., & Dramicanin, M. D. (2017). *Appl. Catal. B: Environ.*, 203, 740.

16. Ali, N., Zada, A., Zahid, M., Ismail, A., Rafiq, M., Riaz, A., & Khan, A. (2019). *J Chin Chem Soc*., 66, 402.

17. Djebli, A., Boudjemaa, A., Bendjeffal, H., Mamine, H., Metidji, T., Bekakria, H., & Bouhedja, Y. (2020). *Inorg. Nano-Met Chem*.., 50, 1115.

18. Liu, L., Wu, D., Zhao, B., Han, X., Wu, J., Hou, H., & Fan, Y. (2015). *Dalton Trans*.**,** 44**,** 1406.

19. Saha, U., Si, T. K., Nandi, P. K., & Mukherjea, K.K. (2013). *Inorg. Chem. Commun*., 38, 43.

20. Suramwar, N. V., Thakare, S. R., & Khaty, N. T. (2013). *Syn. React. Inorg. Metaorg. Nanometal Chem*., 43, 57.

PART VII

MOLECULAR MODELING STUDIES OF THE DIPHENYL GLYCOLIC ACID -AMINO ACID COMPLEXES

CHAPTER I

INTRODUCTION

The emergence of quantum chemistry leads a new stepping stone to the development in the field of the coordination complexes. The study of the energies and structure of the coordination complexes was made effortless with the upcoming of the mathematical methods accomplished by computer programme. The quantum mechanical treatment is emerged from the great Schrodinger equation. The expenditure met by the high cost of chemicals and the hazards can be reduced to great extent by the new frame to study chemical phenomena by studying the reactions and compounds by running calculations on computer.

In 1998, John Pople and Walter Kohn won the Noble Prize in Chemistry for the convergence of traditional quantum chemical methodology and DFT. DFT describes the interacting system of fermions through its density not through its many body wave function[1]. DFT comes out as a commercial method for the computation of molecular structure, vibration frequencies and energies of chemical reactions. The great accuracy of the DFT in replicating the experimental values in terms of geometry, dipole moment, vibrational frequencies, thermodynamic properties etc is very appreciable. The molecular structures and vibrational frequencies predicted by DFT are much trustworthy than any other computational methods[2].

CHAPTER 2

DFT METHOD

2.1. Geometry optimization

Geometry optimization is the method to attain the configuration of minimum energy of a molecule. A molecular structure with minimum energy will not have any imaginary frequencies. Single crystal X-ray diffraction data of the molecule can act as a starting point for geometry optimization, whenever possible. Hohenberg and Kohn[3, 4] proposed the optimization of gas phase structures of the compounds with the help of DFT method.

2. 2. GAUSSVIEW -GUI-for GAUSSIAN 09 program

Gaussview is a cost effective, full-featured graphical user interface for GAUSSIAN 09 program[5] which helps in preparation of input for the submission to Gaussian and to examine graphically the output that Gaussian produces[6]. The results of a variety of Gaussian calculations such as molecular orbitals, atomic charges, surfaces from the electron density, electrostatic potential, NMR shielding density and other properties can be graphically displayed with the aid of Gauss view. Surfaces can be demonstrated by different ways such as in solid, translucent and wire mesh modes and these surfaces can be colored by a separate property .Gaussview can be used to generate the animation of the normal modes of vibrational frequencies, animations of the steps in geometry optimizations,

potential energy surface scans, intrinsic reaction coordinate(IRC) paths.

2.3. HOMO-LUMO

The reactivity and stability of the compounds can be elucidated with the help of most reactive position in conjugated systems, molecular orbitals and their properties like energy are utilized[7]. The positive and negative values for the wave function can be symbolized using the red and green colors in the picture. The biological activity of the molecule can be recognized by the charge exchange inside the molecule which can be computed from the HOMO-LUMO energy gap[8]. The HOMO-LUMO energy can be used an identification factor of stability index[9]. The small HOMO-LUMO energy gap is an indication of high chemical reactivity and low kinetic stability and such molecules having less energy gap are named as delicate ones[10].

2.4. Global descriptors

From the DFT method the global descriptive parameters can be calculated with the help of HOMO-LUMO energy gap of the molecule. According to Koopman's theorem HOMO-LUMO energies are associated with the gas phase vertical electron affinities (A) and vertical ionization energies (I) through the equations $A= -E_{LUMO}$, $I= -E_{HOMO}$[11]. Electron affinity is the potential of a ligand to accept an electron from a donor. Byusing HOMO and

LUMO energy values, global descriptors such as chemical hardness (η), chemical softness (ζ), chemical potential (μ) and Global electronegativity index (ω) were calculated[12]. The formulas for the calculation of global descriptive parameters are described below.

Electronegativity(χ) = $(I+A) \div 2$ (1)

Chemical potential (μ) = $-\chi$ (2)

Chemical hardness (η) = $(I-A) \div 2$ (3)

Chemical softness (S) = $1 \div (2\eta)$ (4)

Electrophilicity index (ω) = $\mu^2 \div (2\eta)$ (5)

where I and A represent ionization potential and electron affinity respectively.

Ionization potential= $-E_{Homo}$ (6)

Electron affinity = $-E_{Lumo}$ (7)

Chemical potential (μ) can be depicted as the escaping tendency of electrons from an equilibrium system[13]. Electrophilicity index measures the capacity of a species to accept electrons[11, 14]. It is a measure of stabilization in energy after a system accepts additional amount of electronic charge from the environment[15, 16].

2.5. Molecular electrostatic potential (MEP/ESP)

MEP is the indicator of the net electric charge distribution of an atom or molecule. The total charge distribution of the atom or molecule at a point in the space around the molecule is the MEP.MEP is used to identify the electrophilic and nucleophilic sites in a molecule which helps to determine the chemical reactivity of the compound[17]. Different colors are used to denote discrete values of the electrostatic potential at the surface, i.e, red depicts the most negative electrostatic potential and blue denotes the most positive electrostatic potential and green stands for the zero potential regions. The order of increasing potential is red < orange < yellow < green < blue.

2.6. Natural Bond Orbital Analysis (NBO)

NBO provides a reflective approach towards the intra- and intermolecular orbital interactions in molecules between filled donor and empty acceptor NBOs, which also gives information regarding the charge-transfer or conjugative interactions in molecular systems[18, 19]. An idea about the origin of stabilization of a molecule can be provided by the method by analyzing the interactions between occupied Lewis NBO (bond pair or lone pair) as donor and an unoccupied non-Lewis NBO (anti-bonding or Rydberg) as acceptor[20]. NBO analysis makes us to recognize which orbital interactions are primarily involved in the stability of the observed conformer. Second order perturbation energies ($E^{(2)}$) are

used to treat the delocalizing interactions of filled NBOs, since the occupied NBOs are highly condensed.

$$(E^{(2)}) = -q_i F_{ij} \, / _{Ei-Ej}$$

Where q_i is the population of donor orbital or donor orbital occupancy; $_{Ei,\ Ej}$ are orbital energies of donor and acceptor NBOs, respectively, and F_{ij} is the off-diagonal Fock or Kohn-Sham matrix element between i and j NBOs[21].

CHAPTER 3

RESULT AND DISCUSSION

The computational calculations of the synthesized molecules were done using GAUSSIAN 09 software package and GAUSS-VIEW 5.0.9 visualization program[22]. The optimization of the prepared compounds was done by using Density functional theory with Beck's three parameter[23] for the exchange interaction and Lee-Yang-Parr[24] to consider correlation functional (B3LYP) with the 6-31+G (d, p) basis sets. The starting geometries of molecules were drawn with the aid of Gauss view program. The detailed description about the compounds such as HOMO-LUMO energy gap, global reactivity descriptors, the molecular electrostatic potential map and natural bond analysis (NBO) were obtained from the DFT method.

The following novel ligands synthesized by us were selected for computational studies:

1. Diphenyl glycolic acid–Tyrosine ligand (HBT)

2. Diphenyl glycolic acid–Glycine ligand (HBG))

3. Diphenyl glycolic acid–Histidine ligand (HBH)

4. Diphenyl glycolic acid–Valine ligand (HBV)

5. Diphenyl glycolic acid–Leucine ligand (HBL)

3.1 Computational details of Diphenyl glycolic acid–tyrosine ligand

The Gaussian 09 program package[2, 31] was utilized to computationally investigate the synthesized Diphenyl glycolic acid -tyrosine ligand. All calculations were carried out using density functional theory (DFT) with the B3LYP functional, which incorporates Becke's three parameters and the Lee-Yang-Parr functional, in conjunction with a pople type 6-311+G (d,p) basis set. In this research, we examined various aspects of the ligand in the gas phase, including its geometrical parameters, global descriptive parameters, electrostatic potential map (ESP), and NBO parameters. Moreover, a frontier molecular orbital (FMO) analysis was conducted to determine key quantum chemical parameters such as the highest occupied molecular orbital (HOMO), lowest unoccupied molecular orbital (LUMO), and the HOMO-LUMO gap (E_g).

3.1.1 Geometrical optimization of Diphenyl glycolic acid–tyrosine ligand

The geometrical optimization of the Diphenyl glycolic acid -tyrosine ligand was conducted in the gas phase using the DFT/B3LYP/6-311+G (d,p) basis set. During the optimization process, no symmetry constraints were imposed, allowing the structure to attain its lowest energy state and highest stability[25-27]. Fig. 1.1 illustrates the geometrically optimized structure of the

Diphenyl Glycolic acid-tyrosine ligand, while Tables 1.1, 1.2, and 1.3 present the associated geometric parameters, such as bond lengths, bond angles, and dihedral angles, respectively.

The optimized structure of the Diphenyl glycolic acid-tyrosine ligand exhibits three six-membered rings. The C-C bond lengths within these rings range from 1.39 to 1.40 Å, indicating that the ligand contains three aromatic rings, as these bond lengths are consistent with the typical C-C bond lengths observed in aromatic rings. The ligand includes two carboxylic acid functional groups, each with C-O double and single bonds measuring 1.20 Å, 1.21 Å, 1.35 Å, and 1.35 Å, as well as O-H bond lengths of 0.97 Å. The two aromatic rings in the ligand are connected through the C1 atom, which exhibits bond lengths of 1.55 Å for each connection. Furthermore, the C1 atom is attached to the N31 atom of the tyrosine moiety via a bond length of 1.47 Å, and it is also linked to the carboxylic acid group through a C1-C24 bond of 1.55 Å.

The key dihedral angles that determine the orientation of the ligand are ϕ(C13-C1-C2-C3), ϕ(C13-C1-C2-C3), ϕ(C1-N31-C33-C32), ϕ(C1-N31-C33-C37), ϕ(C2-C1-C24-O25), and ϕ(C2-C1-C24-O25), with corresponding values of 139.720, -44.280, 93.770, -146.000, -71.940, and 106.630, respectively. These dihedral angles indicate that the Diphenyl glycolic acid-tyrosine ligand does not possess a planar structure.

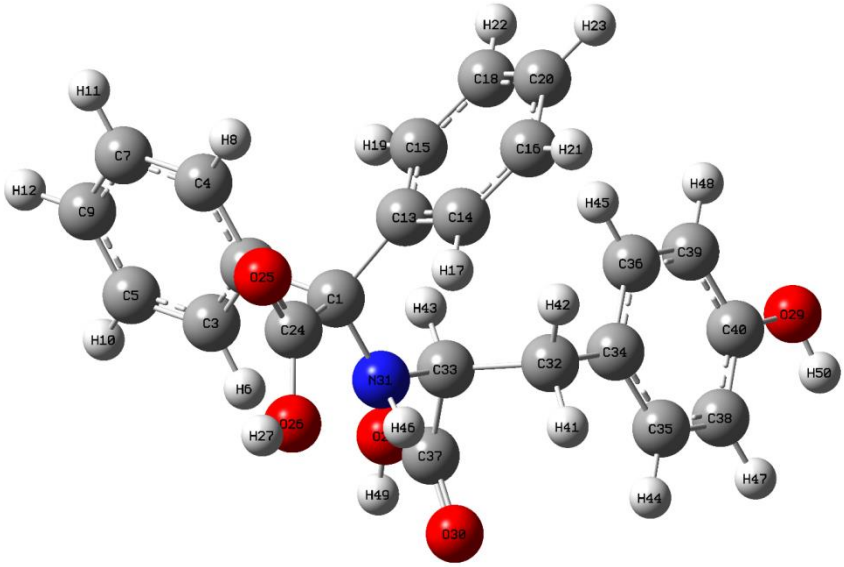

Fig.1.1. Optimized geometry of the Diphenyl glycolic acid-tyrosine ligand

Table 1.1 Optimized bond lengths of Diphenyl glycolic acid-tyrosine ligand

Bond	Bond angle	Bond	Bond angle
C1-C2	1.5545	C24-O25	1.2027
C1-C13	1.5472	C24-O26	1.3528
C1-C24	1.5518	O26-H27	0.9696
C1-N31	1.4707	O28-C37	1.3518
C2-C3	1.3954	O28-H49	0.9703
C2-C4	1.4018	O29-C40	1.3708
C3-C5	1.3958	O29-H50	0.9628
C3-H6	1.0802	O30-C37	1.2064
C4-C7	1.3911	N31-C33	1.4640
C4-H8	1.0824	N31-H46	1.0104
C5-C9	1.3911	C32-C33	1.5517
C5-H10	1.0844	C32-C34	1.5141
C7-C9	1.3952	C32-H41	1.0940

C7-H11	1.0843	C32-H42	1.0905
C9-H12	1.0843	C33-C37	1.5319
C13-C14	1.4003	C33-H43	1.0897
C13-C15	1.3983	C34-C35	1.3976
C14-C16	1.3918	C34-C36	1.4017
C14-H17	1.0842	C35-C38	1.3942
C15-C18	1.3952	C35-H44	1.0845
C15-H19	1.0831	C36-C39	1.3897
C16-C20	1.3943	C36-H45	1.0853
C16-H21	1.0842	C38-C40	1.3941
C18-C20	1.3920	C38-H47	1.0864
C18-H22	1.0845	C39-C40	1.3953
C20-H23	1.0840	C39-H48	1.0835

Table 1.2. Optimized bond angles of Diphenyl glycolic acid-tyrosine ligand

Bond angle	Angle(degree)	Bond angle	Angle(degree)
C2-C1-C13	112.2904	C1-C24-O25	124.1185
C2-C1-C24	103.1527	C1-C24-O26	113.5921
C2-C1-N31	111.2053	O25-C24-O26	122.2734
C13-C1-C24	108.5883	C24-O26-H27	106.7281
C13-C1-N31	112.4614	C37-O28-H49	107.2124
C24-C1-N31	108.6355	C40-O29-H50	109.6706
C1-C2-C3	120.9681	C1-N31-C33	121.7148
C1-C2-C4	120.1918	C1-N31-H46	112.8497
C3-C2-C4	118.7220	C33-N31-H46	112.0539
C2-C3-C5	120.5938	C33-C32-C34	113.8533
C2-C3-H6	119.3675	C33-C32-H41	107.5238
C5-C3-H6	120.0375	C33-C32-H42	107.9176
C2-C4-C7	120.6260	C34-C32-H41	109.8512
C2-C4-H8	119.8353	C34-C32-H42	109.9849

C7-C4-H8	119.5336	H41-C32-H42	107.4842
C3-C5-C9	120.3523	N31-C33-C32	114.9876
C3-C5-H10	119.4709	N31-C33-C37	105.4881
C9-C5-H10	120.1762	N31-C33-H43	108.8708
C4-C7-C9	120.2917	C32-C33-C37	109.0824
C4-C7-H11	119.5598	C32-C33-H43	110.0894
C9-C7-H11	120.1481	C37-C33-H43	108.0322
C5-C9-C7	119.3952	C32-C34-C35	121.4638
C5-C9-H12	120.3541	C32-C34-C36	120.7918
C7-C9-H12	120.2496	C35-C34-C36	117.7431
C1-C13-C14	120.6473	C34-C35-C38	121.3119
C1-C13-C15	120.9612	C34-C35-H44	119.5331
C14-C13-C15	118.1481	C38-C35-H44	119.1549
C13-C14-C16	121.0774	C34-C36-C39	121.6248
C13-C14-H17	120.2708	C34-C36-H45	119.3799
C16-C14-H17	118.6511	C39-C36-H45	118.9905
C13-C15-C18	120.9292	O28-C37-O30	122.6857
C13-C15-H19	119.9272	O28-C37-C33	112.8529
C18-C15-H19	119.1401	O30-C37-C33	124.4494
C14-C16-C20	120.2289	C35-C38-C40	119.8947
C14-C16-H21	119.6168	C35-C38-H47	119.9866
C20-C16-H21	120.1538	C40-C38-H47	120.1183
C15-C18-C20	120.3160	C36-C39-C40	119.6682
C15-C18-H22	119.5360	C36-C39-H48	121.2695
C20-C18-H22	120.1462	C40-C39-H48	119.0607
C16-C20-C18	119.2997	O29-C40-C38	122.7720
C16-C20-H23	120.3102	O29-C40-C39	117.4707
C18-C20-H23	120.3896	C38-C40-C39	119.7568

Table 1.3. Optimized dihedral angles of Diphenyl glycolic acid-tyrosine ligand

Dihedral	Dihedral angle (degree)	Dihedral	Dihedral angle (degree)
C13-C1-C2-C3	139.7172	C14-C16-C20-H23	179.8642
C13-C1-C2-C4	-44.2837	H21-C16-C20-C18	-179.6370
C24-C1-C2-C3	-103.5660	H21-C16-C20-H23	0.1133
C24-C1-C2-C4	72.4333	C15-C18-C20-C16	0.1338
N31-C1-C2-C3	12.7073	C15-C18-C20-H23	-179.6170
N31-C1-C2-C4	-171.2940	H22-C18-C20-C16	179.6550
C2-C1-C13-C14	150.6082	H22-C18-C20-H23	-0.0954
C2-C1-C13-C15	-35.1638	C1-C24-O26-H27	-177.3920
C24-C1-C13-C14	37.1972	O25-C24-O26-H27	1.2131
C24-C1-C13-C15	-148.5750	H49-O28-C37-O30	-0.3892
N31-C1-C13-C14	-83.0578	H49-O28-C37-C33	-179.1800
N31-C1-C13-C15	91.1702	H50-O29-C40-C38	-0.2914
C2-C1-C24-O25	-71.9439	H50-O29-C40-C39	179.4676
C2-C1-C24-O26	106.6308	C1-N31-C33-C32	93.7690
C13-C1-C24-O25	47.3668	C1-N31-C33-C37	-146.004
C13-C1-C24-O26	-134.0580	C1-N31-C33-H43	-30.2715
N31-C1-C24-O25	169.9691	H46-N31-C33-C32	-44.2073
N31-C1-C24-O26	-11.4561	H46-N31-C33-C37	76.0193
C2-C1-N31-C33	81.7927	H46-N31-C33-H43	-168.2480
C2-C1-N31-H46	-140.5290	C32-C33-C37-N31	-179.7590
C13-C1-N31-C33	-45.1236	C34-C32-C33-C37	62.0138
C13-C1-N31-H46	92.5547	C34-C32-C33-H43	-56.3646
C24-C1-N31-C33	-165.3510	H41-C32-C33-N31	58.3044
C24-C1-N31-H46	-27.6729	H41-C32-C33-C37	-59.9226
C1-C2-C3-C5	177.6832	H41-C32-C33-H43	-178.3010
C1-C2-C3-H6	-1.9178	H42-C32-C33-N31	-57.3674
C4-C2-C3-C5	1.6264	H42-C32-C33-C37	-175.5950
C4-C2-C3-H6	-177.9750	H42-C32-C33-H43	66.0272
C1-C2-C4-C7	-177.3790	C33-C32-C34-C35	-96.9516
C1-C2-C4-H8	1.7926	C33-C32-C34-C36	82.6101

C3-C2-C4-C7	-1.2911	H41-C32-C34-C35	23.6894
C3-C2-C4-H8	177.8808	H41-C32-C34-C36	-156.7490
C2-C3-C5-C9	-0.8570	H42-C32-C34-C35	141.8008
C2-C3-C5-H10	179.4238	H42-C32-C34-C36	-38.6375
H6-C3-C5-C9	178.7413	N31-C33-C37-O28	107.5049
H6-C3-C5-H10	-0.9779	N31-C33-C37-O30	-71.2607
C2-C4-C7-C9	0.1799	C32-C33-C37-O28	-128.4610
C2-C4-C7-H11	179.9624	C32-C33-C37-O30	52.7735
H8-C4-C7-C9	-178.995	H43-C33-C37-O28	-8.8012
H8-C4-C7-H11	0.7880	H43-C33-C37-O30	172.4332
C3-C5-C9-C7	-0.2785	C32-C34-C35-C38	179.4154
C3-C5-C9-H12	-179.8820	C32-C34-C35-H44	-0.4979
H10-C5-C9-C7	179.4386	C36-C34-C35-C38	-0.1591
H10-C5-C9-H12	-0.1646	C36-C34-C35-H44	179.9276
C4-C7-C9-C5	0.6131	C32-C34-C36-C39	-179.3540
C4-C7-C9-H12	-179.7830	C32-C34-C36-H45	1.4442
H11-C7-C9-C5	-179.1680	C35-C34-C36-C39	0.2235
H11-C7-C9-H12	0.4356	C35-C34-C36-H45	-178.9780
C1-C13-C14-C16	174.5050	C34-C35-C38-C40	-0.0256
C1-C13-C14-H17	-5.8043	C34-C35-C38-H47	179.7450
C15-C13-C14-C16	0.1180	H44-C35-C38-C40	179.8880
C15-C13-C14-H17	179.8087	H44-C35-C38-H47	-0.3414
C1-C13-C15-C18	-174.237	C34-C36-C39-C40	-0.1014
C1-C13-C15-H19	6.4536	C34-C36-C39-H48	-179.6410
C14-C13-C15-C18	0.1317	H45-C36-C39-C40	179.1032
C14-C13-C15-H19	-179.1780	H45-C36-C39-H48	-0.4362
C13-C14-C16-C20	-0.2422	C35-C38-C40-O29	179.9065
C13-C14-C16-H21	179.5100	C35-C38-C40-C39	0.1528
H17-C14-C16-C20	-179.9380	C40-C38-C40-O29	0.1363
H17-C14-C16-H21	-0.1856	H47-C38-C40-C39	-179.6180
C13-C15-C18-C20	-0.2593	C36-C39-C40-O29	-179.857
C13-C15-C18-H22	-179.7830	C36-C39-C40-C38	-0.0903
H19-C15-C18-C20	179.0556	H48-C39-C40-O29	-0.3073
H19-C15-C18-H22	-0.4685	H48-C39-C40-C38	179.4593
C14-C16-C20-C18	0.1137		

3.1.2 Frontier molecular orbital (FMO) analysis

The study includes an analysis of the frontier molecular orbitals (FMO), namely the highest occupied molecular orbital (HOMO) and the lowest unoccupied molecular orbital (LUMO), using the optimized structure of the Diphenyl glycolic acid-tyrosine ligand. FMO analysis is a valuable method for investigating the chemical reactivity of compounds[28], as it provides insights into their electron donation and acceptance capabilities. The HOMO orbital, characterized by higher energy, signifies a propensity for electron donation, whereas the LUMO orbital, with greater energy, indicates a tendency to receive electrons. The disparity between HOMO and LUMO is quantified by the band gap (E_g).

To visualize the FMOs and illustrate the HOMO, LUMO, and band gap of the Diphenyl glycolic -tyrosine ligand, Fig. 1.2 is provided. The figure employs red and blue shading to represent the positive and negative lobes of the orbitals, respectively. The corresponding orbital energies are presented in Table 1.4. The calculated band gap of the ligand is determined to be 5.0131 eV. This relatively large band gap suggests that the ligand possesses reactivity.

In the FMO diagram, the HOMO is primarily localized over one of the aromatic rings and the tyrosine moiety, while the LUMO is concentrated on the two aromatic rings in the Diphenyl glycolic acid portion. The regions corresponding to the HOMO serve as

electron-donating sites, whereas those associated with the LUMO act as electron-accepting sites.

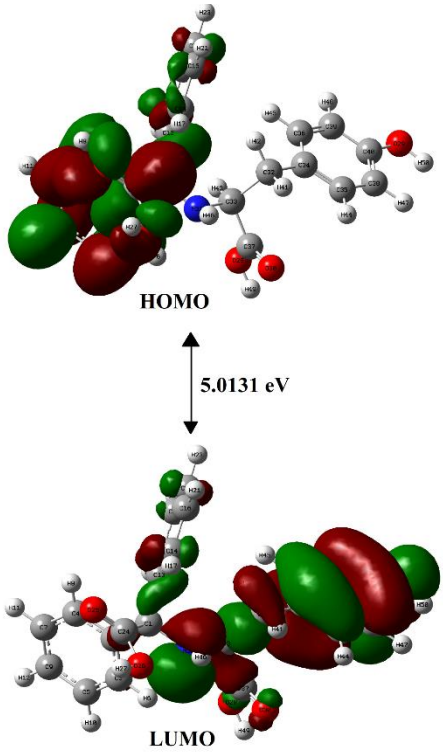

Fig.1.2. Frontier molecular orbitals of Diphenyl glycolic acid-tyrosine ligand

Table 1.4.HOMO, LUMO energies, and calculated band gap of Diphenyl glycolic acid-tyrosine ligand

E_{HOMO} (eV)	E_{LUMO}(eV)	Band gap(eV)
-6.1062	-1.0931	5.0131

3.1.3 Global reactivity parameters

The global reactivity descriptors of the Diphenyl glycolic acid-tyrosine ligand are derived using **Eqs. (1–7)**.The global descriptive parameters provide valuable information for comparing the behaviours and reactions of different molecules. Some of these parameters include Electronegativity (χ), Chemical Potential (ϰ), Chemical Hardness (ɳ), Chemical Softness (S), and Electrophilicity Index (ω) [29]. Electronegativity describes a molecule's ability to attract electrons, while chemical potential describes the tendency of electrons to flow from areas of higher potential to areas of lower chemical potential. Softness measures a molecule's inclination to receive electrons, whereas hardness indicates its tendency to donate electrons[30].

In Table 1.5, we present the calculated global descriptive parameters for the Diphenyl glycolic acid-tyrosine ligand. The ligand's calculated Ionization Potential (IP) value is 6.1062 eV, suggesting that it may be challenging to remove electrons from the ligand. On the other hand, the ligand's Electron Affinity (EA) value is 1.0931 eV, indicating its ability to accept electrons. The ligand's computed electrophilicity index is 2.5847 eV, suggesting a relatively low electron transfer from donor to acceptor[31, 32]. Furthermore, the predicted chemical hardness is significantly higher (2.5066 eV) compared to the calculated chemical softness (0.1830), implying that the molecule is relatively hard and stable.

This indicates that hard molecules require substantial energy for excitation and are less susceptible to polarization.

Table 1.5. Calculated global descriptive parameters of Diphenyl glycolic acid-tyrosine ligand

Descriptors	Values(eV)
Ionization potential (IP)	6.1062
Electron affinity (EA)	1.0931
Chemical hardness (η)	2.5066
Chemical softness (S)	0.1830
Electronegativity (χ)	3.5997
Electrophilicity index (ω)	2.5847
Chemical potential (ϰ)	-3.5997

3.1.4 Electrostatic potential maps (ESP)

The reactivity of chemical systems in electrophilic and nucleophilic reactions can be estimated by utilizing the three-dimensional electrostatic potential map (ESP) [33]. This map aids in visualizing the molecule's size, shape, and charge distribution, thereby predicting the reactivity of interactions within or between molecules. The ESP is based on the electrostatic potential energy, which evaluates the strength of surrounding charges, nuclei, and electrons at specific locations[34].

In **Fig. 1.3**, we present the calculated ESP diagram for the Diphenyl glycolic acid-tyrosine ligand. The diagram employs color to represent different electrostatic potentials, where blue indicates

positive sites and red indicates regions rich in electrons or more negative. The obtained ESP map of the Diphenyl glycolic acid-tyrosine ligand reveals that the electron density is concentrated at the positions of the two carboxylic groups. The red-colored regions in the COO groups can potentially act as acceptors for hydrogen bonding, indicating nucleophilic sites, while the blue-colored regions observed in the hydrogen atoms of the COOH group can act as electrophilic sites.

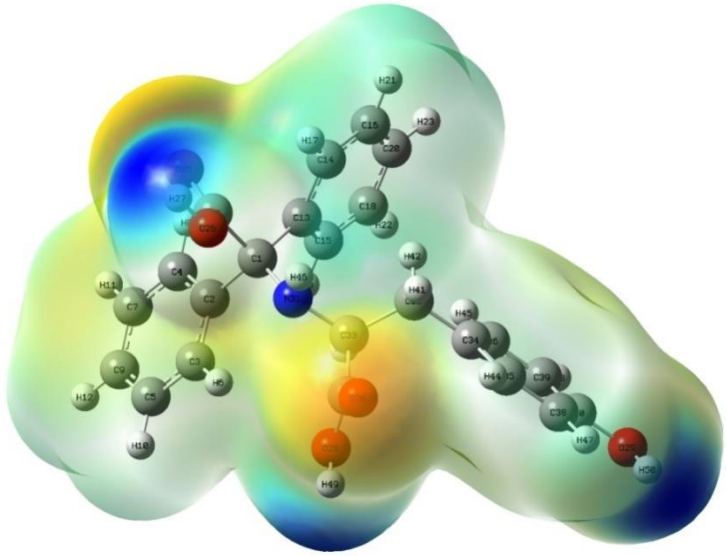

Fig.1.3. ESP diagram of Diphenyl glycolic acid -tyrosine ligand

3.1.5. NBO Analysis

The NBO (Natural Bond Orbital) analysis is a valuable technique used for visualizing electron orbitals and population analysis[35]. In conjunction with second-order perturbation energy, NBO analysis

provides insights into the interactions between Lewis-type orbitals (bonding or lone pairs) with non-Lewis-type orbitals (antibonding), which measure the extent of delocalization or hyperconjugation within and between molecules. The NBO output file includes concepts like bond orbital occupancies and natural atomic hybrids, which assist in predicting compound aromaticity and differentiating between kinetic and thermal stability[36].

Table 1.6.presents the occupancies and hybrids of various atoms or groups in the Diphenyl glycolic acid-tyrosine ligand. This information summarizes the effective valence electron configuration of each atom in the molecule. NBO analysis helps explain the presence of two aromatic rings in the ligand. The first ring consists of atoms C2, C3, C4, C5, C7, and C9, while the second ring comprises atoms C13, C14, C15, C16, C18, and C20. Atom C1 connects the aromatic rings through two σ bonds, C1-C2 and C1-C13. Additionally, C1 is connected to a carboxylic group and a tyrosine moiety through the C1 atom.

In NBO analysis, the electronic wave function is characterized by considering occupied and empty Lewis delocalized orbitals. Table 1.**7.**presents the crucial electronic wave functions of the donor and acceptor orbitals, along with the interaction energy (E(2)) between these two. The ligand's interaction energies are influenced by the lone pairs of atoms, including Oxygen, Nitrogen, Carbon, and Hydrogen. As the donor-acceptor interaction increases, the

interaction energy (E(2)) also increases. For the donors O26-H27 and O28-H49, and the acceptors C24-O25 and O30-C37, the interactions between the donor and acceptor result in interaction energies of 0.83kcal/mol and 0.87kcal/mol, respectively. These interaction energies are relatively weak, suggesting that the removal of protons H27 and H49 is easily achievable.

Table 1.6. Occupancy of NBOs and hybrids of Diphenyl glycolic acid -tyrosine ligand

NBOs	Hybrid	occupancy	AO%
σC1-C2	C $sp^{2.73}$	1.95195	s(26.82%)p(73.14%)d(0.04%)
	C $sp^{2.32}$		s(30.14%)p(69.82%)d(0.05%)
σC1-N31	C $sp^{3.34}$	1.97789	s(23.03%)p(76.86%)d(0.10%)
	N $sp^{2.00}$		s(33.34%)p(66.60%)d(0.05%)
σN31-C33	N $sp^{2.02}$	1.97837	s(33.08%)p(66.87%)d(0.05%)
	C $sp^{3.23}$		s(23.59%)p(76.30%)d(0.11%)
σN31-H46	N $sp^{3.06}$	1.98116	s(24.62%)p(75.31%)d(0.07%)
	H s		s(99.93%)p(0.07%)
σC33-H43	C $sp^{3.18}$	1.97108	s(23.91%)p(76.02%)d(0.07%)
	H s		s(99.96%)p(0.04%)
σC33-C37	C $sp^{3.21}$	1.96965	s(23.75%)p(76.18%)d(0.07%)
	C $sp^{1.59}$		s(38.64%)p(61.31%)d(0.06%)
σO30-C37	O $sp^{1.43}$	1.99542	s(41.09%)p(58.79%)d(0.12%)
	C $sp^{1.98}d^{0.01}$		s(33.45%)p(66.37%)d(0.17%)
ΠO30-C37	O $sp^{99.99}d^{0.29}$	1.99177	s(0.42%)p(99.45%)d(0.12%)
	C $sp^{99.99}d^{1.64}$		s(0.32%)p(99.15%)d (0.53%)
σO28-C37	O $sp^{1.94}$	1.99483	s(33.95%)p(65.96%)d(0.09%)
	C $sp^{2.62}d^{0.01}$		s(27.56%)p(72.21%)d(0.23%)
σO28-H49	O $sp^{3.74}$	1.98684	s(21.08%)p(78.83%)d(0.09%)

	H s		s(99.85%)p(0.15%)
σC32-C33	C $sp^{2.80}$	1.96576	s(26.28%)p(73.67%)d(0.05%)
	C $sp^{2.47}$		s(28.81%)p(71.16%)d(0.03%)
σC32-H42	C $sp^{3.41}$	1.9734	s(22.66%)p(77.27%)d(0.07%)
	H s		s(99.97%)p(0.03%)
σC32-H41	C $sp^{3.57}$	1.97605	s(21.89%)p(78.05%)d(0.06%)
	H s		s(99.97%)p(0.03%)
σC32-C34	C $sp^{2.43}$	1.97408	s(29.15%)p(70.81%)d(0.04%)
	C $sp^{2.15}$		s(31.77%)p(68.20%)d(0.03%)
σO29-C40	O $sp^{1.90}$	1.99454	s(34.40%)p(65.52%)d(0.08%)
	C $sp^{3.07}d^{0.01}$		s(24.53%)p(75.25%)d(0.22%)
σO29-H50	O $sp^{3.80}$	1.98752	s(20.82%)p(79.09%)d(0.09%)
	H s		s(99.88%)p(0.12%)
σC1-C13	C $sp^{2.53}$	1.96019	s(28.34%)p(71.62%)d(0.04%)
	C $sp^{2.28}$		s(30.50%)p(69.45%)d(0.05%)
σC1-C2	C $sp^{2.73}$	1.95195	s(26.82%)p(73.14%)d(0.04%)
	C $sp^{2.32}$		s(30.14%)p(69.82%)d(0.05%)
σC1-C24	C $sp^{3.59}$	1.95639	s(21.76%)p(78.17%)d(0.07%)
	C $sp^{1.59}$		s(38.57%)p(61.37%)d(0.06%)
σC24-O25	C $sp^{1.95}$	1.99477	s(33.86%)p(65.98%)d(0.17%)
	O $sp^{1.39}$		s(41.75%)p(58.14%)d(0.12%)
ΠC24-O25	C $sp^{99.99}d^{2.06}$	1.99168	s(0.25%)p(99.25%)d(0.51%)
	O $sp^{99.99}d^{0.46}$		s(0.28%)p(99.60%)d(0.13%)
σC24-O26	C $sp^{2.65}d^{0.01}$	1.99466	s(27.36%)p(72.41%)d(0.23%)
	O $sp^{1.93}$		s(34.11%)p(65.81%)d(0.09%)
σO26-H27	O $sp^{3.69}$	1.98419	s(21.31%)p(78.60%)d(0.09%)
	H s		s(99.86%)p(0.14%)

Table 1.7. Donor-Acceptor interactions of Diphenyl glycolic acid-tyrosine ligand in terms of E (2)

Donor NBO(i)	Acceptor NBO(j)	E(2) (kcal/mol)	Ej-Ei (a.u)	F(I,j) (a.u)
σC1-C2	σ*C1-C13	1.14	0.99	0.03
σC1-C2	σ*C1-C24	0.67	0.93	0.022
σC1-C2	σ*C2-C3	1.76	1.19	0.041
σC1-C2	σ*C2-C4	1.55	1.18	0.038
σC1-C2	σ*C3-C5	2.12	1.2	0.045
σC1-C2	σ*C4-C7	2.15	1.2	0.046
σC1-C2	σ*C13-C14	2.63	1.18	0.05
σC1-C2	Π*C24-O25	3.67	0.61	0.044
σC1-C2	σ*C24-O26	0.78	0.94	0.024
σC1-C2	σ*N31-H46	1.64	1.04	0.037
σC1-C13	σ*C1-C2	1.27	1	0.032
σC1-C13	σ*C1-C24	0.6	0.95	0.022
σC1-C13	σ*C2-C3	1.96	1.21	0.044
σC1-C13	Π*C2-C3	0.67	0.66	0.02
σC1-C13	σ*C13-C14	1.79	1.19	0.041
σC1-C13	σ*C13-C15	1.78	1.19	0.041
σC1-C13	σ*C14-C16	2.2	1.2	0.046
σC1-C13	σ*C15-C18	2.31	1.2	0.047
σC1-C13	Π*C24-O25	1.16	0.62	0.025
σC1-C13	σ*C24-O26	1.79	0.95	0.037
σC1-C24	σ*C1-C2	0.9	1.01	0.027
σC1-C24	σ*C2-C3	0.95	1.22	0.031
σC1-C24	Π*C2-C3	2.95	0.68	0.043
σC1-C24	σ*C13-C15	2.98	1.21	0.054
σC1-C24	σ*C24-O25	0.9	1.24	0.03
σC1-C24	σ*O26-H27	2.19	1.02	0.042
σC1-C24	σ*N31-C33	2.96	0.99	0.049

σC1-N31	σ*C1-C2	0.7	1.11	0.025
σC1-N31	σ*C1-C13	0.89	1.11	0.028
σC1-N31	σ*C2-C4	1.84	1.31	0.044
σC1-N31	Π*C13-C15	1.59	0.76	0.034
σC1-N31	σ*C24-O25	1.76	1.34	0.043
σC1-N31	σ*N31-C33	0.5	1.09	0.021
σC24-O25	σ*C1-C24	1.51	1.43	0.042
σC24-O25	σ*C1-N31	0.67	1.46	0.028
ΠC24-O25	σ*C1-C2	0.75	0.78	0.022
ΠC24-O25	σ*C1-C13	0.5	0.79	0.018
ΠC24-O25	Π*C2-C3	0.55	0.45	0.015
ΠC24-O25	Π*C24-O25	0.89	0.41	0.018
σC24-O26	σ*C1-C13	0.69	1.34	0.027
σO26-H27	σ*C1-C24	4.34	1.09	0.062
σO26-H27	σ*C24-O25	0.83	1.37	0.03
σO28-C37	σ*C32-C33	0.53	1.31	0.024
σO28-H49	σ*O30-C37	0.87	1.36	0.031
σO28-H49	σ*C33-C37	3.69	1.12	0.058
σO29-C40	σ*C35-C38	1.12	1.49	0.037
σO29-C40	σ*C36-C39	1.29	1.5	0.039
σO29-C40	σ*C38-C40	0.81	1.48	0.031
σO29-C40	σ*C39-C40	0.61	1.48	0.027
σO29-H50	σ*C39-C40	4.21	1.31	0.067
σO30-C37	σ*C33-C37	1.37	1.45	0.041
ΠO30-C37	Π*O30-C37	0.73	0.42	0.016
ΠO30-C37	σ*N31-C33	1.39	0.75	0.029
σN31-C33	σ*C1-C24	1.09	1.05	0.031
σN31-C33	σ*C1-N31	0.64	1.07	0.024
σN31-C33	σ*O28-C37	0.67	1.07	0.024
σN31-C33	Π*O30-C37	2.12	0.75	0.037
σN31-C33	σ*C32-C34	1.21	1.16	0.033
σN31-H46	σ*C1-C2	2.03	0.99	0.04

σN31-H46	σ*C1-C24	0.97	0.94	0.027
σN31-H46	σ*C33-H43	2.02	1.03	0.041
σC32-C33	σ*C1-N31	0.81	0.94	0.025
σC32-C33	σ*O28-C37	1.84	0.94	0.038
σC32-C33	Π*O30-C37	1.5	0.61	0.028
σC32-C33	σ*C32-C34	1.03	1.03	0.029
σC32-C33	σ*C33-H43	0.53	1.01	0.021
σC32-C33	σ*C34-C35	0.77	1.19	0.027
σC32-C33	Π*C34-C35	2.16	0.64	0.036
σC32-C34	σ*N31-C33	2.4	0.97	0.043
σC32-C34	σ*C32-C33	0.76	0.98	0.024
σC32-C34	σ*C32-H41	0.54	1.02	0.021
σC32-C34	σ*C32-H42	0.68	1.04	0.024
σC32-C34	σ*C34-C35	2.11	1.2	0.045
σC32-C34	σ*C34-C36	2.02	1.2	0.044
σC32-C34	σ*C35-C38	2.43	1.2	0.048
σC32-C34	σ*C36-C39	2.35	1.21	0.048
σC32-H41	σ*C33-H43	2.94	0.9	0.046
σC32-H41	Π*C34-C35	0.52	0.53	0.016
σC32-H41	σ*C34-C36	3.96	1.07	0.058
σC32-H42	σ*C32-C34	0.51	0.92	0.019
σC32-H42	σ*C33-C37	2.63	0.85	0.043
σC32-H42	σ*C34-C35	3.31	1.08	0.053
σC32-H42	Π*C34-C35	1.61	0.53	0.029
σC33-C37	σ*C1-N31	3.15	0.98	0.05
σC33-C37	σ*O28-H49	2.31	1.01	0.043
σC33-C37	σ*O30-C37	1.13	1.24	0.034
σC33-C37	σ*C32-H42	1.66	1.06	0.038
σC33-H43	σ*O28-C37	0.66	0.85	0.022
σC33-H43	σ*O30-C37	4.31	1.12	0.062
σC33-H43	σ*N31-H46	3.15	0.94	0.049
σC33-H43	σ*C32-H41	2.21	0.91	0.04

Π*C24-O25	σ*C1-C2	0.86	0.37	0.045
Π*C24-O25	σ*C1-C13	0.61	0.38	0.038
Π*C24-O25	Π*C2-C3	4.83	0.04	0.023
Π*C24-O25	σ*C24-O25	0.61	0.6	0.051
σ*O28-C37	σ*O28-H49	1.69	0.04	0.029
σ*O28-C37	σ*N31-C33	2.58	0.01	0.021
σ*O28-C37	σ*C32-C33	3.16	0.02	0.029
σ*O28-C37	σ*C33-H43	2.7	0.07	0.05
Π*O30-C37	σ*O30-C37	0.89	0.59	0.061
Π*O30-C37	σ*N31-C33	1.37	0.34	0.057
Π*O30-C37	σ*C32-C33	0.67	0.35	0.039
Π*C34-C35	σ*C32-C33	1.82	0.32	0.048
Π*C34-C35	σ*C32-H42	0.54	0.38	0.03
Π*C38-C40	Π*C34-C35	197.83	0.02	0.08

3.2. Computational details of Diphenyl glycolic acid–glycine ligand

Computational study of synthesized Diphenyl glycolic acid - glycine ligand was performed using density functional theory. It is treated according to hybrid Becke's three parameters and the Lee-Yang-Parr functional (B3LYP) supplemented with pople type 6-311+G (d, p) basis set. All calculations in this study have been performed with the Gaussian-09 program package. Quantum chemical parameters such as the highest occupied molecular orbital (HOMO), lowest unoccupied molecular orbital (LUMO), and HOMO-LUMO gap (E) were calculated as part of the frontier molecular orbital analysis. Theoretical studies were also conducted on geometrical parameters, global descriptive parameters,

electrostatic potential map and NBO parameters. All the calculations were performed in the gas phase.

3.2.1 Geometrical optimization of Diphenyl glycolic acid-glycine ligand

Geometrical optimization of Diphenyl glycolic acid-glycine ligand was performed at DFT/B3LYP level of theory and 6-311+G (d, p) basis set. Optimizations have been carried out without any symmetry constraints in the ground state. The optimized structure had been given in the Fig.1.4 and is used for further analysis.

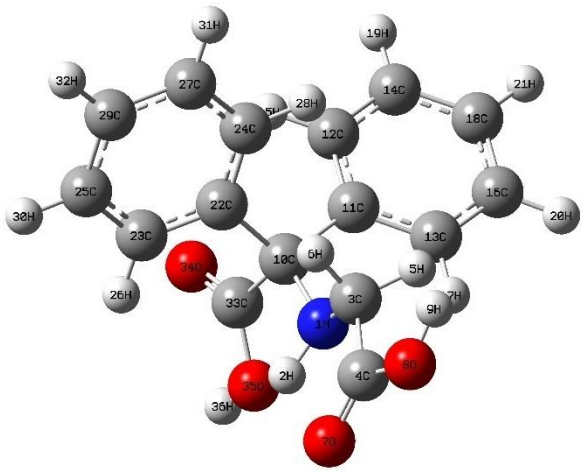

Fig. 1.4. Optimized structure of Diphenyl glycolic acid -glycine ligand

Geometrical parameters include bond length, bond angle and dihedral angles. The nature of bond can identify from these values.

Tables 1.8, 1.9 and 1.10 show the optimized bond lengths, bond angles, and dihedral angles for Diphenyl glycolic acid -glycine ligand.

Table 1.8. Optimized bond length of Diphenyl glycolic acid -glycine ligand

Bond	Bond length	Bond	Bond length
R (1,2)	1.0135	R(14,19)	1.0843
R (1,3)	1.4463	R(16,18)	1.392
R (1,10)	1.4705	R(16,20)	1.0844
R (3,4)	1.5225	R(18,21)	1.0843
R (3,5)	1.098	R(22,23)	1.4006
R (3,6)	1.1033	R(22,24)	1.3983
R (4,7)	1.1986	R(23,25	1.3914
R(4,8)	1.3575	R(23,26)	1.0846
R(8,9)	0.9655	R(24,27)	1.3958
R(10,11)	1.5503	R(24,28)	1.0831
R(10,22)	1.5465	R(25,29)	1.3945
R(10,33)	1.5507	R(25,30)	1.0841
R(11,12)	1.4007	R(27,29)	1.3915
R(11,13)	1.397	R(27,31)	1.0844
R(12,14)	1.3919	R(29,32)	1.084
R(12,15)	1.0825	R(33,34)	1.2031
R(13,16)	1.3952	R(33,35)	1.35
R(13,17)	1.0824	R(35,36)	0.9697
R(14,18)	1.3948		

Table 1.9. Optimized bond angles of Diphenyl glycolic acid - glycine ligand

Bond	Angle	Bond	Angle
A(2,1,3)	110.1991	A(18,14,19)	120.1124
A(2,1,10)	112.7712	A(13,16,18)	120.2641
A(3,1,10)	118.5142	A(13,16,20)	119.5820
A(1,3,4)	109.7847	A(18,16,20)	120.1507
A(1,3,5)	110.7644	A(14,18,16)	119.4360
A(1,3,6)	114.0113	A(14,18,21)	120.2390
A(4,3,5)	109.5194	A(16,18,21)	120.3211
A(4,3,6)	106.1596	A(10,22,23)	119.7878
A(5,3,6)	106.4098	A(10,22,24)	121.7176
A(3,4,7)	124.2735	A(23,22,24)	118.1236
A(3,4,8)	115.2666	A(22,23,25)	121.1026
A(7,4,8)	120.4200	A(22,23,26)	120.1497
A(4,8,9)	110.8023	A(25,23,26)	118.7465
A(1,10,11)	110.3571	A(22,24,27)	120.9259
A(1,10,22)	111.3639	A(22,24,28)	119.9036
A(1,10,33)	108.9978	A(27,24,28)	119.1677
A(11,10,22)	113.6246	A(23,25,29)	120.2088
A(11,10,33)	103.6040	A(23,25,30)	119.6201
A(22,10,33)	108.5141	A(29,25,30)	120.1707
A(10,11,12)	120.8387	A(24,27,29)	120.3067
A(10,11,13)	120.2591	A(24,27,31)	119.5364
A(12,11,13)	118.7597	A(29,27,31)	120.1568
A(11,12,14)	120.5480	A(25,29,27)	119.3254
A(11,12,15)	119.8281	A(25,29,32)	120.2989
A(14,12,15)	119.6173	A(27,29,32)	120.3757
A(11,13,16)	120.6235	A(10,33,34)	123.8997
A(11,13,17)	118.9321	A(10,33,35)	113.4240
A(16,13,17)	120.4270	A(34,33,35)	122.6619
A(12,14,18)	120.3402	A(33,35,36)	106.8266
A(12,14,19)	119.5464		

Table 1.10. Optimized dihedrals of Diphenyl glycolic acid -glycine ligand

Bond	Dihedral	Bond	Dihedral
D(2,1,3,4)	27.9769	D(12,11,13,16)	1.9037
D(2,1,3,5)	149.0508	D(12,11,13,17)	-176.581
D(2,1,3,6)	-90.9723	D(11,12,14,18)	0.2985
D(10,1,3,4)	159.9842	D(11,12,14,19)	179.9491
D(10,1,3,5)	-78.9420	D(15,12,14,18)	-178.768
D(10,1,3,6)	41.0349	D(15,12,14,19)	0.8828
D(2,1,10,11)	-149.567	D(11,13,16,18)	-0.8175
D(2,1,10,22)	83.2677	D(11,13,16,20)	179.8331
D(2,1,10,33)	-36.4208	D(17,13,16,18)	177.6448
D(3,1,10,11)	79.5730	D(17,13,16,20)	-1.7046
D(3,1,10,22)	-47.5925	D(12,14,18,16)	0.814
D(3,1,10,33)	-167.281	D(12,14,18,21)	-179.905
D(1,3,4,7)	-16.5630	D(19,14,18,16)	-178.835
D(1,3,4,8)	165.7328	D(19,14,18,21)	0.4463
D(5,3,4,7)	-138.384	D(13,16,18,14)	-0.5572
D(5,3,4,8)	43.9123	D(13,16,18,21)	-179.837
D(6,3,4,7)	107.1108	D(20,16,18,14)	178.7885
D(6,3,4,8)	-70.5933	D(20,16,18,21)	-0.4917
D(3,4,8,9)	-3.5805	D(10,22,23,25)	174.0916
D(7,4,8,9)	178.6195	D(10,22,23,26)	-6.3232
D(1,10,11,12)	-169.592	D(24,22,23,25)	0.9617
D(1,10,11,13)	14.8010	D(24,22,23,26)	-179.453
D(22,10,11,12)	-43.6900	D(10,22,24,27)	-173.804
D(22,10,11,13)	140.7028	D(10,22,24,28)	6.8012
D(33,10,11,12)	73.8547	D(23,22,24,27)	-0.8136
D(33,10,11,13)	-101.753	D(23,22,24,28)	179.7914
D(1,10,22,23)	-78.6636	D(22,23,25,29)	-0.4657
D(1,10,22,24)	94.2123	D(22,23,25,30)	179.3107

D(11,10,22,23)	155.9698	D(26,23,25,29)	179.9435
D(11,10,22,24)	-31.1542	D(26,23,25,30)	-0.2801
D(33,10,22,23)	41.3112	D(22,24,27,29)	0.1711
D(33,10,22,24)	-145.813	D(22,24,27,31)	-179.702
D(1,10,33,34)	170.4876	D(28,24,27,29)	179.5705
D(1,10,33,35)	-10.8628	D(28,24,27,31)	-0.3028
D(11,10,33,34)	-72.0061	D(23,25,29,27)	-0.2005
D(11,10,33,35)	106.6435	D(23,25,29,32)	179.791
D(22,10,33,34)	49.0483	D(30,25,29,27)	-179.976
D(22,10,33,35)	-132.302	D(30,25,29,32)	0.0158
D(10,11,12,14)	-177.317	D(24,27,29,25)	0.3458
D(10,11,12,15)	1.7471	D(24,27,29,32)	-179.646
D(13,11,12,14)	-1.6453	D(31,27,29,25)	-179.782
D(13,11,12,15)	177.419	D(31,27,29,32)	0.2269
D(10,11,13,16)	177.6014	D(10,33,35,36)	-177.851
D(10,11,13,17)	-0.8836	D(34,33,35,36)	0.8177

The carbon-carbon bond length of phenyl ring ranges between 1.4 and 1.39 Angstrom, which agrees with the average C-C bond length of an aromatic ring and confirm the presence of two aromatic rings in the ligand HBG. The C=O bond length ranges from 1.1986 to 1.2031, the C-O bond length ranges from 1.35 to 1.47, and the C-N bond length ranges from 1.44 to 1.47. The significant dihedral angles are -36.4208, -149.567, 83.2677, 79.573, -47.5925, -167.281, -16.563, and 165.7328. These values give an idea about orientation of the benzene rings and other groups in Diphenyl glycolic acid -glycine ligand.

3.2.2 Frontier Molecular orbital Analysis

Frontier molecular orbitals comprise the HOMO and LUMO. Where HOMO denotes electron donor activity and LUMO denotes electron accepting tendencies. Schematic diagram of HOMO, LUMO and their band gap are given in Fig.1.5 where positive and negative regions are represented by red and green color respectively.

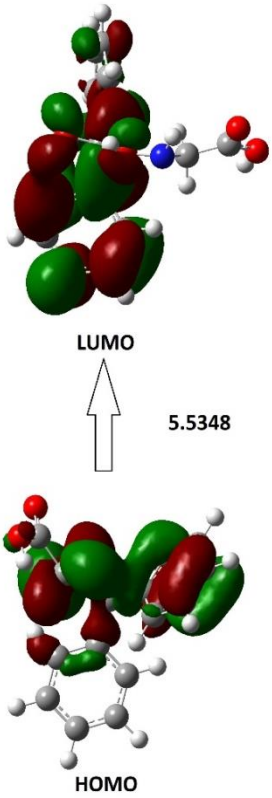

Fig.1.5.HOMO and LUMO of Diphenyl glycolic acid -glycine ligand

The frontier molecular orbitals of the optimized Diphenyl glycolic acid -glycine ligand are analyzed and the band gap is calculated given in Table 1.11.

Table 1.11 Energies of HOMO and LUMO and Band gap of Diphenyl glycolic acid -glycine ligand

E(HOMO)eV	E(LUMO) eV	Band gap(eV)
-6.7048	-1.1700	5.5348

HOMO and LUMO energies are important quantum chemical parameters for molecules and reactions that they are involved. The band gap (ΔE) is defined as the difference between HOMO and LUMO. The band gap of HBG is calculated to be 5.5348 eV. Since the band gap of the compound is appreciably high indicates the molecule is relatively stable.

3.2.3 Global Reactivity parameters

Global reactivity parameters such as Electronegativity(χ), Chemical hardness(η), Chemical potential(ϒ), Chemical softness(S), Electrophilicity index (ω) were calculated using the following equations listed(Eqn 1-7).The global descriptive parameters are helpful to compare the behaviour of different compounds and their reactivities. The electronegativity is the tendency of an object to attract electrons, whereas the chemical potential is the tendency of electrons to flow from a region of higher chemical potential to a region of lower chemical potential. Hardness shows the resistance

of the molecule to use electrons and its inverse gives softness. Hardness is identified as the charge density, which in turn is the ability to retain electronic charge once it has been acquired. The hardness is an important stability index as it is related to the HOMO-LUMO energy gap of the molecule. The large value for ionization potential (6.7048 eV) indicates that it is difficult to remove electrons from HBG. The electron affinity value (1.1700) is comparatively small, so that it can gain electrons. Chemical hardness value (2.7674ev) is much higher than chemical softness value (0.1806ev) confirms molecule is relatively hard and stable. Hard molecules are less polarizable since they need high energy for excitation. Global descriptive parameters of HBG are listed in table 1.12.

Table 1.12. Global descriptive parameters of Diphenyl glycolic acid -glycine ligand

Descriptors	Values(eV)
Ionisation potential	6.7048
Electron affinity	1.1700
Chemical hardness	2.7674
Chemical softness	0.1806
Electronegativity	3.9374
Electrophilicity	2.8010
Chemical potential	-3.9374

3.2.4 Molecular electrostatic potential maps (ESP)

Electrostatic potential maps are three-dimensional diagrams of molecules (**Fig.1.6**). These diagrams help to visualize the size, shape, and charge distribution of molecules. It is also used to predict reactivity and inter or intra-molecular interactions in the molecule. The key parameter of the ESP map is electrostatic potential energy; which measures the strength of nearby charges, nuclei, and electrons at a particular position. Different colours in this diagram indicate different electrostatic potentials. The red colour represents the electron-rich area or a more negative site, while the blue colour represents a positive site. Here electron density is concentrated in two carboxylic group positions thus they can act as ligand sites for metal ions. These ligands are capable of donating electrons to metal ions forming a metal-ligand complex.

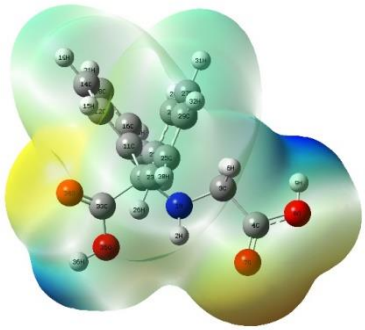

Fig.1.6.ESP diagram of Diphenyl glycolic acid -glycine ligand

3.2.5 NBO Analysis

Natural bond orbital analysis is a useful tool for generating a visual representation of electron orbitals and population analysis. This analysis is based on the approach of transforming multi-electron wave functions of molecules into a localized form that corresponds to single-center (Lone pair) and two-center (natural bond antibonding orbitals) elements. It also helps to understand intra-intermolecular bonding interactions, hyper-conjugation interactions, bond type determination, and intramolecular charge transfer in molecular systems. Moreover, the NBO analysis with their second-order perturbation energy gives information about interactions between Lewis type (bonding or lone pair) filled orbitals and non-Lewis type (antibonding) empty orbitals, which are a measure of the intra and inter -molecular delocalization or hyper conjugation.

Electron density delocalization between occupied Lewis type orbitals and initially unoccupied non-Lewis orbitals corresponds to a stabilizing donor-acceptor interaction. The stabilization energies of the parent depside were investigated using second-order perturbation theory to better understand intra and intermolecular interactions. The stabilization energy E (2) associated with electron delocalization between donor and acceptor is estimated for each donor, NBO (i), and acceptor, NBO (j) as.

$$E(2)= -q_i\frac{F_{ij}^2}{\Delta E}= -q_i\frac{<i|F|j>^2}{Ej-Ei}$$

Where qi is the donor orbital occupancy, Fij is the off-diagonal NBO fock matrix element and Ei and Ej are diagonal elements (orbital energies). The second order perturbation theory analysis of the fock matrix at B3LYP/6-311+G(d, p) level of theory are studied in the gas phase.

Bonding concepts such as bond orbital occupancies and natural atomic hybrids are obtained from the NBO output file. This data helps in predicting the relative aromaticity and the difference between kinetic and thermal stability of compounds. The occupancies and hybrids of various atoms/groups of HBG are given in Table.13, which summarizes the information regarding effective valence electron configuration of each atom in the molecule. The atom label and hybrid label showing the hybrid orbital(sp^x) composition i.e., the amount of s and p character.

From the table it is clear that HBG is composed of two aromatic rings. The 1st aromatic ring (A) is composed of carbon atoms such as C11, C12, C13, C14, C16, C18 and the other aromatic ring (B) is composed of carbon atoms C22, C23, C24, C25, C27, C29.There are 36 sigma bonds and 8 pi bonds in the whole aromatic system. The occupancies of all sigma bonds of the aromatic rings come in the range of 1.96-1.98Angstrom.The pi bonds have occupancy 1.66536, 1.66152, 1.66703, 1.66519, 1.66249, 1.66644 respectively

for C 11 - C 13, C 12 - C 14,C 16 - C 18, C 22 - C 24, C 23 - C 25, and C 27 - C 29. This is a clear indication of delocalization of pi electrons in the aromatic systems. The pi bond is characterized by p orbitals only, that in all the cases contribution from s orbital is less than 1%. There are two other pi bonds in the system which corresponds to C4 - O7 and C33 - O34 having occupancies 1.99118 and 1.99173 respectively, indicates that there is no delocalization and these two bonds are in isolated state.

Table 1.12. Occupancy of NBOs and hybrids of Diphenyl glycolic acid -glycine ligand

NBO	Hybrid	Occupancy	AO%
	N 1 sp 3.07		N 1 s (24.55%) p(75.38%) d (0.07%)
σN 1 - H 2	H 2 sp 0	1.97891	H 2 s (99.92%) p(0.08%)
	N 1 sp 2.25		N 1 s (30.77%) p(69.18%)
σN 1 - C 3	C 3 sp 2.83	1.98598	C 3 s (26.11%) p(73.78%) d (0.05%)
	C 3 sp 2.83		N 1 s (32.53%) p (67.41%) d (0.06%)
σN 1 - C 10	C 10sp 3.40	1.97866	C 10s (22.73%) p(77.17%) d (0.11%)
	C 3 sp 2.93		C 3 s (25.44%) p (74.50%) d (0.06%)
σC 3 - C 4	C 4 sp 1.62	1.98411	C 4 s (38.17%) p(61.79%) d (0.05%)
	C 3 sp 3.14		C 3 s (24.15%) p (75.78%) d (0.06%)
σC 3 - H 5	H 5 sp 0.00	1.97224	H 5 s (99.97%) p(0.03%)
	C 3 sp 3.09		C 3 s (24.43%) p (75.50%) d(0.07%)
σC 3 - H 6	H 6 sp 0.00	1.96507	H 6 s (99.97%) p (0.03%)
	C 4 sp 1.93		C 4 s (34.02%) p (65.83%) d (0.15%)
σC 4 - O 7	O 7 sp 1.43	1.99529	O 7 s (41.08%) p(58.80%) d (0.13%)
	C 4 sp 99.99 d 2.04		C 4 s (0.24%) p (99.27%) d (0.49%)
ΠC 4 - O 7	O 7 sp 99.99 d 0.37	1.99118	O 7 s (0.35%) p (99.52%) d(0.13%)
σO 8 - H 9	O 8 sp 3.64	1.98524	O 8 s (21.52%) p(78.39%) d (0.09%)

	H 9 sp 0.00		H 9 s (99.84%) p(0.16%)
	C 10sp 2.71		C 10s (26.93%) p(73.03%) d(0.04%)
σC 10 - C 11	C 11sp 2.30	1.95327	C 11s (30.26%) p (69.69%) d(0.05%)
	C 10sp 2.53		C 10s (28.34%) p(71.62%) d(0.04%)
σC 10 - C 22	C 22sp 2.27	1.96083	C 22s (30.53%) p(69.43%) d(0.05%)
	C 10sp 3.55		C 10s (21.98%) p(77.95%) d (0.07%)
σC 10 - C 33	C 33sp 1.60	1.95635	C 33s (38.38%) p(61.56%) d(0.06%)
	C 11sp 1.88		C 11s (34.76%) p(65.20%) d (0.04%)
σC 11 - C 12	C 12sp 1.80	1.97251	C 12s (35.73%) p(64.23%) d(0.04%)
	C 11sp 1.86		C 11s (34.94%) p(65.02%) d(0.04%)
σC 11 - C 13	C 13sp 1.81	1.97212	C 13s (35.60%) p(64.35%) d (0.04%)
	C 11 sp99.99d 1.78		C 11s (0.02%) p (99.95%) d(0.03%)
ΠC 11 - C 13	C 13sp 1.00	1.66536	C 13s (0.00%) p(99.95%) d(0.05%)
	C 12sp 1.79		C 12s (35.82%) p(64.14%) d(0.04%)
σC 12 - C 14	C 14sp 1.78	1.97696	C 14sp(63.99%) d(0.04%)
	C 12sp 1.00		C 12s (0.00%) p(99.95%) d(0.04%)
ΠC 12 - C 14	C 14sp 1.00	1.66152	C 14s (0.00%) p(99.95%) d(0.05%)
	C 13sp 1.80		C 13s (35.74%) p(64.22%) d (0.04%)
σC 13 - C 16	C 16sp 1.79	1.97665	C 16 s(35.82%)p (64.13%)d (0.04%)

	C 14sp 1.80		C 14 s(35.74%)p (64.22%)d(0.04%)
σC 14 - C 18	C 18sp 1.80	1.9793	C 18 s(35.65%)p (64.30%)d(0.04%)
	C 16sp 1.79		C 16 s(35.88%)p (64.08%)d(0.04%)
σC 16 - C 18	C 18sp 1.79	1.97936	C 18 s(35.79%)p (64.16%)d(0.04%)
	C 16sp 1.00		C 16 s(0.00%)p(99.96%)d (0.04%)
ΠC 16 - C 18	C 18sp 1.00	1.66703	C 18 s(0.00%)p (99.96%)d(0.04%)
	C 22sp 1.91		C 22 s(34.34%)p (65.61%)d (0.04%)
σC 22 - C 23	C 23sp 1.76	1.97157	C 23 s(36.18%)p (63.78%)d(0.04%)
	C 22sp 1.85		C 22 s(35.03%)p (64.92%)d(0.04%)
σC 22 - C 24	C 24sp 1.78	1.97185	C 24 s(36.01%)p (63.95%)d(0.04%)
	C 22 sp99.99d 0.59		C 22 s(0.06%)p(99.90%)d (0.04%)
ΠC 22 - C 24	C 24sp 1.00	1.66519	C 24 s(0.00%)p (99.95%)d (0.05%)
	C 23sp 1.78		C 23 s(35.98%)p (63.98%)d (0.04%)
σC 23 - C 25	C 25sp 1.79	1.97753	C 25 s(35.86%)p (64.10%)d (0.04%)
	C 23sp 1.00		C 23 s(0.00%)p (99.96%)d(0.04%)
ΠC 23 - C 25	C 25sp 1.00	1.66249	C 25 s(0.00%)p(99.95%)d(0.05%)
	C 24sp 1.80		C 24 s(35.75%)p (64.22%)d(0.04%)
σC 24 - C 27	C 27sp 1.79	1.97688	C 27 s(35.89%)p (64.07%)d (0.04%)
σC 25 - C 29	C 25sp 1.80	1.97903	C 25 s(35.76%)p (64.19%)d (0.04%)

	C 25sp 1.80		C 29 s(35.61%)p (64.34%)d(0.04%)
	C 27sp 1.79		C 27 s(35.88%)p(64.08%)d(0.04%)
σC 27 - C 29	C 29sp 1.80	1.97929	C 29 s(35.75%)p (64.20%)d (0.04%)
	C 27sp 1.00		C 27 s(0.00%)p (99.96%)d (0.04%)
ΠC 27 - C 29	C 29sp 1.00	1.66644	C 29 s(0.00%)p (99.96%)d (0.04%)
	C 33sp 1.94d 0.01		C 33 s(33.98%)p (65.85%)d (0.17%)
σC 33 - O 34	O 34sp 1.39	1.99498	O 34 s(41.74%)p (58.14%)d (0.12%)
	C 33 sp99.99d 2.90		C 33 s(0.17%)p(99.32%)d (0.51%)
ΠC 33 - O 34	O 34 sp99.99d 0.65	1.99173	O 34 s(0.19%)p(99.68%)d(0.13%)
	C 33sp 2.63d 0.01		C 33 s(27.49%)p (72.27%)d(0.23%)
σC 33 - O 35	O 35sp 1.93	1.99466	O 35 s(34.13%)p (65.78%)d (0.09%)
	O 35sp 3.72		O 35 s(21.17%)p (78.74%)d(0.09%)
σO 35 - H 36	H 36 s	1.98389	H 36 s(99.86%)p (0.14%)
	C 12sp 2.52		C 12 s(28.42%)p(71.53%)d (0.05%)
σC 12 - H 15	H 15 s	1.97756	H 15 s(99.96%)p (0.04%)
	C 13sp 2.49		C 13 s(28.64%)p(71.32%)d (0.05%)
σC 13 - H 17	H 17 s	1.97716	H 17 s(99.96%)p (0.04%)
	C 14sp 2.54		C 14 s(28.24%)p (71.72%)d (0.04%)
σC 14 - H 19	H 19 s	1.97963	H 19 s(99.96%)p (0.04%)

	C 16sp 2.54		C 16 s(28.25%)p (71.70%)d (0.04%)
σC 16 - H 20	H 20 s	1.97972	H 20 s(99.96%)p (0.04%)
	C 18sp 2.51		C 18 s(28.51%)p (71.44%)d (0.04%)
σC 18 - H 21	H 21 s	1.98007	H 21 s(99.96%)p (0.04%)
	C 23sp 2.60		C 23 s(27.80%)p (72.15%)d (0.05%)
σC 23 - H 26	H 26 s	1.97797	H 26 s(99.96%)p (0.04%)
	C 24sp 2.54		C 24 s(28.21%)p (71.74%)d (0.05%)
σC 24 - H 28	H 28 s	1.97778	H 28 s(99.96%)p (0.04%)
	C 25sp 2.53		C 25 s(28.33%)p(71.63%)d (0.04%)
σC 25 - H 30	H 30 s	1.9794	H 30 s(99.96%)p (0.04%)
	C 27sp 2.55		C 27 s(28.19%)p (71.77%)d(0.04%)
σC 27 - H 31	H 31 s	1.97959	H 31 s(99.96%)p (0.04%)
	C 29sp 2.50		C 29 s(28.59%)p (71.36%)d(0.04%)
σC 29 - H 32	H 32 s	1.97984	H 32 s(99.96%)p (0.04%)

The bonding efficiency in a molecule is often explained by bond order values and this is also obtained from NBO output file. From the result, the strength of each bond obtained and the weakest which is broken first can be predicted. Formulation of metal complexes involves breaking and making of bonds. This in turn, signifies the study of bond orders in a molecule. The bond order of each of the bonds in Diphenyl glycolic acid -glycine ligand is given in Table 1.13.From this table it is clear that among 2 O-H bond O8-H9 and O35-H36 the weakest bond is O35-H36.So the bond O35-H36 will break easily and generate a proton. This is clear evidence that this site will act as a ligand for metal ions easily.

Table 1.13. Bond order values of Diphenyl glycolic acid -glycine ligand

Bond	Bond order	Bond	Bond order
N1-H2	0.7976	C27-H31	0.9244
N1-C3	1.0036	C29-H32	0.9244
N1-C10	0.9763	C25-H30	0.9238
C3-H5	0.909	C23-H26	0.9216
C3-H6	0.8891	C33-O35	1.0573
C3-C4	0.9803	C33-O34	1.7738
C4-O7	1.7878	C22-C23	1.3929
C4-O8	1.0334	C22-C24	1.4058
O8-H9	0.7597	C25-C29	1.4245
C10-C33	0.92	C27-C29	1.44
C10-C11	0.96	C11-C12	1.3899
C10-C22	0.9637	C11-C13	1.4105
C13-H17	0.9105	C12-C14	1.4459
C16-H20	0.9248	C14-C18	1.425
C18-H21	0.9252	C16-C16	1.4261
C14-H19	0.9244	C16-C18	1.4436
C12-H15	0.9144	O35-H36	0.7345
C24-H28	0.9169		

In NBO analysis, the electronic wave function is elucidated in terms of occupied Lewis and unoccupied Lewis delocalized orbitals. The important electronic wave function of donor and acceptor orbitals and the E (2) interaction energy between these two have given in Table 1.14.The lone pair of electrons of Nitrogen and Oxygen atoms is responsible for the majority of Diphenyl glycolic acid -glycine ligand interaction energies. The E (2) value increases with increase in interaction between donor and acceptor pair. In the case of donor σN1-H2, it having highest E (2) value with acceptor σ*C3-H11. So, the donor σN1-H2 and acceptor σ*C3-H11 have strong interaction. In the same way, the donors σ N1-C3, σ N1-C10, σ C3-C4 are showing high interaction with acceptors σ*C3-O8, σ*C3-C12, σ* C3-C10 respectively. The highest donor-acceptor interaction in the case of molecule Diphenyl glycolic acid -glycine ligand is seen between the donor Π C16-C18 and the acceptor Π*C11-C13.

Table 1.14. Donor-Acceptor interactions of HBG in terms of E (2)

Donor NBO(i)		Acceptor NBO(j)		E(2) in Kcal/mol	Ej-Ei in a.u	F(I,j) in a.u
Σ	N1-H2	σ*	C3-C4	0.97	0.97	0.028
Σ	N1-H2	σ*	C3-H5	1.77	0.98	0.037
Σ	N1-H2	σ*	C3-C11	2.3	0.99	0.043
Σ	N1-H2	σ*	C3-C33	0.87	0.94	0.026
Σ	N1-C3	σ*	C3-C10	0.69	1.08	0.025
Σ	N1-C3	σ*	C3-O8	2.08	1.08	0.043
Σ	N1-C3	σ*	C3-C33	1.37	1.07	0.035
Σ	N1-C10	σ*	C3-C4	0.81	1.08	0.027
Σ	N1-C10	σ*	C3-C11	0.71	1.11	0.025
Σ	N1-C10	σ*	C3-C22	0.88	1.11	0.028
Σ	N1-C10	σ*	C3-C12	1.97	1.3	0.045
Σ	N1-C10	σ*	C3-C24	0.5	1.3	0.023
Σ	N1-C10	Π*	C3-C24	1.66	0.76	0.035
Σ	N1-C10	σ*	C3-O34	1.75	1.34	0.043
Σ	C3-C4	σ*	C3-C10	3.19	1	0.051
Σ	C3-C4	σ*	C3-O7	1.24	1.29	0.036
Σ	C3-C5	σ*	C3-H2	2.25	0.96	0.042
Σ	C3-H5	σ*	C3-O7	2.6	1.16	0.049

Σ	C3-H5	Π*	C3-O7	3.49	0.54	0.041
Σ	C3-H6	σ*	C3-O7	1.61	1.15	0.039
Σ	C3-H6	Π*	C3-O7	5.46	0.54	0.05
Σ	C3-O7	σ*	C3-C4	1.12	1.46	0.037
Σ	C3-O7	σ*	C3-H9	0.87	1.48	0.032
Π	C3-O7	σ*	C3-H5	1.13	0.77	0.026
Π	C3-O7	σ*	C3-H6	1.34	0.77	0.029
Π	C3-O8	Π*	C3-O7	0.69	0.41	0.016
Σ	C4-O8	σ*	N1-C3	0.73	1.3	0.028
Σ	O8 -H9	σ*	C4-O7	4.8	1.4	0.073
Σ	C10-C11	σ*	N1-H2	1.79	1.04	0.039
Σ	C10-C11	σ*	C10-C22	1.21	1	0.031
Σ	C10-C11	σ*	C10-C33	0.73	0.94	0.024
Σ	C10-C11	σ*	C11-C12	1.66	1.19	0.04
Σ	C10-C11	σ*	C11-C13	1.79	1.19	0.041
Σ	C10-C11	σ*	C12-C14	2.13	1.2	0.045
Σ	C10-C11	σ*	C13-C16	2.15	1.2	0.046
Σ	C10-C11	σ*	C22-C23	2.49	1.18	0.049
Σ	C10-C11	Π*	C33-O34	3.52	0.62	0.043
Σ	C10-C11	σ*	C33-O35	0.79	0.95	0.025
Σ	C10-C22	σ*	C10-C11	1.35	1	0.033
Σ	C10-C22	σ*	C10-C33	0.65	0.95	0.022

Σ	C10-C22	σ*	C11-C13	1.92	1.2	0.043
Σ	C10-C22	Π*	C11-C13	0.64	0.66	0.02
Σ	C10-C22	σ*	C22-C23	1.73	1.19	0.041
Σ	C10-C22	σ*	C22-C24	1.85	1.19	0.042
Σ	C10-C22	σ*	C23-C25	2.21	1.2	0.046
Σ	C10-C22	σ*	C24-C27	2.26	1.2	0.047
Σ	C10-C22	Π*	C33-O34	1.18	0.63	0.025
Σ	C10-C22	σ*	C33-O35	1.73	0.96	0.037
Σ	C10-C33	σ*	N1-C3	2.9	1	0.048
Σ	C10-C33	σ*	C10-C11	0.94	1.01	0.028
Σ	C10-C33	σ*	C11-C13	0.88	1.21	0.029
Σ	C10-C33	Π*	C11-C13	2.98	0.67	0.043
Σ	C10-C33	σ*	C22-C24	2.92	1.2	0.053
Σ	C10-C33	σ*	C33-034	0.89	1.25	0.03
Σ	C10-C33	σ*	O35-H36	2.22	1.02	0.043
Σ	C11-C12	σ*	N1-C10	1.41	1.04	0.034
Σ	C11-C12	σ*	C10-C11	1.65	1.07	0.038
Σ	C11-C12	σ*	C11-C13	3.75	1.27	0.062
Σ	C11-C12	σ*	C12-14	3.28	1.28	0.058
Σ	C11-C12	σ*	C12-H15	1.12	1.15	0.032
Σ	C11-C12	σ*	C13-H17	2.55	1.14	0.048
Σ	C11-C12	σ*	C14-H19	2.13	1.13	0.044

Σ	C11-C13	σ*	C10-C11	1.96	1.07	0.041
Σ	C11-C13	σ*	C10-C22	1.16	1.08	0.032
Σ	C11-C13	σ*	C11-C12	3.8	1.27	0.062
Σ	C11-C13	σ*	C12-H15	2.56	1.15	0.049
Σ	C11-C13	σ*	C13-C16	3.25	1.28	0.058
Σ	C11-C13	σ*	C13-H17	1.24	1.15	0.034
Σ	C11-C13	σ*	C16-H20	2.12	1.13	0.044
Π	C11-C13	σ*	C10-C22	1.6	0.63	0.031
Π	C11-C13	σ*	C10-C33	3.11	0.58	0.04
Π	C11-C13	Π*	C12-C14	20.13	0.29	0.068
Π	C11-C13	Π*	C16-C18	19.47	0.29	0.067
Π	C11-C13	Π*	C33-O34	2.07	0.26	0.021
Σ	C12-C14	σ*	C10-C11	3.9	1.07	0.058
Σ	C12-C14	σ*	C11-C12	3.77	1.27	0.062
Σ	C12-C14	σ*	C12-H15	1.03	1.15	0.031
Σ	C12-C14	σ*	C14-C18	2.76	1.28	0.053
Σ	C12-C14	σ*	C14-H19	0.92	1.13	0.029
Σ	C12-C14	σ*	C18-H21	2.39	1.13	0.047
Π	C12-C14	Π*	C11-C13	20.29	0.28	0.068
Π	C12-C14	Π*	C16-C18	20.62	0.28	0.068
Σ	C12-H15	σ*	C11-C12	0.89	1.08	0.028
Σ	C12-H15	σ*	C11-C13	4.73	1.09	0.064

Σ	C12-H15	σ*	C12-C14	0.77	1.1	0.026
Σ	C13-H15	σ*	C14-C18	3.68	1.09	0.057
Σ	C13-H15	σ*	C14-H19	0.59	0.95	0.021
Σ	C13-C16	σ*	C10-C11	3.99	1.07	0.059
Σ	C13-C16	σ*	C11-C13	3.79	1.27	0.062
Σ	C13-C16	σ*	C13-H17	1.07	1.14	0.031
Σ	C13-C16	σ*	C16-C18	2.75	1.28	0.053
Σ	C13-C16	σ*	C16-H20	0.89	1.13	0.028
Σ	C13-C16	σ*	C18-H21	2.44	1.13	0.047
Σ	C13-H17	σ*	C11-C12	4.89	1.08	0.065
Σ	C13-H17	σ*	C11-C13	1.03	1.09	0.03
Σ	C13-H17	σ*	C13-C16	0.73	1.09	0.025
Σ	C14-H17	σ*	C16-C18	3.58	1.09	0.056
Σ	C14-H17	σ*	C16-H20	0.56	0.95	0.021
Σ	C14-C18	σ*	C12-C14	2.82	1.28	0.054
Σ	C14-C18	σ*	C12-H15	2.46	1.15	0.047
Σ	C14-C18	σ*	C14-H19	0.93	1.13	0.029
Σ	C14-C18	σ*	C16-C18	2.67	1.28	0.052
Σ	C14-C18	σ*	C16-H20	2.56	1.13	0.048
Σ	C14-C18	σ*	C18-H21	0.9	1.13	0.029
Σ	C14-H19	σ*	C11-C12	4.14	1.08	0.06
Σ	C14-H19	σ*	C12-C14	0.64	1.1	0.024

Σ	C14-H19	σ*	C12-H15	0.51	0.97	0.02
Σ	C14-H19	σ*	C14-C18	0.55	1.09	0.022
Σ	C16-H19	σ*	C16-C18	3.56	1.1	0.056
Σ	C16-H19	σ*	C18-H21	0.51	0.95	0.02
Σ	C16-C18	σ*	C13-C16	2.78	1.28	0.053
Σ	C16-C18	σ*	C13-H17	2.51	1.15	0.048
Σ	C16-C18	σ*	C14-C18	2.67	1.28	0.052
Σ	C16-C18	σ*	C14-H19	2.5	1.13	0.048
Σ	C16-C18	σ*	C16-H20	0.95	1.13	0.029
Σ	C16-C18	σ*	C18-H21	0.94	1.14	0.029
Π	C16-C18	Π*	C11-C13	20.82	0.28	0.069
Π	C16-C18	Π*	C12-C14	19.55	0.29	0.067
Σ	C16-H20	σ*	C11-C13	4.07	1.09	0.06
Σ	C16-H20	σ*	C13-C16	0.6	1.1	0.023
Σ	C16-H20	σ*	C14-C18	3.58	1.09	0.056
Σ	C18-H20	σ*	C16-C18	0.58	1.1	0.022
Σ	C18-H20	σ*	C18H21	0.51	0.95	0.02
Σ	C18-H21	σ*	C12-C14	3.73	1.1	0.057
Σ	C18-H21	σ*	C13-C16	3.75	1.1	0.057
Σ	C18-H21	σ*	C14-C18	0.56	1.09	0.022
Σ	C18-H21	σ*	C14-H19	0.5	0.95	0.02
Σ	C22-H21	σ*	C16-C18	0.59	1.1	0.023

Σ	C22-H21	σ*	C16-H20	0.51	0.95	0.02
Σ	C22-C23	σ*	C10-C11	1.49	1.07	0.036
Σ	C22-C23	σ*	C10-C22	1.93	1.08	0.041
Σ	C22-C23	σ*	C22-C24	3.72	1.27	0.061
Σ	C22-C23	σ*	C23-C25	3.45	1.28	0.059
Σ	C22-C23	σ*	C23-H26	1.14	1.13	0.032
Σ	C22-C23	σ*	C24-H28	2.82	1.14	0.051
Σ	C22-C23	σ*	C25-H30	2.06	1.13	0.043
Σ	C22-C24	σ*	C10-C22	2	1.08	0.042
Σ	C22-C24	σ*	C10-C33	0.77	1.03	0.025
Σ	C22-C24	σ*	C22-C23	3.68	1.27	0.061
Σ	C22-C24	σ*	C23-H26	2.71	1.13	0.05
Σ	C22-C24	σ*	C24-C27	3.4	1.28	0.059
Σ	C22-C24	σ*	C24-H28	1.18	1.14	0.033
Σ	C22-C24	σ*	C27-H31	2.07	1.13	0.043
Π	C22-C24	σ*	N1-C10	4.64	0.6	0.051
Π	C22-C24	σ*	C10-C33	1.48	0.58	0.028
Π	C23-C24	Π*	C23-C25	19.77	0.29	0.068
Π	C23-C24	Π*	C27-C29	20.13	0.29	0.068
Σ	C23-C25	σ*	C10-C22	3.7	1.08	0.057
Σ	C23-C25	σ*	C22-C23	3.89	1.27	0.063
Σ	C23-C25	σ*	C23-H26	1.01	1.13	0.03

Σ	C23-C25	σ*	C25-C29	2.69	1.28	0.052
Σ	C23-C25	σ*	C25-H30	0.92	1.14	0.029
Σ	C23-C25	σ*	C29-H32	2.4	1.14	0.047
Π	C23-C25	Π*	C22-C24	20.77	0.28	0.069
Π	C23-C25	Π*	C27-C29	20.41	0.28	0.068
Σ	C23-H26	σ*	C22-C23	0.88	1.09	0.028
Σ	C23-H26	σ*	C22-C24	4.77	1.09	0.064
Σ	C23-H26	σ*	C23-C25	0.69	1.1	0.025
Σ	C24-H26	σ*	C25-C29	3.61	1.09	0.056
Σ	C24-H26	σ*	C25-H30	0.56	0.95	0.021
Σ	C24-H27	σ*	C10-C22	3.92	1.08	0.058
Σ	C24-H27	σ*	C22-C24	3.87	1.27	0.063
Σ	C24-H27	σ*	C24-H28	1.01	1.14	0.03
Σ	C24-H27	σ*	C27-C29	2.79	1.28	0.053
Σ	C24-H27	σ*	C29-H31	0.9	1.13	0.029
Σ	C24-H27	σ*	C29-H32	2.42	1.13	0.047
Σ	C24-H28	σ*	C22-C23	4.72	1.09	0.064
Σ	C24-H28	σ*	C22-C24	0.97	1.09	0.029
Σ	C24-H28	σ*	C24-C27	0.7	1.09	0.025
Σ	C25-H28	σ*	C27-C29	3.6	1.1	0.056
Σ	C16-C28	σ*	C27-H31	0.56	0.95	0.021
Σ	C25-C29	σ*	C23-C25	2.76	1.28	0.053

Σ	C25-C29	σ*	C23-H26	2.49	1.13	0.047
Σ	C25-C29	σ*	C25-H30	0.93	1.13	0.029
Σ	C25-C29	σ*	C27-C29	2.68	1.28	0.052
Σ	C25-C29	σ*	C27-H31	2.57	1.13	0.048
Σ	C25-C29	σ*	C29-H32	0.91	1.13	0.029
Σ	C25-H30	σ*	C22-C23	4.23	1.09	0.061
Σ	C25-H30	σ*	C23-C25	0.62	1.1	0.023
Σ	C25-H30	σ*	C23-H26	0.54	0.95	0.02
Σ	C25-H30	σ*	C25-C29	0.56	1.09	0.022
Σ	C27-H30	σ*	C27-C29	3.52	1.1	0.056
Σ	C27-H30	σ*	C29-H32	0.5	0.95	0.02
Σ	C27-C29	σ*	C24-C27	2.85	1.28	0.054
Σ	C27-C29	σ*	C24-H28	2.5	1.14	0.048
Σ	C27-C29	σ*	C25-C29	2.65	1.28	0.052
Σ	C27-C29	σ*	C25-H30	2.5	1.14	0.048
Σ	C27-C29	σ*	C27-H31	0.95	1.13	0.029
Σ	C27-C29	σ*	C29-H32	0.94	1.14	0.029
Π	C27-C29	Π*	C22-C24	20.4	0.28	0.068
Π	C27-C29	Π*	C23-C25	19.9	0.29	0.068
Σ	C27-H31	σ*	C22-C24	4.21	1.09	0.06
Σ	C27-H31	σ*	C24-C27	0.6	1.09	0.023
Σ	C27-H31	σ*	C25-C29	3.57	1.09	0.056

Σ	C29-H31	σ*	C27-C29	0.58	1.1	0.022
Σ	C29-H31	σ*	C29-H32	0.51	0.95	0.02
Σ	C29-H32	σ*	C23-C25	3.67	1.1	0.057
Σ	C29-H32	σ*	C24-C27	3.84	1.09	0.058
Σ	C29-H32	σ*	C25-C29	0.57	1.09	0.022
Σ	C33-H32	σ*	C27-H29	0.61	1.1	0.023
Σ	C33-H32	σ*	C27-H31	0.51	0.95	0.02
Σ	C33-O34	σ*	N1-C10	0.63	1.45	0.027
Σ	C33-O34	σ*	C10-C33	1.54	1.44	0.043
Π	C33-O34	σ*	C10-C11	0.77	0.78	0.022
Π	C33-O34	Π*	C11-C13	0.55	0.44	0.015
Π	C35-O34	Π*	C33-O34	0.91	0.41	0.018
Σ	C35-O35	σ*	C10-C22	0.68	1.34	0.027
Σ	O35-H36	σ*	C10-C33	4.39	1.09	0.063
Σ	O35-H36	σ*	C33-O34	0.83	1.37	0.03

3.3 Computational details of Diphenyl glycolic acid-histidine ligand

3.3.1. Geometrical optimization of Diphenyl glycolic acid - histidine ligand

Geometrical optimization of the Diphenyl glycolic acid -histidine ligand was performed using the DFT/B3LYP/6-311G+ (d, p) basis set. These Geometry optimizations in the ground state are carried out without using any symmetry constraints. The geometrically optimized structure of the Diphenyl glycolic acid -histidine ligand is given in Fig. 1.7. The geometrical parameters including bond lengths, bond angles, and dihedral angles are analyzed and are given in Table 1.15, Table 1.16, and Table 1.17.The optimized structure of the Diphenyl glycolic acid -histidine ligand contains two six-membered rings. The C-C bond lengths of these rings range between 1.39 - 1.40 A^0. These bond lengths fall in the average C-C bond length range of aromatic rings confirming the presence of two aromatic rings in the ligand. The carboxylic acid functional groups in the ligand have two C-O double bonds with bond lengths of 1.2042 A^0 and 1.2117 A^0. The C-O single bond length of the acid functional groups is 1.3572 A^0 and 1.3438 A^0 and the respective O-H bond lengths are 0.9690A^0 and 0.9698 A^0. The optimized structure of the ligand contains an additional five-membered ring, in which the C-N single bond length is 1.3834 A^0 and the C-N double bond lengths are 1.3133A^0 and 1.3651 A^0. Bond lengths of the N1-C3 and N1-C20 single bonds that join

various rings in the ligand are 1.4671A^0 and 1.4747 A^0, respectively. The significant dihedral angles that determine the orientation of the ligand are ϕ(C5-C3-N1-C20), ϕ(N1-C3-C5-C9), ϕ(C32-C20-N1-C3), ϕ(O45-C43-C20-N1), ϕ(C21-C20-N1-C3), and ϕ(C6-C3-C5-C9)with respective values of 77.6559^0, 179.1776^0, 43.4689^0, -31.0751^0, 163.5096^0, and 60.1642^0. The reported values of dihedral angles demonstrate that the Diphenyl glycolic acid -histidine ligand is not planar.

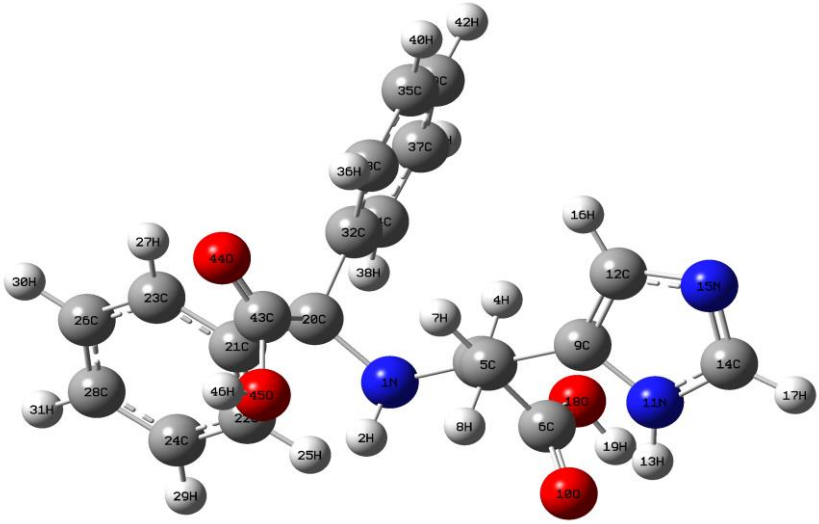

Fig. 1.7.Optimized geometry of the Diphenyl glycolic acid -histidine ligand

Table 1.15. Optimized bond lengths of Diphenyl glycolic acid - histidine ligand

Bond	Bond length(A^0)	Bond	Bond length(A^0)
R(1,2)	1.0145	R(21,23)	1.4008
R(1,3)	1.4671	R(22,24)	1.3960
R(1,20)	1.4747	R(22,25)	1.0815
R(3,4)	1.0896	R(23,26)	1.3912
R(3,5)	1.5487	R(23,27)	1.0836
R(3,6)	1.5294	R(24,28)	1.3913
R(5,7)	1.0919	R(24,29)	1.0844
R(5,8)	1.0945	R(26,28)	1.3950
R(5,9)	1.4965	R(26,30)	1.0842
R(6,10)	1.2117	R(28,31)	1.0841
R(6,18)	1.3438	R(32,33)	1.3981
R(9,11)	1.3834	R(32,34)	1.4013
R(9,12)	1.3753	R(33,35)	1.3960
R(11,13)	1.0103	R(33,36)	1.0803
R(11,14)	1.3651	R(34,37)	1.3907
R(12,15)	1.3762	R(34,38)	1.0830
R(12,16)	1.0797	R(35,39)	1.3909
R(14,15)	1.3133	R(35,40)	1.0842
R(14,17)	1.0796	R(37,39)	1.3946
R(18,19)	0.9698	R(37,41)	1.0842
R(20,21)	1.5576	R(39,42)	1.0841
R(20,32)	1.5394	R(43,44)	1.2042
R(20,43)	1.5553	R(43,45)	1.3572
R(21,22)	1.3955	R(45,46)	0.9690

Table 1.16. Optimized bond angles of Diphenyl glycolic acid - histidine ligand

Bond angle	Angle(degree)	Bond angle	Angle(degree)
A(2,1,3)	110.0610	A(20,21,23)	119.3182
A(2,1,20)	109.7464	A(22,21,23)	118.8957
A(3,1,20)	120.4905	A(21,22,24)	120.4277
A(1,3,4)	108.1837	A(21,22,25)	119.7002
A(1,3,5)	115.7437	A(24,22,25)	119.8541
A(1,3,6)	104.3964	A(21,23,26)	120.5769
A(4,3,5)	109.4759	A(21,23,27)	119.8233
A(4,3,6)	107.2572	A(26,23,27)	119.5988
A(5,3,6)	111.3635	A(22,24,28)	120.4160
A(3,5,7)	107.8261	A(22,24,29)	119.4501
A(3,5,8)	108.7340	A(28,24,29)	120.1335
A(3,5,9)	115.1392	A(23,26,28)	120.2787
A(7,5,8)	106.8090	A(23,26,30)	119.5590
A(7,5,9)	107.5360	A(28,26,30)	120.1620
A(8,5,9)	110.4427	A(24,28,26)	119.4042
A(3,6,10)	124.9104	A(24,28,31)	120.3284
A(3,6,18)	112.5091	A(26,28,31)	120.2670
A(10,6,18)	122.5642	A(20,32,33)	123.8649
A(5,9,11)	123.5228	A(20,32,34)	117.5465
A(5,9,12)	132.0513	A(33,32,34)	118.4835
A(11,9,12)	104.4147	A(32,33,35)	120.5353
A(9,11,13)	124.7406	A(32,33,36)	120.5673
A(9,11,14)	107.5582	A(35,33,36)	118.8849
A(13,11,14)	127.6382	A(32,34,37)	120.9416
A(9,12,15)	111.1114	A(32,34,38)	119.4973
A(9,12,16)	127.4883	A(37,34,38)	119.5605
A(15,12,16)	121.3983	A(33,35,39)	120.4945
A(11,14,15)	111.6476	A(33,35,40)	119.3406

A(11,14,17)	122.4310	A(39,35,40)	120.1648
A(15,14,17)	125.9213	A(34,37,39)	120.1734
A(12,15,14)	105.2677	A(34,37,41)	119.6296
A(6,18,19)	107.5935	A(39,37,41)	120.1969
A(1,20,21)	109.1345	A(35,39,37)	119.3706
A(1,20,32)	109.4304	A(35,39,42)	120.3160
A(1,20,43)	112.0651	A(37,39,42)	120.3134
A(21,20,32)	109.6929	A(20,43,44)	127.1094
A(21,20,43)	102.8517	A(20,43,45)	110.9996
A(32,20,43)	113.4223	A(44,43,45)	121.7570
A(20,21,22)	121.7823	A(43,45,46)	107.0379

Table 1.17. Optimized dihedral angles of Diphenyl glycolic acid - histidine ligand

Dihedral	Dihedral angle	Dihedral	Dihedral angle
D(2,1,3,4)	-174.8029	D(21,20,32,34)	-49.2168
D(2,1,3,5)	-51.5733	D(43,20,32,33)	20.2128
D(2,1,3,6)	71.1999	D(43,20,32,34)	-163.5793
D(20,1,3,4)	-45.5737	D(1,20,43,44)	153.1120
D(20,1,3,5)	77.6559	D(1,20,43,45)	-31.0751
D(20,1,3,6)	-159.5709	D(21,20,43,44)	-89.8065
D(2,1,20,21)	-67.1220	D(21,20,43,45)	86.0064
D(2,1,20,32)	172.8373	D(32,20,43,44)	28.5859
D(2,1,20,43)	46.1240	D(32,20,43,45)	-155.6012
D(3,1,20,21)	163.5096	D(20,21,22,24)	-179.4754
D(3,1,20,32)	43.4689	D(20,21,22,25)	-1.0237
D(3,1,20,43)	-83.2444	D(23,21,22,24)	-0.1933
D(1,3,5,7)	-60.7882	D(23,21,22,25)	178.2584
D(1,3,5,8)	54.6677	D(20,21,23,26)	179.4897
D(1,3,5,9)	179.1776	D(20,21,23,27)	-0.1477
D(4,3,5,7)	61.7600	D(22,21,23,26)	0.1895

D(4,3,5,8)	177.2159	D(22,21,23,27)	-179.4478
D(4,3,5,9)	-58.2742	D(21,22,24,28)	-0.0215
D(6,3,5,7)	-179.8015	D(21,22,24,29)	179.7732
D(6,3,5,8)	-64.3456	D(25,22,24,28)	-178.4708
D(6,3,5,9)	60.1642	D(25,22,24,29)	1.3239
D(1,3,6,10)	-93.8815	D(21,23,26,28)	0.0293
D(1,3,6,18)	84.6747	D(21,23,26,30)	-179.7724
D(4,3,6,10)	151.4662	D(27,23,26,28)	179.6675
D(4,3,6,18)	-29.9775	D(27,23,26,30)	-0.1342
D(5,3,6,10)	31.7042	D(22,24,28,26)	0.2414
D(5,3,6,18)	-149.7395	D(22,24,28,31)	-179.9734
D(3,5,9,11)	-78.1574	D(29,24,28,26)	-179.5519
D(3,5,9,12)	103.2578	D(29,24,28,31)	0.2333
D(7,5,9,11)	161.6490	D(23,26,28,24)	-0.2451
D(7,5,9,12)	-16.9359	D(23,26,28,31)	179.9696
D(8,5,9,11)	45.4530	D(30,26,28,24)	179.5555
D(8,5,9,12)	-133.1318	D(30,26,28,31)	-0.2299
D(3,6,18,19)	-177.0710	D(20,32,33,35)	176.525
D(10,6,18,19)	1.5242	D(20,32,33,36)	-4.7759
D(5,9,11,13)	3.5671	D(34,32,33,35)	0.3503
D(5,9,11,14)	-179.1335	D(34,32,33,36)	179.0494
D(12,9,11,13)	-177.5178	D(20,32,34,37)	-176.5719
D(12,9,11,14)	-0.2184	D(20,32,34,38)	3.1386
D(5,9,12,15)	178.9468	D(33,32,34,37)	-0.1540
D(5,9,12,16)	-0.5282	D(33,32,34,38)	179.5565
D(11,9,12,15)	0.1649	D(32,33,35,39)	-0.2567
D(11,9,12,16)	-179.3101	D(32,33,35,40)	179.6750
D(9,11,14,15)	0.2080	D(36,33,35,39)	-178.9774
D(9,11,14,17)	-179.845	D(36,33,35,40)	0.9543
D(13,11,14,15)	177.4055	D(32,34,37,39)	-0.1393
D(13,11,14,17)	-2.6475	D(32,34,37,41)	179.9308
D(9,12,15,14)	-0.0441	D(38,34,37,39)	-179.8497

D(16,12,15,14)	179.4678	D(38,34,37,41)	0.2204
D(11,14,15,12)	-0.1016	D(33,35,39,37)	-0.0410
D(17,14,15,12)	179.9536	D(33,35,39,42)	179.9524
D(1,20,21,22)	-3.8462	D(40,35,39,37)	-179.9722
D(1,20,21,23)	176.8745	D(40,35,39,42)	0.0213
D(32,20,21,22)	116.0326	D(34,37,39,35)	0.2372
D(32,20,21,23)	-63.2466	D(34,37,39,42)	-179.7563
D(43,20,21,22)	-122.9899	D(41,37,39,35)	-179.8333
D(43,20,21,23)	57.7309	D(41,37,39,42)	0.1732
D(1,20,32,33)	-105.7268	D(20,43,45,46)	-173.8979
D(1,20,32,34)	70.4812	D(44,43,45,46)	2.1755
D(21,20,32,33)	134.5753		

3.3.2. Frontier molecular orbital analysis

The frontier molecular orbitals (FMO) include the highest occupied molecular orbital (HOMO) and the lowest unoccupied molecular orbital (LUMO).The optimized structure of the Diphenyl glycolic acid -histidine ligand is used for the visualization of these orbitals. FMO analysis is an efficient method for studying the chemical reactivity of compounds. It predicts the electron donating and accepting tendency of molecules. The higher energy of the HOMO orbital indicates electron donating ability, while the higher energy of LUMO indicates electron-accepting tendency. The difference between HOMO and LUMO is known as the band gap. The diagrammatic representation of HOMO, LUMO, and band gap of the ligand is given in Fig.1.8, where red and blue color represents the positive and negative lobes of the orbitals. The obtained

energies of HOMO and LUMO orbitals of Diphenyl glycolic acid - histidine ligand and the calculated band gap are given in Table 1.18.The obtained band gap of the ligand is 4.9476eV, since the band gap is neither too small nor too large suggests that the ligand could be reactive. In the obtained FMO diagram, HOMO is localized in the aromatic rings and carboxylic groups while LUMO is concentrated on the five-membered ring. The locations of HOMO act as electron-donating sites, whereas the locations of LUMO act as electron-accepting sites.

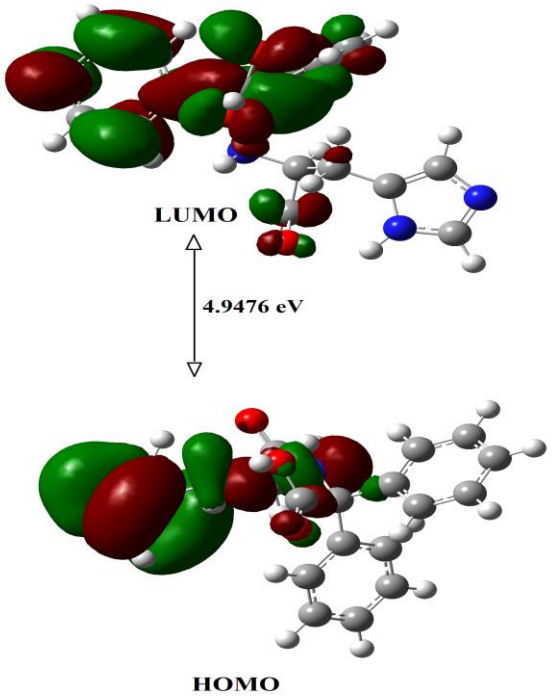

Fig. 1.8. Frontier molecular orbitals of Diphenyl glycolic acid - histidine ligand

Table 1.18.HOMO, LUMO energies, and calculated band gap of Diphenyl glycolic acid -histidine ligand

E(HOMO)eV	E(LUMO) eV	Band gap(eV)
-6.1606	-1.2130	4.9476

3.3.3. Global reactivity parameters

The global reactivity parameters of the Diphenyl glycolic acid -histidine ligand are calculated using Eq. (1 to**7)**.The global descriptive parameters are a useful tool for comparing the behavior and reactivities of different compounds. The global descriptive parameters include Electronegativity (χ), Chemical potential (ꭓ), Chemical softness (S), Chemical hardness (ɳ), and Electrophilicity index (ω). Where electronegativity is the tendency of a molecule to attract electrons, and chemical potential is the tendency of electrons to flow from a region of higher potential to a region of lower chemical potential. Softness is defined as the measure of the tendency of a molecule to receive electrons and its inverse gives hardness.The calculated global descriptive parameters of the Diphenyl glycolic acid-histidine ligand are given in Table 1.19. The computed IP value of the ligand is 6.1606 eV; this high value suggests that it is difficult to remove electrons from the ligand. The obtained EA value of the ligand is 1.2130 eV, this small value indicates that the ligand is capable of accepting electrons. The calculated electrophilicity index of the ligand is 2.7472 eV. This low value of ω indicates the maximal flow of

electrons from the donor to the acceptor.The calculated chemical hardness (2.4738 eV) is much higher than chemical softness (0.2021) confirming that the molecule is relatively hard and stable. Since hard molecules require a lot of energy to excite, they are less polarizable.

Table 1.19 Calculated global descriptive parameters of Diphenyl glycolic acid -histidine ligand

Descriptors	Values(eV)
Ionization potential (IP)	6.1606
Electron affinity (EA)	1.2130
Chemical hardness (η)	2.4738
Chemical softness (S)	0.2021
Electronegativity (χ)	3.6868
Electrophilicity index (ω)	2.7472
Chemical potential (ϰ)	-3.6868

3.3.4 Electrostatic potential maps (ESP)

The three-dimensional electrostatic potential map (ESP) is used for predicting the reactive behavior of chemical systems in both electrophilic and nucleophilic reactions. The ESP diagram predicts the reactivity of inter- or intra-molecular interactions and helps in visualizing the size, shape, and charge distribution of the molecule. ESP is based on electrostatic potential energy, which measures the strength of nearby charges, nuclei, and electrons at a particular position. The calculated ESP diagram of the Diphenyl glycolic

acid-histidine ligand is given in Fig. 1.9. The diagram contains various colors that represent various electrostatic potentials. The blue color denotes a positive site, while the red color denotes an area that is rich in electrons or is more negative. The obtained ESP map of the Diphenyl glycolic acid -histidine ligand shows that the electron density is concentrated in the two carboxylic group positions. Since these sites can serve as the ligand sites for metal ions, it is possible to assume that the Diphenyl glycolic acid -histidine can form complexes with a variety of metal ions.

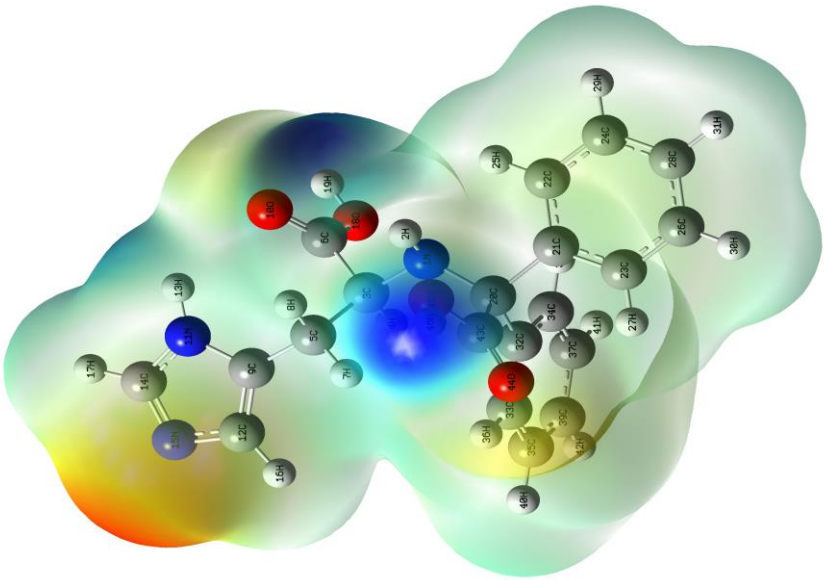

Fig.1.9ESP diagram of Diphenyl glycolic acid -histidine ligand

3.3.5 NBO Analysis

NBO analysis is a useful tool for creating the visual depiction of electron orbitals and population analysis. The NBO analysis, in conjunction with the second-order perturbation energy, provides information about interactions between lewis type (bonding or lone pair) filled orbitals and non-lewis type (antibonding) empty orbitals, which is a measure of intra and intermolecular delocalization or hyperconjugation. The NBO output file contains bonding ideas such as bond orbital occupancies and natural atomic hybrids. This information helps in predicting the relative aromaticity of compounds as well as the difference between kinetic and thermal stability. The occupancies and hybrids of various atoms or groups of Diphenyl glycolic acid -histidine ligand are given in Table 1.20. This data summarizes the information regarding the effective valence electron configuration of each atom in the molecule.NBO analysis explains the presence of two aromatic rings in the ligand. The first ring is composed of atoms C21, C22, C24, C28, C26, and, C23 and the second ring is composed of C32, C33, C35, C39, C37, and C34.The aromatic rings are joined by the two σ bonds, C20-C21, and C20-C32.The atom C20 is further linked with a carboxylic group and an N atom through which the additional 5-membered ring is connected. The 5-membered ring in the ligand contains two N atoms and has five σ bonds and two Π bonds. The Π bonds are seen between C9-C12 and C14-N15 bonds having occupancy of 1.8378 and 1.9859.

In NBO analysis, the electronic wave function is described in terms of occupied lewis and unoccupied lewis delocalized orbitals. The important electronic wave function of the donor and acceptor orbitals as well as the E(2) interaction energy between these two have been provided in Table 1.21. The interaction energies of the ligand are due to the lone pair of atoms in the Oxygen atom and other atoms like Nitrogen, Carbon, and Hydrogen. The interaction energy (E (2)) increases with an increase in the donor-acceptor interaction. For the donors, O45-H46 and O18-H19and the acceptors C43-O44 and C6-O10 the interaction between donor and acceptor is 0.78 kcal/mol and 0.90 kcal/mol. Since the interaction is very weak, the metal chelation between the atoms O45 and O18 by the removal of the protons H46 and H19 is feasible.

Table 1.20. Occupancy of NBOs and hybrids of Diphenyl glycolic acid -histidine ligand

NBOs	Hybrid	occupancy	AO%
	N $sp^{3.39}$		s(22.77%) p(77.15%) d(0.08%)
σN1-H2	H s	1.9795	s(99.93%) p(0.07%)
	N $sp^{2.12}$		s(32.07%) p(67.87%) d(0.05%)
σN1-C3	C $sp^{3.24}$	1.9763	s(23.57%) p(76.32%) d(0.11%)
	N $sp^{2.05}$		s(32.76%) p(67.18%) d(0.06%)
σN1-C20	C $sp^{3.41}$	1.9763	s(22.63%) p(77.27%) d(0.10%)
	C $sp^{3.24}$		s(23.58%) p(76.35%) d(0.07%)
σC3-H4	H s	1.9662	s(99.96%) p(0.04%)
	C $sp^{2.42}$		s(29.23%) p(70.74%) d(0.03%)
σC3-C5	C $sp^{2.68}$	1.9718	s(27.19%) p(72.77%) d(0.04%)
	C $sp^{3.22}$		s(23.68%) p(76.25%) d(0.07%)
σC3-C6	C $sp^{1.58}$	1.9703	s(38.73%) p(61.22%) d(0.05%)
	C $sp^{3.56}$		s(21.89%) p(78.04%) d(0.07%)
σC3-H7	H s	1.9705	s(99.97%) p(0.03%)

	C $sp^{3.49}$		s(22.24%) p(77.70%) d(0.06%)
σC3-H8	H s	1.9729	s(99.97%) p(0.03%)
	C $sp^{2.48}$		s(28.70%) p(71.25%) d(0.05%)
σC5-C9	C $sp^{1.70}$	1.9778	s(37.05%) p(62.93%) d(0.02%)
	C $sp^{2.01}d^{0.01}$		s(33.20%) p(66.62%) d(0.18%)
σC5-O10	O $sp^{1.46}$	1.9956	s(40.55%) p(59.33%) d(0.12%)
	C $sp^{99.99}d^{1.55}$		s(0.35%) p(99.11%) d(0.54%)
σC6-O10	C $sp^{99.99}d^{0.22}$	1.9896	s(0.54%) p(99.34%) d(0.12%)
	C $sp^{2.60}d^{0.01}$		s(27.71%) p(72.07%) d(0.22%)
σC6-O18	O $sp^{1.92}$	1.9947	s(34.26%) p(65.64%) d(0.09%)
	C $sp^{2.91}$		s(25.52%) p(74.37%) d(0.11%)
σC9-N11	N $sp^{1.83}$	1.9832	s(35.35%) p(64.60%) d(0.04%)
	C $sp^{1.67}$		s(37.41%) p(62.55%) d(0.04%)
σC9-C12	C $sp^{1.68}$	1.9798	s(37.24%) p(62.71%) d(0.05%)
	C sp		s(0.01%) p(99.94%) d(0.06%)
ΠC9-C12	C sp	1.8378	s(0.00%) p(99.92%) d(0.08%)
	N $sp^{2.35}$		s(29.85%) p(70.12%) d(0.04%)
σN11-H13	H s	1.9888	s(99.93%) p(0.07%)
	N $sp^{1.88}$		s(34.67%) p(65.29%) d(0.05%)
σN11-C14	C $sp^{2.30}$	1.9893	s(30.30%) p(69.58%) d(0.12%)
	C $sp^{2.35}$		s(29.80%) p(70.09%) d(0.11%)
σC12-N15	N $sp^{2.12}$	1.9776	s(32.02%) p(67.89%) d(0.09%)
	C $sp^{2.04}$		s(32.93%) p(67.03%) d(0.03%)
σC12-H16	H s	1.9839	s(99.95%) p(0.05%)
	C $sp^{1.84}$		s(35.13%) p(64.78%) d(0.09%)
σC14-N15	N $sp^{1.89}$	1.9859	s(34.55%) p(65.34%) d(0.10%)
	C p		s(0.00%) p(99.83%) d(0.17%)
ΠC14-N15	N p	1.8714	s(0.00%) p(99.83%) d(0.17%)
	C $sp^{1.88}$		s(34.69%) p(65.27%) d(0.04%)
σC14-H17	H s	1.9853	s(99.94%) p(0.06%)
	O $sp^{3.74}$		s(21.09%) p(78.82%) d(0.09%)
σO18-H19	H s	1.9850	s(99.87%) p(0.13%)
	C $sp^{2.89}$		s(25.71%) p(74.25%) d(0.04%)
σC20-C21	C $sp^{2.33}$	1.9463	s(30.01%) p(69.94%) d(0.05%)
σC12-C32	C $sp^{2.49}$	1.9581	s(28.65%) p(71.32%) d(.03%)

	C $sp^{2.29}$		s(30.35%) p(69.60%) d(0.05%)
	C $sp^{3.35}$		s(22.98%) p(76.95%) d(0.07%)
σC20-C43	C $sp^{1.56}$	1.9643	s(39.07%) p(60.88%) d(0.06%)
	C $sp^{1.98}$		s(33.54%) p(66.29%) d(0.16%)
σC43-O44	O $sp^{1.43}$	1.9950	s(41.14%) p(58.74%) d(0.12%)
	C $sp^{99.99}d^{0.76}$		s(0.67%) p(98.82%) d(0.51%)
ΠC43-O44	O $sp^{99.99}d^{0.14}$	1.9903	s(0.91%) p(98.96%) d(0.12%)
	C $sp^{2.73}$		s(26.78%) p(72.98%) d(0.24%)
σC43-O45	O $sp^{1.92}$	1.9939	s(34.18%) p(65.73%) d(0.09%)
	O $sp^{3.64}$		s(21.52%) p(78.40%) d(0.09%)
σO45-H46	H s	1.9850	s(99.82%) p(0.18%)

Table 1.21. Donor-Acceptor interactions of Diphenyl glycolic acid -histidine ligand in terms of E (2)

Donor NBO(i)		**Acceptor NBO(j)**		**E(2) (kcal/mol)**	**Ej-Ei (a.u)**	**F(I,j) (a.u)**
σ	N 1 - H 2	σ*	C 3 - H 4	2.32	1.02	0.0430
σ	N 1 - H 2	σ*	C 20 - C 32	2.91	1.01	0.0490
σ	N 1 - C 3	σ*	N 1 - C 20	0.60	1.07	0.0230
σ	N 1 - C 3	σ*	C 5 - C 9	1.19	1.17	0.0330
σ	N 1 - C 3	σ*	C 6 - O 10	0.93	1.31	0.0310
σ	N 1 - C 3	Π*	C 6 - O 10	2.41	0.73	0.0390
σ	N 1 - C 3	σ*	C 20 - C 21	1.16	1.10	0.0320
σ	N 1 - C 20	σ*	C 3 - C 6	0.61	1.08	0.0230
σ	N 1 - C 20	σ*	C 20 - C 21	0.62	1.10	0.0230
σ	N 1 - C 20	σ*	C 20 - C 32	0.81	1.12	0.0270
σ	N 1 - C 20	σ*	C 21 - C 23	2.00	1.31	0.0460
σ	N 1 - C 20	σ*	C 32 - C 33	0.80	1.31	0.0290
σ	N 1 - C 20	Π*	C 32 - C 33	1.49	0.77	0.0330
σ	N 1 - C 20	σ*	C 43 - O 44	1.56	1.32	0.0410
σ	N 1 - C 20	Π*	C 43 - O 44	0.63	0.74	0.0200
σ	C 3 - H 4	σ*	N 1 - H 2	3.09	0.92	0.0480
σ	C 3 - H 4	σ*	C 5 - H 8	2.38	0.91	0.0420
σ	C 3 - H 4	σ*	C 6 - O 10	3.56	1.09	0.0560
σ	C 3 - H 4	Π*	C 6 - O 10	2.04	0.51	0.0300
σ	C 3 - H 4	σ*	C 6 - O 18	0.53	0.85	0.0190

σ	C 3 - C 5	σ*	C 3 - H 4	0.54	1.02	0.0210
σ	C 3 - C 5	σ*	C 5 - C 9	1.13	1.05	0.0310
σ	C 3 - C 5	σ*	C 6 - O 18	2.34	0.95	0.0430
σ	C 3 - C 5	σ*	C 9 - C 12	1.16	1.22	0.0340
σ	C 3 - C 5	Π*	C 9 - C 12	1.94	0.66	0.0340
σ	C 3 - C 6	σ*	N 1 - C 20	3.78	0.99	0.0550
σ	C 3 - C 6	σ*	C 5 - H 7	1.45	1.05	0.0350
σ	C 3 - C 6	σ*	C 6 - O 10	1.01	1.23	0.0320
σ	C 3 - C 6	σ*	O 18 - H 19	2.37	1.02	0.0440
σ	C 5 - H 7	σ*	C 3 - C 6	3.00	0.85	0.0460
σ	C 5 - H 7	σ*	C 5 - C 9	0.57	0.94	0.0210
σ	C 5 - H 7	σ*	C 9 - N 11	6.51	0.96	0.0700
σ	C 5 - H 8	σ*	C 3 - H 4	2.73	0.90	0.0440
σ	C 5 - H 8	σ*	C 9 - C 12	3.03	1.11	0.0520
σ	C 5 - H 8	Π*	C 9 - C 12	2.46	0.54	0.0350
σ	C 5 - C 9	σ*	N 1 - C 3	2.45	0.99	0.0440
σ	C 5 - C 9	σ*	C 3 - C 5	0.85	1.01	0.0260
σ	C 5 - C 9	σ*	C 5 - H 7	0.57	1.05	0.0220
σ	C 5 - C 9	σ*	C 5 - H 8	0.58	1.04	0.0220
σ	C 5 - C 9	σ*	C 9 - N 11	0.87	1.10	0.0280
σ	C 5 - C 9	σ*	C 9 - C 12	3.40	1.26	0.0580
σ	C 5 - C 9	σ*	N 11 - C 14	1.94	1.12	0.0420
σ	C 5 - C 9	σ*	C 12 - N 15	0.87	1.16	0.0280
σ	C 6 - O 10	σ*	C 3 - C 6	1.21	1.45	0.0380
Π	C 6 - O 10	σ*	N 1 - C 3	1.57	0.76	0.0310
Π	C 6 - O 10	σ*	C 3 - H 4	0.57	0.82	0.0190
Π	C 6 - O 10	Π*	C 6 - O 10	0.72	0.42	0.0160
σ	C 6 - O 18	σ*	C 3 - C 5	0.86	1.32	0.0300
σ	C 9 - N 11	σ*	C 5 - H 7	0.64	1.19	0.0250
σ	C 9 - N 11	σ*	C 5 - C 9	0.88	1.23	0.0290
σ	C 9 - N 11	σ*	C 9 - C 12	1.14	1.40	0.0360
σ	C 9 - N 11	σ*	N 11 - H 13	0.79	1.21	0.0280
σ	C 9 - N 11	σ*	N 11 - C 14	1.63	1.26	0.0410
σ	C 9 - N 11	σ*	C 12 - N 15	0.59	1.30	0.0250

σ	C 9 - N 11	σ*	C 12 - H 16	3.01	1.23	0.0540
σ	C 9 - N 11	σ*	C 14 - N 15	0.52	1.37	0.0240
σ	C 9 - N 11	σ*	C 14 - H 17	2.57	1.20	0.0500
σ	C 9 - C 12	σ*	C 5 - C 9	3.50	1.14	0.0560
σ	C 9 - C 12	σ*	C 9 - N 11	0.83	1.15	0.0280
σ	C 9 - C 12	σ*	N 11 - H 13	4.25	1.11	0.0610
σ	C 9 - C 12	σ*	C 12 - N 15	0.69	1.20	0.0260
σ	C 9 - C 12	σ*	C 12 - H 16	1.47	1.14	0.0370
Π	C 9 - C 12	σ*	C 3 - C 5	3.93	0.61	0.0450
Π	C 9 - C 12	σ*	C 5 - H 8	2.19	0.65	0.0350
Π	C 9 - C 12	Π*	C 14 - N 15	15.24	0.27	0.0610
σ	N 11 - H 13	σ*	C 9 - N 11	0.57	1.14	0.0230
σ	N 11 - H 13	σ*	C 9 - C 12	1.46	1.29	0.0390
σ	N 11 - H 13	σ*	C 14 - N 15	1.35	1.27	0.0370
σ	N 11 - C 14	σ*	C 5 - C 9	4.08	1.24	0.0640
σ	N 11 - C 14	σ*	C 9 - N 11	1.66	1.26	0.0410
σ	N 11 - C 14	σ*	N 11 - H 13	0.73	1.22	0.0270
σ	C 12 - N 15	σ*	C 5 - C 9	4.71	1.18	0.0670
σ	C 12 - N 15	σ*	C 9 - N 11	0.97	1.20	0.0300
σ	C 12 - N 15	σ*	C 9 - C 12	1.31	1.35	0.0380
σ	C 12 - N 15	σ*	N 11 - C 14	1.41	1.21	0.0370
σ	C 12 - N 15	σ*	C 14 - N 15	0.61	1.33	0.0250
σ	C 12 - N 15	σ*	C 14 - H 17	5.19	1.16	0.0690
σ	C 12 - H 16	σ*	C 9 - N 11	2.43	0.97	0.0440
σ	C 12 - H 16	σ*	C 9 - C 12	1.19	1.12	0.0330
σ	C 12 - H 16	σ*	C 14 - N 15	2.34	1.10	0.0450
σ	C 14 - N 15	σ*	N 11 - H 13	2.50	1.23	0.0500
σ	C 14 - N 15	σ*	C 12 - N 15	0.56	1.32	0.0240
σ	C 14 - N 15	σ*	C 12 - H 16	3.39	1.26	0.0580
σ	C 14 - N 15	σ*	C 14 - H 17	0.97	1.23	0.0310
Π	C 14 - N 15	Π*	C 9 - C 12	19.91	0.33	0.0760
σ	C 14 - H 17	σ*	C 9 - N 11	2.70	1.00	0.0470
σ	C 14 - H 17	σ*	C 12 - N 15	2.82	1.05	0.0490
σ	C 14 - H 17	σ*	C 14 - N 15	0.76	1.13	0.0260

σ	O 18 - H 19	σ*	C 3 - C 6	3.73	1.12	0.0580
σ	O 18 - H 19	σ*	C 6 - O 10	0.90	1.35	0.0310
σ	C 20 - C 21	σ*	N 1 - C 3	2.76	0.95	0.0460
σ	C 20 - C 21	σ*	C 20 - C 32	1.66	1.00	0.0360
σ	C 20 - C 21	σ*	C 21 - C 22	1.71	1.19	0.0410
σ	C 20 - C 21	σ*	C 21 - C 23	1.39	1.18	0.0370
σ	C 20 - C 21	σ*	C 22 - C 24	2.05	1.19	0.0440
σ	C 20 - C 21	σ*	C 23 - C 26	2.19	1.20	0.0460
σ	C 20 - C 21	σ*	C 32 - C 33	2.54	1.19	0.0490
σ	C 20 - C 21	Π*	C 32 - C 33	0.86	0.65	0.0230
σ	C 20 - C 21	σ*	C 43 - O 44	1.62	1.20	0.0400
σ	C 20 - C 21	Π*	C 43 - O 44	3.69	0.62	0.0440
σ	C 20 - C 32	σ*	N 1 - H 2	2.13	1.04	0.0420
σ	C 20 - C 32	σ*	N 1 - C 20	0.59	0.96	0.0210
σ	C 20 - C 32	σ*	C 20 - C 21	1.87	0.99	0.0390
σ	C 20 - C 32	σ*	C 21 - C 22	1.58	1.20	0.0390
σ	C 20 - C 32	Π*	C 21 - C 22	1.42	0.66	0.0300
σ	C 20 - C 32	σ*	C 32 - C 33	2.04	1.20	0.0440
σ	C 20 - C 32	σ*	C 32 - C 34	1.60	1.20	0.0390
σ	C 20 - C 32	σ*	C 33 - C 35	2.04	1.21	0.0450
σ	C 20 - C 32	σ*	C 34 - C 37	2.19	1.22	0.0460
σ	C 20 - C 32	σ*	C 43 - O 45	1.85	0.95	0.0380
σ	C 20 - C 43	σ*	C 20 - C 21	0.68	1.01	0.0230
σ	C 20 - C 43	σ*	C 20 - C 32	0.55	1.03	0.0210
σ	C 20 - C 43	σ*	C 21 - C 22	2.01	1.22	0.0440
σ	C 20 - C 43	Π*	C 21 - C 22	2.04	0.68	0.0360
σ	C 20 - C 43	σ*	C 32 - C 34	2.64	1.21	0.0510
σ	C 20 - C 43	σ*	C 43 - O 44	1.07	1.23	0.0320
σ	C 20 - C 43	σ*	O 45 - H 46	2.15	1.02	0.0420
σ	C 21 - C 22	σ*	C 20 - C 21	1.92	1.07	0.0410
σ	C 21 - C 22	σ*	C 20 - C 32	0.70	1.09	0.0250
σ	C 21 - C 22	σ*	C 21 - C 23	3.67	1.27	0.0610
σ	C 21 - C 22	σ*	C 22 - C 24	3.33	1.28	0.0580
σ	C 21 - C 22	σ*	C 22 - H 25	1.31	1.15	0.0350

σ	C 21 - C 22	σ*	C 23 - H 27	2.50	1.15	0.0480
σ	C 21 - C 22	σ*	C 24 - H 29	2.05	1.14	0.0430
Π	C 21 - C 22	σ*	C 20 - C 32	2.37	0.64	0.0380
Π	C 21 - C 22	σ*	C 20 - C 43	2.40	0.57	0.0350
Π	C 21 - C 22	Π*	C 23 - C 26	19.52	0.29	0.0670
Π	C 21 - C 22	Π*	C 24 - C 28	19.61	0.29	0.0670
Π	C 21 - C 22	Π*	C 43 - O 44	1.27	0.26	0.0170
σ	C 21 - C 23	σ*	N 1 - C 20	1.63	1.03	0.0370
σ	C 21 - C 23	σ*	C 20 - C 21	1.45	1.06	0.0350
σ	C 21 - C 23	σ*	C 21 - C 22	3.68	1.27	0.0610
σ	C 21 - C 23	σ*	C 22 - H 25	2.61	1.14	0.0490
σ	C 21 - C 23	σ*	C 23 - C 26	3.42	1.28	0.0590
σ	C 21 - C 23	σ*	C 23 - H 27	1.09	1.14	0.0320
σ	C 21 - C 23	σ*	C 26 - H 30	2.10	1.13	0.0440
σ	C 22 - C 24	σ*	C 20 - C 21	4.24	1.06	0.0600
σ	C 22 - C 24	σ*	C 21 - C 22	3.97	1.27	0.0630
σ	C 22 - C 24	σ*	C 22 - H 25	1.06	1.14	0.0310
σ	C 22 - C 24	σ*	C 24 - C 28	2.72	1.28	0.0530
σ	C 22 - C 24	σ*	C 24 - H 29	0.87	1.13	0.0280
σ	C 22 - C 24	σ*	C 28 - H 31	2.43	1.13	0.0470
σ	C 22 - H 25	σ*	C 21 - C 22	1.09	1.09	0.0310
σ	C 22 - H 25	σ*	C 21 - C 23	4.85	1.08	0.0650
σ	C 22 - H 25	σ*	C 22 - C 24	0.72	1.09	0.0250
σ	C 22 - H 25	σ*	C 24 - C 28	3.56	1.10	0.0560
σ	C 22 - H 25	σ*	C 24 - H 29	0.55	0.95	0.0200
σ	C 23 - C 26	σ*	C 20 - C 21	3.89	1.06	0.0580
σ	C 23 - C 26	σ*	C 21 - C 23	3.90	1.27	0.0630
σ	C 23 - C 26	σ*	C 23 - H 27	1.06	1.14	0.0310
σ	C 23 - C 26	σ*	C 26 - C 28	2.71	1.28	0.0530
σ	C 23 - C 26	σ*	C 26 - H 30	0.90	1.13	0.0290
σ	C 23 - C 26	σ*	C 28 - H 31	2.39	1.13	0.0470
Π	C 23 - C 26	Π*	C 21 - C 22	20.62	0.28	0.0680
Π	C 23 - C 26	Π*	C 24 - C 28	20.33	0.28	0.0680
σ	C 23 - H 27	σ*	C 21 - C 22	4.79	1.09	0.0640

σ	C 23 - H 27	σ*	C 21 - C 23	0.92	1.08	0.0280
σ	C 23 - H 27	σ*	C 23 - C 26	0.79	1.10	0.0260
σ	C 23 - H 27	σ*	C 26 - C 28	3.65	1.09	0.0560
σ	C 23 - H 27	σ*	C 26 - H 30	0.58	0.95	0.0210
σ	C 24 - C 28	σ*	C 22 - C 24	2.76	1.28	0.0530
σ	C 24 - C 28	σ*	C 22 - H 25	2.46	1.15	0.0470
σ	C 24 - C 28	σ*	C 24 - H 29	0.96	1.13	0.0290
σ	C 24 - C 28	σ*	C 26 - C 28	2.68	1.28	0.0520
σ	C 24 - C 28	σ*	C 26 - H 30	2.51	1.14	0.0480
σ	C 24 - C 28	σ*	C 28 - H 31	0.94	1.14	0.0290
σ	C 24 - C 28	Π*	C 21 - C 22	20.4	0.28	0.0680
σ	C 24 - C 28	Π*	C 23 - C 26	19.71	0.29	0.0670
σ	C 24 - H 29	σ*	C 21 - C 22	4.01	1.09	0.0590
σ	C 24 - H 29	σ*	C 22 - C 24	0.57	1.09	0.0220
σ	C 24 - H 29	σ*	C 24 - C 28	0.58	1.10	0.0230
σ	C 24 - H 29	σ*	C 26 - C 28	3.59	1.09	0.0560
σ	C 24 - H 29	σ*	C 28 - H 31	0.51	0.95	0.0200
σ	C 26 - C 28	σ*	C 23 - C 26	2.79	1.28	0.0530
σ	C 26 - C 28	σ*	C 23 - H 27	2.46	1.14	0.0470
σ	C 26 - C 28	σ*	C 24 - C 28	2.68	1.28	0.0520
σ	C 26 - C 28	σ*	C 24 - H 29	2.57	1.13	0.0480
σ	C 26 - C 28	σ*	C 26 - H 30	0.93	1.13	0.0290
σ	C 26 - C 28	σ*	C 28 - H 31	0.91	1.13	0.0290
σ	C 26 - H 30	σ*	C 21 - C 23	4.09	1.09	0.0600
σ	C 26 - H 30	σ*	C 23 - C 26	0.63	1.10	0.0240
σ	C 26 - H 30	σ*	C 24 - C 28	3.53	1.10	0.0560
σ	C 26 - H 30	σ*	C 26 - C 28	0.55	1.09	0.0220
σ	C 28 - H 31	σ*	C 22 - C 24	3.77	1.10	0.0570
σ	C 28 - H 31	σ*	C 23 - C 26	3.66	1.10	0.0570
σ	C 28 - H 31	σ*	C 24 - C 28	0.60	1.10	0.0230
σ	C 28 - H 31	σ*	C 24 - H 29	0.51	0.95	0.0200
σ	C 28 - H 31	σ*	C 26 - C 28	0.56	1.09	0.0220
σ	C 32 - C 33	σ*	C 20 - C 21	0.91	1.07	0.0280
σ	C 32 - C 33	σ*	C 20 - C 32	2.17	1.09	0.0440

σ	C 32 - C 33	σ*	C 32 - C 34	3.74	1.27	0.0620
σ	C 32 - C 33	σ*	C 33 - C 35	3.27	1.28	0.0580
σ	C 32 - C 33	σ*	C 33 - H 36	1.28	1.15	0.0340
σ	C 32 - C 33	σ*	C 34 - H 38	2.51	1.15	0.0480
σ	C 32 - C 33	σ*	C 35 - H 40	2.00	1.14	0.0430
Π	C 32 - C 33	σ*	N 1 - C 20	4.59	0.59	0.0500
Π	C 32 - C 33	σ*	C 20 - C 21	1.81	0.62	0.0320
Π	C 32 - C 33	Π*	C 34 - C 37	19.89	0.29	0.0680
Π	C 32 - C 33	Π*	C 35 - C 39	19.16	0.29	0.0660
σ	C 32 - C 34	σ*	C 20 - C 32	1.90	1.08	0.0410
σ	C 32 - C 34	σ*	C 20 - C 43	1.53	1.01	0.0360
σ	C 32 - C 34	σ*	C 32 - C 33	3.58	1.27	0.0600
σ	C 32 - C 34	σ*	C 33 - H 36	2.77	1.14	0.0500
σ	C 32 - C 34	σ*	C 34 - C 37	3.31	1.28	0.0580
σ	C 32 - C 34	σ*	C 34 - H 38	1.10	1.14	0.0320
σ	C 32 - C 34	σ*	C 37 - H 41	2.11	1.13	0.0440
σ	C 33 - C 35	σ*	C 20 - C 32	4.38	1.08	0.0620
σ	C 33 - C 35	σ*	C 32 - C 33	3.80	1.27	0.0620
σ	C 33 - C 35	σ*	C 33 - H 36	1.02	1.14	0.0310
σ	C 33 - C 35	σ*	C 35 - C 39	2.73	1.28	0.0530
σ	C 33 - C 35	σ*	C 35 - H 40	0.86	1.13	0.0280
σ	C 33 - C 35	σ*	C 39 - H 42	2.43	1.13	0.0470
σ	C 33 - H 36	σ*	C 32 - C 33	1.00	1.09	0.0290
σ	C 33 - H 36	σ*	C 32 - C 34	4.79	1.08	0.0640
σ	C 33 - H 36	σ*	C 33 - C 35	0.73	1.09	0.0250
σ	C 33 - H 36	σ*	C 35 - C 39	3.62	1.10	0.0560
σ	C 33 - H 36	σ*	C 35 - H 40	0.57	0.95	0.0210
σ	C 34 - C 37	σ*	C 20 - C 32	3.62	1.08	0.0560
σ	C 34 - C 37	σ*	C 32 - C 34	3.78	1.27	0.0620
σ	C 34 - C 37	σ*	C 34 - H 38	1.02	1.14	0.0310
σ	C 34 - C 37	σ*	C 37 - C 39	2.73	1.28	0.0530
σ	C 34 - C 37	σ*	C 37 - H 41	0.92	1.13	0.0290
σ	C 34 - C 37	σ*	C 39 - H 42	2.40	1.14	0.0470
Π	C 34 - C 37	Π*	C 32 - C 33	20.2	0.28	0.0680

Π	C 34 - C 37	Π*	C 35 - C 39	20.52	0.28	0.0680
σ	C 34 - H 38	σ*	C 32 - C 33	4.64	1.08	0.0630
σ	C 34 - H 38	σ*	C 32 - C 34	0.91	1.08	0.0280
σ	C 34 - H 38	σ*	C 34 - C 37	0.75	1.10	0.0260
σ	C 34 - H 38	σ*	C 37 - C 39	3.64	1.09	0.0560
σ	C 34 - H 38	σ*	C 37 - H 41	0.58	0.95	0.0210
σ	C 35 - C 39	σ*	C 33 - C 35	2.73	1.28	0.0530
σ	C 35 - C 39	σ*	C 33 - H 36	2.34	1.15	0.0460
σ	C 35 - C 39	σ*	C 35 - H 40	0.97	1.14	0.0300
σ	C 35 - C 39	σ*	C 37 - C 39	2.67	1.28	0.0520
σ	C 35 - C 39	σ*	C 37 - H 41	2.53	1.14	0.0480
σ	C 35 - C 39	σ*	C 39 - H 42	0.94	1.14	0.0290
Π	C 35 - C 39	Π*	C 32 - C 33	20.97	0.28	0.0690
Π	C 35 - C 39	Π*	C 34 - C 37	19.48	0.29	0.0670
σ	C 35 - H 40	σ*	C 32 - C 33	4.21	1.09	0.0600
σ	C 35 - H 40	σ*	C 33 - C 35	0.59	1.09	0.0230
σ	C 35 - H 40	σ*	C 33 - H 36	0.50	0.96	0.0200
σ	C 35 - H 40	σ*	C 35 - C 39	0.59	1.10	0.0230
σ	C 35 - H 40	σ*	C 37 - C 39	3.58	1.09	0.0560
σ	C 35 - H 40	σ*	C 39 - H 42	0.51	0.95	0.0200
σ	C 37 - C 39	σ*	C 34 - C 37	2.80	1.28	0.0540
σ	C 37 - C 39	σ*	C 34 - H 38	2.50	1.14	0.0480
σ	C 37 - C 39	σ*	C 35 - C 39	2.67	1.28	0.0520
σ	C 37 - C 39	σ*	C 35 - H 40	2.56	1.13	0.0480
σ	C 37 - C 39	σ*	C 37 - H 41	0.93	1.13	0.0290
σ	C 37 - C 39	σ*	C 39 - H 42	0.90	1.13	0.0290
σ	C 37 - H 41	σ*	C 32 - C 34	4.20	1.08	0.0600
σ	C 37 - H 41	σ*	C 34 - C 37	0.64	1.10	0.0240
σ	C 37 - H 41	σ*	C 34 - H 38	0.50	0.96	0.0200
σ	C 37 - H 41	σ*	C 35 - C 39	3.51	1.10	0.0550
σ	C 37 - H 41	σ*	C 37 - C 39	0.55	1.09	0.0220
σ	C 39 - H 42	σ*	C 33 - C 35	3.77	1.09	0.0570
σ	C 39 - H 42	σ*	C 34 - C 37	3.68	1.10	0.0570
σ	C 39 - H 42	σ*	C 35 - C 39	0.60	1.10	0.0230

σ	C 39 - H 42	σ*	C 35 - H 40	0.51	0.95	0.0200
σ	C 39 - H 42	σ*	C 37 - C 39	0.55	1.09	0.0220
σ	C 43 - O 44	σ*	N 1 - C 20	0.50	1.44	0.0240
σ	C 43 - O 44	σ*	C 20 - C 43	1.39	1.42	0.0410
Π	C 43 - O 44	σ*	N 1 - C 20	0.77	0.76	0.0220
Π	C 43 - O 44	σ*	C 20 - C 21	0.88	0.79	0.0240
Π	C 43 - O 44	Π*	C 43 - O 44	0.74	0.43	0.0170
σ	C 43 - O 45	σ*	C 20 - C 32	1.16	1.34	0.0350
σ	O 45 - H 46	σ*	C 20 - C 43	4.05	1.09	0.0610
σ	O 45 - H 46	σ*	C 43 - O 44	0.78	1.36	0.0290
Π*	C 6 - O 10	σ*	N 1 - C 3	1.37	0.34	0.0570
Π*	C 6 - O 10	σ*	C 6 - O 10	1.08	0.58	0.0650
Π*	C 9 - C 12	σ*	C 3 - C 5	1.96	0.32	0.0520
Π*	C 9 - C 12	σ*	C 5 - H 8	0.86	0.35	0.0380
Π*	C 14 - N 15	Π*	C 9 - C 12	70.11	0.02	0.0600
Π*	C 21 - C 22	σ*	C 20 - C 32	1.02	0.36	0.0390
Π*	C 21 - C 22	σ*	C 20 - C 43	1.03	0.28	0.0320
Π*	C 32 - C 33	σ*	N 1 - C 20	2.17	0.30	0.0520
Π*	C 32 - C 33	σ*	C 20 - C 21	0.69	0.33	0.0300
Π*	C 43 - O 44	σ*	N 1 - C 20	0.61	0.33	0.0370
Π*	C 43 - O 44	σ*	C 20 - C 21	0.85	0.36	0.0450
Π*	C 43 - O 44	Π*	C 21 - C 22	7.88	0.03	0.0240
Π*	C 43 - O 44	Π*	C 23 - C 26	0.51	0.03	0.0060
Π*	C 43 - O 44	Π*	C 32 - C 33	0.89	0.03	0.0080
Π*	C 43 - O 44	σ*	C 43 - O 44	2.01	0.58	0.0910

3.4 Computational details of Diphenyl glycolic acid-Valine ligand

Computational investigation of synthesized Diphenyl glycolic acid -valine ligand was performed using the Gaussian09 program package.All calculations are performed using density functional

theory (DFT) with the hybrid Becke's three parameters and the Lee-Yang-Parr functional (B3LYP) augmented with a pople type 6-311+G(d,p) basis set. Theoretical investigation of geometrical parameters, global descriptive parameters, electrostatic potential map (ESP), and NBO parameters is conducted in the gas phase. Quantum chemical parameters such as the highest occupied molecular orbital (HOMO), lowest unoccupied molecular orbital (LUMO), and HOMO-LUMO gap (E_g) were also determined as part of the frontier molecular orbital (FMO) analysis.

3.4.1 Geometrical optimization of Diphenyl glycolic acid-Valine ligand

Geometrical optimization of the Diphenyl glycolic acid -valine ligand was carried out in the gas phase using the DFT/B3LYP/6-311+G(d,p) basis set. There are no symmetry constraints throughout the whole geometry optimization process and the resultant structure possesses the lowest energy and highest stability. The geometrically optimized structure of the Diphenyl glycolic acid-valine ligand is shown in Fig. 1.10, and the corresponding geometrical parameters, including bond lengths, bond angles, and dihedral angles, are given in Tables 1.22, 1.23, and 1.24, respectively.

The optimized structure of the Diphenyl glycolic acid -valine ligand has two six-membered rings. The C-C bond lengths of these rings range from 1.39 to 1.40 A^0.Since the bond lengths are consistent with the usual C-C bond length of aromatic rings, the

ligand contains two aromatic rings. There are two carboxylic acid functional groups with C-O double and single bonds of 1.2073 A^0, 1.2030 A^0, 1.3515 A^0, and 1.3527 A^0 and O-H bond lengths of 0.9701 A^0 and 0.9696 A^0, respectively. The two aromatic rings in the ligand are connected through the C19 atom, which has bond lengths of 1.5484A^0 and 1.5529 A^0, respectively. The C19 atom is also linked to a carboxylic acid functional group and the valine ligand through the N1-C19 bond (1.4785 A^0).

The significant dihedral angles that determine the orientation of the ligand are ϕ(C3-N1-C19-C20), ϕ(C3-N1-C19-C31), ϕ(C3-N1-C19-C42), ϕ(C19-N1-C3-C6), ϕ(C19-N1-C3-C5), and ϕ(C6-C3-C5-C9)with respective values of42.96^0,-84.27^0,163.07^0,-90.24^0, 146.78^0. The obtained dihedral angles show that the Diphenyl glycolic acid -valine ligand is not planar.

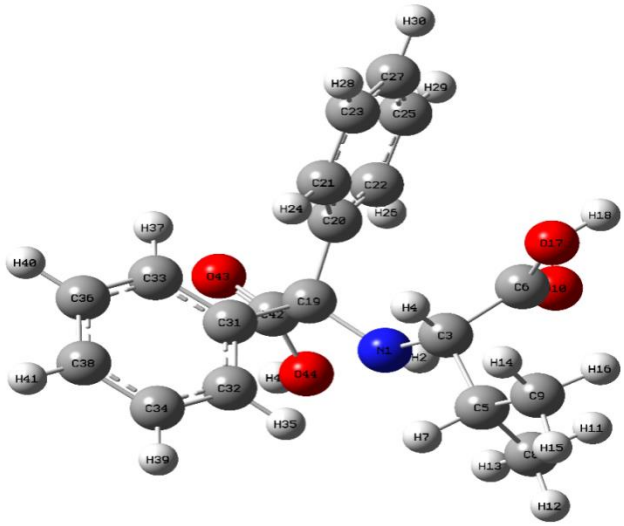

Fig. 1.10. Optimized geometry of the Diphenyl glycolic acid -valine ligand

Table 1.22. Optimized bond lengths of Diphenyl glycolic acid - valine ligand

Bond	Bond length(A^0)	Bond	Bond length(A^0)
N1-H2	1.0127	C21-C23	1.3947
N1-C3	1.4615	C21-H24	1.0828
N1-C19	1.4785	C22-C25	1.3912
C3-H4	1.0902	C22-H26	1.0839
C3-C5	1.5646	C23-C27	1.3916
C3-C6	1.5310	C23-H28	1.0843
C5-H7	1.0947	C25-C27	1.3944
C5-C8	1.5338	C25-H29	1.0842
C5-C9	1.5349	C27-H30	1.0843
C6-O10	1.2073	C31-C32	1.3960
C6-O17	1.3515	C31-C33	1.4018
C8-H11	1.0937	C32-C34	1.3956
C8-H12	1.0937	C32-H35	1.0808
C8-H13	1.0922	C33-C36	1.3914
C9-H14	1.0936	C33-H37	1.0823
C9-H15	1.0935	C34-C38	1.3914
C9-H16	1.0931	C34-H39	1.0845
O17-H18	0.9701	C36-C38	1.3951
C19-C20	1.5484	C36-H40	1.0844
C19-C31	1.5529	C38-H41	1.0843
C19-C42	1.5517	C42-O43	1.2030
C20-C21	1.3986	C42-O44	1.3527
C20-C22	1.4004	O44-H45	0.9696

Table 1.23. Optimized bond angles of Diphenyl glycolic acid - valine ligand

Bond angle	Angle(degree)	Bond angle	Angle(degree)
H2-N1-C3	109.7286	C21-C20-C22	118.0940
H2-N1-C19	110.2724	C20-C21-C23	120.9874
C3-N1-C19	118.9294	C20-C21-H24	120.0022
N1-C3-H4	109.4568	C23-C21-H24	119.0061
N1-C3-C5	110.4337	C20-C22-C25	121.0911
N1-C3-C6	111.3522	C20-C22-H26	120.1826
H4-C3-C5	107.1996	C25-C22-H26	118.7262
H4-C3-C6	107.9145	C21-C23-C27	120.2659
C5-C3-C6	110.3573	C21-C23-H28	119.5220
C3-C5-H7	103.7055	C27-C23-H28	120.2121
C3-C5-C8	113.2206	C22-C25-C27	120.2163
C3-C5-C9	112.7012	C22-C25-H29	119.5781
H7-C5-C8	107.6309	C27-C25-H29	120.2054
H7-C5-C9	107.5610	C23-C27-C25	119.3404
C8-C5-C9	111.4367	C23-C27-H30	120.3554
C3-C6-O10	124.5255	C25-C27-H30	120.3042
C3-C6-O17	112.8680	C19-C31-C32	120.7681
O10-C6-O17	122.5720	C19-C31-C33	120.5137
C5-C8-H11	111.8637	C32-C31-C33	118.5898
C5-C8-H12	109.8383	C31-C32-C34	120.7425
C5-C8-H13	111.5801	C31-C32-H35	118.8633
H11-C8-H12	107.7134	C34-C32-H35	120.3830
H11-C8-H13	108.1153	C31-C33-C36	120.6338
H12-C8-H13	107.5558	C31-C33-H37	119.8278
C5-C9-H14	111.7316	C36-C33-H37	119.5333
C5-C9-H15	109.8069	C32-C34-C38	120.2847
C5-C9-H16	112.0759	C32-C34-H39	119.5447
H14-C9-H15	107.8851	C38-C34-H39	120.1682
H14-C9-H16	107.6084	C33-C36-C38	120.3624

H15-C9-H16	107.5482	C33-C36-H40	119.5280
C6-O17-H18	107.2582	C38-C36-H40	120.1092
N1-C19-C20	112.8011	C34-C38-C36	119.3590
N1-C19-C31	110.5338	C34-C38-H41	120.3706
N1-C19-C42	108.6558	C36-C38-H41	120.2676
C20-C19-C31	112.7278	C19-C42-O43	124.1249
C20-C19-C42	108.3130	C19-C42-O44	113.5931
C31-C19-C42	103.2755	O43-C42-O44	122.2631
C19-C20-C21	121.5596	C42-O44-H45	106.5511
C19-C20-C22	120.1582		

Table 1.24 Optimized dihedral angles of Diphenyl glycolic acid -valine ligand

Dihedral	**Dihedral angle (degree)**	**Dihedral**	**Dihedral angle (degree)**
H2-N1-C3-H4	157.2167	C20-C19-C31-C32	-139.6482
H2-N1-C3-C5	-84.9899	C20-C19-C31-C33	44.5305
H2-N1-C3-C6	37.9829	C42-C19-C31-C32	103.6823
C9-N1-C3-H4	28.9898	C42-C19-C31-C33	-72.1390
C19-N1-C3-C5	146.7833	N1-C19-C42-O43	-170.3239
C19-N1-C3-C6	-90.244	N1-C19-C42-O44	11.2280
H2-N1-C19-C20	-85.0159	C20-C19-C42-O43	-47.4639
H2-N1-C19-C31	147.7556	C20-C19-C42-O44	134.088
H2-N1-C19-C42	35.0951	C19-C20-C22-C25	-175.8571
C3-N1-C19-C20	42.9585	C19-C20-C22-H26	4.0529
C3-N1-C19-C31	-84.2700	C21-C20-C22-C25	-0.7646
C3-N1-C19-C42	163.0695	C21-C20-C22-H26	179.1454
N1-C3-C5-H7	-57.1727	C20-C21-C23-C27	0.0049
N1-C3-C5-C8	59.1784	C20-C21-C23-H28	179.8906
N1-C3-C5-C9	-173.1920	H24-C21-C23-C27	-179.2421
H4-C3-C5-H7	61.9990	H24-C21-C23-H28	0.6436
H4-C3-C5-C8	178.3501	C20-C22-C25-C27	0.3160
H4-C3-C5-C9	-54.0198	C20-C22-C25-H29	-179.5292
C6-C3-C5-H7	179.2767	H26-C22-C25-C27	-179.5952
C6-C3-C5-C8	-64.3722	H26-C22-C25-H29	0.5595
C6-C3-C5-C9	63.2579	C21-C23-C27-C25	-0.4682

N1-C3-C6-O10	-33.7849	C21-C23-C27-H30	179.4895
N1-C3-C6-O17	148.3104	H28-C23-C27-C25	179.6469
H4-C3-C6-O10	-153.9340	H28-C23-C27-H30	-0.3954
H4-C3-C6-O17	28.1617	C22-C25-C27-C23	0.3099
C5-C3-C6-O10	89.2316	C22-C25-C27-H30	-179.6478
C5-C3-C6-O17	-88.6732	H29-C25-C27-C23	-179.8459
C3-C5-C8-H11	65.6057	H29-C25-C27-H30	0.1964
C3-C5-C8-H12	-174.8380	C19-C31-C32-C34	-177.8185
C3-C5-C8-H13	-55.6589	C19-C31-C32-H35	0.9714
H7-C5-C8-H11	179.6143	C33-C31-C32-C34	-1.9182
H7-C5-C8-H12	-60.8289	C33-C31-C32-H35	176.8717
H7-C5-C8-H13	58.3496	C19-C31-C33-C36	177.5186
C9-C5-C8-H11	-62.6815	C19-C31-C33-H37	-1.6561
C9-C5-C8-H12	56.8753	C32-C31-C33-C36	1.6075
C9-C5-C8-H13	176.0538	C32-C31-C33-H37	-177.5672
C3-C5-C9-H14	51.4540	C31-C32-C34-C38	0.8990
C3-C5-C9-H15	171.1204	C31-C32-C34-H39	-179.6706
C3-C5-C9-H16	-69.4148	H35-C32-C34-C38	-177.8726
H7-C5-C9-H14	-62.2350	H35-C32-C34-H39	1.5578
H7-C5-C9-H15	57.4314	C31-C33-C36-C38	-0.2744
H7-C5-C9-H16	176.8963	C31-C33-C36-H40	179.9807
C8-C5-C9-H14	-179.9810	H37-C33-C36-C38	178.9028
C8-C5-C9-H15	-60.3149	H37-C33-C36-H40	-0.8421
C8-C5-C9-H16	59.1499	C32-C34-C38-C36	0.4668
C3-C6-O17-H18	179.0649	C32-C34-C38-H41	179.8559
O10-C6-O17-H18	1.1133	H39-C34-C38-C36	-178.9600
N1-C19-C20-C21	-94.6628	H39-C34-C38-H41	0.4291
N1-C19-C20-C22	80.2560	C33-C36-C38-C34	-0.7749
C31-C19-C20-C21	31.3960	C33-C36-C38-H41	179.8353
C31-C19-C20-C22	-153.6850	H40-C36-C38-C34	178.9685
C42-C19-C20-C21	145.0294	H40-C36-C38-H41	-0.4212
C42-C19-C20-C22	-40.0518	C19-C42-O44-H45	177.8891
N1-C19-C31-C32	-12.3792	O43-C42-O44-H45	-0.5917
N1-C19-C31-C33	171.7994		

3.4.2 Frontier molecular orbital (FMO) analysis

The frontier molecular orbitals (FMO) entail the highest occupied molecular orbital (HOMO) and the lowest unoccupied molecular

orbital (LUMO).These orbitals are visualized using the optimized structure of the Diphenyl glycolic acid -valine ligand. FMO analysis is an effective approach for investigating the chemical reactivity of compounds. It foretells the ability of molecules to donate and accept electrons. The higher HOMO orbital energy shows the tendency to donate electrons, whereas greater LUMO orbital energy indicates a tendency to receive electrons.

The distinction between HOMO and LUMO is expressed by the band gap (E_g).The HOMO, LUMO, and E_g of the ligand are depicted diagrammatically in Fig. 1.11, with red and blue designating the positive and negative lobes of the orbitals, respectively, and the associated orbital energies are provided in Table 1.24. The obtained band gap of the ligand is 5.4532eV since the band gap is somewhat large, suggesting that the ligand could be reactive. In the obtained FMO diagram, HOMO is localized over one of the aromatic rings and valine moiety while LUMO is concentrated on the two rings. The locations of HOMO act as electron-donating sites, whereas the locations of LUMO act as electron-accepting sites.

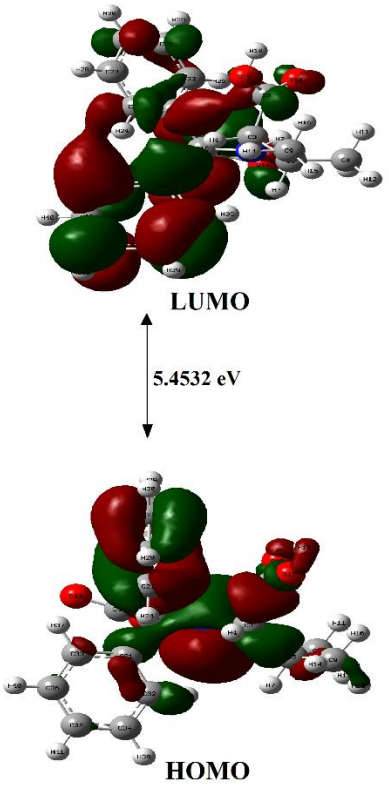

Fig.1.11. Frontier molecular orbitals of Diphenyl glycolic acid -valine

Table 1.24.HOMO, LUMO energies, and calculated band gap of Glycolic acid Diphenyl glycolic acid -valine ligand

E_{HOMO} (eV)	E_{LUMO}(eV)	Band gap(eV)
-6.5117	-1.0585	5.4532

3.4.3 Global reactivity parameters

The global reactivity descriptors of the Diphenyl glycolic acid -valine ligand are derived using **Eqs. (1–7)**.The global descriptive

parameters are a great resource for contrasting the behaviours and reactivities of different molecules. The following are some of them: Electronegativity (χ), Chemical Potential (ϒ), Chemical Hardness (η), Chemical Softness (S), and Electrophilicity Index (ω).Electronegativity describes the tendency of a molecule to attract electrons, and chemical potential describes the tendency of electrons to flow from a region of higher potential to a region of lower chemical potential. Softness measures the tendency of a molecule to receive electrons while hardness measures the tendency to donate electrons .The calculated global descriptive parameters of the Diphenyl glycolic acid-valine ligand are given in Table 1.25.The calculated IP value of the ligand is 6.5117 eV; this high value implies that it may be difficult to remove electrons from the ligand. The obtained EA value of the ligand is 1.0585 eV; this low value implies that the ligand can take electrons. The computed electrophilicity index of the ligand is 2.6273 eV. This low value denotes the maximum electron transfer from donor to acceptor. The predicted chemical hardness (2.7266 eV) is significantly more than the calculated chemical softness (0.1834), indicating that the molecule is relatively hard and stable. Considering that hard molecules take a lot of energy to excite, they are less polarizable.

Table 1.25. Calculated global descriptive parameters of Diphenyl glycolic acid -valine ligand

Descriptors	**Values(eV)**
Ionization potential (IP)	6.5117
Electron affinity (EA)	1.0585
Chemical hardness (η)	2.7266
Chemical softness (S)	0.1834
Electronegativity (χ)	3.7851
Electrophilicity index (ω)	2.6273
Chemical potential (ϰ)	-3.7851

3.4.4 Electrostatic potential maps (ESP)

The reactive behaviour of chemical systems in electrophilic and nucleophilic reactions is estimated using the three-dimensional electrostatic potential map (ESP).This map assists in visualizing the size, shape, and charge distribution of the molecule and predicts the reactivity of inter- or intramolecular interactions. The basis of ESP is electrostatic potential energy, which assesses the intensity of surrounding charges, nuclei, and electrons at a certain place. The calculated ESP diagram of the Diphenyl glycolic acid -valine ligand is given in Fig.1.12. The diagram is colored to show different electrostatic potentials. The blue colour represents a positive site, whereas the red colour represents a region that is rich in electrons or is more negative. The obtained ESP map of the Diphenyl glycolic acid -valine ligand shows that the electron density is concentrated in the two carboxylic group positions. The positions of red colour in the COO groups may act as acceptors of

H bonds and are nucleophilic sites while the blue colour regions seen in the Hydrogen atoms of the COOH group act as electrophilic sites.

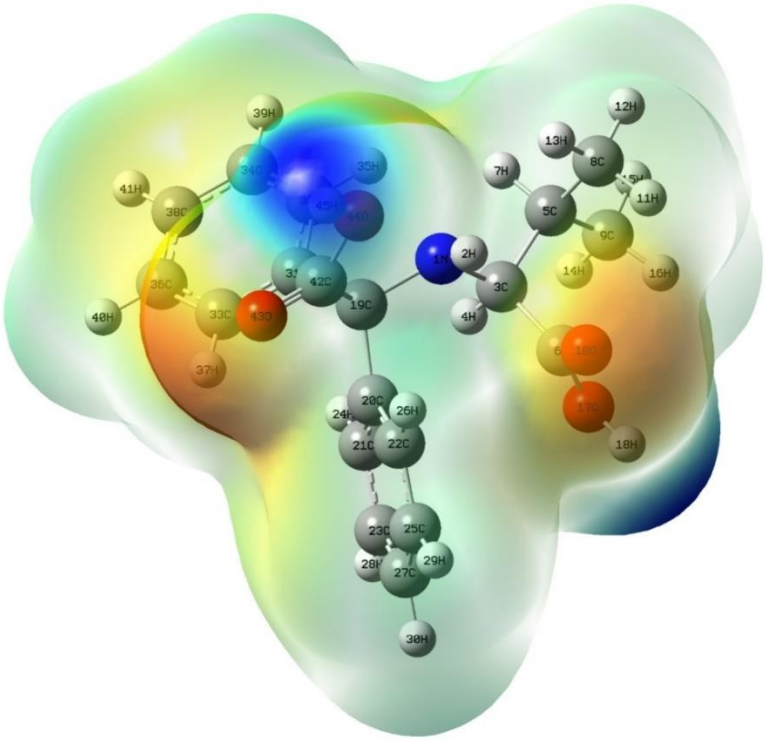

Fig. 1.12.ESP diagram of Diphenyl glycolic acid -valine ligand

3.4.5 NBO Analysis

NBO analysis is an important method for constructing visual representations of electron orbitals and population analysis . Together with the second-order perturbation energy, the NBO analysis provides information about interactions between Lewis-

type (bonding or lone pair) filled orbitals and non-Lewis type (antibonding) empty orbitals, which is a measure of intra and intermolecular delocalization or hyperconjugation. Bonding ideas like bond orbital occupancies and natural atomic hybrids are included in the NBO output file, which aids in predicting compound aromaticity and the difference between kinetic and thermal stability. Table 1.26 and 1.27 depicts the occupancies and hybrids of various atoms or groups of the Diphenyl glycolic acid - valine ligand. This information summarizes the effective valence electron configuration of each atom in the molecule. The existence of two aromatic rings in the ligand can be explained using NBO analysis. The first ring is made up of atoms C20, C21, C22, C23, C25, and C27, whereas the second ring is made up of atoms C31, C32, C33, C34, C36, and C38. The atom C19 connects the aromatic rings through two σ bonds, C19-C20 and C19-C31. C19 is also connected to a carboxylic group and a valine moiety via the N1 atom.

The electronic wave function is characterised in NBO analysis in terms of occupied and empty Lewis delocalized orbitals. Table 1.27 shows the key electronic wave functions of the donor and acceptor orbitals, as well as the E (2) interaction energy between these two. The interaction energies of the ligand are caused by the lone pair of atoms in the Oxygen atom and other atoms such as Nitrogen, Carbon, and Hydrogen. With an increase in the donor-acceptor interaction, the interaction energy (E (2)) rises as well. For the

donors, O17-H18 and O44-H45and the acceptors C6-O10 and C42-O43the interaction between donor and acceptor is 0.84 kcal/mol and 0.85 kcal/mol. Since the interaction is very weak, the removal of the protons H46 and H19 is easily feasible.

Table 1.26. Occupancy of NBOs and hybrids of Diphenyl glycolic acid -valine ligand

NBOs	Hybrid	occupancy	AO%
σN1-H2	N $sp^{3.27}$	1.9795	s(23.38%) p(76.54%) d(0.08%)
	H s		s(99.92%) p(0.08%)
σN1-C3	N $sp^{2.15}$	1.9807	s(31.69%) p(68.25%) d(0.06%)
	C $sp^{3.16}$		s(24.01%) p(75.89%) d(0.10%)
σN1-C19	N $sp^{2.17}$	1.9775	s(31.53%) p(68.41%) d(0.06%)
	C $sp^{3.35}$		s(22.97%) p(76.93%) d(0.10%)
σC3-H4	C $sp^{3.24}$	1.9675	s(23.55%) p(76.38%) d(0.07%)
	H s		s(99.96%) p(0.04%)
σC3-C5	C $sp^{2.58}$	1.9562	s(27.92%) p(72.05%) d(0.03%)
	C $sp^{2.91}$		s(25.57%) p(74.37%)
σC3-C6	C $sp^{3.06}$	1.9729	s(24.62%) p(75.32%) d(0.07%)
	C $sp^{1.57}$		s(38.90%) p(61.05%) d(0.05%)
σC5-C9	C $sp^{2.69}$	1.9825	s(27.11%) p(72.85%) d(0.04%)
	C $sp^{2.35}$		s(29.82%) p(70.14%) d(0.04%)
σC5-C8	C $sp^{2.68}$	1.9834	s(27.15%) p(72.81%) d(0.04%)
	C $sp^{2.38}$		s(29.54%) p(70.42%) d(0.04%)
σC6-O10	C $sp^{1.97}$	1.9954	s(33.63%) p(66.21%) d(0.16%)
	C $sp^{1.41}$		s(41.50%%) p(58.38%) d(0.12%)
ΠC6-O10	C $sp^{99.99}d^{13.71}$	1.9919	s(0.04%) p(99.43%) d(0.53%)
	O p		s(0.00%) p(99.88%) d(0.12%)
σC6-O17	C $sp^{2.62}d^{0.01}$	1.9945	s(27.53%) p(72.23%) d(0.24%)
	O $sp^{1.93}$		s(34.13%) p(65.78%) d(0.09%)
σO17-H18	O $sp^{3.73}$	1.9865	s(21.11 %) p(78.80 %) d(0.09%)

	H s		s(99.83 %) p(0.17 %)
σC19-C42	C $sp^{3.59}$	1.9566	s(21.76%) p(78.17%) d(0.07%)
	C $sp^{1.59}$		s(38.59%) p(61.34%) d(0.06%)
σC42-O43	C $sp^{1.94}$	1.9947	s(33.91%) p(65.92%) d(0.17%)
	O $sp^{1.39}$		s(41.82%) p(58.06%) d(0.12%)
ΠC42-O43	C $sp^{99.99}$ $d^{3.07}$	1.9916	s(0.17%) p(99.33%) d(0.51%)
	O $sp^{99.99}d^{0.67}$		s(0.19%) p(99.69%) d(0.13%)
σC42-O44	C $sp^{2.65}d^{0.01}$	1.9946	s(27.35%) p(72.41%) d(0.23%)
	O $sp^{1.93}$		s(34.08%) p(65.83%) d(0.09%)
σO44-H45	O $sp^{3.72}$	1.984	s(21.18%) p(65.83%) d(0.09%)
	H s		s(99.86%) p(0.14%)
σC19-C20	C $sp^{2.51}$	1.9606	s(28.45%) p(71.51%) d(0.04%)
	C $sp^{2.28}$		s(30.46%) p(69.49%) d(0.05%)
σC19-C31	C $sp^{2.73}$	1.9528	s(26.77%) p(73.19%) d(0.04%)
	C $sp^{2.29}$		s(30.34%) p(69.62%) d(0.05%)

Table 1.27. Donor-Acceptor interactions of Diphenyl glycolic acid -valine ligand in terms of E (2)

Donor NBO(i)		**Acceptor NBO(j)**		**E(2) (kcal/mol)**	**Ej-Ei (a.u)**	**F(I,j) (a.u)**
σ	N 1 - H 2	σ*	C 3 - H 4	2.25	1.02	0.043
σ	N 1 - H 2	σ*	C 19 - C 31	2.31	0.99	0.043
σ	N 1 - H 2	σ*	C 19 - C 42	0.95	0.93	0.027
σ	N 1 - C 3	σ*	N 1 - C 19	0.63	1.06	0.023
σ	N 1 - C 3	σ*	C 3 - C 5	0.67	1.08	0.024
σ	N 1 - C 3	σ*	C 5 - C 9	1.56	1.11	0.037
σ	N 1 - C 3	Π*	C 6 - O 10	0.52	0.73	0.018
σ	N 1 - C 3	σ*	C 6 - O 17	1.63	1.07	0.038
σ	N 1 - C 3	σ*	C 19 - C 42	1.18	1.05	0.032
σ	N 1 - C 19	σ*	C 3 - C 5	0.95	1.08	0.029
σ	N 1 - C 19	σ*	C 19 - C 20	0.81	1.1	0.027
σ	N 1 - C 19	σ*	C 19 - C 31	0.65	1.1	0.024

σ	N 1 - C 19	σ*	C 20 - C 21	0.51	1.29	0.023
σ	N 1 - C 19	Π*	C 20 - C 21	1.52	0.76	0.033
σ	N 1 - C 19	σ*	C 31 - C 33	1.99	1.29	0.045
σ	N 1 - C 19	σ*	C 42 - O 43	1.85	1.33	0.044
σ	C 3 - H 4	σ*	N 1 - H 2	2.85	0.94	0.046
σ	C 3 - H 4	σ*	C 3 - C 5	0.53	0.87	0.019
σ	C 3 - H 4	σ*	C 5 - C 8	3.35	0.9	0.049
σ	C 3 - H 4	σ*	C 6 - O 10	3.9	1.13	0.059
σ	C 3 - H 4	Π*	C 6 - O 10	1.19	0.52	0.023
σ	C 3 - C 5	σ*	N 1 - C 3	0.57	0.95	0.021
σ	C 3 - C 5	σ*	N 1 - C 19	2.64	0.93	0.044
σ	C 3 - C 5	σ*	C 3 - H 4	0.53	1	0.021
σ	C 3 - C 5	σ*	C 3 - C 6	0.51	0.95	0.02
σ	C 3 - C 5	σ*	C 5 - C 8	0.6	0.98	0.022
σ	C 3 - C 5	σ*	C 6 - O 10	0.6	1.2	0.024
σ	C 3 - C 5	Π*	C 6 - O 10	3.64	0.59	0.043
σ	C 3 - C 5	σ*	C 8 - H 12	1.38	1	0.033
σ	C 3 - C 5	σ*	C 9 - H 15	1.34	1	0.033
σ	C 3 - C 6	σ*	N 1 - C 19	0.63	0.98	0.022
σ	C 3 - C 6	σ*	C 3 - C 5	0.56	1	0.021
σ	C 3 - C 6	σ*	C 5 - H 7	1.29	1.05	0.033
σ	C 3 - C 6	σ*	C 6 - O 10	0.98	1.26	0.031
σ	C 3 - C 6	σ*	O 17 - H 18	2.27	1.02	0.043
σ	C 5 - H 7	σ*	C 3 - C 6	3.35	0.83	0.048
σ	C 5 - H 7	σ*	C 8 - H 11	3.14	0.89	0.047
σ	C 5 - H 7	σ*	C 9 - H 16	3.21	0.88	0.048
σ	C 5 - C 8	σ*	C 3 - H 4	1.52	1.01	0.035
σ	C 5 - C 8	σ*	C 3 - C 5	0.56	0.96	0.021
σ	C 5 - C 8	σ*	C 5 - H 7	0.54	1.01	0.021
σ	C 5 - C 8	σ*	C 5 - C 9	0.71	0.99	0.024
σ	C 5 - C 8	σ*	C 9 - H 14	1.65	1.01	0.037
σ	C 5 - C 9	σ*	N 1 - C 3	2.38	0.96	0.043
σ	C 5 - C 9	σ*	C 5 - H 7	0.51	1.01	0.02
σ	C 5 - C 9	σ*	C 5 - C 8	0.73	0.99	0.024

σ	C 5 - C 9	σ*	C 8 - H 13	1.64	1.02	0.037
σ	C 6 - O 10	σ*	C 3 - C 6	1.46	1.46	0.042
Π	C 6 - O 10	Π*	C 6 - O 10	0.76	0.4	0.016
σ	C 6 - O 17	σ*	N 1 - C 3	0.96	1.31	0.032
σ	O 17 - H 18	σ*	C 3 - C 6	3.97	1.11	0.06
σ	O 17 - H 18	σ*	C 6 - O 10	0.84	1.37	0.03
σ	C 19 - C 20	σ*	C 19 - C 31	1.28	1	0.032
σ	C 19 - C 20	σ*	C 19 - C 42	0.6	0.95	0.022
σ	C 19 - C 20	σ*	C 20 - C 21	1.81	1.19	0.042
σ	C 19 - C 20	σ*	C 20 - C 22	1.75	1.19	0.041
σ	C 19 - C 20	σ*	C 21 - C 23	2.25	1.2	0.047
σ	C 19 - C 20	σ*	C 22 - C 25	2.19	1.21	0.046
σ	C 19 - C 20	σ*	C 31 - C 32	1.94	1.2	0.043
σ	C 19 - C 20	Π*	C 31 - C 32	0.7	0.66	0.021
σ	C 19 - C 20	Π*	C 42 - O 43	1.16	0.62	0.025
σ	C 19 - C 20	σ*	C 42 - O 44	1.8	0.95	0.038
σ	C 19 - C 31	σ*	N 1 - H 2	1.59	1.04	0.037
σ	C 19 - C 31	σ*	C 19 - C 20	1.14	1	0.03
σ	C 19 - C 31	σ*	C 19 - C 42	0.66	0.94	0.022
σ	C 19 - C 31	σ*	C 20 - C 22	2.57	1.18	0.049
σ	C 19 - C 31	σ*	C 31 - C 32	1.81	1.19	0.042
σ	C 19 - C 31	σ*	C 31 - C 33	1.6	1.18	0.039
σ	C 19 - C 31	σ*	C 32 - C 34	2.15	1.2	0.046
σ	C 19 - C 31	σ*	C 33 - C 36	2.14	1.2	0.046
σ	C 19 - C 31	Π*	C 42 - O 43	3.66	0.62	0.044
σ	C 19 - C 31	σ*	C 42 - O 44	0.78	0.94	0.025
σ	C 19 - C 42	σ*	N 1 - C 3	2.75	1	0.047
σ	C 19 - C 42	σ*	C 19 - C 31	0.89	1.01	0.027
σ	C 19 - C 42	σ*	C 20 - C 21	2.92	1.21	0.053
σ	C 19 - C 42	Π*	C 20 - C 21	0.52	0.67	0.018
σ	C 19 - C 42	σ*	C 31 - C 32	0.97	1.21	0.031
σ	C 19 - C 42	σ*	C 31 - C 32	2.99	0.67	0.043
σ	C 19 - C 42	σ*	C 42 - O 43	0.92	1.24	0.03
σ	C 19 - C 42	σ*	O 44 - H 45	2.18	1.02	0.042

σ	C 42 - O 43	σ*	N 1 - C 19	0.71	1.45	0.029
σ	C 42 - O 43	σ*	C 19 - C 42	1.5	1.44	0.042
Π	C 42 - O 43	σ*	C 19 - C 31	0.77	0.78	0.022
Π	C 42 - O 43	Π*	C 31 - C 32	0.55	0.44	0.015
Π	C 42 - O 43	Π*	C 42 - O 43	0.89	0.41	0.018
σ	C 42 - O 44	σ*	C 19 - C 20	0.67	1.34	0.027
σ	O 44 - H 45	σ*	C 19 - C 42	4.35	1.09	0.062
σ	O 44 - H 45	σ*	C 42 - O 43	0.85	1.37	0.031

3.5 Computational details of Diphenyl glycolic acid-leucine ligand

We utilized the Gaussian-09 software package to conduct a computational investigation on a synthesized ligand comprising Diphenyl glycolic acid and leucine. All computations were performed using density functional theory (DFT) with the B3LYP functional, which combines Becke's three parameters and the Lee-Yang-Parr functional, along with a pople type 6-311 + G(d, p) basis set. The analysis is focused on various aspects, including the examination of geometrical parameters, global descriptive parameters, electrostatic potential map, and NBO parameters, all conducted in the gas phase. Additionally, as part of the investigation into frontier molecular orbitals, quantum chemical parameters such as the highest occupied molecular orbital (HOMO), lowest unoccupied molecular orbital (LUMO), and the HOMO-LUMO gap (E) were also calculated.

3.5.1 Geometrical optimization of Diphenyl glycolic acid - leucine ligand

The Diphenyl glycolic acid -leucine ligand underwent geometrical optimization using the DFT/B3LYP/6-311G + (d, p) basis set. These optimizations were performed in the ground state, without employing any symmetry constraints. The resulting geometrically optimized structure of the Diphenyl glycolic acid -leucine ligand is depicted in Fig. 1.13. Furthermore, the analysis of the geometrical parameters, such as bond lengths, bond angles, and dihedral angles, is presented in Table1.28, Table 1.29 and Table 1.30, respectively.

The optimized structure of the Diphenyl Glycolic acid-leucine ligand reveals the presence of two six-membered rings. The C-C bond lengths within these rings range from 1.39 to 1.40 Å, falling within the average range of C-C bond lengths observed in aromatic rings. This confirms the existence of two aromatic rings in the ligand. The carboxylic acid functional groups in the ligand display C-O double bonds with bond lengths of 1.21 Å and 1.20 Å, while the C-O single bond lengths of the acid functional groups measure 1.35 Å for both bonds. Additionally, the corresponding O-H bond lengths are 0.97 Å for both bonds. The optimized structure of the ligand contains the leucine moiety attached to the Diphenyl glycolic acid part via N1-C22 single bond (1.47 A^0).The orientation of the ligand is determined by several significant dihedral angles, namely ϕ(H2-N1-C22-C45), ϕ(H2-N1-C22-C34), ϕ(C23-C22-C45-O46), ϕ(C23-C22-C45-O47), ϕ(C3-C6-O20-H21), and ϕ(N1-C3-C6-O10), with corresponding values of 34.02°, 146.780°,

47.590°, 133.930°, 178.760°, and 39.490°, respectively. These reported dihedral angles indicate that the Diphenyl glycolic acid - leucine ligand does not possess a planar structure.

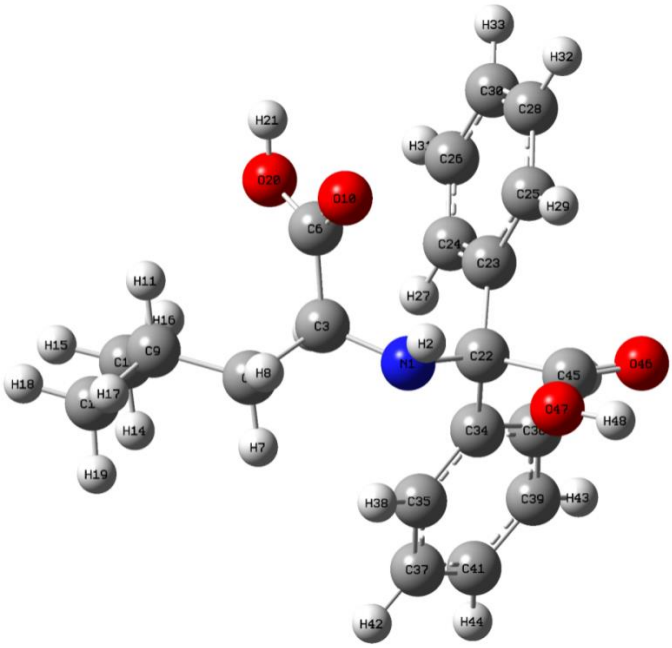

Fig. 1.13. Optimized geometry of the Diphenyl glycolic acid - leucine ligand

Table 1.28. Optimized bond lengths of Diphenyl glycolic acid - leucine ligand

Bond	**Bond length(A^0)**	**Bond**	**Bond length(A^0)**
N1-H2	1.0129	C23-C25	1.4004
N1-C3	1.4607	C24-C26	1.3945
N1-C22	1.4763	C24-H27	1.0828
C3-H4	1.0893	C25-C28	1.3911
C3-C5	1.5503	C25-H29	1.0840
C3-C6	1.5320	C26-C30	1.3916
C5-H7	1.0946	C26-H31	1.0843
C5-H8	1.0957	C28-C30	1.3946
C5-C9	1.5402	C28-H32	1.0842
C6-O10	1.2068	C30-H33	1.0843
C6-O20	1.3515	C34-C35	1.3960
C9-H11	1.0968	C34-C36	1.4016
C9-C12	1.5356	C35-C37	1.3957
C9-C13	1.5359	C35-H38	1.0810
C12-H14	1.0958	C36-C39	1.3914
C12-H15	1.0938	C36-H40	1.0824
C12-H16	1.0922	C37-C41	1.3914
C13-H17	1.0939	C37-H42	1.0845
C13-H18	1.0937	C39-C41	1.3952
C13-H19	1.0956	C39-H43	1.0844
O20-H21	0.9701	C41-H44	1.0843
C22-C23	1.5484	C45-O46	1.2030
C22-C34	1.5534	C45-O47	1.3525
C22-C45	1.5515	O47-H48	0.9696
C23-C24	1.3983		

Table 1.29. Optimized bond angles of Diphenyl glycolic acid - leucine ligand

Bond angle	Angle(degree)	Bond angle	Angle(degree)
H2-N1-C3	109.9294	C34-C22-C45	103.3910
H2-N1-C22	111.0758	C22-C23-C24	121.4938
C3-N1-C22	119.4414	C22-C23-C25	120.1906
N1-C3-H4	109.3437	C24-C23-C25	118.1276
N1-C3-C5	108.6188	C23-C24-C26	120.9709
N1-C3-C6	111.9249	C23-C24-H27	119.9782
H4-C3-C5	109.7241	C26-C24-H27	119.0475
H4-C3-C6	108.8140	C23-C25-C28	121.0724
C5-C3-C6	108.3922	C23-C25-H29	120.2054
C3-C5-H7	106.6632	C28-C25-H29	118.7221
C3-C5-H8	107.3527	C24-C26-C30	120.2719
C3-C5-C9	117.3451	C24-C26-H31	119.5223
7H-C5-H8	106.4878	C30-C26-H31	120.2057
7H-C5-C9	109.1367	C25-C28-C30	120.2090
8H-C5-C9	109.3201	C25-C28-H32	119.5746
C3-C6-O10	124.1634	C30-C28-H32	120.2162
C3-C6-O20	113.0325	C26-C30-C28	119.3433
O10-C6-O20	122.7445	C26-C30-H33	120.3705
C5-C9-H11	108.6906	C28-C30-H33	120.2862
C5-C9-C12	112.4278	C22-C34-C35	120.7997
C5-C9-C13	109.5235	C22-C34-C36	120.4713
H11-C9-C12	107.8858	C35-C34-C36	118.6244
H11-C9-C13	107.4059	C34-C35-C37	120.7045
C12-C9-C13	110.7460	C34-C35-H38	118.9416
C9-C12-H14	110.8083	C37-C35-H38	120.3437
C9-C12-H15	110.6714	C34-C36-C39	120.6356
C9-C12-H16	112.0869	C34-C36-H40	119.7698
H14-C12-H15	107.6078	C39-C36-H40	119.5893
H14-C12-H16	108.1449	C35-C37-C41	120.3030
H15-C12-H16	107.3402	C35-C37-H42	119.5435

C9-C13-H17	111.4280	C41-C37-H42	120.1514
C9-C13-H18	111.0273	C36-C39-H41	120.3479
C9-C13-H19	110.9817	C36-C39-H43	119.5316
H17-C13-H18	107.8577	H41-C39-H43	120.1202
H17-C13-H19	107.7460	C37-C39-H43	119.3633
H18-C13-H19	107.6335	C37-C41-H44	120.3674
C6-O20-H21	107.3456	C39-C41-H44	120.2671
N1-C22-C23	112.9027	C22-C45-O46	124.1131
N1-C22-C34	110.3798	C22-C45-O47	113.6019
N1-C22-C45	108.7282	O46-C45-O47	122.2668
C23-C22-C34	112.6110	C45-O47-H48	106.5746
C23-C22-C45	108.3059		

Table 1.30. Optimized dihedral angles of Diphenyl glycolic acid - leucine ligand

Dihedral	**Dihedral angle**	**Dihedral**	**Dihedral angle**
H2-N1-C3-H4	163.7507	N1-C22-C34-C35	11.1074
H2-N1-C3-C5	76.5330	N1-C22-C34-C36	172.6617
H2-N1-C3-C6	43.1042	C23-C22-C34-C35	138.2960
C22-N1-C3-H4	33.6690	C23-C22-C34-C36	45.4730
C22-N1-C3-C5	153.3854	C45-C22-C34-C35	105.0305
C22-N1-C3-C6	86.9774	C45-C22-C34-C36	71.2004
H2-N1-C22-C23	86.1920	N1-C22-C45-O46	170.6200
H2-N1-C22-C34	146.7809	N1-C22-C45-O47	10.9057
H2-N1-C22-C45	34.0241	C23-C22-C45-O46	47.5956
C3-N1-C22-C23	43.3756	C23-C22-C45-O47	133.9298
C3-N1-C22-C34	83.6515	C34-C22-C45-O46	72.0772
C3-N1-C22-C45	163.5918	C34-C22-C45-O47	106.3980
N1-C3-C5-H7	55.6938	C22-C23-C24-C26	175.6443
N1-C3-C5-H8	58.1288	C22-C23-C24-H27	5.0241
N1-C3-C5-C9	178.3790	C25-C23-C24-C26	0.6210
H4-C3-C5-H7	63.7850	C25-C23-C24-H27	179.9527
H4-C3-C5-H8	177.6076	C22-C23-C25-C28	175.8370
H4-C3-C5-H9	58.9005	C22-C23-C25-H29	4.0794
C6-C3-C5-H7	177.5130	C24-C23-C25-C28	0.7463
C6-C3-C5-H8	63.6906	C24-C23-C25-H29	179.1699

C6-C3-C5-H9	59.8013	C23-C24-C26-C30	0.0281
N1-C3-C6-O10	39.4981	C23-C24-C26-H31	179.8795
N1-C3-C6-O20	143.2470	H27-C24-C26-C30	179.3660
H4-C3-C6-O10	160.4520	H27-C24-C26-H31	0.5417
H4-C3-C6-O20	22.2932	C23-C25-C28-C30	0.2785
C5-C3-C6-O10	80.2721	C23-C25-C28-H32	179.5330
C5-C3-C6-O20	96.9828	H29-C25-C28-C30	179.6390
C3-C5-C9-H11	57.8906	H29-C25-C28-H32	0.5495
C3-C5-C9-C12	61.4749	C24-C26-C30-C28	0.4543
C3-C5-C9-C13	174.956	C24-C26-C30-H33	179.4654
H7-C5-C9-H11	179.3000	H31-C26-C30-C28	179.6388
H7-C5-C9-C12	59.9343	H31-C26-C30-H33	0.4415
H7-C5-C9-C13	63.6345	C25-C28-C30-C26	0.3307
H8-C5-C9-H11	64.5968	C25-C28-C30-H33	179.5890
H8-C5-C9-C12	176.038	H32-C28-C30-C26	179.8590
H8-C5-C9-C13	52.4689	H32-C28-C30-H33	0.2212
C3-C6-O20-H21	178.7617	C22-C34-C35-C37	177.9850
O10-C6-O20-H21	1.4623	C22-C34-C35-H38	0.8549
C5-C9-C12-H14	58.1883	C36-C34-C35-C37	1.6863
C5-C9-C12-H15	177.4803	C36-C34-C35-H38	177.1540
C5-C9-C12-H16	62.7255	C22-C34-C36-C39	177.6892
H11-C9-C12-H14	178.0220	C22-C34-C36-H40	1.4699
H11-C9-C12-H15	62.6860	C35-C34-C36-C39	1.3775
H11-C9-C12-H16	57.1082	C35-C34-C36-H40	177.7820
C13-C9-C12-H14	64.6962	C34-C35-C37-C41	0.8195
C13-C9-C12-H15	54.5958	C34-C35-C37-H42	179.7040
C13-C9-C12-H16	174.3899	H38-C35-C37-C41	178.0050
C5-C9-C13-H17	57.8661	H38-C35-C37-H42	1.4722
C5-C9-C13-H18	178.1173	C34-C36-C39-C41	0.1980
C5-C9-C13-H19	62.2126	C34-C36-C39-H43	179.9780
H11-C9-C13-H17	60.0048	C40-C36-C39-C41	178.9626
H11-C9-C13-H18	60.2464	C40-C36-C39-H43	0.8176
H11-C9-C13-H19	179.9165	C35-C37-C41-C39	0.3874
C12-C9-C13-H17	177.5810	C35-C37-C41-H44	179.8477
C12-C9-C13-H18	57.3296	H42-C37-C41-C39	179.0860
C12-C9-C13-H19	62.3405	H42-C37-C41-H44	0.3741
N1-C22-C23-C24	94.6244	C36-C39-C41-C37	0.6943
N1-C22-C23-C25	80.2976	C36-C39-C41-H44	179.8449
C34-C22-C23-C24	31.2121	H43-C39-C41-C37	179.0847

C34-C22-C23-C25	153.8660	H43-C39-C41-H44	0.3762
C45-C22-C23-C24	144.9177	C22-C45-O47-H48	177.8166
C45-C22-C23-C25	40.1603	O46-C45-O47-H48	0.6899

3.5.2. Frontier molecular orbital analysis

The frontier molecular orbitals (FMO) encompass the highest occupied molecular orbital (HOMO) and the lowest unoccupied molecular orbital (LUMO). The optimized structure of the Diphenyl glycolic acid -leucine ligand is utilized to visualize these orbitals. FMO analysis is an effective technique for investigating the chemical reactivity of compounds. It provides insights into the electron-donating and electron-accepting tendencies of molecules. A higher energy level of the HOMO orbital signifies electron-donating ability, while a higher energy level of the LUMO indicates an electron-accepting tendency. The disparity between the HOMO and LUMO energy levels is referred to as the band gap. The representation of the HOMO, LUMO, and band gap of the ligand is depicted in Fig. 1.14, where the red and blue colours represent the positive and negative lobes of the orbitals. The calculated energies of the HOMO and LUMO orbitals of the Diphenyl glycolic acid -leucine ligand, along with the computed band gap, are presented in Table 1.31. The determined band gap of the ligand is 5.4477 eV, suggesting a relatively large band gap, indicating the potential reactivity of the ligand. In the obtained FMO diagram, the HOMO is primarily localized in one of the

aromatic rings and the leucine component, while the LUMO is concentrated on the two aromatic rings and the carboxylic acid group. The locations of the HOMO serve as electron-donating sites, whereas the locations of the LUMO function as electron-accepting sites.

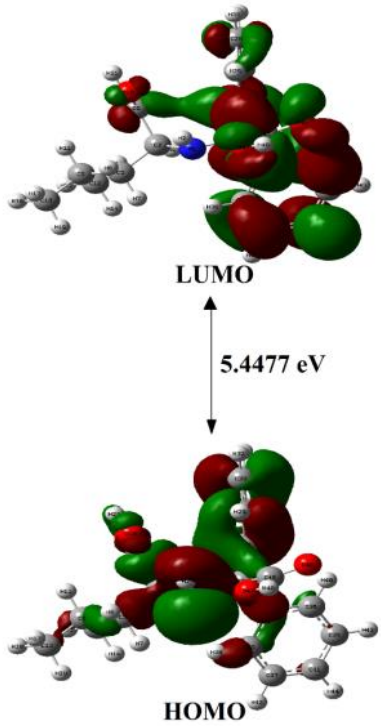

Fig. 1.14. Frontier molecular orbitals of Diphenyl glycolic acid -leucine ligand

Table 1.31.HOMO, LUMO energies, and calculated band gap of Diphenyl glycolic acid -leucine ligand

E(HOMO)eV	E(LUMO) eV	Band gap(eV)
-6.4981	-1.0504	5.4477

3.5.3 Global reactivity parameters

The global reactivity parameters of the Diphenyl glycolic acid - leucine ligand are calculated using **Eq. (1 to 7)**.Global descriptive parameters serve as a valuable tool for comparing the behaviour and reactivity of different compounds. These parameters include electronegativity (χ), chemical potential (ϒ), chemical softness (S), chemical hardness (η), and electrophilicity index (ω). Electronegativity indicates a molecule's tendency to attract electrons, while chemical potential represents the tendency of electrons to flow from regions of higher potential to lower chemical potential. Softness measures a molecule's inclination to receive electrons, and its inverse corresponds to hardness. The computed global descriptive parameters of the Diphenyl Glycolic acid-histidine ligand are listed in Table 1.32. The calculated ionization potential (IP) value of the ligand is 6.4981 eV, indicating a high value that suggests the removal of electrons from the ligand is challenging. The obtained electron affinity (EA) value of the ligand is 1.0504 eV, reflecting a small value that signifies the ligand's ability to accept electrons. The computed electrophilicity index (ω) of the ligand is 2.6149 eV. This relatively low value indicates a maximal flow of electrons from the donor to the acceptor. The calculated chemical hardness is 2.7239 eV, significantly higher than the chemical softness value of 0.1836, confirming that the molecule is relatively hard and stable. Hard molecules require substantial energy for excitation and exhibit reduced polarizability.

Table 1.32. Calculated global descriptive parameters of Diphenyl glycolic acid -leucine ligand

Descriptors	**Values(eV)**
Ionization potential (IP)	6.4981
Electron affinity (EA)	1.0504
Chemical hardness (η)	2.7239
Chemical softness (S)	0.1836
Electronegativity (χ)	3.7743
Electrophilicity index (ω)	2.6149
Chemical potential (ϰ)	-3.7743

3.5.4 Electrostatic potential maps (ESP)

The three-dimensional electrostatic potential map (ESP) is utilized to predict the reactive behaviour of chemical systems, encompassing both electrophilic and nucleophilic reactions. This map provides insights into the reactivity of inter- or intra-molecular interactions and aids in visualizing the molecule's size, shape, and charge distribution. ESP is based on the electrostatic potential energy, which quantifies the strength of nearby charges, nuclei, and electrons at specific positions. The computed ESP diagram of the Diphenyl glycolic acid -leucine ligand is presented in Fig. 1.15. The diagram employs various colours to represent distinct electrostatic potentials. The blue colour signifies a positive site, while the red colour indicates regions with a higher electron density or a more negative charge. The obtained ESP map of the Diphenyl glycolic acid -leucine ligand reveals that the electron density is

concentrated in the positions of the two carboxylic groups. This concentration suggests that these sites can potentially serve as ligand-binding sites for metal ions. Consequently, it is plausible to hypothesize that the Diphenyl glycolic acid -leucine ligand can form complexes with a variety of metal ions.

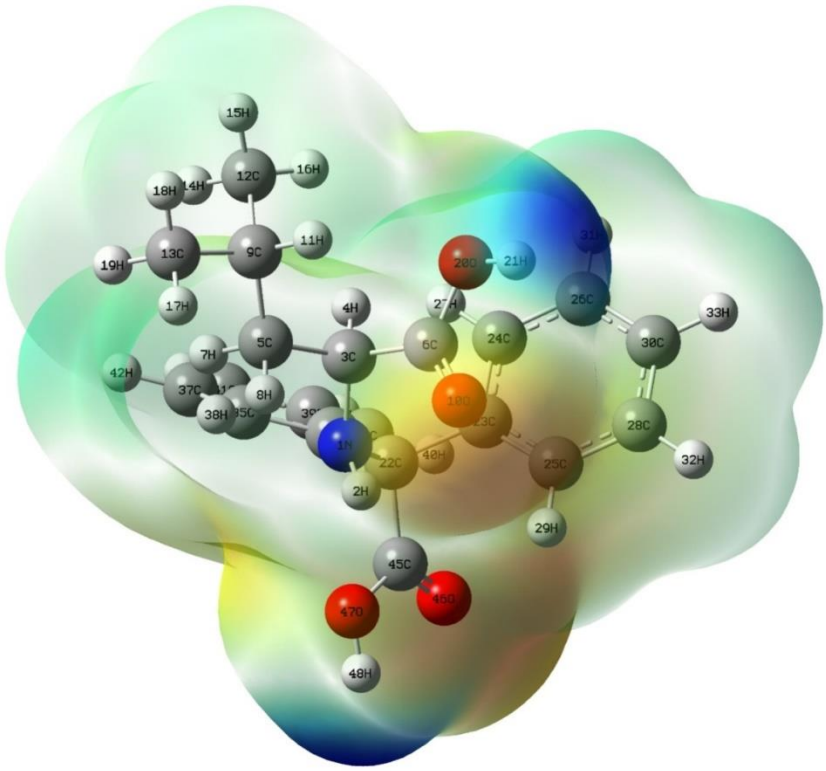

Fig.1.15. ESP diagram of Diphenyl glycolic acid -leucine ligand

3.5.5. NBO Analysis

NBO analysis is a valuable tool for visualizing electron orbitals and conducting population analysis. This analysis, in conjunction with

second-order perturbation energy, provides insights into the interactions between Lewis-type (bonding or lone pair) filled orbitals and non-Lewis-type (antibonding) empty orbitals, thereby quantifying intra- and intermolecular delocalization or hyperconjugation. The NBO output file contains valuable information, such as bond orbital occupancies and natural atomic hybrids, which assist in predicting the relative aromaticity of compounds and discerning the difference between kinetic and thermal stability. The occupancies and hybrids of various atoms or groups in the Diphenyl glycolic acid-leucine ligand are presented in Table 1.33. This data summarizes the effective valence electron configuration of each atom in the molecule. The NBO analysis clarifies the presence of two aromatic rings in the ligand. The first ring comprises atoms C23, C24, C25, C26, C28, and C30, while the second ring consists of C34, C35, C36, C37, C39, and C41. These aromatic rings are connected by two single bonds, namely C22-C23 and C22-C34. The occupancies of these Sigma bonds are reported as 1.96036 and 1.95258, respectively. Additionally, atom C22 is linked to a carboxylic group (C22-C45) and an N atom that connects to the leucine moiety (C22-N1). The occupancies of these two Sigma bonds are specified as 1.95670 and 1.97776, respectively.

In NBO analysis, the electronic wave function is described in terms of occupied Lewis and unoccupied Lewis delocalized orbitals**.** Table 1.34 presents the key electronic wave functions of the donor

and acceptor orbitals, along with the interaction energy (E(2)) between them. The ligand's interaction energies arise from the lone pairs of atoms such as oxygen, nitrogen, carbon, and hydrogen. The strength of the donor-acceptor interaction is reflected by the interaction energy (E(2)), which increases as the interaction between the donor and acceptor intensifies. For the donors, O47-H48 and O20-H21, and the acceptors C45-O46 and C6-O10, the interaction energies between the donor and acceptor are reported as 0.85kcal/mol and 0.78kcal/mol, respectively. Since the interaction is relatively weak, it is feasible for the metal chelation to occur between the atoms O47 and O20 through the removal of the protons H48 and H21.

Table1.33.Occupancy of NBOs and hybrids of Diphenyl glycolic acid -leucine ligand

NBOs	**Hybrid**	**occupancy**	**AO%**
σN1-H2	N $sp^{3.24}$	1.98005	s(23.56%) p(76.36%) d(0.08%)
	H s		s(99.92%) p(0.08%)
σN1-C3	N $sp^{2.15}$	1.98024	s(31.70%) p(68.24%) d(0.06%)
	C $sp^{3.17}$		s(23.97%) p(75.93%) d(0.10%)
σN1-C22	N $sp^{2.14}$	1.97776	s(31.85%) p(68.09%) d(0.06%)
	C $sp^{3.35}$		s(22.99%) p(76.91%) d(0.10%)
σC3-H4	N $sp^{3.18}$	1.96932	s(23.92%) p(76.01%) d(0.07%)
	H s		s(99.96%) p(0.04%)
σC3-C5	C $sp^{2.62}$	1.96057	s(27.64%) p(72.33%) d(0.03%)
	C $sp^{2.71}$		s(26.95%) p(72.99%) d(0.06%)
σC3-C6	C $sp^{3.06}$	1.97211	s(24.62%) p(75.32%) d(0.07%)
	C $sp^{1.58}$		s(38.80%) p(61.15%) d(0.05%)

σC5-H7	C $sp^{3.55}$	1.97408	s(21.95%) p(77.99%) d(0.07%)
	H s		s(99.97%) p(0.03%)
σC5-H8	C $sp^{3.56}$	1.97755	s(21.91%) p(78.02%) d(0.07%)
	H s		s(99.97%) p(0.03%)
σC5-C9	C $sp^{2.42}$	1.97745	s(29.22%) p(70.75%) d(0.04%)
	C $sp^{2.75}$		s(26.69%) p(73.27%) d(0.04%)
σC6-O10	C $sp^{1.96}$	1.99558	s(33.68%) p(66.16%) d(0.16%)
	O $sp^{1.40}$		s(41.55%) p(58.33%) d(0.12%)
ΠC6-O10	C $sp^{99.99}d^{12.27}$	1.99258	s(0.04%) p(99.42%) d(0.54%)
	O $sp^{1.00}$		s(0.00%) p(99.88%) d(0.12%)
σC6-O20	C $sp^{2.61}d^{0.01}$	1.99495	s(27.60%) p(72.14%) d(0.26%)
	O $sp^{1.93}$		s(34.12%) p(65.80%) d(0.08%)
σC9-C12	C $sp^{2.75}$	1.98302	s(26.65%) p(73.31%) d(0.04%)
	C $sp^{2.35}$		s(29.80%) p(70.16%) d(0.04%)
σC9-C13	C $sp^{2.78}$	1.98095	s(26.47%) p(73.48%) d(0.04%)
	C $sp^{2.34}$		s(29.93%) p(70.04%) d(0.04%)
σO20-H21	O $sp^{3.70}$	1.98684	s(21.24%) p(78.67%) d(0.08%)
	H s		s(99.82%) p(0.18%)
σC22-C23	C $sp^{2.52}$	1.96036	s(28.42%) p(71.54%) d(0.04%)
	C $sp^{2.28}$		s(30.45%) p(69.50%) d(0.05%)
σC22-C34	C $sp^{2.74}$	1.95258	s(26.74%) p(73.22%) d(0.04%)
	C $sp^{2.30}$		s(30.30%) p(69.65%) d(0.05%)
σC22-C45	C $sp^{3.58}$	1.95670	s(21.80%) p(78.13%) d(0.07%)
	C $sp^{1.59}$		s(38.58%) p(61.36%) d(0.06%)
σC45-O46	C $sp^{1.94}$	1.99468	s(33.92%) p(65.91%) d(0.17%)
	O $sp^{1.39}$		s(41.82%) p(58.07%) d(0.12%)
ΠC45-O46	C $sp^{99.99}d^{3.18}$	1.99169	s(0.16%) p(99.33%) d(0.51%)

	O $sp^{99.99}d^{0.69}$		s(0.18%) p(99.69%) d(0.13%)
σC45-O47	C $sp^{2.65}d^{0.01}$	1.99461	s(27.36%) p(72.41%) d(0.23%)
	O $sp^{1.93}$		s(34.09%) p(65.82%) d(0.09%)
σO47-H48	O $sp^{3.71}$	1.98406	s(21.20%) p(78.72%) d(0.09%)
	H s		s(99.86%) p(0.14%)

Table 1.34. Donor-Acceptor interactions of Diphenyl glycolic acid -leucine ligand in terms of E (2)

Donor NBO(i)	**Acceptor NBO(j)**	**E(2) (kcal/mol)**	**Ej-Ei (a.u)**	**F(I,j) (a.u)**
σN1-H2	σ*C3-H4	2.29	1.02	0.043
σN1-H2	σ*C22-C34	2.23	0.99	0.042
σN1-H2	σ*C22-C45	0.95	0.93	0.027
σN1-C3	σ*N1-C22	0.61	1.07	0.023
σN1-C3	σ*C3-C5	0.71	1.09	0.025
σN1-C3	σ*C5-C9	1.57	1.12	0.037
σN1-C3	Π*C6-O10	0.67	0.73	0.021
σN1-C3	σ*C6-O20	1.44	1.07	0.036
σN1-C3	σ*C22-C45	1.18	1.05	0.032
σN1-C22	σ*C3-C5	0.99	1.09	0.029
σN1-C22	σ*C22-C23	0.84	1.11	0.027
σN1-C22	σ*C22-C34	0.66	1.10	0.024
σN1-C22	σ*C23-C24	0.50	1.30	0.023
σN1-C22	Π*C23-C24	1.52	0.76	0.033
σN1-C22	σ*C34-C36	1.99	1.30	0.045
σN1-C22	σ*C45-O46	1.84	1.33	0.044
σC3-H4	σ*N1-H2	3.01	0.94	0.048
σC3-H4	σ*C3-C5	0.56	0.88	0.020
σC3-H4	σ*C5-H8	2.29	0.92	0.041

σC3-H4	σ*C6-O10	4.03	1.13	0.060
σC3-H4	Π*C6-O10	0.61	0.52	0.017
σC3-C5	σ*N1-C3	0.55	0.96	0.021
σC3-C5	σ*N1-C22	2.98	0.94	0.047
σC3-C5	σ*C3-H4	0.75	1.01	0.025
σC3-C5	σ*C3-C6	0.56	0.95	0.021
σC3-C5	σ*C5-C9	0.61	0.99	0.022
σC3-C5	Π*C6-O10	3.84	0.61	0.045
σC3-C5	σ*C6-O20	0.51	0.94	0.020
σC3-C5	σ*C9-C13	1.55	0.99	0.035
σC3-C6	σ*C3-C5	0.58	1.01	0.022
σC3-C6	σ*C5-H7	1.77	1.05	0.039
σC3-C6	σ*C6-O10	0.95	1.26	0.031
σC3-C6	σ*O20-H21	2.25	1.03	0.043
σC5-H7	σ*C3-C6	2.84	0.84	0.044
σC5-H7	σ*C9-H11	2.94	0.89	0.046
σC5-H8	σ*C3-H4	2.94	0.90	0.046
σC5-H8	σ*C9-C12	3.41	0.88	0.049
σC5-C9	σ*N1-C3	1.68	0.96	0.036
σC5-C9	σ*C3-C5	0.51	0.96	0.020
σC5-C9	σ*C9-C12	0.73	0.99	0.024
σC5-C9	σ*C9-C13	0.67	0.98	0.023
σC5-C9	σ*C12-H15	1.48	1.00	0.035
σC5-C9	σ*C13-H18	1.52	1.00	0.035
σC6-O10	σ*C3-C6	1.43	1.46	0.042
ΠC6-O10	σ*N1-C3	0.62	0.76	0.019
ΠC6-O10	σ*C3-C5	0.93	0.76	0.024
ΠC6-O10	Π*C6-O10	0.77	0.40	0.017
σC6-O20	σ*N1-C3	0.80	1.31	0.029
σC9-C12	σ*C5-H8	1.76	1.00	0.038
σC9-C12	σ*C5-C9	0.78	0.99	0.025
σC9-C12	σ*C9-C13	0.76	0.98	0.024

σC9-C12	σ*C13-H17	1.70	1.00	0.037
σC9-C13	σ*C3-C5	2.78	0.96	0.046
σC9-C13	σ*C5-C9	0.93	0.98	0.027
σC9-C13	σ*C9-C12	0.75	0.98	0.024
σC9-C13	σ*C12-H16	1.75	1.01	0.038
σO20-H21	σ*C3-C6	3.82	1.11	0.059
σO20-H21	σ*C6-O10	0.78	1.38	0.029
σC22-C23	σ*C22-C34	1.28	1.00	0.032
σC22-C23	σ*C22-C45	0.61	0.95	0.022
σC22-C23	σ*C23-C24	1.81	1.19	0.042
σC22-C23	σ*C23-C25	1.75	1.19	0.041
σC22-C23	σ*C24-C26	2.26	1.20	0.047
σC22-C23	σ*C25-C28	2.19	1.20	0.046
σC22-C23	σ*C34-C35	1.90	1.20	0.043
σC22-C23	Π*C34-C35	0.74	0.66	0.021
σC22-C23	Π*C45-O46	1.17	0.62	0.025
σC22-C23	σ*C45-O47	1.81	0.95	0.038
σC22-C34	σ*N1-H2	1.63	1.04	0.037
σC22-C34	σ*C22-C23	1.15	0.99	0.030
σC22-C34	σ*C22-C45	0.66	0.94	0.022
σC22-C34	σ*C23-C25	2.59	1.18	0.050
σC22-C34	σ*C34-C35	1.79	1.19	0.042
σC22-C34	σ*C34-C36	1.59	1.18	0.039
σC22-C34	σ*C35-C37	2.15	1.19	0.046
σC22-C34	σ*C36-C39	2.15	1.20	0.046
σC22-C34	Π*C45-O46	3.65	0.61	0.044
σC22-C34	σ*C45-O47	0.79	0.94	0.025
σC22-C45	σ*N1-C3	2.71	1.00	0.047
σC22-C45	σ*C22-C34	0.90	1.01	0.027
σC22-C45	σ*C23-C24	2.90	1.21	0.053
σC22-C45	Π*C23-C24	0.52	0.67	0.018
σC22-C45	σ*C34-C35	1.02	1.21	0.032

σC22-C45	Π*C34-C35	2.93	0.67	0.043
σC22-C45	σ*C45-O46	0.92	1.24	0.030
σC22-C45	σ*O47-H48	2.18	1.02	0.042
σC45-O46	σ*N1-C22	0.71	1.45	0.029
σC45-O46	σ*C22-C45	1.50	1.44	0.042
ΠC45-O46	σ*C22-C34	0.78	0.78	0.022
ΠC45-O46	Π*C34-C35	0.54	0.44	0.015
ΠC45-O46	Π*C45-O46	0.89	0.41	0.018
σC45-O47	σ*C22-C23	0.67	1.34	0.027
σO47-H48	σ*C22-C45	4.35	1.09	0.062
σO47-H48	σ*C45-O46	0.85	1.37	0.030
Π*C6-O10	σ*N1-C3	0.71	0.36	0.042
Π*C6-O10	σ*C3-C5	1.01	0.36	0.05
Π*C6-O10	Π*C23-C24	0.95	0.03	0.009
σ*C6-O20	σ*N1-C3	6.24	0.02	0.041
σ*C6-O20	σ*C3-H4	2.31	0.07	0.045
σ*C6-O20	σ*O20-H21	1.42	0.04	0.029
Π*C23-C24	σ*N1-C22	2.49	0.31	0.056
Π*C23-C24	σ*C22-C45	0.57	0.29	0.025
Π*C34-C35	σ*C22-C23	0.68	0.34	0.031
Π*C34-C35	σ*C22-C45	1.45	0.29	0.040
Π*C45-O46	σ*C22-C23	0.62	0.38	0.038
Π*C45-O46	σ*C22-C34	0.85	0.37	0.045
Π*C45-O46	Π*C23-C24	0.51	0.03	0.007
Π*C45-O46	Π*C34-C35	5.28	0.03	0.023

Conclusion

The molecular modeling studies of the newly synthesized ligands have been carried out. The geometrical optimization of the new compounds has been done. The global parameters have also been calculated and their structural relationship with its reactivity and their corrosion inhibition efficiency is studied. The three-dimensional electrostatic potential map (ESP) of the newly prepared compounds is utilized to predict the reactive behaviour of chemical systems, encompassing both electrophilic and nucleophilic reactions. This map provides insights into the reactivity of inter- or intra-molecular interactions and aids in visualizing the molecule's size, shape, and charge distribution. ESP is based on the electrostatic potential energy, which quantifies the strength of nearby charges, nuclei, and electrons at specific positions. The NBO analysis of the synthesized compounds has also studied. The NBO analyzed data contains valuable information, such as bond orbital occupancies and natural atomic hybrids, which assist in predicting the relative aromaticity of compounds and discerning the difference between kinetic and thermal stability.

References :

1. Parr, R., &Yang, W. (1989). Density-Functional Theory of Atoms and Molecules, Oxford University Press, New York.

2. Kohn, W., & Sham, L. (1965). *Phys. Rev*., 140, 1133.

3. Frisch, A., Dennington, I. I. R., Keith, T., Millam, J., Nielsen, A. B., Holder, A. J., & Hiscocks, J. (2007). Reference, Version 4.0, Gaussian Inc. Inc Pittsburgh.

4. Hohenberg, P., & Kohn, W. (1964). *Phys. Rev*., 136, 864.

5. Frisch, M. J., Trucks, G. W., Schlegel, H. B., Scuseria, G. E., Robb, M. A., Cheeseman, J. R., Scalmani, G., Barone, V., Mennucci, B., Petersson, G. A., Nakatsuji, H., Caricato, M., Li, X., Hratchian, H. P., Izmaylov, A. F., Bloino, J., Zheng, G., Sonnenberg, J. L., Hada, M., Ehara, M., Toyota, K., Fukuda, R., Hasegawa, J., Ishida, M., Nakajima, T., Honda, Y., Kitao, O., Nakai, H., Vreven, T., Montgomery, J. A., Jr., Peralta, J. E., Ogliaro, F., Bearpark, M. Heyd, J. J., Brothers, E. Kudin, K. N., Staroverov, V. N., Iyengar, R. Kobayashi, J. Normand, K. Raghavachari, A. Rendell, J. C. Burant, S. S., Tomasi, J., Cossi, M., Rega, N., Millam, J. M., Klene, M., Knox, J. E., Cross, J. B., Bakken, V., Adamo, C., Jaramillo, J., Gomperts, R., Stratmann, R. E., Yazyev, O., Austin, A. J., Cammi, R., Pomelli, C. Ochterski, J. W., Martin, R. L., Morokuma, K., Zakrzewski, V. G., Voth, G. A., Salvador, P., Dannenberg, J. J. Dapprich, S., Daniels, A. D., Farkas, Ö., Foresman, J. B., Ortiz, J. V., Cioslowski, J., & Fox, D. J. (2009). *Gaussian 09* (Gaussian, Inc., Wallingford CT.

6. Frisch E., Hratchian H. P.,Dennington R. D. II, Keith T. A., Millam J., Nielsen B., Holder A. J., & Hiscocks J. 2009. *GaussView*, version 5.0.8.; Gaussian Inc.

7. Choudhary, N., Bee, S., Gupta, A., &Tandon, P. (2013). *Comput. Theor. Chem*., 1016, 8.

8. Kavitha, E., Sundaraganesan, N., & Sebastian, S., (2010). *J. Pure Ap. Phy*., 48, 20.

9. Despaigne, A. A. R., da Silva, J. G., do Carmo, A. C. M., Sives, F., Piro, O. E., Castellano, E. E., & H. Beraldo, (2009). *Polyhedron*, 28, 3797.

10. Orbitals, I. F. F. (1976). Organic Chemical Reactions, John Wiley and Sons, New York City, New York.

11. Vektariene, A., & Vektaris, G. (2009). *J. Svoboda, Arkivoc*, 7, 311.

12. Pearson, R. G. (1986). *Proc. Natl. Acad. Sci*., 83, 8440.

13. Chattaraj, P. K., & Maiti, B. (2003). *J. Am. Chem. Soc*., 125, 2705.

14. Parr, R. G., Szentpaly, L.V, & Liu, S., (1999). *J. Am. Chem Soc*., 121, 1922.

15. Koopmans, T. (1933). *Physica*., 1, 104.

16. Liu, S. (2005). *J. Chem. Sci*., 117, 477.

17. Scrocco, E., Tomasi, J., & Lowdin P. (Ed.). (1978). Advances in Quantum Chemistry, Academic Press, New York City, New York,115.

18. Scrocco, E., & Tomasi, J. (1973). *Topics Current Chem*.,Vol. 42,95.

19. Reed, A. E., Weinhold, R. B., & Weinhold, F. (1985). *J. Chem. Phys*., 83, 735.

20. Reed, A.E., Curtiss, L. A., & Weinhold, F., (1988). *Chem. Rev*., 88, 899.

21. Gunter, P. 2000. Nonlinear Optical Effects and Materials, *Springer,72.*

22. Frisch, M. J., Trucks, G. W., Schlegel, H. B., Scuseria, G. E., Robb, M. A., Cheeseman, J. R., & Pople, J. A. (2003). Gaussian 03, Revision B. 03, Gaussian, Inc., Pittsburgh (PA). *J. Chem. Phys.*, *118*, 1101.

23. Becke, A. D. (1988). *Phys. Rev. B. Condens.Matter*, 37, 785.

24. Lee, C., Yang, W., & Parr, R.G. (1988). *Phys. Rev. B.*, 37, 785.

25. Krishna, P. N., & Muraleedharan,K. (2023). *Comput. Theor. Chem.*, 1220, 113996.

26. Krishna, P. N., Jalala, V. K., & Muraleedharan, K. (2023). *Struct. Chem.*, *34*, 2139.

27. Krishna, P. N., & Muraleedharan, K. (2023). *Mater. Today Commun.*, 36, 106453.

28. Kaviani, S., Izadyar, M., & Housaindokht, M. R. (2020). *Comput. Biol. Chem.*, 86, 107267.

29. Rajan, V. K., Hasna, C. K. & Muraleedharan, K., (2018). *Food Chem.*, 262, 184.

30. Pearson, R. G.(1997). Chemical Hardness, Wiley: New York.

31. Meenakshi, R. (2017). *J. Mol. Struct.*, 1127, 694.

32. Hussan, K. P. S., Thayyil, M. S., Rajan, V. K., & Muraleedharan, K. (2019). *Comput. Biol. Chem.*, 80, 46.

33. Bebu, A., Szabo, L., Leopold, N., Berindean, C., & David, L. (2011). *J. Mol. Struct.*, *993*, 52.

34. Politzer, P., & Truhlar D.G. (1981). (Eds.), Chemical Application of Atomic and Molecular Electrostatic Potentials, Plenum, New York.

35. Adeowo, F. Y., Honarparvar, B., & Skelton, A. A. (2017). *J. Phys. Chem. A*, 121, 6054.

36. Kaviani, S., Izadyar, M., & Housaindokht, M. R. (2017). *Comput. Biol. Chem*, 67, 114.

SUMMARY AND FUTURE PERSPECTIVES

SUMMARY AND FUTURE PERSPECTIVES

Amino acid complexes are a significant group of complexes in coordination chemistry and find ample applications in different spheres. Transition metal complexes of Diphenyl Glycolic acidhave been amongst the widely studied coordination compounds. Because of the green nature of the amino acid ligands many ligands of diverse structural type have been synthesized. The present study is focused mainly on the metal complexes of Diphenyl glycolic acid-amino acid. Five new ligands viz Diphenyl glycolic acid-tyrosine (HBT), Diphenyl glycolic acid-glycine(HBG), Diphenyl glycolic acid-histidine(HBH), Diphenyl glycolic acid-valine(HBH) and Diphenyl glycolic acid-leucine(HBL) their transition metal chelates have been synthesized and characterised. The thesis is divided into seven parts. Part I deals with the synthesis and characterization of various complexes derived from Diphenyl glycolic acid-amino acid ligands. Part I comprises of seven chapters. The first chapter consists of an introduction and a critical review of the published work on metal complexes of Schiff bases. In the second chapter, materials, methods and instruments used for the various studies are described. Synthesis and characterisation of Cr(III),Mn(II), Fe(III),Co(II), Ni(II), Cu(II), Zn(II) and Cd(II) complexes of HBT are described in the Chapter 3. Structural elucidation of these complexes has been made on the basis of micro analytical, spectral and magnetic data. These data suggest that HBT act as a dianionic

bidendate ligand for the metal ions. Majority of the complexes possess 1:1 whereas some among them possess 1:2 metal ligand stoichiometry and they are non-electrolyte in nature. All complexes are found to be paramagnetic except Zn (II) and Cd (II) complex which are diamagnetic. Based on the above physicochemical studies, an octahedral structure is suggested for all the seven complexes except Cd(II) complex, showing tetrahedral geometry. The synthesis and characterisation of Cr(III),Mn(II), Fe(III),Co(II), Ni(II), Cu(II), Zn(II) and Cd(II) complexes of HBG, HBH, HBV and HBL are described in the Chapters 4, 5, 6 and 7. These complexes are characterised and structural elucidation have been made. Majority of the complexes of HBG, HBH, HBV and HBL possess 1:1 metal ligand stoichiometry whereas some among them possess 1:2 metal ligand stoichiometry and they are non electrolyte in nature. The ligands HBG, HBH, HBV and HBL acted as dianionic tridendate and the geometry of their complexes are found to be octahedral one. Part I ends with reference.

Part II deals with the thermogravimetric analysis of the selected nine complexes of Diphenyl glycolic acid- glycine, Diphenyl glycolic acid- leucine and Diphenyl glycolic acid- histidine ligands. Chapter I and II discuss about the introduction, materials and methods used for the study respectively. Chapter III consists of the thermogravimetric analysis of the Mn (II), Fe (III), Cu (II) and Zn (II) complexes of HBG, Cu (II) and Cr (III) complexes of HBH and Cu (II), Ni (II) and Cr (III) complexes of HBL. The decomposition

pattern and kinetic analysis of the complexes were carried out. From the TG curves various kinetic parameters such as energy of activation, Arrhenius frequency factor and entropy of activation for decomposition have been calculated using nine equations and Coats- Redfern equation. Based on the temperature of inflection and initial decomposition, the relative thermal stabilities of the complexes were determined. The Zn (II), Fe (III) and Cu (II) complexes of HBG follow a two stage decomposition pattern while the Mn (II) complexes follow a single stage decomposition pattern. The Cr (III) and Cu (II) complexes of HBH follow a two stage decomposition pattern while the Cr (III) and Cu (II) of HBH follow a two stage decomposition pattern while the Ni (II) complexes follow a three stage decomposition pattern. The thermal decomposition data of the above mentioned nine complexes are represented in figures 3.1 to 3.9. The temperature ranges, peak temperature, probable assignments and total mass from TG curves of the Mn (II), Fe (III), Cu (II) and Zn (II) complexes of HBG, Cu (II) and Cr (III) complexes of HBH and Cu (II), Ni (II) and Cr (III) complexes of HBL are summarized in the tables 3.1 to 3.9 respectively. The kinetic parameters data from the Coats-Redfern kinetic equation and nine equations are given in the table 3.10-3.15.The relative thermal stabilities of HBG complexes follow the order, Mn (II) < Zn (II) < Fe (III) < Cu (II) while the HBH complexes follows the order Cu (II) < Cr (III). In the case HBL complexes the order is Cr (III) < Cu (II) < Ni (II). The part II concludes with reference.

Part III consists of X-ray diffraction study of the selected complexes of Diphenyl glycolic acid- glycine, Diphenyl glycolic acid- tyrosine and Diphenyl glycolic acid- histidine ligands. Chapter I and II give the introduction, materials and methods employed respectively. In Chapter III, the X - ray diffraction studies of the HBT, HBG and HBH ligands and Mn (II), Fe (III), Co (II) complexes of HBT, Mn (II), Fe (III), Co (II), Ni (II), Cu (II), Zn (II), and Cd (II) complexes of HBG, and Mn (II), Fe (III), Co (II), Ni (II), Cu (II), Zn (II), and Cd (II) complexes of HBH ligands are presented. All the three ligands and their seventeen complexes have been found to be orthorhombic. The calculated density of each complex was in good agreement with experimental value found out, which confirm the proposed molecular formula of the complexes and the existence of 1: 1 stoichiometry between the metal ion and the ligand for all complexes, except for the Mn (II) complexes of HBT, Co (II) and Mn (II) complexes of HBG, Mn (II) complexes of HBH where it is 1: 2 stoichiometry. Chapter III concludes with reference.

Studies of corrosion inhibition efficiency of five Diphenyl glycolic acid-amino acid ligands HBT, HBG, HBH, HBV and HBL towards mild steel in hydrochloric acid are described in Part IV. A critical review of Schiff base based corrosion inhibitors is included in first chapter. A detailed description about the theory and methods used for the corrosion inhibition studies are discussed in Chapter 2. In Chapter 3, the results of the corrosion inhibition efficiency

determined using laboratory corrosion immersion technique (weight loss method) and adsorption studies are presented. Results reveal that among five ligands HBH and HBV ligands act as good corrosion inhibitors, and various parameters were carried with. HBH and HBV are having efficiency of 97 and 93 % respectively towards mild steel in 0.5M hydrochloric acid solutions. Hence they can be used as corrosion inhibitors for industrial applications. The efficiency of the investigated compounds varied depending upon their chemical structure and constituents present in them. The adsorption isotherm analysis and thermodynamic parameters calculated indicate that the prepared ligandsinhibit corrosion through the physical adsorption process and follow Langmuir adsorption isotherm. Relevant references are given at the end of Part IV.

Part V of this thesis consists of studies on anti fungal activity of Diphenyl glycolic acid-amino acid ligands and its transition metal complexes against various fungal strains such as Pencillium sp., Fusarium sp.,Pythium sp., Lasiodiplodia theobromae and Aspergillus sp. Chapter I and II give the introduction to antifungal treatment, materials, methods and instruments employed in the present study. Chapter III comprises the results of the above-mentioned studies in a detailed manner. The results of the study at 48 hours were tabulated in the tables 1.1- 1.5 and their graphical representations are shown in fig.1.1-1.5. The antifungal activity of the ligand and its complexes were shown in fig 1.6-1.10. All the

studies confirm the fact that at higher concentration the inhibition of the complexes is maxima. The experimental results revealed that most of these compounds possess anti fungal activity. Some of them showed less activity at low concentration, but upon increasing the concentration, they also showed considerable activity.

Part VI of this thesis consists of studies on catalytic activity of selected transition metal complexes of Diphenyl glycolic acid-amino acid ligands Chapter I and II give the introduction to catalytic activity of compounds, materials, methods and instruments employed in the present study. Chapter III comprises the results of the above-mentioned studies in a detailed manner. The catalytic activity of the newly synthesized complexes towards the degradation of methyl orange was also studied using H_2O_2 as an oxidant. The reactivity order is CoBG >CoBV >CoBL >CuBG >CuBL >CuBV >NiBV >NiBL >NiBG. Among these complexes, a Cobalt complex shows the maximum degradation of the dye and among them Cobalt complex of the HBG is the highest with an efficiency of 91%. Optimum values were found to be the reaction time (1 hour), amount of catalyst (0.005g), amount of oxidant (1ml). Any further increase in the optimum values results in the lower yield of methyl orange dye. Among the nine catalysts Co-gly was found to be the efficient candidate for the degradation process.The catalytic activity order of the newly synthesized complexes towards the degradation of methylene blue with the use of oxidizing agent H_2O_2 is CoBV >CoBG >CoBL >CuBG >CuBV

>CuBL >NiBG >NiBV >NiBL. Among these complexes, Cobalt complexes exhibits high percentage conversion efficiency and among them Cobalt complex of the HBV is the highest with an efficiency of 96%. Hence these catalysts are found to be an efficient catalyst for the decomposition of methylene blue. Detailed study of the catalytic activity of the complexes was carried out by varying the parameters like catalyst amount, reaction time and amount of oxidant. At optimum conditions Cobalt-gly complex gives high efficiency towards the degradation of the methylene blue dye. These complexes are environment friendly thereby reducing the environmental pollution.

Part VII of this thesis consists of molecular modeling studies of Diphenyl glycolic acid-amino acid ligands using Gaussian program 6-31G. Chapter I and II give the introduction to molecular modeling materials, methods and instruments employed in the present study. Chapter III comprises the results of the above-mentioned studies in a detailed manner. The starting geometries of molecules were drawn with the aid of Gauss view program. The detailed description about the compounds such as HOMO-LUMO energy gap, global reactivity descriptors, the molecular electrostatic potential map and natural bond analysis (NBO) were obtained from the DFT method. The global parameters have also been calculated and their structural relationship with its reactivity and their corrosion inhibition efficiency is studied. The three-dimensional electrostatic potential map (ESP) of the newly prepared compounds

is utilized to predict the reactive behaviour of chemical systems, encompassing both electrophilic and nucleophilic reactions. This map provides insights into the reactivity of inter- or intra-molecular interactions and aids in visualizing the molecule's size, shape, and charge distribution. ESP is based on the electrostatic potential energy, which quantifies the strength of nearby charges, nuclei, and electrons at specific positions. The NBO analysis of the synthesized compounds has also studied. The NBO analyzed data contains valuable information, such as bond orbital occupancies and natural atomic hybrids, which assist in predicting the relative aromaticity of compounds and discerning the difference between kinetic and thermal stability.

Future Perspectives

The present work give a wonderful idea of user friendly protocol for the successful preparation of five important amino acid ligands obtained from initial materials ie diphenyl glycolic acid, amino acids (tyrosine, glycine, histidine, valine and leucine). These ligands on further complexation with eight transition metal chlorides/acetates results in formation of bidentate complexes which show tremendous corrosion inhibition efficiency, catalytic activity and biological activity as compare to parent ligands whether it is antimicrobial, corrosion inhibition and catalytic activities. The extract of this research revealed that all the prepared diphenyl glycolic acid-amino acid ligands and their transition metal complexes could lead to development of better antifungal, catalyst

and corrosion inhibitor. Results has given clear indications of antimicrobial activity of Schiff base ligands and their transition metal complexes are very active against fungi Aspergillus sp., Pythium sp., Pencillium sp., Lasiodiplodia sp. and Fusarium sp. Pythium sp. and Lasiodiplodia sp., hence study should be done against other species of micro-organism to see the diversity of results. Along with positivity, investigations should also be done for possible side effects of prepared compounds on affected and normal living cells. Because on getting harmful effects, possible changes could be made in structure of the compounds or concentration to minimize the side effects. The results of catalytic activity and corrosion inhibition efficiency has also lighten the importance of prepared diphenyl glycolic acid-amino acid ligands and their transition metal complexes in area of corrosion and catalysis due to their excellent role in inhibition of corrosion and excellent efficiency for the degradation of dyes . It is expected that further investigation in prepared compounds could contribute further development of diphenyl glycolic acid-amino acid ligands and their metal complexes so that they can be used to cure diseases in clinical and pharmacological fields after necessary modifications and also in the field of organic inhibitors and in catalysis.